



Conceptual Mathematical Models for Climate Change and Sustainability

A Thesis Submitted in Partial Fulfilment of the Requirements
for the Degree of Doctor of Philosophy in

Sustainable Development and Climate Change

Doctoral Programme of National Interest



In the Curriculum
EARTH SYSTEM AND ENVIRONMENT

by

Marta Lenzi

Supervisor: Prof. Franco Flandoli

Co-Supervisor: Dott. Gianmarco Del Sarto

07, 2026

ABSTRACT

This thesis develops idealised mathematical models for the study of ongoing climate change and of the sustainability of human life on the territory. The models deliberately favour conceptual simplicity and qualitative insight over exhaustive physical detail, and they employ randomness to encapsulate those climate variables that would otherwise require complex physical descriptions. A central tool is the energy balance model, a simplified representation of the Earth's incoming and outgoing radiative budget that nonetheless captures, qualitatively, the response of temperature to radiative forcing.

The main line of research builds on the pioneering ideas of Klaus Hasselmann, who recognised that slow-timescale climate variables exhibit non-negligible fluctuations, inherited from the fast-timescale variables acting on them, which transfer their own fluctuating behaviour to the slow ones. Within this framework, a particular stochastic energy balance model is derived, and it is shown that the stationary temperature variance increases with greenhouse gas concentrations, such as CO_2, once the mean temperature enters the ice-sensitive regime of the albedo; the same result is then recovered in a spatial setting that accounts for horizontal heat transport. This growth in variance is already observed in the surface temperature of the Arctic seas today.

The same slow-fast contrast motivates the second contribution: for a coupled velocity-temperature ocean model (three-dimensional Navier-Stokes coupled, through a buoyancy term, with an advection-diffusion equation for the temperature), in which the effect of the fast atmosphere is encoded as a noise acting on the boundary where ocean and atmosphere meet, a global well-posedness result for small data is established.

The final part follows the thread of CO_2 into a volcanic setting. It first asks whether volcanic eruptions can emit greenhouse gases in amounts able to affect present-day climate change: an overview of the past and present role of volcanic emissions in the carbon budget shows that they cannot, given the marked disproportion between anthropogenic and volcanic CO_2. Volcanoes then become the bridge towards sustainable development, through the case of the

Campi Flegrei, one of the active calderas in Europe, affected for over twenty years by bradyseism and by a persistent seismicity that the past shows may become dangerous. For this area, a simplified subsurface model is proposed, describing the upward dynamics of magmatic fluids so as to reproduce the observed ground uplift, and hence the associated seismic activity.

ACKNOWLEDGEMENTS

This thesis was produced while attending the PhD programme in PhD in Sustainable Development And Climate Change at the University School for Advanced Studies IUSS Pavia, Cycle XXXVIII, with the support of a scholarship financed by the Ministerial Decree no. 351 of 9th April 2022, based on the NRRP - funded by the European Union - NextGenerationEU - Mission 4 "Education and Research", Component 1 "Enhancement of the offer of educational services: from nurseries to universities" - Investment 3.4 "Advanced teaching and university skills".

The author declares that Artificial Intelligence tools were used to support the drafting of this thesis — specifically Claude (Anthropic) — mainly for language revision. All contents have been critically reviewed and independently reworked by the author.

Table of Contents

INTRODUCTION **1**

1 INTRODUCTION **2**
1.1 Arctic EBM 4
1.1.1 Background and motivation 4
1.1.2 Introduction to the modelling framework 6
1.1.3 From the classical EBM to a fast-slow system . . 7
1.1.4 Hasselmann reduction 9
1.1.5 Summary of models 12
1.1.6 Main results 13
1.1.7 Observational comparison 15
1.1.8 Contributions, limitations, and future directions 16
1.2 Boundary noise model 19
1.2.1 Background and motivation 19
1.2.2 Modelling framework and applicability 20
1.2.3 Main results 22
1.3 Climate, sustainability and volcanoes 27
References 28

VARIABILITY AMPLIFICATION IN AN ARCTIC EBM **33**

2 VARIABILITY AMPLIFICATION IN AN ARCTIC EBM **34**
2.1 Radiative forcing amplifies variance in a multiplicative-noise EBM 34
2.1.1 Preliminaries: energy balance models and Wong-Zakai principle 34
2.1.2 Fast–slow insolation–temperature model and reduction to a multiplicative-noise EBM 37
2.1.3 Stationary variance and monotone dependence on radiative forcing 41
2.2 Spatial anomaly model and finite-dimensional approximation 44
2.2.1 Spatial EBM with Dirichlet data and anomaly formulation 44

2.2.2 Finite-difference semi-discretisation 45
2.2.3 Stationary covariance for the semi-discrete anomaly SDE 48
2.2.4 Monotonicity of the stationary covariance in the radiative forcing parameter 54
2.3 Analysis of observational sea surface temperature data 60
References 69

TEMPERATURE-VELOCITY MODEL: BOUNDARY NOISE 73

3 TEMPERATURE-VELOCITY MODEL: BOUNDARY NOISE 74
3.1 Notations and functional setting 74
3.2 Preliminaries and main results 77
3.3 Temperature problem 83
3.3.1 Stochastic linear problem with non-homogeneous Dirichlet boundary conditions 83
3.3.2 The remainder temperature equation 89
3.4 Velocity problem 100
3.4.1 Stokes operator in weak setting, $\mathcal{H}^\infty$-calculus and maximal regularity 101
3.4.2 Global for small data for the 3D Navier-Stokes problem 105
3.5 Well-posedness for the 3D-coupled temperature-velocity model with boundary noise 107
References 111

CLIMATE, SUSTAINABILITY, AND VOLCANOES 113

4 CLIMATE, SUSTAINABILITY, AND VOLCANOES 114
4.1 The effects of volcanic eruptions 114
4.1.1 Warming effect 115
4.1.2 Cooling effect 116
4.2 The case of Campi Flegrei Caldera 124
4.2.1 First model: layers 130
4.2.2 Second model: cavities 141
References 148

CONCLUSIONS 153

5 CONCLUSIONS 154

Chapter 1



Introduction

1 INTRODUCTION

This dissertation presents the research carried out during the Doctoral Programme of National Interest PhD SDC – Sustainable Development and Climate Change. Developed within the Earth System and Environment curriculum, this work approaches the subject from a mathematical point of view, focusing on idealised mathematical models aimed at studying climate dynamics and environmental sustainability, as the title suggests.

Present-day climate change is a serious and pressing challenge that can be examined from many different perspectives. Among these, the present pages bring together the description of some of the CO_2-driven mechanisms involved and the study of how climate quantities acting on different timescales relate to one another – such as temperature, which evolves slowly, and radiation, which responds rapidly. Sustainable development, too, poses a challenging problem. It is addressed here by building on some considerations concerning volcanic emissions, again within the framework of CO_2-driven mechanisms, through the study of a representative case: a densely populated volcanic area that, as such, must be closely monitored to ensure the safety and sustainability of human life in the region.

The structure of this thesis is as follows.
Chapter 2 constitutes the main focus and deals with the ability to assess changes in climate quantities in response to external forcing, specifically the *variability* of temperature under increased CO_2. This enhancing behaviour is already happening, for instance, in the Arctic seas, and one of the drivers of this mechanism is the ice-albedo feedback, that is, the surface's response to radiative solar input as a function of the ice cover.
This theme is addressed starting from a simplified mathematical framework, namely *energy balance models*, which are conceptual models based on the Earth's radiative balance. The aim is to derive a model able to explain the increase in extreme events – here understood as a growing temperature variance – as greenhouse gas emissions rise.
This work relies on the distinction between fast and slow climate

variables, acting on different timescales, and on the way they interact. In the classical setting, fast variables enter the slow dynamics through an averaged version of themselves, leading to a deterministic model. On the contrary, in this work a reduced model is derived in which the effect of the fast variables (insolation, described by an Ornstein–Uhlenbeck process) on the slow ones (temperature, described by an energy balance model) is not averaged out; rather, it enters the slow dynamics while preserving its fluctuating behaviour and transferring it to the slow variable, thus leading to a stochastic model with multiplicative, and therefore state-dependent, noise. In this way, the slow variable acquires stochastic paths, that is, it develops its own variability. This variability depends on the forcing through the albedo function; therefore, in a certain regime, the model is able to explain the increased variability as greenhouse gas emissions rise. This contribution builds on the pioneering insight of Klaus Hasselmann [1], who first recognised that the slow variables (macroweather scales) develop their own fluctuations by integrating the forcing of the fast ones (weather scale), which acts on them as a random driving. His original idea is here framed within an energy balance model for the Arctic sea surface temperature.

Chapter 3 also starts from Hasselmann's stochastic climate paradigm, large-scale dynamics are driven by fast, random perturbations, and investigates the interplay between the slow ocean and the fast atmosphere above it.
In particular, the ocean is described through a coupled temperature-velocity system, and the action of the fast variables on the slow ones is modelled by considering a noisy boundary condition for the temperature equation, so as to encode the effect of the fast variables on the slow dynamics directly.
It is worth underlining how this represents, in a sense, a further declination of Hasselmann's insight. Whereas in the previous chapter Hasselmann's paradigm was declined in a purely temporal sense, here the same principle is transposed into a spatial context, in which the fast-slow separation is realised geometrically: the fast fluctuations are confined to the interface between the two systems and act on the slow dynamics through the boundary. The temperature equation thus already constitutes the reduced model, in which the fast variables are incorporated into the boundary rather than into the interior dynamics.
This is quite a technical chapter: an existence and uniqueness result is proved for the velocity-temperature system with boundary noise.

Lastly, Chapter 4 draws on all the preceding discussion of greenhouse gases and timescales to provide an overview of the past and

present role of volcanic emissions in terms of greenhouse gases, and of their current potential to enhance atmospheric CO_2. This leads to a short digression on environmental sustainability in the context of volcanoes, and in particular to the case of the Campi Flegrei, for which a past and present overview is given, together with a contribution to the study of the subsurface: simplified models of layers and cavities are proposed, able to account for the seismic activity and the bradyseism typical of that area, a condition that has already proved hazardous in the past and is under constant monitoring at present.

1.1 Arctic EBM

1.1.1 Background and motivation

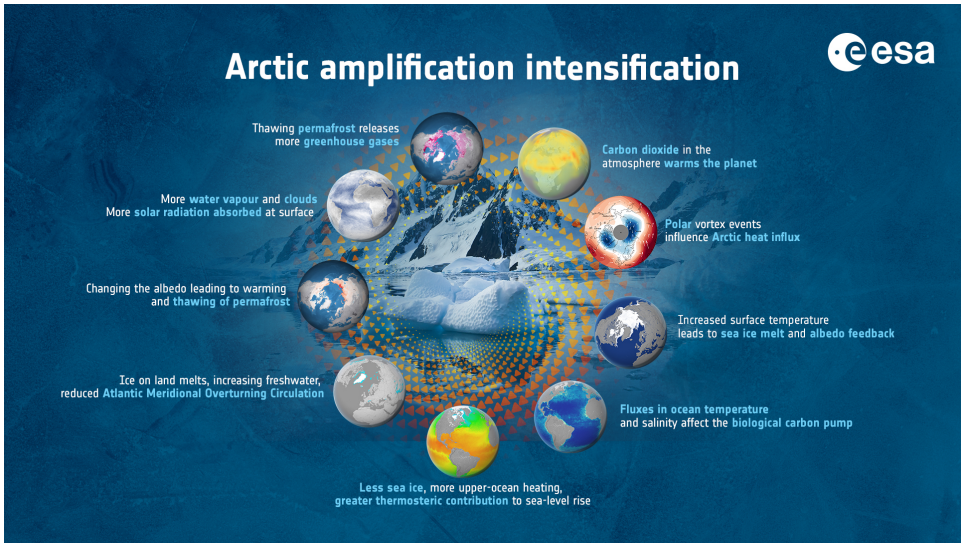

Figure 1.1: *Arctic amplification intensification. Image: ©ESA. Available at esa.int*

The Arctic is warming significantly faster than the global average, a phenomenon known as *Arctic Amplification* [2]. One of the primary driver is the ice–albedo feedback [3]: rising atmospheric carbon dioxide concentrations of anthropogenic origin warm the planet and trigger substantial ice loss; as snow and sea ice melt, the surface darkens and absorbs more shortwave radiation, magnifying the regional temperature response to greenhouse-gas forcing. Figure 1.1 outlines the main feedbacks involved and some of the possible consequences of a warming Arctic. Land ice loss increases freshwater input and alters ocean salinity, which may in turn weaken

the Atlantic Meridional Overturning Circulation (AMOC); warming also destabilises permafrost, whose thaw releases additional carbon dioxide and methane into the atmosphere, thereby reinforcing the original forcing [4].

Extreme events may arise as a consequence of a change in climate variability. Assessing such a change, however, is far from straightforward, primarily because an increase in the frequency of extremes can in many cases be explained by a shift in the mean alone. Yet an increase in variance also widens the distribution, making persistent or extreme warm events more likely [5, 4] (see Figure 1.2); distinguishing these two contributions is therefore of fundamental importance.

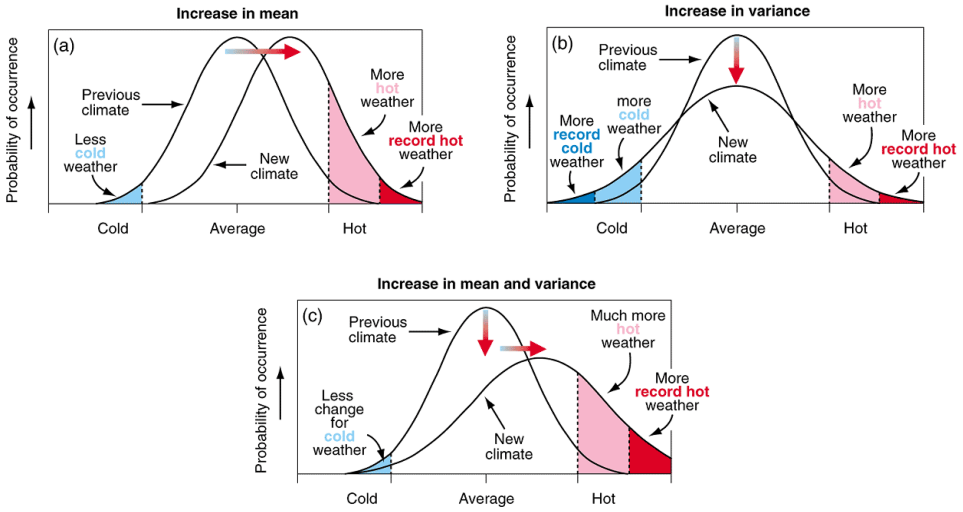

Figure 1.2: *Schematic effect of changes in the temperature distribution on extremes: (a) increase in the mean, (b) increase in the variance, (c) increase in both. Reproduced from [5], Figure 2.32.*

A clear illustration of this difficulty is offered by the Arctic. While the increase in the mean temperature of both the overlying atmosphere and the ocean surface is beyond dispute, whether the variability of this temperature is also changing remains an open question. From the standpoint of sea surface temperature (SST), the physical mechanism is a further consequence of the ice-albedo feedback: when sea ice is present, SST is constrained to remain near the freezing point and cannot fluctuate appreciably, whereas its retreat removes this thermodynamic constraint, freeing SST to respond to atmospheric forcing and thereby enhancing its variability [6]. This may explain why observations, forecasts and simulations point towards an increase in variance for SST.

The first practically ice-free September is expected to occur as

a fluctuation well before the mean state reaches that condition – the IPCC assesses it as likely at least once before 2050 under all scenarios [4].

Projections indicate that Arctic SST variability will be enhanced in the future [6]. Global climate models exhibit significant increases in SST variance over the Arctic in both March and September, with the largest relative changes occurring where sea ice disappears (summer). This enhancement is not uniform: SST variance peaks at the marginal ice zone and tracks the ice edge poleward, with an increase near the retreating margin offset by a decrease behind it rather than a uniform rise – a pattern testable against observations. A clear contrast emerges between the Arctic and lower-latitude regions, for example, in the shape of the projected future SST probability distribution.

This projected behaviour is consistent with the observed record, which shows large year-to-year variations in summer SST over the marginal seas: August values in the Beaufort Sea differed by several degrees between consecutive years, while the Chukchi Sea has recently seen anomalously cool summers against the warming trend [7, 8].

Among warm extreme events, a manifestation of a changing variability is the emergence, since 2007, of Arctic marine heatwaves [9]. These are primarily triggered by an abrupt retreat of sea ice, coinciding with the maximum in incoming solar radiation, and their likelihood has increased under anthropogenic greenhouse-gas forcing.

The aim of this work is to bring these elements (anthropogenic CO_2 forcing, ice-albedo feedback, increasing variance) together within the simplest conceptual model that can *explain* the causal relationships described above among them: a stochastic energy balance model (EBM). This study proposes and analyses, within a mathematically tractable framework, a mechanism by which CO_2-driven radiative forcing can *increase Arctic temperature variability* through the temperature-dependent ice-albedo feedback.

1.1.2 Introduction to the modelling framework

We work within the class of energy balance models, an elementary class of climate models [10]. In their simplest form, EBMs describe the evolution of a representative near-surface temperature through the balance between absorbed shortwave radiation and emitted longwave radiation [11, 12, 13]. EBMs are appreciated for their mathematical tractability [14, 15, 16, 17], and for capturing key mechanisms driving Earth's climate [18, 19, 20, 21].

A central ingredient in Sellers-type EBMs is a *Lipschitz* co-albedo function $\beta(T)$ encoding the reduction of albedo with warming as sea ice and snow retreat [22, 23, 24]. This co-albedo nonlinearity is the simplest representation of the ice-albedo feedback and is known to generate multiple regimes and tipping-like behaviour in low-order climate models [25, 26, 27]. In the present work, rather than focusing on regime shifts, we address how radiative forcing modifies the *stationary variance and covariance* of temperature anomalies around a stable equilibrium.

A standard approach to modelling unresolved "weather" variability in climate dynamics is to introduce stochastic forcing, in the spirit of Hasselmann-type stochastic climate models [1, 28, 29]. His theory is based on multiscale analysis: the physical variables are divided into two groups, the fast (weather) and the slow (macroweather) ones, depending on their characteristic timescale. In the classical version of multiscale analysis, the fast variables are suitably averaged out, leading to a reduced closed model for the slow variables alone. The fluctuations, however, are thereby lost at the macroweather scale. Hasselmann's theory modifies classical averaging in such a way that it yields a stochastic model for the slow variables. In physical terms, this noise represents the cumulative effect of fast weather fluctuations on the slow temperature dynamics, reproducing the variability seen in observational records. A further common simplification in EBMs is that the noise is assumed to be additive. Yet this is only an approximation: as already pointed out in the Hasselmann programme, the physically correct form of the noise is *multiplicative* [1].

This motivates our starting point: a fast-slow formulation in which insolation (or a proxy) evolves on a fast weather timescale (e.g. one day) while temperature evolves on a slow macroweather timescale (e.g. one year). A related fast-slow insolation–temperature setup was recently considered in [30]; here we focus on the reduction to a closed equation for the slow variable and the resulting monotone variance/covariance amplification.

1.1.3 From the classical EBM to a fast-slow system

We start considering a classical deterministic EBM, a simple mathematical framework that aims to provide a conceptual description of the time evolution of the Earth's (near-surface) temperature T in terms of the energy budget absorbed and emitted by the Earth's surface. Namely, we have:

$$\frac{dT}{dt} = \mathcal{R}_a - \mathcal{R}_e,$$

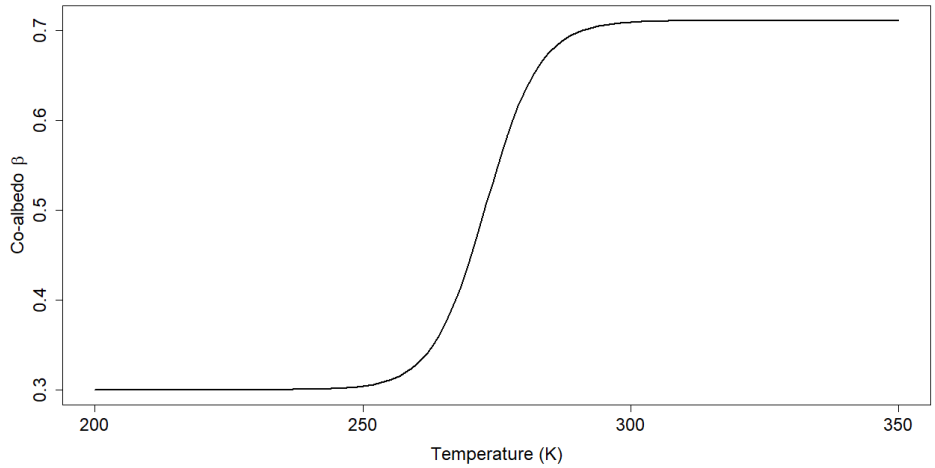

Figure 1.3: *Co-albedo function in its smooth shape.*

where $\mathcal{R}_a$ denotes the absorbed shortwave radiation and $\mathcal{R}_e$ the emitted longwave radiation.

In the simplest setting, the absorbed radiation is $\mathcal{R}_a(T) = Q\beta(T)$ and the emitted one is $\mathcal{R}_e(T) = \sigma\,\epsilon\,T^4$. The quantity Q represents the globally averaged incoming solar radiation, modulated by the *co-albedo* function $\beta \in (0, 1)$, i.e. the fraction of incident solar radiation that is absorbed ($\beta = 1 - \alpha$, with α the albedo). The co-albedo depends on the presence of ice and therefore on the temperature itself. Its general shape is shown in Figure 1.3, although we will employ a piecewise linear version of it. The emitted radiation follows from the Stefan–Boltzmann law, with the quantity σ representing the Stefan–Boltzmann constant and ϵ the globally averaged emissivity.

In this work, for the term $\mathcal{R}_e$ we adopt the classical Budyko empirical formula and assume

$$\mathcal{R}_e(T) = r_0 + r_1 T,$$

with $r_0 \in \mathbb{R}$ and $r_1 > 0$, thereby approximating the emitted radiation over the temperatures associated with the Earth's current climate state. This empirical linear relation considerably simplifies the analysis of the model while also provide a more realistic fit to observations [11, 10].

For the term $\mathcal{R}_a$, we impose that the absorbed shortwave radiation is of the form

$$\mathcal{R}_a(T, X, \lambda) = X\,\beta(T) + \lambda,$$

where X plays the same role as Q above, but is now time-dependent, while λ models the effect of greenhouse gases on the radiation balance – the larger the emissions, the larger λ, and the more radiation is absorbed.

The quantity X represents the *effective* incoming solar radiation available at the surface, which fluctuates on the fast, weather scale – variations in cloud cover, aerosols and atmospheric conditions, for instance, continuously modulate how much shortwave radiation actually reaches and is absorbed at the surface. In this sense, X is no longer a fixed solar input but a solar forcing that evolves in time according to its own dynamics, as a result of various atmospheric filters, encoding the fast, weather-scale variability of the radiation balance. To do so, we impose that the term X has stochastic dynamics; more precisely, we model the insolation X by a rapidly mean-reverting Ornstein–Uhlenbeck process, fluctuating around a climatological mean level Q, with correlation time $\tau \ll 1$:

$$dX_t = -\frac{1}{\tau}(X_t - Q)dt + \frac{1}{\sqrt{\tau}}dW_t,$$

where $(W_t)_t$ denotes a Brownian motion. The parameter τ also plays the role of separating the timescales of the two dynamics under consideration, once we couple the equations and consider the fast-slow system: the first equation describes the fast variable and the second the relatively slow temperature, as discussed above. Since τ, representing the ratio of the fast and slow timescales, and λ, representing the radiative forcing, both play a fundamental role, we emphasize the dependence of the variables on these two quantities and obtain the following system:

$$\begin{cases} dX_t^\tau = -\frac{1}{\tau}(X_t^\tau - Q)dt + \frac{1}{\sqrt{\tau}}dW_t, & X_0^\tau = x_0, \\ \frac{dT_t^{\tau,\lambda}}{dt} = X_t^\tau \beta(T_t^{\tau,\lambda}) + \lambda - (r_0 + r_1 T_t^{\tau,\lambda}), & T_0^{\tau,\lambda} = \theta_0. \end{cases} \tag{1.1}$$

1.1.4 Hasselmann reduction

The next step is to derive a closed stochastic equation for the slow variable, the temperature, using Hasselmann's theory.
Coupled fast–slow systems are not a novelty in climate studies; indeed, they lie at the core of most climate models and numerical simulations. Whether one starts from a stochastic or a deterministic equation for the fast variable, the classical approach is to obtain a closed equation via an *averaging principle*, that is, by closing the equation for the slow variable through the mean state of the fast

variable. The main limitation of this method is that the fluctuations due to the fast variable are thereby lost and the averaged equation only describes the long-term climate evolution, with no trace of the macroweather-scale variability.

Hasselmann's insight [1] starts exactly from this point. His idea likely originates from the observation of real data: indeed, looking at the global mean temperature (GMT) time series, one can see that its behaviour is noisy, with the time series fluctuating like the path of a stochastic process. Consequently, Hasselmann states that the closed equation for the slow variable at the macroweather scale should be stochastic.

In more detail, consider the deterministic fast-slow system

$$\begin{cases} \dot{x} = \dfrac{1}{\tau} f(x, y), \\ \dot{y} = g(x, y), \end{cases}$$

where the factor $1/\tau$ makes x the fast variable and y the slow one – adopting the slow timescale as reference, x evolves much faster and, under suitable ergodicity assumptions, rapidly settles to a statistical equilibrium. The classical averaging principle then approximates y by the solution of the averaged equation

$$\dot{\bar{y}} = \bar{g}(\bar{y}),$$

where $\bar{g}(y) = \int g(x, y)\, d\mu_y(x)$ is obtained by averaging g over the invariant measure μ_y of the fast dynamics at fixed y.
Hasselmann, instead, argues that at the macroweather scale the fast fluctuations still affect the slow variable and should not be averaged out. He therefore proposes that the reduced equation should instead be an SDE of the form

$$d\tilde{Y}_t = \bar{g}(\tilde{Y}_t)\, dt + \sigma(\tilde{Y}_t) \circ dW_t,$$

where the diffusion coefficient σ is non-trivial, and the noise is understood in the Stratonovich sense. In this way, the fast fluctuations are not discarded but survive as an effective noise, leaving a visible imprint on the slow variable and thus a more realistic approximation of the original system.

In Hasselmann's original work the full system is deterministic, and the stochasticity of the slow variable is obtained through a physical argument. In our setting, where the fast insolation is modelled as the OU process X_t^τ, the reduction yields a stochastic equation of the form

$$d\tilde{T}_t^\tau = \bar{g}(\tilde{T}_t^\tau)dt + \sqrt{\tau}\sigma(\tilde{T}_t^\tau) \circ dW_t.$$

Our work builds on Hasselmann's novel insight: starting from system (1.1), we derive a closed stochastic equation for the temperature, whose key feature is a *multiplicative noise*, that is, a noise with amplitude depending on the state itself, as opposed to an additive noise of constant intensity. In our specific model, the noise intensity will turn out to increase with temperature, thereby affecting its variance. Specifically, the model is able to explain the causal chain by which a CO_2-driven increase in the equilibrium temperature also enhances its variance, all of this through the ice-albedo feedback.

More precisely, we start from system (1.1) and derive the reduced equation as follows.
First, we prove that the integrated fast fluctuations converge to Brownian motion as $\tau \to 0$.

Lemma 1.1. *For any $t > 0$, it holds*

$$\lim_{\tau \to 0} \mathbb{E} \left| \frac{1}{\sqrt{\tau}} \int_0^t (X_s^\tau - Q)\, ds - W_t \right|^2 = 0.$$

Heuristically speaking, dropping the τ dependence, this result means that, to a first approximation,

$$X - Q \sim \sqrt{\tau}\, \frac{dW}{dt},$$

so that, expanding $\mathcal{R}_a$ to first order in X around Q,

$$\mathcal{R}_a(T, X, \lambda) \sim \mathcal{R}_a(T, Q, \lambda) + \partial_X \mathcal{R}_a(T, Q, \lambda)\, \sqrt{\tau}\, \frac{dW}{dt},$$

and we obtain

$$\begin{aligned} dT &\sim \big(\mathcal{R}_a(T, Q, \lambda) - \mathcal{R}_e(T)\big)\, dt + \sqrt{\tau}\, \partial_X \mathcal{R}_a(T, Q, \lambda)\, dW \\ &= (Q\beta(T) + \lambda - (r_0 + r_1 T))\, dt + \sqrt{\tau}\, \beta(T)\, dW, \end{aligned} \tag{1.2}$$

i.e., a formulation with state-dependent noise, whose amplitude is modulated by the co-albedo.

To be more rigorous, define

$$W_t^\tau := \frac{1}{\sqrt{\tau}} \int_0^t (X_s^\tau - Q)\, ds.$$

Since the integrated forcing is smooth for fixed $\tau > 0$, we can write the following random ODE for the temperature:

$$dT_t^{\tau,\lambda} = \Big(Q\beta(T_t^{\tau,\lambda}) + \lambda - (r_0 + r_1 T_t^{\tau,\lambda})\Big)\, dt + \sqrt{\tau}\, \beta(T_t^{\tau,\lambda})\, dW_t^\tau. \tag{1.3}$$

This naturally leads to a Wong-Zakai reduction: replacing the smooth driver W^τ by its Brownian limit W (Lemma 1.1) leads to the Stratonovich approximation

$$d\widetilde{T}_t^{\tau,\lambda} = \Big(Q\beta(\widetilde{T}_t^{\tau,\lambda}) + \lambda - (r_0 + r_1\widetilde{T}_t^{\tau,\lambda})\Big)\, dt + \sqrt{\tau}\,\beta(\widetilde{T}_t^{\tau,\lambda}) \circ dW_t \qquad (1.4)$$

which in Itô form becomes

$$d\widetilde{T}_t^{\tau,\lambda} = \Big(Q\beta(\widetilde{T}_t^{\tau,\lambda}) + \lambda - (r_0 + r_1\widetilde{T}_t^{\tau,\lambda}) + \frac{\tau}{2}\beta(\widetilde{T}_t^{\tau,\lambda})\beta'(\widetilde{T}_t^{\tau,\lambda})\Big)\, dt + \sqrt{\tau}\,\beta(\widetilde{T}_t^{\tau,\lambda})dW_t. \qquad (1.5)$$

This provides a derivation linking fast weather variability to a reduced stochastic climate model with state-dependent noise. It is worth noting that this is not a *limit* procedure as $\tau \to 0$: the parameter τ is small – recall that it quantifies the separation between the weather and the macroweather scales, say one day against one year – but not so small as to justify taking the limit. Indeed, letting $\tau \to 0$ would suppress the noise altogether and bring us back to the deterministic averaged equation. It is precisely because τ is small but finite that the fast fluctuations, although weak, survive in the reduced dynamics. In this sense, Hasselmann's theory is a *reduction* method rather than a limit procedure. Consistently, the Itô correction in (1.5) carries a factor $\tau \ll \sqrt{\tau}$, and can therefore be neglected, so that we recover the heuristic equation (1.2) derived above.

1.1.5 Summary of models

For the reader's convenience and to improve readability, in this brief section we restate the main models discussed so far and add a few comments.

We started from the fast-slow system

$$\begin{cases} dX_t^\tau = -\dfrac{1}{\tau}(X_t^\tau - Q)dt + \dfrac{1}{\sqrt{\tau}}dW_t \\ \dfrac{dT_t^{\tau,\lambda}}{dt} = \underbrace{X_t^\tau\beta(T_t^{\tau,\lambda}) + \lambda}_{\text{absorbed radiation}} - \underbrace{(r_0 + r_1 T_t^{\tau,\lambda})}_{\text{emitted radiation}}. \end{cases}$$

The classical averaging principle would replace the fast component X with its average Q, leading to the simple deterministic equation

$$\frac{dT_t^\lambda}{dt} = \underbrace{Q\beta(T_t^\lambda) + \lambda}_{\text{absorbed}} - \underbrace{(r_0 + r_1 T_t^\lambda)}_{\text{emitted}}.$$

The contribution of Hasselmann's theory is to retain, in the slow component, the additional term of random fluctuations, not a generic

one, but tuned to the specific interaction between the fluctuations of the fast scales and the nonlinearity of the slow-variable equation, leading to

$$dT_t^{\tau,\lambda} = \left(\underbrace{Q\beta(T_t^{\tau,\lambda}) + \lambda}_{\text{absorbed}} - \underbrace{(r_0 + r_1 T_t^{\tau,\lambda})}_{\text{emitted}} \right) dt + \underbrace{\sqrt{\tau}\, \beta(T_t^{\tau,\lambda}) \circ dW_t}_{\text{fluctuations}}.$$

In the next section we show that, with this reduced model, in a certain regime the specific shape of the co-albedo β causes the fluctuations to increase as CO_2 increases.

1.1.6 Main results

Our main result quantifies a *forcing-induced variance amplification mechanism*.
We study fluctuations around the stable equilibrium $T^{*,\lambda}$. To this end we introduce the *temperature anomaly*

$$Y_t^{\tau,\lambda} := \widetilde{T}_t^{\tau,\lambda} - T^{*,\lambda}$$

and we linearise the co-albedo function β around $T^{*,\lambda}$. This yields the linear stochastic differential equation

$$dY_t^{\tau,\lambda} = \left(Q\beta'(T^{*,\lambda}) - r_1 \right) Y_t^{\tau,\lambda} dt + \sqrt{\tau} \left(\beta(T^{*,\lambda}) + \beta'(T^{*,\lambda}) Y_t^{\tau,\lambda} \right) dW_t.$$

With the shorthand notation

$$b^\lambda := -Q\beta'(T^{*,\lambda}) + r_1, \qquad \sigma_0^\lambda := \beta(T^{*,\lambda}), \qquad \sigma_1^\lambda := \beta'(T^{*,\lambda}),$$

the linear EBM assumes the compact form

$$dY_t^{\tau,\lambda} = -b^\lambda Y_t^{\tau,\lambda} dt + \sqrt{\tau}(\sigma_0^\lambda + \sigma_1^\lambda Y_t^{\tau,\lambda}) dW_t, \qquad Y_0^{\tau,\lambda} = y_0.$$

We first calculate, under the stability condition $b^\lambda > 0$, the limit for large time t of the expected value

$$\lim_{t \to +\infty} \mathbb{E}[Y_t^{\tau,\lambda}] = 0.$$

Assuming in addition $y_0 = 0$, we derive an explicit formula for the stationary variance of the temperature anomaly Y.

Proposition 1.1. *Assume*

$$b^\lambda > 0, \qquad 2b^\lambda - \tau(\sigma_1^\lambda)^2 > 0.$$

Then the following limit exists

$$\lim_{t \to +\infty} \mathbb{E}[|Y_t^{\tau,\lambda}|^2] = \frac{\tau(\sigma_0^\lambda)^2}{2b^\lambda - \tau(\sigma_1^\lambda)^2}.$$

Our main result concerns the dependence of this stationary variance on the radiative forcing parameter λ.

Proposition 1.2. *Assume*

$$b^\lambda > 0, \qquad 2b^\lambda - \tau(\sigma_1^\lambda)^2 > 0, \qquad T^{*,\lambda} \in (T_l, T_u).$$

Then the stationary variance is monotone increasing.
In other words, setting

$$\lambda \mapsto \mathrm{Var}_\infty(\lambda) := \lim_{t\to+\infty} \mathbb{E}[|Y_t^{\tau,\lambda}|^2] = \frac{\tau(\sigma_0^\lambda)^2}{2b^\lambda - \tau(\sigma_1^\lambda)^2} = \frac{\tau\beta(T^{*,\lambda})^2}{2(r_1 - Q\beta'(T^{*,\lambda})) - \tau\beta'(T^{*,\lambda})^2},$$

we have $\mathrm{Var}_\infty(\lambda)' > 0$.

Namely, we state that the stationary variance increases monotonically with λ whenever $T^{*,\lambda}$ lies in the *ice-sensitive* regime of the co-albedo (i.e. where β has positive slope). The mechanism is clear. Increasing radiative forcing shifts the equilibrium temperature upward; in the ice-sensitive regime the co-albedo is increasing, so the effective amplitude of multiplicative noise and its impact on the anomaly dynamics increase accordingly, leading to higher stationary variance.

Spatial results

We move from a single temperature variable to the following spatial model on $\mathcal{D} \subset \mathbb{R}^2$, a bounded domain with sufficiently regular boundary $\partial\mathcal{D}$, that accounts for horizontal heat transport:

$$\begin{cases} dT_t^{\tau,\lambda} = \left(\Delta T_t^{\tau,\lambda} + Q\,\beta(T_t^{\tau,\lambda}) + \lambda - (r_0 + r_1 T_t^{\tau,\lambda})\right) dt + \sqrt{\tau}\,\beta(T_t^{\tau,\lambda})\,dW_t, \\ T^{\tau,\lambda}|_{\partial\mathcal{D}} = \theta \\ T^{\tau,\lambda}|_{t=0} = T_0 \end{cases} \tag{1.6}$$

We study the temperature anomaly Y around a reference equilibrium profile and approximate the resulting stochastic dynamics on a grid. This leads to a finite-dimensional stochastic model for the anomaly field, for which we can analyse the long-time covariance explicitly. Consistently with the previous result, we prove the following:

Proposition 1.3. *Under suitable assumptions on the matrices arising from the discretisation and on the coefficients* r_1 *and* $Q(x)$*, if* $T^{*,\lambda}(x)$ *lies in the interval on which the co-albedo has positive slope for all* $x \in \mathcal{D}$*, the stationary spatial variance* $\mathrm{Var}_{\mathrm{sp},\infty}(\lambda)$ *is monotone increasing in* λ*.*

Under standard stability assumptions and non-negative noise correlations, we show that increasing radiative forcing increases the stationary covariance matrix component-wise, and hence increases the stationary spatial variance (its trace), which we use as a second-moment proxy for fluctuation intensity and for the likelihood of large anomalies.

1.1.7 Observational comparison

In the last part of the work we compare our theoretical results with observations, asking whether the model-predicted variability changes can be seen in real data. Sea surface temperature in the Arctic provides a crucial measure of the power of ice–albedo feedback during a given summer season [7]. Since the ice-albedo feedback is expected to be strongest when the mean state lies near the melt-sensitive temperature range, we focus on August sea surface temperature in the Arctic and adjacent northern high latitudes and track changes in both the mean and variability over the satellite era. More generally, variance changes under warming can depend strongly on the region [31]; here this suggests that variability changes should be spatially non-uniform, with Arctic seas and transition zones behaving differently from persistently ice-covered or warm open-ocean areas.

An example of our investigation on our first result can be seen in Figure 1.4, which shows the case of the Kara Sea: the histogram in the top right displays the spatially averaged daily temperature in August over the decades 1983–1992 and 2016–2025. It can be seen that not only is there a clear shift in the mean temperature, but also a widening of the tails, and hence an increase in variance. Both increasing trends can also be seen in the bottom panels, showing the one-year moving-window mean SST and standard deviation.
In contrast, Figure 1.5 shows the case in which the mechanism described above has not yet been activated, namely that of the Arctic Ocean, which has so far remained perennially ice-covered, with no ice-free periods. Indeed, the data reveal an almost unchanged statistics between the two decades considered. A possible explanation is provided by our model: the equilibrium temperature of that region has not yet entered the range where the co-albedo has positive slope. Details of the data analysis for the second result are provided in the corresponding chapter.

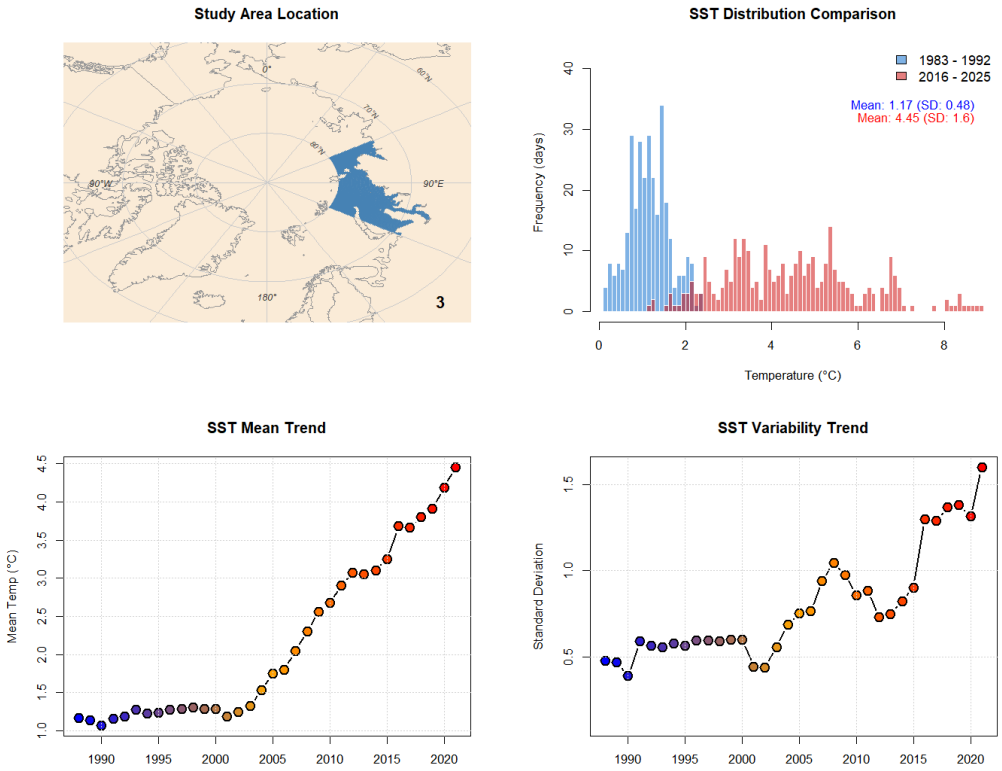

Figure 1.4: *Kara Sea. Top-left: location of the study area. Top-right: comparison between the histograms (number of days) of the spatial-averaged daily August SST for the first decade (1983-1992, blue) and the last calculable decade (2016-2025, red), along with their respective mean and standard deviation values. Bottom-left: decadal spatial mean trend of August SST (centred on the mid-year of each decade, one year moving window). Bottom-right: decadal spatial standard deviation trend of August SST (centred on the mid-year of each decade, one year moving window). The blue-to-red colour scale represents the progression of time across the decades, in accordance with the colour scheme used in the histogram.*

1.1.8 Contributions, limitations, and future directions

The key ingredient of the present model is the form of the stochastic perturbation, since the fluctuations of temperature produced will be the direct consequence of this term. In many studies, the stochastic perturbation is chosen in a generic way, typically as an additive white noise. On the contrary, in this investigation the choice of the noise is expected to play a central role in the discrimination of different behaviours of the fluctuations; hence a generic choice certainly cannot be sufficient. Moreover, the aim is to pro-

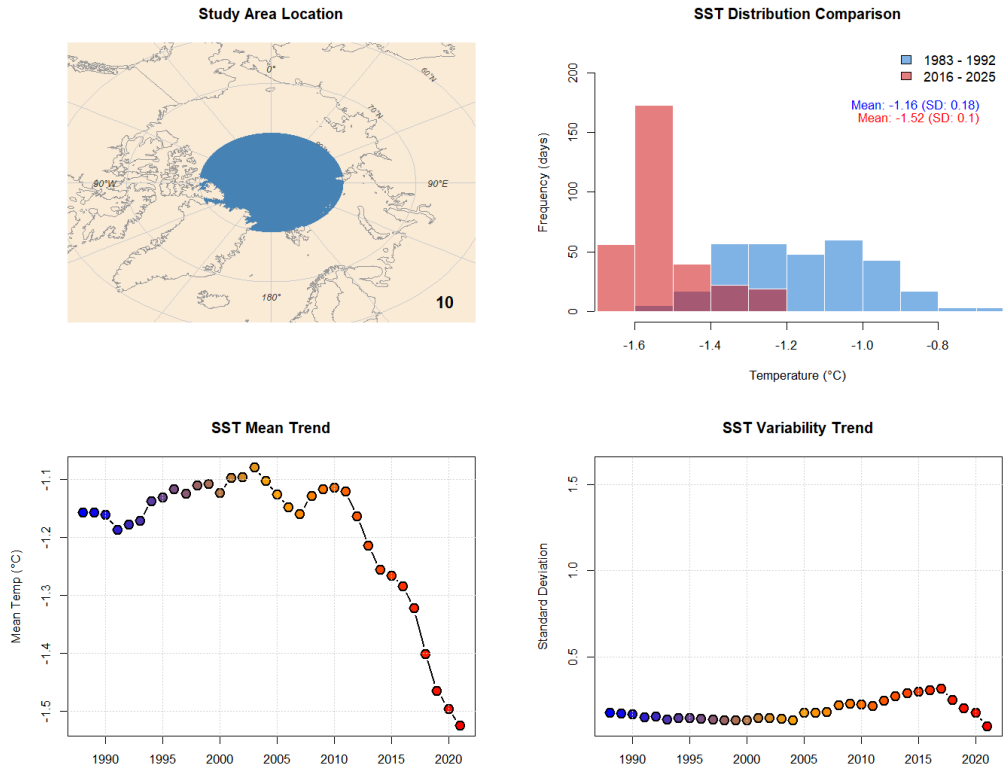

Figure 1.5: *Arctic Sea. Refer to Figure 1.4 for the panel description; further details in the text.*

vide an explanation of the physical phenomenon described above, therefore the choice of the noise made here has been done with scientific criteria, and it represents a balance of simplicity and physical realism.

Opposite to an enormous literature on the different levels of complexity and realism that deterministic models for climate dynamics can provide, the literature about the choice of the noise is very limited. The fundamental exception is the deep theory of Klaus Hasselmann, exposed in [1]. This type of stochasticity inherits the variations of the fast variables, modulated by the slow ones, leading to specific noise forms. The noise thus incorporates both the properties of fast scales and the mechanisms of the slow ones. This work is based on a simplified stochastic dynamics of the fast scales, still physically motivated, in place of the complex deterministic dynamical system and the following ideas are those developed in Hasselmann fundamental paper [1]. The final stochastic EBM is new in the literature, to our knowledge.



Figure 1.6: *Patchwork of sea-ice floes drifting on the ocean surface during the Northern Hemisphere summer of 2016. Photo by NOAA Ocean Exploration.*

The focus of the model is to explain the arctic temperature variability, its fluctuations, and precisely whether they increase with the CO_2 increasing. One of the purpose of the investigation on this variability on real data from different areas is to extract a logical qualitative explanation of the causes why in some cases the fluctuations increase, while in others they don't. A limitation of this study is to have found a correct link between phenomena, but maybe not so relevant compared to other concurring phenomena of largest intensity or influence. Here we employed a simple stochastic EBM that cannot incorporate every climate variables and physical laws with their specific charachteristics. There are several concurring atmospheric factors and maybe some of them also contribute to explain the increase of fluctuations with CO_2. If, in certain cases, the factors identified in the present work play a secondary role with respect to others not taken here into account, the explanation given by our study has a limited value.

In addition, our results are conditional on the existence of a stable deterministic temperature equilibrium $T^{*,\lambda}$ around which we linearise and compute stationary second moments. For Arctic applications this assumption is not automatic: it is essentially guaranteed in polar winter (when mean insolation is close to zero), but

it can be questionable if the forcing is interpreted as summer or annual-mean, when the ice-albedo feedback is strongest. We nevertheless adopt stability as a first-order working hypothesis, since key EBM parameters are uncertain and hard to calibrate regionally (i.e. in our Arctic setting), and because a more complete treatment would incorporate seasonality by prescribing a periodically time-dependent insolation, following the natural seasonality of the arctic ice development and therefore of the ice-albedo feedback. This would lead to a non-autonomous problem where the reference equilibrium $T^{*,\lambda}(t)$(time dependent) describes a seasonal cycle rather than a fixed equilibrium. We leave this extension to future work.

1.2 Boundary noise model

1.2.1 Background and motivation

The large-scale circulation of the ocean is, to a good approximation, a slowly evolving system: its velocity and temperature fields respond on time scales of months, years, and decades. The atmosphere sitting above it, by contrast, is a fast and turbulent medium, fluctuating on scales of hours to days. The two systems meet along the air–sea interface, and it is precisely across this surface that the ocean is continually forced by an atmosphere whose evolution is, from the ocean's standpoint, effectively unpredictable. Understanding how these fast surface fluctuations shape the slow oceanic dynamics is the physical starting question of this research.
The atmospheric processes acting on the ocean surface – turbulent winds, latent heat fluxes, weather systems, the instabilities of the atmospheric boundary layer – operate on temporal scales far below those of the oceanic circulation. Resolving them explicitly would require coupling the ocean to a fully resolved atmospheric model, defeating the purpose of a reduced description. From a physical point of view, stochastic boundary forcing represents the effect of unresolved fast fluctuations, such as boundary-layer instabilities or small-scale convection, that cannot be described deterministically at the scale of our models.
In the present setting these fluctuations do not permeate the interior of the ocean but act upon it through its upper boundary, the air–sea interface: the natural mathematical object encoding their influence is therefore not a distributed noise but a stochastic forcing on the boundary. Related approaches that model boundary-layer effects through non-standard boundary mechanisms can be found, for instance, in [32]. In climate science, and as already discussed in the previous section, this philosophy traces back to Hasselmann's

stochastic climate paradigm [1], in which, slow, large-scale dynamics are driven by fast, random perturbations.
The air–sea forced convection considered here is an instance of this mechanism and the boundary-noise employed thus provides a mathematically tractable way to "close" the system with respect to the unmodelled atmosphere: the latter does not have its own equation, but is summarized through a stochastic term acting on the boundary, yielding a self-contained coupled velocity–temperature system. In this spirit, we plan to investigate in a future work in which sense the studied system described in the following section arises as a limit of a multiscale fast–slow model.

1.2.2 Modelling framework and applicability

Let $\mathcal{D} \subset \mathbb{R}^3$ be a bounded, open domain (i.e. non-empty, connected set) with smooth boundary $\partial\mathcal{D}$, and let $T > 0$ be a fixed final time. We study the coupled velocity-temperature system for an incompressible fluid in $\mathcal{D}$, modelled by Navier-Stokes equations with thermal advection-diffusion, and perturbed by Dirichlet boundary noise. Concretely, for each $\varepsilon > 0$ we consider

$$\begin{cases} \partial_t u^\varepsilon + u^\varepsilon \cdot \nabla u^\varepsilon + \nabla p^\varepsilon - \Delta u^\varepsilon = -\theta^\varepsilon e_3, & \text{in } \mathcal{D}\times(0,T), \\ \operatorname{div}(u^\varepsilon) = 0, & \text{in } \mathcal{D}\times(0,T), \\ u^\varepsilon|_{\partial\mathcal{D}} = 0, & \text{in } \partial\mathcal{D}\times(0,T), \\ \partial_t \theta^\varepsilon + u^\varepsilon \cdot \nabla \theta^\varepsilon - \Delta \theta^\varepsilon = 0, & \text{in } \mathcal{D}\times(0,T), \\ \theta^\varepsilon_{|\partial\mathcal{D}} = \sqrt{\varepsilon}\,\dfrac{dW}{dt}, & \text{in } \partial\mathcal{D}\times(0,T), \\ u^\varepsilon|_{t=0} = u_0, \quad \theta^\varepsilon|_{t=0} = \theta_0. \end{cases} \tag{1.7}$$

where $u^\varepsilon \colon \mathcal{D}\times(0,T) \to \mathbb{R}^3$ is the fluid velocity, $\theta^\varepsilon \colon \mathcal{D}\times(0,T) \to \mathbb{R}$ is the temperature field, $p^\varepsilon \colon \mathcal{D}\times(0,T) \to \mathbb{R}$ is the pressure, $e_3 = (0,0,1)^T$, and $(W_t)_{t\geq 0}$ is a $\mathcal{Q}$-Wiener process acting only on the boundary with intensity which scales depending on the parameter ε.

The parameter ε influences the probability of global existence up to time T. Indeed, the three-dimensional (3D) Navier-Stokes equations are only known to be globally well-posed under smallness conditions on initial data and forcing (see, e.g., [33, Chapter 9]). Since stochastic boundary forcing enters the velocity equation through buoyancy coupling, we impose a small-noise regime in order to retain a nonzero probability of well-posedness on $[0,T]$. However, even for arbitrarily small $\varepsilon > 0$, the boundary noise may assume large values with positive probability. Consequently, we construct the solution $(u^\varepsilon, \theta^\varepsilon)$ up to a random stopping time $\tau^\varepsilon \leq T$, defined to interrupt the evolution if the stochastic forcing becomes too large.

A key difficulty of the model comes from the fact that Dirichlet boundary noise is much rougher than the forcing acting in the interior of the domain. Even in the linear heat equation with boundary noise, the stochastic convolution produced by the boundary forcing typically lives only slightly below the threshold $H^{-1/2}(\mathcal{D})$. We quantify this loss through a small exponent $\delta_\theta > 0$, which measures how far the noise-driven component falls into $H^{-1/2-\delta_\theta}(\mathcal{D})$.

To couple this temperature field back into the three-dimensional Navier-Stokes equation via the buoyancy term $-\theta^\varepsilon e_3$, we solve the fluid problem in a (slightly) weaker Sobolev scale $H^{-1/2-\delta_u}(\mathcal{D})$, chosen so that *both* the noise contribution and the initial temperature can be interpreted as forcing terms at the fluid level. This leads to the compatibility requirement

$$\delta_u \geq \max\{\delta_\theta,\ \tfrac{1}{2} - s\},$$

where $s \in (0, 1/2)$ is the Sobolev regularity of the initial temperature $\theta_0 \in W^{s,6/5}(\mathcal{D})$.

Under this condition (and for $p > 4$ in the maximal-regularity framework), we prove the existence and uniqueness of the coupled system on the interval $[0, \tau^\varepsilon]$, satisfying

$$\begin{aligned} u^\varepsilon &\in W^{1,p}(0, \tau^\varepsilon; H^{-\frac{1}{2}-\delta_u}(\mathcal{D})) \cap L^p(0, \tau^\varepsilon; H^{\frac{3}{2}-\delta_u}(\mathcal{D})) \\ \theta^\varepsilon &\in C(0, \tau^\varepsilon; H^{-\frac{1}{2}-\delta_u}(\mathcal{D})) \end{aligned}$$

Furthermore, we establish the high-probability estimate $\mathbb{P}(\tau^\varepsilon = T) \geq 1 - C\varepsilon$.

It is worth underlining the mathematical difficulties of the boundary noise. Da Prato and Zabczyk were the first to rigorously demonstrate in [34] that solutions to the heat equation subject to Dirichlet boundary noise exhibit significantly reduced regularity compared to solutions driven by interior stochastic forcing, even in one spatial dimension. Specifically, due to the presence of boundary noise, the best regularity that one can hope for, even in the linear case, is continuity in time with values in a negative-order Bessel potential space, namely $C(0, T; H^{-\frac{1}{2}-\delta_\theta}(\mathcal{D}))$ for any $\delta_\theta > 0$ and any final time $T > 0$. This limitation reflects the difficulties of noisy Dirichlet boundary conditions.

The low spatial regularity of the stochastic convolution in the Dirichlet setting is a major obstruction for non-linear problems: even basic products and non-linear maps may fail to be well-defined in a classical sense, and standard energy methods or fixed-point arguments often require additional structure. As a consequence, the

available well-posedness theory for non-linear PDEs with Dirichlet white-noise boundary data is rather limited and typically concerns only a limited class of non-linearities (see for instance [35]). Other works treat situations where the boundary forcing is regularised (e.g. coloured in space and/or fractional in time) or otherwise smoothed at the boundary, which can lead to better regularity and allow one to handle genuinely non-linear dynamics; see [36, 37]. In our setting the boundary noise enters the temperature equation linearly, but the resulting rough temperature acts as a forcing in the Navier-Stokes component, and its interplay with the convective non-linearity is one of the main analytic difficulties. It is also worth noting that the $H^{-\frac{1}{2}-\delta_\theta}$ limitation is closely related to a boundary-layer singularity: solutions to the associated linear Dirichlet problem may blow up as one approaches $\partial\mathcal{D}$, while remaining smooth in the interior, (e.g. in [38]).

In parallel, the velocity field u^ε enjoys, in this context, the maximal regularity of the Stokes operator in the same low-regularity framework introduced above. This constitutes the optimal regularity according to the maximal regularity theory for the Stokes operator on $H^{-\frac{1}{2}-\delta_u}(\mathcal{D})$, with suitable divergence-free and boundary conditions on the spaces. Our maximal regularity approach follows the framework developed by Prüss and Wilke in [39, Section 5].

1.2.3 Main results

First, we decouple the model (1.7) into a system for temperature only, given a prescribed fluid velocity; and a system for velocity only, given a prescribed temperature. Namely, we study first the equation for the temperature $\theta^\varepsilon\colon \mathcal{D}\times(0,T)\to\mathbb{R}$, which reads as

$$\begin{cases} \partial_t\theta^\varepsilon + u\cdot\nabla\theta^\varepsilon - \Delta\theta^\varepsilon = 0, & \text{in } \mathcal{D}\times(0,T),\\ \theta^\varepsilon|_{\partial\mathcal{D}} = \sqrt{\varepsilon}\dfrac{dW}{dt}, & \text{in } \partial\mathcal{D}\times(0,T),\\ \theta^\varepsilon|_{t=0} = \theta_0, & \text{in } \mathcal{D}. \end{cases} \tag{1.8}$$

Here, $u\colon \mathcal{D}\times(0,T)\to\mathbb{R}^3$ is a given velocity and θ_0 is the initial condition. Second, we study the 3D Navier-Stokes equations for the velocity $u\colon \mathcal{D}\times(0,T)\to\mathbb{R}^3$ given by

$$\begin{cases} \partial_t u + u\cdot\nabla u + \nabla p - \Delta u = f^\theta, & \text{in } \mathcal{D}\times(0,T),\\ \operatorname{div}(u) = 0, & \text{in } \mathcal{D}\times(0,T),\\ u|_{\partial\mathcal{D}} = 0, & \text{in } \partial\mathcal{D}\times(0,T),\\ u|_{t=0} = u_0, & \text{in } \mathcal{D}. \end{cases} \tag{1.9}$$

Here, $f^\theta\colon \mathcal{D}\times(0,T)\to\mathbb{R}^3$ is a prescribed forcing, $p\colon \mathcal{D}\times(0,T)\to\mathbb{R}$ is the pressure, and u_0 denotes the initial condition.

Then, following the idea in [40, 41], we split the analysis of (1.8) into two problems, corresponding to the decomposition $\theta_t^\varepsilon = Z_t^\varepsilon + \zeta_t^\varepsilon$. The first term Z_t^ε corresponds to the stochastic linear problem with non-homogeneous Dirichlet boundary conditions given by

$$\begin{cases} \partial_t Z^\varepsilon = \Delta Z^\varepsilon, & \text{in } \mathcal{D}\times(0,T),\\ Z^\varepsilon|_{\partial\mathcal{D}} = \sqrt{\varepsilon}\dfrac{dW}{dt}, & \text{in } \partial\mathcal{D}\times(0,T),\\ Z^\varepsilon|_{t=0} = 0, & \text{in } \mathcal{D}. \end{cases} \tag{1.10}$$

The solution of the previous equation can be interpreted in mild form, as in [34]. Next, we consider the remainder $\zeta_t^\varepsilon := \theta_t^\varepsilon - Z_t^\varepsilon$, which satisfies

$$\begin{cases} \partial_t\zeta^\varepsilon + u\cdot\nabla\zeta^\varepsilon + u\cdot\nabla Z^\varepsilon - \Delta\zeta^\varepsilon = 0, & \text{in } \mathcal{D}\times(0,T),\\ \zeta^\varepsilon|_{\partial\mathcal{D}} = 0, & \text{in } \partial\mathcal{D}\times(0,T),\\ \zeta^\varepsilon|_{t=0} = \theta_0, & \text{in } \mathcal{D}. \end{cases} \tag{1.11}$$

Here, we interpret again the solution $\zeta^\varepsilon\colon \mathcal{D}\times(0,T)\to\mathbb{R}$ in the mild form, namely

$$\zeta_t^\varepsilon = e^{t\Delta}\theta_0 - \int_0^t e^{(t-r)\Delta}\,(u_r\cdot\nabla\zeta_r^\varepsilon)\,dr - \int_0^t e^{(t-r)\Delta}\,(u_r\cdot\nabla Z_r^\varepsilon)\,dr.$$

We refer the reader to Section 3.2 for all the technical details (precise exponents, assumptions, preliminary lemmas, functional setting and so on) concerning the theorems and corollaries presented below and for minor results.
The first main result concerns the well-posedness of the system (1.11).

Theorem 1.1. *Let $T>0$, $s\in(0,\frac12)$ and $p>4$. With a suitable choice of γ, λ, $\bar\delta_\theta(s,p)$, $\bar\delta_u(s,p)$, for every*

$$0<\delta_\theta<\bar\delta_\theta(s,p), \qquad 0<\delta_u<\bar\delta_u(s,p),$$

the following holds. Set

$$\alpha_\theta = \frac14+\frac{\delta_\theta}{2}, \qquad \beta_\theta = \frac14-\frac{\delta_\theta}{4},$$

and let $Z_t^\varepsilon = -\sqrt{\varepsilon}\int_0^t \Delta e^{(t-r)\Delta}D\,dW_r$ be the continuous version in $H^{-2\alpha_\theta}(\mathcal{D})$. Then, for every divergence-free velocity field

$$u\in L^p\big(0,T;{}_0H_\sigma^{\frac32-\delta_u}(\mathcal{D})\big)\cap L^\infty\big(0,T;{}_0H_\sigma^{\frac12-\delta_u}(\mathcal{D})\big)$$

and every initial datum $\theta_0 \in W^{s,6/5}(\mathcal{D})$, there exists a unique mild solution ζ^ε of (1.11) *of the form*

$$\zeta_t^\varepsilon = e^{t\Delta}\theta_0 - \int_0^t e^{(t-r)\Delta}\big(u_r \cdot \nabla \zeta_r^\varepsilon\big)\, dr - \int_0^t e^{(t-r)\Delta}\big(u_r \cdot \nabla Z_r^\varepsilon\big)\, dr,$$

with trajectories in

$$\zeta^\varepsilon \in C(0,T;W^{s,6/5}(\mathcal{D})) \qquad \mathbb{P}\text{-}\textbf{\textit{a.s.}}$$

A straightforward but important consequence of the proof of the previous result is the following estimate.

Corollary 1.1. *Under the assumptions of Theorem 1.1, let $\zeta \in C(0,T;W^{s,\frac{6}{5}}(\mathcal{D}))$ and define*

$$\tilde{\zeta}_t := e^{t\Delta}\theta_0 - \int_0^t e^{(t-r)\Delta}\,(u_r \cdot \nabla \zeta_r)\, dr - \int_0^t e^{(t-r)\Delta}\,(u_r \cdot \nabla Z_r^\varepsilon)\, dr,$$

Then, for any $0 < \lambda < 1 - \delta_u$, it holds

$$\begin{aligned}\left\|\tilde{\zeta}\right\|_{C(0,T;W^{s,\frac{6}{5}}(\mathcal{D}))} &\le \left\|e^{t\Delta}\theta_0\right\|_{C(0,T;W^{s,\frac{6}{5}}(\mathcal{D}))} \\ &+ C\,\|u\|_{L^{\frac{p}{\lambda+\delta_u}}(0,T;W^{\frac{1}{2}+\lambda,2}(\mathcal{D}))}\left(\|\zeta\|_{C(0,T;W^{s,\frac{6}{5}}(\mathcal{D}))} + \|\xi^\varepsilon\|_{C(0,T;L^2(\mathcal{D}))}\right),\end{aligned} \tag{1.12}$$

where $C = C(p,\lambda,\delta_u,\delta_\theta,s,T) > 0$.

So far, together with Proposition 3.1 from the dedicated chapter, we have investigated the well-posedness of the temperature equation (1.8). Moreover, we can control the norm of its solution $\theta^\varepsilon = Z^\varepsilon + \zeta^\varepsilon$ with high probability depending on ε, since we are able to estimate the norms of Z^ε (by Proposition 3.1) and ζ^ε (by Corollary 1.1).

We now turn to the analysis of the 3D Navier-Stokes equations (1.9), assuming that f^θ is a prescribed forcing term. Global well-posedness results for the 3D Navier–Stokes equations are well known under smallness assumptions on the initial datum and the forcing; see for instance [33, Chapter 9]. In the classical energy setting one typically assumes $f^\theta \in L^2(0,T;L^2(\mathcal{D}))$ and $u_0 \in H^1(\mathcal{D})$.

In our coupled model the forcing is of buoyancy type, $f^\theta = -\theta^\varepsilon e_3$, and the temperature is decomposed as $\theta^\varepsilon = Z^\varepsilon + \zeta^\varepsilon$. The noise component Z^ε is, in general, only continuous in time with values in $H^{-\frac{1}{2}-\delta_\theta}(\mathcal{D})$, for any $\delta_\theta > 0$ compatible with a suitable covariance summability condition; the remainder ζ^ε is controlled in

$W^{s,6/5}(\mathcal{D})$. We therefore work in the ambient space $H^{-\frac{1}{2}-\delta_u}(\mathcal{D})$ for the Stokes/Navier-Stokes maximal regularity theory, choosing δ_u so that

$$\delta_u \geq \max\{\delta_\theta,\ \tfrac{1}{2} - s\},$$

which ensures that both Z^ε and ζ^ε can be interpreted as forcing terms in $H^{-\frac{1}{2}-\delta_u}(\mathcal{D})$. Accordingly, we formulate the Navier-Stokes well-posedness result for general forcing

$$f^\theta \in L^p(0,T;H^{-\frac{1}{2}-\delta_u}(\mathcal{D})), \quad p > \frac{2}{1-\delta_u},$$

which is the natural class arising from the maximal regularity framework in the low-regularity setting.

The notion of solution considered for the 3D Navier-Stokes problem (1.9) is the one of mild solution in the weak setting determined by the weak Stokes operator A_w. We now formalise this notion.

Definition 1.1. A function u is a solution of the 3D Navier-Stokes equations (1.9) on the time interval $[0,T]$ if

$$u_t = e^{-tA_w}u_0 + \int_0^t e^{-(t-r)A_w} P\left(-u_r \cdot \nabla u_r + f_r^\theta\right) dr, \tag{1.13}$$

for any $0 \leq t \leq T$, and possesses the regularity

$$u \in \mathbb{E}_{T,p}^{\delta_u} = W^{1,p}(0,T;{}_0H_\sigma^{-\frac{1}{2}-\delta_u}(\mathcal{D})) \cap L^p(0,T;{}_0H_\sigma^{\frac{3}{2}-\delta_u}(\mathcal{D})).$$

Here, and throughout the rest of the work, P denotes the Helmholtz projection, defined by interpolation from $H^{-\frac{1}{2}-\delta_u}(\mathcal{D})$ to $H_\sigma^{-\frac{1}{2}-\delta_u}(\mathcal{D})$. The global existence results for the velocity problem read as follows.

Theorem 1.2 (Global well-posedness for small data)**.** *Let $\delta_u \in (0,1)$, $f^\theta \in L^p(0,T;H^{-\frac{1}{2}-\delta_u}(\mathcal{D}))$, with $p > \frac{2}{1-\delta_u}$, and $u_0 \in V_p^{\delta_u}$. There exist $\tilde{\eta} = \tilde{\eta}(p,\delta_u,T) > 0$ and $M = M(p,\delta_u,T) > 0$ such that if $\eta \in (0,\tilde{\eta})$ and*

$$\max\left(\|u_0\|_{V_p^{\delta_u}}, \left\|f^\theta\right\|_{L^p(0,T;H^{-\frac{1}{2}-\delta_u}(\mathcal{D}))}\right) \leq \frac{\eta}{4M},$$

then there exists a unique solution $u \in \mathbb{E}_{T,p}^{\delta_u}$ with $\|u\|_{\mathbb{E}_{T,p}^{\delta_u}} \leq \eta$ of the 3D Navier-Stokes equation (1.9) *in the sense of Definition 1.1.*

We now shift our focus to the fully coupled velocity-temperature system (1.7). The corresponding notion of solution is the following.

Definition 1.2. The triple $(u^\varepsilon, \theta^\varepsilon, \tau^\varepsilon)$ is a *solution* of (1.7) on $[0,T]$ if $\tau^\varepsilon \colon \Omega \to [0,T]$ is a stopping time and $(u^\varepsilon, \theta^\varepsilon)$ is a stochastic process with trajectories $\mathbb{P}$-a.s. in

$$\mathbb{E}^{\delta_u}_{\tau^\varepsilon,p} \times C\big(0,\tau^\varepsilon; H^{-\frac{1}{2}-\delta_u}(\mathcal{D})\big),$$

where u^ε is adapted to $(\mathcal{F}_t)_t$ as a process in ${}_0H^{-\frac{1}{2}-\delta_u}_\sigma(\mathcal{D})$, and progressively measurable as a process in ${}_0H^{\frac{3}{2}-\delta_u}_\sigma(\mathcal{D})$, while θ^ε is adapted as a process in $H^{-\frac{1}{2}-\delta_u}(\mathcal{D})$, and, for any $0 \le t \le \tau^\varepsilon$, it holds

$$\begin{aligned}
u^\varepsilon_t &= e^{-tA_w}u_0 + \int_0^t e^{-(t-r)A_w} P\left(-u^\varepsilon_r \cdot \nabla u^\varepsilon_r - \theta^\varepsilon_r e_3\right) dr,\\
\theta^\varepsilon_t &= \zeta^\varepsilon_t + Z^\varepsilon_t,\\
\zeta^\varepsilon_t &= e^{t\Delta}\theta_0 - \int_0^t e^{(t-r)\Delta}\left(u^\varepsilon_r \cdot \nabla \zeta^\varepsilon_r\right) dr - \int_0^t e^{(t-r)\Delta}\left(u^\varepsilon_r \cdot \nabla Z^\varepsilon_r\right) dr,\\
Z^\varepsilon_t &= -\sqrt{\varepsilon}\int_0^t \Delta e^{(t-r)\Delta} D dW_r,
\end{aligned}$$

with probability one.

Lastly, we state the comprehensive main result of our work.

Theorem 1.3. *Let $T>0$, $s \in (0,\frac{1}{2})$ and $p>4$. Given a suitable choice of γ, λ, $\bar\delta_\theta(s,p)$, $\bar\delta_u(s,p)$, let parameters δ_θ, δ_u satisfy*

$$0 < \delta_\theta < \bar\delta_\theta, \qquad 0 < \delta_u < \bar\delta_u,$$

subject to the compatibility conditions

$$\delta_u \ge \max\left\{\delta_\theta, \frac{1}{2} - s\right\}, \qquad \delta_u < 1 - \frac{2}{p}, \tag{1.14}$$

which define a non-empty set for the given range of s and p. Set

$$\alpha_\theta := \frac{1}{4} + \frac{\delta_\theta}{2}, \qquad \beta_\theta := \frac{1}{4} - \frac{\delta_\theta}{4},$$

and assume a suitable covariance summability condition for the Q-Wiener process.
Then there exist constants $\eta > 0$ and $\widetilde{M} = \widetilde{M}(\delta_\theta, \delta_u, T) \ge 2$ such that the following holds: if

$$(\theta_0, u_0) \in W^{s,6/5}(\mathcal{D}) \times V^{\delta_u}_p, \qquad \max\{\|\theta_0\|_{W^{s,6/5}(\mathcal{D})},\ \|u_0\|_{V^{\delta_u}_p}\} \le \frac{\eta}{16\widetilde{M}},$$

then for every $\varepsilon > 0$ there exists a unique solution $(u^\varepsilon, \theta^\varepsilon, \tau^\varepsilon)$ of (1.7) on $[0,T]$ in the sense of Definition 1.2, such that

$$\|u^\varepsilon\|_{\mathbb{E}^{\delta_u}_{\tau^\varepsilon,p}} \le \eta, \qquad \|\theta^\varepsilon\|_{C\left(0,\tau^\varepsilon; H^{-\frac{1}{2}-\delta_u}(\mathcal{D})\right)} \le \eta, \qquad \mathbb{P}-\textbf{a.s.}$$

Moreover, there exists a constant $C(\delta_\theta, T) > 0$ *such that*

$$\mathbb{P}(\tau^\varepsilon = T) \geq 1 - \frac{64\,\widetilde{M}^2\,\varepsilon}{\eta^2}\,C(\delta_\theta, T)\sum_k \lambda_k^2 \|(-\Delta)^{\beta_\theta} De_k\|_2^2.$$

1.3 Climate, sustainability and volcanoes

Unlike the other two, this chapter does not present findings or proofs in the strict sense; rather, it is the outcome of the exploration undertaken during the doctoral studies on the broader subject of CO_2.

In the EBM work we investigated how an increase in CO_2 can cause an increase in the frequency of extreme events. Here we ask whether the amount needed to trigger this phenomenon is of anthropogenic origin or also natural. In other words, we ask whether human activity alone contributes substantially to the increase in greenhouse gases, or whether volcanic activity plays a role as well.

The main question guiding the first investigation is whether the gases emitted by volcanoes after a major eruption (see [42]) could have a discernible effect on climate change. Specifically, we seek to determine whether a major eruption occurring in the present day could release a quantity of gas sufficient to intensify the greenhouse effect over the long term, thereby exacerbating the warming trend we are already experiencing through a further rise in global temperatures. We find two distinct and competing behaviours (a warming one and a cooling one), arising from two distinct mechanisms operating on different time scales. Characterizing these mechanisms has important implications for contextualizing past events and predicting their modern-day counterparts. This work is situated within the broader framework of *Climate Change*.

Finally, we take advantage of the investigation into volcanic emissions to discuss environmental sustainability and the coexistence of human life with volcanic activity in a broader sense, such as seismicity or ground displacement, from a mathematical modelling prospective.

This second investigation has a substantially different aim. It is the product of a parallel study conducted thanks to the collaboration with INGV (Istituto Nazionale di Geofisica e Vulcanologia) and focuses on the phenomenon of bradyseism affecting the Campi Flegrei area in Italy, that is, the gradual uplift and subsidence of the ground, accompanied by frequent and at times shallow yet strong seismic events (see [43]). Its primary objective is to model the partially unknown subsurface structure under the hypothesis that these ground movements are driven by the dynamics of fluids

at depth. This work is situated within the broader framework of *Sustainable Development*.

References

1. Hasselmann, K. Stochastic climate models part I. Theory. *Tellus* **28,** 473–485. doi:10.1111/j.2153-3490.1976.tb00696.x (1976).
2. Serreze, M. & Barry, R. Processes and impacts of arctic amplification: A research synthesis. *Global and Planetary Change* **77,** 85–96. doi:10.1016/j.gloplacha.2011.03.004 (2011).
3. Hall, A. The role of surface albedo feedback in climate. *Journal of Climate* **17,** 1550–1568. doi:10.1175/1520-0442(2004)017<1550:TROSAF>2.0.CO;2 (2004).
4. *Climate Change 2021: The Physical Science Basis. Contribution of Working Group I to the Sixth Assessment Report of the Intergovernmental Panel on Climate Change* (eds Masson-Delmotte, V. *et al.*) doi:10.1017/9781009157896 (Cambridge University Press, Cambridge, United Kingdom and New York, NY, USA, 2021).
5. *Climate Change 2001: The Scientific Basis. Contribution of Working Group I to the Third Assessment Report of the Intergovernmental Panel on Climate Change* (eds Houghton, J. *et al.*) https://www.ipcc.ch/report/ar3/wg1/ (Cambridge University Press, Cambridge, United Kingdom and New York, NY, USA, 2001).
6. Alexander, M. A. *et al.* Projected sea surface temperatures over the 21st century: Changes in the mean, variability and extremes for large marine ecosystem regions of Northern Oceans. *Elementa: Science of the Anthropocene* **6,** 9. doi:10.1525/elementa.191 (2018).
7. Timmermans, M. & Labe, Z. *Sea Surface Temperature* NOAA Technical Report OAR ARC 23-07. In: Arctic Report Card 2023 (National Oceanic and Atmospheric Administration (NOAA), 2023). doi:10.25923/e8jc-f342.
8. Timmermans, M. & Labe, Z. *Sea Surface Temperature* NOAA Technical Report OAR ARC 24-07. In: Arctic Report Card 2024 (National Oceanic and Atmospheric Administration (NOAA), 2024). doi:10.25923/9z96-aq19.

9. Barkhordarian, A. *et al.* Arctic marine heatwaves forced by greenhouse gases and triggered by abrupt sea-ice melt. *Communications Earth & Environment* **5,** 57. doi:10.1038/s43247-024-01215-y (2024).
10. North, G. & Kim, K. *Energy balance climate models* doi:10.1002/9783527698844 (John Wiley & Sons, Weinheim, 2017).
11. Budyko, M. The effect of solar radiation variations on the climate of the earth. *Tellus* **21,** 611–619. doi:10.1111/j.2153-3490.1969.tb00466.x (1969).
12. Sellers, W. A global climatic model based on the energy balance of the earth-atmosphere system. *Journal of Applied Meteorology and Climatology* **8,** 392–400. doi:10.1175/1520-0450(1969)008<0392:AGCMBO>2.0.CO;2 (1969).
13. Ghil, M. Climate stability for a sellers-type model. *Journal of Atmospheric Sciences* **33,** 3–20. doi:10.1175/1520-0469(1976)033<0003:CSFAST>2.0.CO;2 (1976).
14. Díaz, J. I. in *The mathematics of models for climatology and environment* (ed Díaz, J. I.) 217–251 (Springer, Berlin, 1997). doi:10.1007/978-3-642-60603-8_6.
15. Floridia, G. Nonnegative controllability for a class of nonlinear degenerate parabolic equations with application to climate science. *Electronic Journal of Differential Equations* **2020,** 1–27. doi:10.58997/ejde.2020.59 (2020).
16. Del Sarto, G. *et al.* Dynamic boundary conditions with noise for an energy balance model coupled to geophysical flows. *Mathematische Nachrichten* **299,** 60–84. doi:10.1002/mana.70073 (2026).
17. Fornasaro, F. *et al.* Well-posedness and long time dynamics for a quasi-geostrophic ocean-atmosphere model with radiation balance. *arXiv preprint arXiv:2512.19556.* doi:10.48550/arXiv.2512.19556 (2025).
18. Cannarsa, P. *et al.* Analysis of a two-layer energy balance model: long time behavior and greenhouse effect. *Chaos* **33.** 34 pp., 113111. doi:10.1063/5.0136673 (2023).
19. Bastiaansen, R. *et al.* Fragmented tipping in a spatially heterogeneous world. *Environmental Research Letters* **17,** 045006. doi:10.1088/1748-9326/ac59a8 (Mar. 2022).
20. Goodwin, P. & Williams, R. On the arctic amplification of surface warming in a conceptual climate model. *Physica D: Nonlinear Phenomena* **454,** 133880. doi:10.1016/j.physd.2023.133880 (2023).

21. Del Sarto, G. *et al.* Time-periodic solutions to an energy balance model coupled with an active fluid under arbitrarily large forces. *Nonlinear Analysis: Real World Applications* **90,** 104558. doi:10.1016/j.nonrwa.2025.104558 (2026).
22. North, G. *et al.* Energy balance climate models. *Reviews of Geophysics* **19,** 91–121. doi:10.1029/RG019i001p00091 (1981).
23. Rombouts, J. & Ghil, M. Oscillations in a simple climate–vegetation model. *Nonlinear Processes in Geophysics* **22,** 275–288. doi:10.5194/npg-22-275-2015 (2015).
24. Lohmann, G. Temperatures from energy balance models: The effective heat capacity matters. *Earth System Dynamics* **11,** 1195–1208. doi:10.5194/esd-11-1195-2020 (2020).
25. Ashwin, P. & von der Heydt, A. S. Extreme sensitivity and climate tipping points. *Journal of Statistical Physics* **179,** 1531–1552. doi:10.1007/s10955-019-02425-x (2020).
26. Ghil, M. & Lucarini, V. The physics of climate variability and climate change. *Reviews of Modern Physics* **92,** 035002. doi:10.1103/RevModPhys.92.035002 (July 2020).
27. Lucarini, V. *et al.* Lévy noise versus gaussian-noise-induced transitions in the ghil–sellers energy balance model. *Nonlinear Processes in Geophysics* **29,** 183–205. doi:10.5194/npg-29-183-2022 (2022).
28. Arnold, L. *Hasselmann's program revisited: the analysis of stochasticity in deterministic climate models* in *Stochastic climate models* (eds Imkeller, P. & von Storch, J.-S.) **49** (Birkhäuser, Basel, 2001), 141–157. doi:10.1007/978-3-0348-8287-3_5.
29. Watkins, N. *et al.* The challenge of non-markovian energy balance models in climate. *Chaos: An Interdisciplinary Journal of Nonlinear Science* **34,** 072105. doi:10.1063/5.0187815 (July 2024).
30. Longo, I. *et al.* Nonautonomous modelling in energy balance models of climate. limitations of averaging and climate sensitivity. *Physica D: Nonlinear Phenomena* **485,** 135038. doi:10.1016/j.physd.2025.135038 (2026).
31. Lewis, S. & King, A. Evolution of mean, variance and extremes in 21st century temperatures. *Weather and Climate Extremes* **15,** 1–10. doi:10.1016/j.wace.2016.11.002 (2017).
32. Berselli, L. & Romito, M. On the existence and uniqueness of weak solutions for a vorticity seeding model. *SIAM Journal on Mathematical Analysis* **37,** 1780–1799. doi:10.1137/04061249X (2006).

33. Constantin, P. & Foias, C. *Navier-Stokes equations* (University of Chicago Press, Chicago, IL, 1988).

34. Da Prato, G. & Zabczyk, J. Evolution equations with white-noise boundary conditions. *Stochastics and Stochastics Reports* **42.** MR1291187, 167–182. doi:10.1080/17442509308833817 (1993).

35. Fabbri, G. & Goldys, B. An LQ problem for the heat equation on the halfline with Dirichlet boundary control and noise. *SIAM Journal on Control and Optimization* **48,** 1473–1488. doi:10.1137/070711529 (2009).

36. Agresti, A. *et al.* Global well-posedness of 2D Navier-Stokes with Dirichlet boundary fractional noise. *Nonlinearity* **38.** 41 pp., 075023. doi:10.1088/1361-6544/ade21c (2025).

37. Fan, W. *et al.* Three-dimensional shear driven turbulence with noise at the boundary. *Nonlinearity* **34,** 4764–4786. doi:10.1088/1361-6544/abf84b (2021).

38. Brzeźniak, Z. *et al.* Second order PDEs with Dirichlet white noise boundary conditions. *Journal of Evolution Equations* **15,** 1–26. doi:10.1007/s00028-014-0246-2 (2015).

39. Prüss, J. & Wilke, M. On critical spaces for the Navier-Stokes equations. *Journal of Mathematical Fluid Mechanics* **20.** MR3808592, 733–755. doi:10.1007/s00021-017-0342-5 (2018).

40. Da Prato, G. & Debussche, A. Two-dimensional Navier-Stokes equations driven by a space-time white noise. *Journal of Functional Analysis* **196.** MR1941997, 180–210. doi:10.1006/jfan.2002.3919 (2002).

41. Agresti, A. & Luongo, E. Global well-posedness and interior regularity of 2D Navier-Stokes equations with stochastic boundary conditions. *Mathematische Annalen* **390.** MR4801839, 2727–2766. doi:10.1007/s00208-024-02812-0 (2024).

42. Robock, A. Volcanic eruptions and climate. *Reviews of Geophysics* **38,** 191–219. doi:10.1029/1998RG000054 (2000).

43. INGV-OV. *Campi Flegrei - Bollettino di Sorveglianza mensile – Febbraio 2026* Bollettino di Sorveglianza. https://www.ov.ingv.it/index.php/monitoraggio-e-infrastrutture/bollettini-tutti/bollett-mensili-cf/anno-2026-2/1945-bollettino-mensile-campi-flegrei-2026-02/file (Feb. 2026).

Chapter 2



Variability amplification in an Arctic EBM

This chapter is extensively based on the following preprint:
Del Sarto G., Flandoli F., Lenzi M., (2026) A Multiplicative-Noise Mechanism for Variability Amplification under Radiative Forcing in an Arctic Energy-Balance Model; https://doi.org/10.48550/arXiv.2603.01617

2 VARIABILITY AMPLIFICATION IN AN ARCTIC EBM

This chapter is organised as follows. Section 2.1 introduces the stochastic Sellers-type EBM, derives the multiplicative-noise reduced model via a fast-slow formulation and Wong-Zakai, and proves monotone variance amplification with respect to radiative forcing. Section 2.2 formulates the spatial anomaly model, constructs a finite difference semi-discretisation, derives covariance dynamics and its stationary limit, and establishes monotonicity of the stationary covariance and spatial variance under suitable assumptions. Lastly, Section 2.3 compares the model predictions with observational August *sea surface temperature* from the National Oceanic and Atmospheric Administration (NOAA) north of $60°$N. We track temporal variability with moving decadal statistics and spatial heterogeneity with the within-region standard deviation, contrasting Arctic seas with regions showing little change.

2.1 RADIATIVE FORCING AMPLIFIES VARIANCE IN A MULTIPLICATIVE-NOISE EBM

2.1.1 Preliminaries: energy balance models and Wong-Zakai principle

Energy balance climate models

Among the lowest-complexity levels in the climate-model hierarchy lie the class of *energy balance models* [1]. Introduced independently by Budyko and Sellers in 1969 [2, 3], EBMs describe the evolution of a representative (near-surface) temperature T (in Kelvin) through the balance between absorbed shortwave radiation $\mathcal{R}_a$ and emitted longwave radiation $\mathcal{R}_e$. In its zero-dimensional form, the EBM is given by

$$C_{\text{eff}} \frac{dT}{dt} = \mathcal{R}_a - \mathcal{R}_e, \tag{2.1}$$

where $C_{\text{eff}} > 0$ is an effective heat capacity per unit area; equivalently, upon rescaling time one may set $C_{\text{eff}} = 1$ and recover $\frac{dT}{dt} =$

$\mathcal{R}_a - \mathcal{R}_e$. The model can be enriched by incorporating a spatial variable (typically latitude, after zonal averaging) and representing meridional heat transport by diffusion, which yields a nonlinear parabolic PDE, see [4, 5].

In this work we adopt a reduced, regionally EBM for the Arctic. This choice is motivated by the fact that Arctic temperature variability and trends are strongly constrained by the local radiative energy budget and amplified by cryospheric feedbacks, most notably the sea-ice/snow albedo feedback, which makes reduced energy-balance descriptions informative at regional scales [6, 7]. Consistently, low-order energy-balance and sea-ice models have been adapted for recent studies for sea-ice stability, Arctic warming and ice-loss transitions [8, 9, 10].

For the emitted radiation $\mathcal{R}_e$ we use the classical Budyko empirical formula [2, 1] and assume

$$\mathcal{R}_e(T) = r_0 + r_1 T,$$

with $r_0 \in \mathbb{R}$ and $r_1 > 0$. For the absorbed shortwave radiation we set

$$\mathcal{R}_a(T, Q, \lambda) = Q\beta(T) + \lambda,$$

where Q denotes the (possibly regionally averaged) incoming solar flux and $\beta \in (0, 1)$ is the *co-albedo*, i.e. the fraction of incident shortwave radiation absorbed ($\beta = 1 - \alpha$, with α the albedo). Here, as in [11, 12], λ models the effect of greenhouse gases on the radiation balance; the larger is λ, the larger is the radiative forcing, and thus the greenhouse effect which leads to a higher absorbed radiation. Following continuous piecewise linear parametrisation in the EBM literature as in [13], we consider

$$\beta(T) = \begin{cases} \beta_{\min}, & \text{if } T \le T_l, \\ \beta_{\min} + \dfrac{\beta_{\max} - \beta_{\min}}{T_u - T_l}(T - T_l), & \text{if } T_l < T < T_u, \\ \beta_{\max}, & \text{if } T \ge T_u. \end{cases} \tag{2.2}$$

where $\beta_{\min}$ and $\beta_{\max}$ represent the limiting co-albedo values in, respectively, the ice-covered (cold) and ice-free (warm) regimes; typical values in Sellers-type models are $\beta_{\min} \approx 0.38$ and $\beta_{\max} \approx 0.70$ [5]. Here, $T_l = 263\,\mathrm{K}$ and $T_u = 300\,\mathrm{K}$ as in [13]. We emphasise that these values are not meant to represent the melting temperature of ice, but rather to parametrise the temperature range over which the *effective* (regionally averaged) ice cover, and hence the co-albedo, transitions from its ice-covered to its ice-free limit [5, 13]. This interpretation is consistent with the thermodynamics of melting. Since the phase change involves the latent heat of fusion, a

large amount of energy is required to melt the ice, and the temperature can remain close to the freezing point while melting proceeds. In simple sea-ice/EBM formulations this "latent-heat buffering" is captured by treating melt in terms of an enthalpy (energy) budget when ice is present, see [10, 14]. Lastly, note that our EBM is of Sellers-type, meaning that the co-albedo is Lipschitz continuous. The other main class of EBMs is the Budyko type, which is characterised by a discontinuous co-albedo. In the latter case, it is known that uniqueness may fail; see, for example, [15] for a discussion of non-uniqueness of weak solutions.

Wong-Zakai principle

It is worth recalling the Wong-Zakai principle, a tool that we will use in Section 2.1.2. Roughly speaking, it asserts that if we consider smooth approximations W_t^ε of a Brownian motion W_t such that

$$W_t^\varepsilon \to W_t$$

in a sufficiently strong sense, then the solution Z_t^ε of the corresponding (pathwise deterministic, for fixed ω) differential equation

$$\frac{dZ_t^\varepsilon}{dt} = b(t, Z_t^\varepsilon) + \sigma(t, Z_t^\varepsilon)\frac{dW_t^\varepsilon}{dt},$$

converges (in the same mode of convergence as $W_t^\varepsilon \to W_t$), as $\varepsilon \to 0$, to the solution of the SDE driven by *Stratonovich noise*

$$dZ_t = b(t, Z_t)\,dt + \sigma(t, Z_t) \circ dW_t.$$

See, for instance, [16, Chapter 5.2] or [17, 18] for more details on the Wong-Zakai principle.

For the sake of clarity, we recall that the Stratonovich stochastic integral $\int_0^t \sigma(s, Z_s) \circ dW_s$ is defined as the limit (in probability) of Riemann sums using midpoint evaluation,

$$\sum_k \sigma\left(t_k, \frac{Z_{t_k} + Z_{t_{k+1}}}{2}\right)\left(W_{t_{k+1}} - W_{t_k}\right),$$

whenever the limit exists. This contrasts with the Itô integral $\int_0^t \sigma(s, Z_s)\,dW_s$, which is defined via left-point evaluation $\sigma(t_k, Z_{t_k})$. A key consequence is that Stratonovich calculus obeys the classical chain rule (as in ordinary calculus), while Itô calculus involves an additional quadratic-variation correction term. Concretely, for sufficiently regular coefficients one has the conversion formula

$$\int_0^t \sigma(s, Z_s) \circ dW_s = \int_0^t \sigma(s, Z_s)\,dW_s + \frac{1}{2}\int_0^t \partial_z\sigma(s, Z_s)\sigma(s, Z_s)\,ds,$$

so that an SDE written in Stratonovich form corresponds to an Itô SDE with an extra correction term in the drift term, see [19, Section 4.6].

2.1.2 Fast–slow insolation–temperature model and reduction to a multiplicative-noise EBM

We consider a fast-slow system describing the interaction between a *slow* temperature process T evolving on a macroweather timescale (e.g. one year) and a *fast* component X evolving on a weather timescale (e.g. one day). In our setting, X represents (a proxy for) the insolation. We model X as a mean-reverting Ornstein-Uhlenbeck process fluctuating around a climatological mean level Q, while the temperature follows a radiative balance law. More precisely, on the slow time variable t we consider

$$\begin{cases} dX_t^\tau = -\dfrac{1}{\tau}(X_t^\tau - Q)dt + \dfrac{1}{\sqrt{\tau}}dW_t, & X_0^\tau = x_0, \\ \dfrac{dT_t^{\tau,\lambda}}{dt} = X_t^\tau \beta(T_t^{\tau,\lambda}) + \lambda - (r_0 + r_1 T_t^{\tau,\lambda}), & T_0^{\tau,\lambda} = \theta_0, \end{cases} \tag{2.3}$$

where $(W_t)_t$ denotes a Brownian motion, and x_0, θ_0 are the deterministic initial conditions. The parameter $\tau > 0$ represents the ratio of the fast and slow timescales (e.g. $\tau \approx 1/365$ if the slow scale is one year and the fast one is one day). Even if τ is small, it is not infinitesimal in applications; this will be important in what follows.

A key feature of the scaling in (2.3) is that the variance of the invariant measure for X^τ does not depend on τ: indeed, for the OU process $dX_t^\tau = -(1/\tau)(X_t^\tau - Q)dt + (1/\sqrt{\tau})dW_t$ the stationary law is Gaussian with mean Q and variance $1/2$. Thus τ controls the *correlation time* of X^τ, not its variance.

At this point, we would like to deduce a closed equation for the slow process $T_t^{\tau,\lambda}$.

Lemma 2.1. *For any $t > 0$, it holds*

$$\lim_{\tau \to 0} \mathbb{E}\left| \frac{1}{\sqrt{\tau}} \int_0^t X_s^\tau ds - \frac{Qt}{\sqrt{\tau}} - W_t \right|^2 = 0.$$

Proof. For simplicity, we drop the dependence on τ in X^τ. The fast

process X_t can be written explicitly as

$$\begin{aligned} X_t &= x_0 e^{-t/\tau} + \frac{1}{\tau}\int_0^t Q e^{-(t-s)/\tau} ds + \frac{1}{\sqrt{\tau}}\int_0^t e^{-(t-s)/\tau} dW_s \\ &= x_0 e^{-t/\tau} + Q\left(1 - e^{-t/\tau}\right) + \frac{1}{\sqrt{\tau}}\int_0^t e^{-(t-s)/\tau} dW_s \\ &= (x_0 - Q)\, e^{-t/\tau} + Q + \frac{1}{\sqrt{\tau}}\int_0^t e^{-(t-s)/\tau} dW_s. \end{aligned}$$

Thus, integrating in time, we get

$$\begin{aligned} \int_0^t X_s ds &= \int_0^t \left[(x_0 - Q)\, e^{-s/\tau} + Q + \frac{1}{\sqrt{\tau}}\int_0^s e^{-(s-r)/\tau} dW_r\right] ds \\ &= \tau\left(1 - e^{-t/\tau}\right)(x_0 - Q) + tQ + \frac{1}{\sqrt{\tau}}\int_0^t\int_0^s e^{-(s-r)/\tau} dW_r ds. \end{aligned}$$

The last term on the right-hand side (RHS) can be computed applying Fubini-Tonelli for stochastic integrals

$$\begin{aligned} \frac{1}{\sqrt{\tau}}\int_0^t\int_0^s e^{-(s-r)/\tau} dW_r ds &= \frac{1}{\sqrt{\tau}}\int_0^t\int_r^t e^{-(s-r)/\tau} ds dW_r \\ &= \sqrt{\tau}\int_0^t \left(1 - e^{-(t-r)/\tau}\right) dW_r \\ &= \sqrt{\tau}\left(W_t - \int_0^t e^{-(t-r)/\tau} dW_r\right). \end{aligned}$$

From the previous computations, we deduce

$$\begin{aligned} \mathbb{E}\left|\frac{1}{\sqrt{\tau}}\int_0^t X_s ds - \frac{Qt}{\sqrt{\tau}} - W_t\right|^2 &= \mathbb{E}\left|\sqrt{\tau}\left(1 - e^{-t/\tau}\right)(x_0 - Q) - \int_0^t e^{-(t-r)/\tau} dW_r\right|^2 \\ &\le 2\tau\left(1 - e^{-t/\tau}\right)^2 (x_0 - Q)^2 + 2\mathbb{E}\left|\int_0^t e^{-(t-r)/\tau} dW_r\right|^2 \\ &= 2\tau\left(1 - e^{-t/\tau}\right)^2 (x_0 - Q)^2 + 2\int_0^t e^{-2(t-r)/\tau} dr \\ &= 2\tau\left(1 - e^{-t/\tau}\right)^2 (x_0 - Q)^2 + \tau\left(1 - e^{-2t/\tau}\right) \end{aligned}$$

where the first inequality follows from the Jensen's inequality, and the following inequality by Itô-isometry. Taking the limits in τ, we conclude the proof.

□

Define the centred, integrated fast fluctuations

$$W_t^\tau := \frac{1}{\sqrt{\tau}}\int_0^t (X_s^\tau - Q)\, ds.$$

Since X^τ has continuous paths, W^τ is C^1 and

$$dW_t^\tau = \frac{1}{\sqrt{\tau}}(X_t^\tau - Q)\,dt.$$

Lemma 2.1 yields $W_t^\tau \to W_t$ in L^2 for each fixed t. Using this identity, the temperature equation in (2.3) can be rewritten as the random ODE

$$dT_t^{\tau,\lambda} = \Big(Q\beta(T_t^{\tau,\lambda}) + \lambda - \mathcal{R}_e(T_t^{\tau,\lambda})\Big)\,dt + \sqrt{\tau}\,\beta(T_t^{\tau,\lambda})\,dW_t^\tau, \tag{2.4}$$

where the last integral is understood pathwise (Riemann-Stieltjes), since W^τ is C^1.
We now invoke the Wong–Zakai principle (see Section 2.1.1). Since (2.4) is driven by the smooth process W^τ, replacing W^τ by its Brownian limit W leads to a Stratonovich interpretation of the limiting stochastic integral. Accordingly, for $\tau \ll 1$ we approximate $T^{\tau,\lambda}$ by the solution $\widetilde{T}^{\tau,\lambda}$ of

$$d\widetilde{T}_t^{\tau,\lambda} = \Big(Q\beta(\widetilde{T}_t^{\tau,\lambda}) + \lambda - \mathcal{R}_e(\widetilde{T}_t^{\tau,\lambda})\Big)\,dt + \sqrt{\tau}\,\beta(\widetilde{T}_t^{\tau,\lambda}) \circ dW_t. \tag{2.5}$$

In Itô form, (2.5) becomes

$$d\widetilde{T}_t^{\tau,\lambda} = \Big(Q\beta(\widetilde{T}_t^{\tau,\lambda}) + \lambda - \mathcal{R}_e(\widetilde{T}_t^{\tau,\lambda}) + \frac{\tau}{2}\beta(\widetilde{T}_t^{\tau,\lambda})\beta'(\widetilde{T}_t^{\tau,\lambda})\Big)\,dt + \sqrt{\tau}\,\beta(\widetilde{T}_t^{\tau,\lambda})dW_t. \tag{2.6}$$

We stress that we are not taking a literal limit $\tau \to 0$ from (2.4) to (2.5). Doing so would indeed make the diffusion coefficient vanish. Rather, τ is the (small but positive) ratio between the fast and slow time scales, and the passage from (2.4) to (2.5) is a *model reduction step*: for $\tau \ll 1$, the forcing generated by the fast OU process is approximated by a white-noise forcing, with Stratonovich interpretation suggested by Wong-Zakai.

We study fluctuations near the stable equilibrium $T^{*,\lambda}$, so the *temperature anomaly*

$$Y_t^{\tau,\lambda} := \widetilde{T}_t^{\tau,\lambda} - T^{*,\lambda}$$

stays small and it is natural to linearise $\beta(T)$ around $T^{*,\lambda}$.
The Itô-Stratonovich correction is an $O(\tau)$ drift term, and since $\tau \approx 1/365$ (with β, β' bounded) it is much smaller than the remaining deterministic drift modelling the radiation balance $\mathcal{R}_a - \mathcal{R}_e$. So we can neglect it. Thus, we define $T^{*,\lambda}$ as the stable equilibrium temperature $T^* = T^{*,\lambda}$ of the deterministic stationary equation associated to (2.6). We stress that it is an assumption of our analysis

that $T^{*,\lambda}$ is a stable equilibrium point for the deterministic EBM (2.1). In other words, $T^{*,\lambda}$ is solution of

$$Q\beta(T^{*,\lambda}) + \lambda - \mathcal{R}_e(T^{*,\lambda}) = 0, \tag{2.7}$$

and it is (locally asymptotically) stable for the deterministic dynamics, i.e. the linearisation of $\frac{dT}{dt} = Q\beta(T) + \lambda - \mathcal{R}_e(T)$ at $T^{*,\lambda}$ has negative slope

$$\frac{d}{dT}(Q\beta(T) + \lambda - \mathcal{R}_e(T))|_{T=T^{*,\lambda}} = Q\beta'(T^{*,\lambda}) - \mathcal{R}_e'(T^{*,\lambda}) < 0,$$

equivalently

$$b^\lambda = \mathcal{R}_e'(T^{*,\lambda}) - Q\beta'(T^{*,\lambda}) > 0. \tag{2.8}$$

Since β is piecewise linear by (2.2), for T in a neighbourhood of $T^{*,\lambda}$ that does not cross T_l or T_u we have the affine representation

$$\beta(T) = \beta(T^{*,\lambda}) + \beta'(T^{*,\lambda})(T - T^{*,\lambda}), \tag{2.9}$$

with

$$\beta'(T^{*,\lambda}) = 0 \qquad T^{*,\lambda} \notin [T_l, T_u]$$

outside and

$$\beta'(T^{*,\lambda}) = (\beta_{\max} - \beta_{\min})/(T_u - T_l) \qquad T^{*,\lambda} \in (T_l, T_u).$$

Thus, recalling that $\mathcal{R}_e(T) = r_0 + r_1 T$ is already linear, we get, applying (2.9) in (2.6) and using (2.7) to cancel the constant drift,

$$dY_t^{\tau,\lambda} = \left(Q\beta'(T^{*,\lambda}) - r_1\right) Y_t^{\tau,\lambda} dt + \sqrt{\tau}\left(\beta(T^{*,\lambda}) + \beta'(T^{*,\lambda}) Y_t^{\tau,\lambda}\right) dW_t, \qquad Y_0 = y_0, \tag{2.10}$$

where y_0 is some deterministic initial condition.
Introducing the shorthands

$$b^\lambda := -Q\beta'(T^{*,\lambda}) + r_1, \qquad \sigma_0^\lambda := \beta(T^{*,\lambda}), \qquad \sigma_1^\lambda := \beta'(T^{*,\lambda}),$$

then the linear EBM (2.10) assumes the compact form

$$dY_t^{\tau,\lambda} = -b^\lambda Y_t^{\tau,\lambda} dt + \sqrt{\tau}(\sigma_0^\lambda + \sigma_1^\lambda Y_t^{\tau,\lambda}) dW_t, \qquad Y_0^{\tau,\lambda} = y_0.$$

Remark 2.1 (On the stability condition (2.8))**.** *Condition* (2.8) *is the stability requirement for the deterministic EBM at* $T^{*,\lambda}$*. It is automatic outside the ice-sensitive range (i.e.* $T^{*,\lambda} < T_l$ *or* $T^{*,\lambda} > T_u$*) because* $\beta'(T^{*,\lambda}) = 0$ *and thus* $b^\lambda = r_1 > 0$*. In the ice-sensitive range (i.e.* $T^{*,\lambda} \in (T_l, T_u)$*) the sign of* $b^\lambda = r_1 - Q\beta'(T^{*,\lambda})$ *depends on the magnitude of* Q*. For an Arctic winter mean, we can reasonably consider* $Q \approx 0$*; so stability is expected. On the other hand, for summer or annual-mean forcing the condition can fail. Since our stationary-variance analysis requires a stable linearisation, we treat* (2.8) *as an explicit modelling assumption delimiting the regime of validity. A more realistic approach would introduce seasonal forcing* $Q = Q(t)$*, yielding a non-autonomous model; we leave this for future work.*

2.1.3 Stationary variance and monotone dependence on radiative forcing

In this section we prove that the stationary variance associated to the solution of (2.10) increases monotonically with respect to λ. This means that, as the CO_2 concentration in the atmosphere increases, the same holds for the variance of the climate, i.e. the stationary temperature anomaly.

We start by observing that, since $t \mapsto \int_0^t (\sigma_0^\lambda + \sigma_1^\lambda Y_s^{\tau,\lambda})\, dW_s$ is a martingale, then the expected value of the process $Y_t^{\tau,\lambda}$ satisfies

$$\mathbb{E}[Y_t^{\tau,\lambda}] = y_0 - b^\lambda \int_0^t \mathbb{E}[Y_s^{\tau,\lambda}]\, ds. \tag{2.11}$$

This can be seen by writing (2.10) in the integral form and then considering the expectation.
The solution of (2.11) is

$$\mathbb{E}[Y_t^{\tau,\lambda}] = e^{-b^\lambda t} y_0, \qquad t \geq 0.$$

Thus the limit for large time t of the expected value of $Y_t^{\tau,\lambda}$ exists and it is independent of y_0 if and only if $b^\lambda > 0$. In that case, we have

$$\lim_{t \to +\infty} \mathbb{E}[Y_t^{\tau,\lambda}] = 0.$$

This motivates once more why the assumption $b^\lambda > 0$ from (2.8) is natural in this framework. Further, to simplify the computation, we also assume $y_0 = 0$, which gives $\mathbb{E}[Y_t^{\tau,\lambda}] = 0$ for any $t \geq 0$.

The following result identifies the value of the stationary variance associated to the equation (2.10).

Proposition 2.1 (Value of the stationary variance)**.** *Assume*

$$b^\lambda > 0, \qquad 2b^\lambda - \tau(\sigma_1^\lambda)^2 > 0.$$

Then the following limit exists

$$\lim_{t \to +\infty} \mathbb{E}[|Y_t^{\tau,\lambda}|^2] = \frac{\tau(\sigma_0^\lambda)^2}{2b^\lambda - \tau(\sigma_1^\lambda)^2}.$$

Proof. We drop the superscript τ, λ for readability. We assume for simplicity $y_0 = 0$ and use the notation $V(t) = \mathbb{E}[|Y_t|^2]$. Thus Y_t is a centered process. The Itô formula gives

$$\begin{aligned} d(Y_t)^2 &= 2Y_t dY_t + d[Y.]_t \\ &= 2Y_t \left(-bY_t dt + \sqrt{\tau}(\sigma_0 + \sigma_1 Y_t) dW_t\right) + \tau(\sigma_0 + \sigma_1 Y_t)^2 dt \\ &= \left[-(2b - \tau\sigma_1^2) Y_t^2 + 2\tau\sigma_0\sigma_1 Y_t + \tau\sigma_0^2\right] dt + dM_t, \end{aligned} \tag{2.12}$$

where $[Y.]_t$ denotes the quadratic variation of the process Y_t and M_t is a martingale. Considering the expected value in the previous equality, and using that $\mathbb{E}[Y_t] = 0$, yields

$$\frac{d}{dt}V(t) = -(2b - \tau\sigma_1^2)V(t) + \tau\sigma_0^2.$$

Since $V(0) = 0$, its solution is

$$V(t) = \tau\sigma_0^2 \int_0^t e^{-(2b-\tau\sigma_1^2)(t-s)} ds = \frac{\tau\sigma_0^2}{2b - \tau\sigma_1^2} \left(1 - e^{-(2b-\tau\sigma_1^2)t}\right).$$

Hence

$$\lim_{t\to+\infty} V(t) = \frac{\tau\sigma_0^2}{2b - \tau\sigma_1^2},$$

provided that $2b - \tau\sigma_1^2 > 0$. □

We are now ready to prove the main result of this section, which deals with the increase of the stationary variance under an increase of the radiative forcing, modelled by λ.

Proposition 2.2 (Monotonicity of the stationary variance)**.** *Assume*

$$b^\lambda > 0, \qquad 2b^\lambda - \tau(\sigma_1^\lambda)^2 > 0, \qquad T^{*,\lambda} \in (T_l, T_u).$$

Then the stationary variance is monotone increasing. In other words, setting

$$\lambda \mapsto \mathrm{Var}_\infty(\lambda) := \lim_{t\to+\infty} \mathbb{E}[|Y_t^{\tau,\lambda}|^2] = \frac{\tau(\sigma_0^\lambda)^2}{2b^\lambda - \tau(\sigma_1^\lambda)^2} = \frac{\tau\beta(T^{*,\lambda})^2}{2(r_1 - Q\beta'(T^{*,\lambda})) - \tau\beta'(T^{*,\lambda})^2},$$

we have $\mathrm{Var}_\infty(\lambda)' > 0$.

Proof. Assume for simplicity $y_0 = 0$. Recall that $T^{*,\lambda}$ is defined by

$$Q\beta(T^{*,\lambda}) + \lambda - \mathcal{R}_e(T^{*,\lambda}) = 0,$$

and that the linearised coefficients are

$$b^\lambda = r_1 - Q\beta'(T^{*,\lambda}), \qquad \sigma_0^\lambda = \beta(T^{*,\lambda}), \qquad \sigma_1^\lambda = \beta'(T^{*,\lambda}).$$

By Proposition 2.1, the stationary variance of the temperature anomaly $Y_t^{\tau,\lambda} = \widetilde{T}_t^{\tau,\lambda} - T^{*,\lambda}$ is

$$\mathrm{Var}_\infty(\lambda) = \lim_{t\to\infty} \mathbb{E}|Y_t^{\tau,\lambda}|^2 = \frac{\tau(\sigma_0^\lambda)^2}{2b^\lambda - \tau(\sigma_1^\lambda)^2} = \frac{\tau\,\beta(T^{*,\lambda})^2}{2\big(r_1 - Q\beta'(T^{*,\lambda})\big) - \tau\,\beta'(T^{*,\lambda})^2}.$$

Step 1: increasing λ increases the equilibrium temperature $T^{*,\lambda}$. Differentiating implicitly the equilibrium equation in λ gives

$$\Big(Q\beta'(T^{*,\lambda}) - \mathcal{R}_e'(T^{*,\lambda})\Big)\,\frac{dT^{*,\lambda}}{d\lambda} + 1 = 0.$$

Since $\mathcal{R}_e'(T) \equiv r_1$ and $b^\lambda = r_1 - Q\beta'(T^{*,\lambda})$, this becomes

$$\frac{dT^{*,\lambda}}{d\lambda} = \frac{1}{b^\lambda} > 0.$$

Step 2: monotone increase in stationary variance. For simplicity, set

$$N(\lambda) := \tau\beta(T^{*,\lambda})^2, \qquad D(\lambda) := 2\big(r_1 - Q\beta'(T^{*,\lambda})\big) - \tau\,\beta'(T^{*,\lambda})^2$$

so that

$$\mathrm{Var}_\infty(\lambda) = \frac{N(\lambda)}{D(\lambda)}.$$

In Step 1 we have proved that $\lambda \mapsto T^{*,\lambda}$ is monotone increasing. Further, the co-albedo β is increasing by the standard modelling of EBMs. Hence

$$N'(\lambda) = 2\tau\beta(T^{*,\lambda})\beta'(T^{*,\lambda})\frac{dT^{*,\lambda}}{d\lambda} > 0. \tag{2.13}$$

Note that $\beta'(T^{*,\lambda})$ is non-zero (and positive), since $T^{*,\lambda} \in (T_l, T_u)$, thanks to (2.2). Regarding $D(\lambda)$, since β is piece-wise linear, then $\beta'' = 0$. Hence

$$D'(\lambda) = -2\beta''(T^{*,\lambda})(Q + \tau\beta'(T^{*,\lambda}))\frac{dT^{*,\lambda}}{d\lambda} = 0. \tag{2.14}$$

Combining (2.13) and (2.14), we conclude that

$$\mathrm{Var}_\infty'(\lambda) = \frac{N'(\lambda)D(\lambda) - N(\lambda)D'(\lambda)}{D(\lambda)^2} = \frac{N'(\lambda)D(\lambda)}{D(\lambda)^2} > 0,$$

since $D(\lambda) > 0$ thanks to the assumption $2b^\lambda - \tau(\sigma_1^\lambda)^2 > 0$. □

The previous result indicates, in climate terms, that stronger CO_2 forcing not only warms the equilibrium states, but also that, via the ice-albedo feedback, amplifies the temperature anomaly around the equilibrium state. Indeed, the monotone increase of the stationary variance can be read directly from the explicit formula

$$\mathrm{Var}_\infty(\lambda) = \frac{\tau\,\beta(T^{*,\lambda})^2}{2\big(r_1 - Q\beta'(T^{*,\lambda})\big) - \tau\,\beta'(T^{*,\lambda})^2}.$$

By Step 1 in the previous proof, increasing λ increases the equilibrium temperature $T^{*,\lambda}$. If $T^{*,\lambda} \in (T_l, T_u)$, then β is strictly increasing, hence the numerator $\tau\,\beta(T^{*,\lambda})^2$ increases with λ. Moreover, since β is affine on (T_l, T_u), we have $\beta'(T^{*,\lambda}) \equiv (\beta_{\max} - \beta_{\min})/(T_u - T_l)$, so the denominator $2(r_1 - Q\beta'(T^{*,\lambda})) - \tau\,\beta'(T^{*,\lambda})^2$ is constant (in this regime). Therefore $\mathrm{Var}_\infty(\lambda)$ increases with λ. In climate terms, stronger CO_2 forcing not only warms the equilibrium state, but also amplifies fluctuations around it via the temperature dependence of the co-albedo (ice-albedo feedback).

2.2 Spatial anomaly model and finite-dimensional approximation

In this section we extend the zero-dimensional stochastic energy balance model (2.6) to a space-dependent version, appropriate for a regional model (the Arctic). This is done by introducing horizontal heat transport.

2.2.1 Spatial EBM with Dirichlet data and anomaly formulation

Let $\mathcal{D} \subset \mathbb{R}^2$ be a bounded domain with sufficiently regular boundary $\partial\mathcal{D}$. We consider a Hasselmann-type stochastic energy balance model with diffusion [20], i.e. the spatially dependent extension of equation (2.6). The (near-surface) temperature field $T^{\tau,\lambda}(t,x)$, depending on the time-scale parameter τ and the radiative forcing λ, satisfies non-homogeneous Dirichlet boundary conditions

$$T^{\tau,\lambda}(t,\xi) = \theta(\xi), \qquad t \geq 0,\ \xi \in \partial\mathcal{D}, \tag{2.15}$$

where θ is a prescribed boundary profile; in the following, we assume θ to be independent of the radiative forcing parameter λ, but our analysis extends to the case of $\theta = \theta^\lambda$. On $\mathcal{D}$ we postulate the Itô SPDE

$$\begin{cases} dT_t^{\tau,\lambda} = \left(\Delta T_t^{\tau,\lambda} + Q\,\beta(T_t^{\tau,\lambda}) + \lambda - \mathcal{R}_e(T_t^{\tau,\lambda})\right) dt + \sqrt{\tau}\,\beta(T_t^{\tau,\lambda})\,dW_t, \\ T^{\tau,\lambda}|_{\partial\mathcal{D}} = \theta \\ T^{\tau,\lambda}|_{t=0} = T_0 \end{cases} \tag{2.16}$$

where $Q = Q(x)$ denotes the given insolation function, β is the co-albedo, λ is the radiative forcing parameter, W_t is a Wiener process on $L^2(\mathcal{D})$, and T_0 is the initial condition. We do not specify the details of these objects here, as we use them only heuristically; the interested reader may consult [21].

Assume, for simplicity, that the Dirichlet datum θ is time-independent. We define the reference profile $T^{*,\lambda}$ as a (stable) stationary solution of the deterministic problem with the same boundary values

$$\begin{cases} \Delta T^{*,\lambda}(x) + Q(x)\,\beta(T^{*,\lambda}(x)) + \lambda - \mathcal{R}_e(T^{*,\lambda}(x)) = 0, & x \in \mathcal{D}, \\ T^{*,\lambda}(\xi) = \theta(\xi), & \xi \in \partial\mathcal{D}. \end{cases} \tag{2.17}$$

The temperature anomaly is then defined by

$$Y_t^{\tau,\lambda}(x) := T_t^{\tau,\lambda}(x) - T^{*,\lambda}(x).$$

By construction, (2.15) and (2.17) yield

$$Y_t^{\tau,\lambda}(\xi) = 0, \qquad \xi \in \partial\mathcal{D}, \tag{2.18}$$

i.e. the anomaly satisfies homogeneous Dirichlet boundary conditions. Subtracting (2.17) from (2.16) gives the anomaly SPDE

$$\begin{aligned} dY_t^{\tau,\lambda} = {} & (\Delta Y_t^{\tau,\lambda} + Q(\beta(T^{*,\lambda} + Y_t^{\tau,\lambda}) - \beta(T^{*,\lambda})) - (\mathcal{R}_e(T^{*,\lambda} + Y_t^{\tau,\lambda}) - \mathcal{R}_e(T^{*,\lambda})))dt \\ & + \sqrt{\tau}\,\beta(T^{*,\lambda} + Y_t^{\tau,\lambda})\,dW_t, \end{aligned} \tag{2.19}$$

with homogeneous Dirichlet boundary condition (2.18). As in the zero-dimensional case, if y is small, it holds the relation

$$\beta(T^{*,\lambda} + y) = \beta(T^{*,\lambda}) + \beta'(T^{*,\lambda})\,y.$$

Since in our model $\mathcal{R}_e$ is affine (e.g. $\mathcal{R}_e(T) = r_0 + r_1 T$), we obtain the linear multiplicative SPDE

$$\begin{cases} dY_t^{\tau,\lambda} = \left(\Delta Y_t^{\tau,\lambda} - a^\lambda Y_t^{\tau,\lambda}\right) dt + \sqrt{\tau}\left(\beta(T^{*,\lambda}) + \beta'(T^{*,\lambda})\,Y_t^{\tau,\lambda}\right) dW_t, \\ Y^{\tau,\lambda}|_{\partial\mathcal{D}} = 0, \\ Y^{\tau,\lambda}|_{t=0} = T_0 - T^{*,\lambda}, \end{cases} \tag{2.20}$$

where

$$a^\lambda(x) := -Q(x)\,\beta'(T^{*,\lambda}(x)) + \mathcal{R}_e'(T^{*,\lambda}(x)).$$

Equation (2.20) is complemented with homogeneous Dirichlet boundary conditions (2.18). We are not interested in the well-posedness of (2.20) here; the SPDE is a formal starting point for the semi-discrete covariance analysis.

2.2.2 Finite-difference semi-discretisation

We now derive a finite-difference approximation of (2.20) on a two-dimensional mesh. For simplicity we present the construction on a rectangular grid; the resulting semi-discrete SDE has the same

structure on general meshes, with A_Δ replaced by the corresponding stiffness matrix. We refer to [22, 23] for detailed treatments of finite difference methods for parabolic PDEs.

To describe the numerical discretisation, assume for simplicity $\mathcal{D} = (0, L_x) \times (0, L_y)$. Consider the uniform grid $x_i = ih_x$ for $i = 0, \dots, N_x$ and $y_j = jh_y$ for $j = 0, \dots, N_y$. We denote by

$$\mathcal{I} := \{1, \dots, N_x - 1\} \times \{1, \dots, N_y - 1\}$$

the set of interior index pairs, and by

$$z_{i,j} := (x_i, y_j) \in \mathcal{D}, \qquad (i, j) \in \mathcal{I},$$

the corresponding interior grid points. We enumerate the interior nodes by a single index $m = 1, \dots, d$ (with $d = (N_x - 1)(N_y - 1)$) via the bijection

$$m = m(i, j) := (j - 1)(N_x - 1) + i, \qquad (i, j) \in \mathcal{I},$$

and write $z_m := z_{i,j}$ whenever $m = m(i, j)$. Define the nodal unknowns $Y^{\tau,\lambda}_{i,j}(t) := Y^{\tau,\lambda}_t(z_{i,j})$ for $(i, j) \in \mathcal{I}$. Using the bijection $m = m(i, j)$, we collect these interior nodal values into the vector $Y^{\tau,\lambda}_t \in \mathbb{R}^d$, with $d = (N_x - 1)(N_y - 1)$, by setting $(Y^{\tau,\lambda}_t)_m := Y^{\tau,\lambda}_{i,j}(t)$ whenever $m = m(i, j)$. The five-point stencil for the Laplacian at an interior node reads

$$(\Delta_h Y^{\tau,\lambda})_{i,j} = \frac{Y^{\tau,\lambda}_{i+1,j} - 2Y^{\tau,\lambda}_{i,j} + Y^{\tau,\lambda}_{i-1,j}}{h_x^2} + \frac{Y^{\tau,\lambda}_{i,j+1} - 2Y^{\tau,\lambda}_{i,j} + Y^{\tau,\lambda}_{i,j-1}}{h_y^2},$$

see [23, Section 3.2] for more details on the discretisation of the Laplace operator. Since $Y^{\tau,\lambda}$ satisfies homogeneous Dirichlet boundary conditions (2.18), boundary values are zero and no boundary forcing appears. In matrix form,

$$\Delta_h Y^{\tau,\lambda}_t = A_\Delta Y^{\tau,\lambda}_t, \tag{2.21}$$

where

$$A_\Delta = \frac{1}{h_x^2} \left(I_{N_y - 1} \otimes A_x \right) + \frac{1}{h_y^2} \left(A_y \otimes I_{N_x - 1} \right), \tag{2.22}$$

and $A_x = \operatorname{tridiag}(1, -2, 1) \in \mathbb{R}^{(N_x-1)\times(N_x-1)}$, $A_y = \operatorname{tridiag}(1, -2, 1) \in \mathbb{R}^{(N_y-1)\times(N_y-1)}$. Define the sampled coefficients on interior nodes

$$b^\lambda_m := a^\lambda(z_m), \quad d^\lambda_m := \beta'(T^{*,\lambda}(z_m)), \quad f^\lambda_m := \beta(T^{*,\lambda}(z_m)), \quad m = 1, \dots, d.$$

Set

$$B^\lambda := \operatorname{diag}(b^\lambda) \in \mathbb{R}^{d\times d}, \quad D^\lambda := \operatorname{diag}(d^\lambda) \in \mathbb{R}^{d\times d}, \quad f^\lambda := (f^\lambda_i)_{i=1}^d \in \mathbb{R}^d.$$

To discretise the spatially correlated noise, let $C \in \mathbb{R}^{d\times d}$ be the discrete covariance matrix induced by the covariance operator of W on the grid, and fix a factorisation $C = LL^T$. Let $(W_t)_t$ be a d-dimensional Brownian motion. Then the semi-discrete approximation of (2.20) reads

$$dY_t^{\tau,\lambda} = (A_\Delta - B^\lambda)Y_t^{\tau,\lambda}\,dt + \sqrt{\tau}\,\mathrm{diag}\left(D^\lambda Y_t^{\tau,\lambda} + f^\lambda\right) L dW_t, \qquad Y^{\tau,\lambda}|_{t=0} = y_0. \tag{2.23}$$

We conclude this section by introducing a scalar proxy for the fluctuation level of the semi-discrete anomaly process (2.23), given by the trace of its covariance matrix. From now on, fix $\tau > 0$ and write $Y^\lambda := Y^{\tau,\lambda}$.

Definition 2.1 (Spatial Variance)**.** Let $(Y_t^\lambda)_t$ be the solution of the SDE (2.23) and let $\Gamma_t^\lambda := \mathbb{E}[(Y_t^\lambda - \mathbb{E}[Y_t^\lambda])(Y_t^\lambda - \mathbb{E}[Y_t^\lambda])^T]$ be its covariance matrix. The *spatial variance* at time t is

$$\mathrm{Var}_{\mathrm{sp}}(t;\lambda) := \mathrm{Tr}(\Gamma_t^\lambda),$$

and, whenever the limit exists, the *stationary spatial variance* is

$$\mathrm{Var}_{\mathrm{sp},\infty}(\lambda) := \mathrm{Tr}(\Gamma_\infty^\lambda), \qquad \Gamma_\infty^\lambda := \lim_{t\to\infty} \Gamma_t^\lambda.$$

In the discussion of spatial variance below we assume $y_0 = 0$. In the next subsection we briefly allow general y_0 to describe the mean, and then we set $y_0 = 0$ again to obtain an autonomous covariance equation. Thus, with the assumption $y_0 = 0$, from the fact that the drift is linear and the stochastic integral is a martingale, it follows that $\mathbb{E}[Y_t^\lambda] = 0$ for all $t \geq 0$. In this case,

$$\mathrm{Var}_{\mathrm{sp}}(t;\lambda) = \mathrm{Tr}(\Gamma_t^\lambda) = \sum_{i=1}^d \mathrm{Var}(Y_{t,i}^\lambda) = \mathbb{E}\left[\sum_{i=1}^d |Y_{t,i}^\lambda|^2\right].$$

So $\mathrm{Var}_{\mathrm{sp}}(t;\lambda)$ is the sum of the local fluctuation intensities over the domain, and $\mathrm{Var}_{\mathrm{sp},\infty}(\lambda)$ measures this total variance in the stationary regime.

Remark 2.2 (Stationary spatial variance and extreme weather events)**.** *It is natural to focus on the* stationary *spatial variance* $\mathrm{Var}_{\mathrm{sp},\infty}(\lambda) = \mathrm{Tr}(\Gamma_\infty^\lambda)$*, since it measures the fluctuation level of the temperature anomaly in the long-time regime corresponding to the* climate configuration *determined by the radiative forcing* λ *(after transients have died out). In particular, comparing* $\mathrm{Var}_{\mathrm{sp},\infty}(\lambda_1)$ *and* $\mathrm{Var}_{\mathrm{sp},\infty}(\lambda_2)$ *quantifies how the typical amplitude of persistent spatial fluctuations changes when the forcing level (e.g.* CO_2*) is modified.*

Although extreme events are not determined by second moments alone, $\mathrm{Var}_{\mathrm{sp}}(t;\lambda)$ *provides a useful second-moment control on the probability of observing a large anomaly somewhere in the domain. Assume for simplicity* $y_0 = 0$*, so that* $\mathbb{E}[Y_t^\lambda] = 0$ *for all* $t \geq 0$*. For any* $\vartheta > 0$*, by Markov's inequality*

$$\mathbb{P}\left(\max_{1\leq i\leq d}|Y_{t,i}^\lambda| \geq \vartheta\right) \leq \frac{1}{\vartheta^2}\mathbb{E}\left[\max_{1\leq i\leq d}|Y_{t,i}^\lambda|^2\right] \leq \frac{1}{\vartheta^2}\mathbb{E}\left[\sum_{i=1}^{d}|Y_{t,i}^\lambda|^2\right] = \frac{\mathrm{Var}_{\mathrm{sp}}(t;\lambda)}{\vartheta^2}.$$

and the same estimate holds in the stationary regime with $\mathrm{Var}_{\mathrm{sp},\infty}(\lambda)$*.*

2.2.3 Stationary covariance for the semi-discrete anomaly SDE

Recall from Definition 2.1 that our scalar proxy for the fluctuation level is the spatial variance $\mathrm{Var}_{\mathrm{sp}}(t;\lambda) = \mathrm{Tr}(\Gamma_t^\lambda)$ and its stationary limit $\mathrm{Var}_{\mathrm{sp},\infty}(\lambda) = \mathrm{Tr}(\Gamma_\infty^\lambda)$ whenever it exists. Thus, establishing existence and monotonicity properties for Γ_∞^λ immediately yields corresponding results for $\mathrm{Var}_{\mathrm{sp},\infty}(\lambda)$.

Preliminaries: matrix order, M-matrices, and vectorisation

We collect a few standard facts that will be used to control the sign and monotonicity properties of the stationary covariance. For $A \in \mathbb{R}^{d\times d}$ we denote by $\rho(A)$ its spectral radius,

$$\rho(A) := \max\{|\mu| : \mu \text{ eigenvalue of } A\},$$

and we write $A \geq B$ for the component-wise order. Recall that a matrix A is a *Z-matrix* if $a_{ij} \leq 0$ for all $i \neq j$. A *(non-singular) M-matrix* is a Z-matrix of the form $A = sI - B$ with $B \geq 0$ and $s > \rho(B)$; equivalently, A is a Z-matrix with $\mathrm{Re}(\mu) > 0$ for every eigenvalue μ, see [24, 25]. The key consequence we will use is the element-wise non-negativity of the inverse.

Theorem 2.1. *Let A be a Z-matrix. The following are equivalent:*

(i) A is a non-singular M-matrix,

(ii) $\mathrm{Re}(\mu) > 0$ for every eigenvalue μ of A,

(iii) A is invertible and $A^{-1} \geq 0$ component-wise.

Second, we recall that an *irreducible matrix* A is a square matrix that cannot be transformed, via a permutation matrix P (specifically PAP^T), into a block upper triangular matrix with more than one diagonal block of positive size. Equivalently, A is irreducible if its

associated directed graph is strongly connected. We refer to [25, Chapter 2.2.] for more details and properties on irreducible matrices

Finally, we fix notation for vectorisation and Kronecker products. Given $A = (v_1 \mid \dots \mid v_d) \in \mathbb{R}^{d\times d}$, we define

$$\mathrm{vec}(A) := \begin{pmatrix} v_1 \\ \vdots \\ v_d \end{pmatrix} \in \mathbb{R}^{d^2}.$$

For matrices $A \in \mathbb{R}^{m\times n}$ and $B \in \mathbb{R}^{p\times q}$, we denote by $A \otimes B \in \mathbb{R}^{mp\times nq}$ their *Kronecker product*, defined blockwise by

$$A \otimes B := \begin{pmatrix} a_{11}B & \cdots & a_{1n}B \\ \vdots & \ddots & \vdots \\ a_{m1}B & \cdots & a_{mn}B \end{pmatrix}.$$

We will repeatedly use the identities

$$(A \otimes B)^T = A^T \otimes B^T, \qquad \mathrm{vec}(AXB) = (B^T \otimes A)\,\mathrm{vec}(X), \tag{2.24}$$

as well as bilinearity in each argument.

Covariance dynamics and Lyapunov–vectorised formulation

In this subsection we derive the evolution equation satisfied by the covariance matrix of the semi-discrete anomaly process. By vectorising the resulting Lyapunov-type equation, we obtain a linear ODE in $\mathbb{R}^{d^2}$, whose long-time limit gives an explicit representation of the stationary covariance.

First, observe that SDE (2.23) can be rewritten as

$$dY_t^\lambda = M^\lambda Y_t^\lambda\, dt + \Sigma^\lambda(Y_t^\lambda) dW_t, \quad Y^\lambda|_{t=0} = y_0.$$

with $M^\lambda := A_\Delta - B^\lambda$ and $\Sigma^\lambda(y) = \sqrt{\tau}\,\mathrm{diag}(D^\lambda y + f^\lambda)L$. Then the expected value $\mathbb{E}[Y_t^\lambda]$ satisfies

$$\frac{d}{dt}\mathbb{E}[Y_t^\lambda] = M^\lambda \mathbb{E}[Y_t^\lambda], \qquad \mathbb{E}[Y_0^\lambda] = y_0$$

The solution is

$$\mathbb{E}[Y_t^\lambda] = e^{M^\lambda t} y_0.$$

It is reasonable, as in Section 2.1.3, that the temperature anomaly goes to zero as $t \to +\infty$. This holds for any initial condition y_0 if M^λ is negative definite, an assumption that we will always adopt from now on.

We are interested in the covariance matrix

$$\Gamma_t^\lambda := \mathbb{E}\big[(Y_t^\lambda - \mathbb{E}[Y_t^\lambda])(Y_t^\lambda - \mathbb{E}[Y_t^\lambda])^T\big].$$

For general y_0, the covariance dynamics contain an additional (time-dependent) forcing term through $\mathbb{E}[Y_t^\lambda] = e^{M^\lambda t} y_0$. To keep the covariance equation autonomous and simplify the subsequent vectorised Lyapunov formulation, we impose the simplifying assumption $y_0 = 0$, so that $\mathbb{E}[Y_t^\lambda] = 0$ for all $t \geq 0$ and thus $\Gamma_t^\lambda = \mathbb{E}\big[Y_t^\lambda (Y_t^\lambda)^T\big]$.

Lemma 2.2. *Assume that $M^\lambda = A_\Delta - B^\lambda$ is negative definite and $y_0 = 0$. Then Γ_t^λ satisfies the matrix ODE*

$$\begin{aligned}\frac{d}{dt}\Gamma_t^\lambda &= M^\lambda \Gamma_t^\lambda + \Gamma_t^\lambda (M^\lambda)^T + \mathbb{E}\Big[\Sigma^\lambda(Y_t^\lambda)\,(\Sigma^\lambda(Y_t^\lambda))^T\Big] \\ &= M^\lambda \Gamma_t^\lambda + \Gamma_t^\lambda (M^\lambda)^T + \tau \sum_{k=1}^{d} \mathrm{diag}(l^k)(D^\lambda \Gamma_t^\lambda (D^\lambda)^T + f^\lambda (f^\lambda)^T)\mathrm{diag}(l^k),\end{aligned}$$

where l^k is the k-th column of L.

Proof. Assume for simplicity $\tau = 1$. We drop for the ease of notation the dependence on λ. Using Itô-formula

$$\begin{aligned}d(Y_t Y_t^T) &= (dY_t)(Y_t)^T + Y_t (dY_t)^T + (dY_t)(dY_t)^T \\ &= (MY_t dt + \Sigma dW_t)(Y_t)^T + Y_t (MY_t dt + \Sigma dW_t)^T + (dY_t)(dY_t)^T.\end{aligned}$$

Note that, using Itô isometry, we have

$$(dY_t)(dY_t)^T = (MY_t dt + \Sigma dW_t)(MY_t dt + \Sigma dW_t)^T = \Sigma dW_t (dW_t)^T \Sigma^T.$$

Since $dW_t (dW_t)^T = I dt$, we obtain

$$(dY_t)(dY_t)^T = \Sigma\Sigma^T dt.$$

In conclusion we have

$$d(Y_t Y_t^T) = [MY_t (Y_t)^T + Y_t (Y_t)^T M^T + \Sigma\Sigma^T]dt + \widetilde{M}_t,$$

where $\widetilde{M}_t$ denotes a martingale. Taking the expected values, we deduce

$$\frac{d}{dt}\Gamma_t = M\Gamma_t + \Gamma_t M^T + \mathbb{E}[\Sigma\Sigma^T].$$

But in our setting $\Sigma = \mathrm{diag}(DY_t + f)L$, thus

$$\Sigma\Sigma^T = \mathrm{diag}(DY_t + f)LL^T \mathrm{diag}(DY_t + f)^T.$$

Since

$$LL^T = \sum_{k=1}^{d} l^k (l^k)^T,$$

we obtain

$$\Sigma\Sigma^T = \sum_{k=1}^{d} \mathrm{diag}(DY_t + f) l^k (l^k)^T \mathrm{diag}(DY_t + f)^T,$$

Further, using the property

$$\mathrm{diag}(a)b = \mathrm{diag}(b)a, \quad a, b \in \mathbb{R}^d,$$

we have

$$\Sigma\Sigma^T = \sum_{k=1}^{d} \mathrm{diag}(l^k) \left[(DY_t + f)(DY_t + f)^T\right] \mathrm{diag}(l^k).$$

Since $\mathbb{E}[Y_t] = 0$, we have

$$\mathbb{E}\left[(DY_t + f)(DY_t + f)^T\right] = D\Gamma_t D^T + ff^T,$$

and thus

$$\mathbb{E}\left[\Sigma\Sigma^T\right] = \sum_{k=1}^{d} \mathrm{diag}(l^k)(D\Gamma_t D^T + ff^T)\mathrm{diag}(l^k).$$

□

In the following technical result, we write the ODE satisfied by the covariance matrix Γ_t in more tractable way.

Lemma 2.3. *Assume that $M^\lambda = A_\Delta - B^\lambda$ is negative definite and $y_0 = 0$. The ODE for Γ_t^λ*

$$\frac{d}{dt}\Gamma_t^\lambda = M^\lambda \Gamma_t^\lambda + \Gamma_t^\lambda (M^\lambda)^T + \tau \sum_{k=1}^{d} \mathrm{diag}(l^k)(D^\lambda \Gamma_t^\lambda (D^\lambda)^T + f^\lambda (f^\lambda)^T)\mathrm{diag}(l^k),$$

is equivalent to

$$\frac{d}{dt} q_t^\lambda = K^\lambda q_t^\lambda + F^\lambda, \tag{2.25}$$

with

$$q_t^\lambda = \mathrm{vec}(\Gamma_t^\lambda), \quad K^\lambda := I_d \otimes M^\lambda + M^\lambda \otimes I_d + \tau\, \mathrm{diag}(\mathrm{vec}(C))(D^\lambda \otimes D^\lambda),$$

and

$$F^\lambda = \tau\, \mathrm{diag}(\mathrm{vec}(C))\mathrm{vec}(f^\lambda (f^\lambda)^T),$$

Proof. Assume for simplicity $\tau = 1$. We drop the dependence on λ for the ease of notation. Consider the matrix ODE

$$\frac{d}{dt}\Gamma_t = M\Gamma_t + \Gamma_t M^T + \sum_{k=1}^{d} \mathrm{diag}(l^k)\left(D\Gamma_t D^T + ff^T\right)\mathrm{diag}(l^k).$$

Vectorising both sides gives

$$\frac{d}{dt}q_t = \mathrm{vec}(M\Gamma_t) + \mathrm{vec}(\Gamma_t M^T) + \sum_{k=1}^{d} \mathrm{vec}\left(\mathrm{diag}(l^k)\left(D\Gamma_t D^T + ff^T\right)\mathrm{diag}(l^k)\right).$$

By the Kronecker product property (2.24),

$$\mathrm{vec}(M\Gamma_t) = (I \otimes M)q_t, \qquad \mathrm{vec}(\Gamma_t M^T) = (M \otimes I)q_t.$$

For the noise term, again by (2.24), since $\mathrm{diag}(l^k)^T = \mathrm{diag}(l^k)$,

$$\mathrm{vec}\left(\mathrm{diag}(l^k)X\mathrm{diag}(l^k)\right) = \left(\mathrm{diag}(l^k) \otimes \mathrm{diag}(l^k)\right)\mathrm{vec}(X), \qquad X \in \mathbb{R}^{d\times d}.$$

Apply this with $X = D\Gamma_t D^T + ff^T$ to obtain

$$\sum_{k=1}^{d} \mathrm{vec}\left(\mathrm{diag}(l^k)(D\Gamma_t D^T + ff^T)\mathrm{diag}(l^k)\right) = \left(\sum_{k=1}^{d} \mathrm{diag}(l^k) \otimes \mathrm{diag}(l^k)\right)\mathrm{vec}(D\Gamma_t D^T + ff^T).$$

Finally,

$$\mathrm{vec}(D\Gamma_t D^T) = (D \otimes D)\,\mathrm{vec}(\Gamma_t) = (D \otimes D)\,q_t, \qquad \mathrm{vec}(ff^T) \text{ is constant.}$$

Therefore, since $C = LL^T$ and l^k denotes the k-th column of L, we have

$$\sum_{k=1}^{d} \mathrm{diag}(l^k) \otimes \mathrm{diag}(l^k) = \mathrm{diag}(\mathrm{vec}(C)),$$

because the (i,j) entry of C is $C_{ij} = \sum_{k=1}^{d} l_i^k l_j^k$, and vectorisation turns entrywise multiplication by C into multiplication by $\mathrm{diag}(\mathrm{vec}(C))$. Collecting terms yields

$$\frac{d}{dt}q_t = \left(I_d \otimes M + M \otimes I_d + \mathrm{diag}(\mathrm{vec}(C))(D \otimes D)\right)q_t + \mathrm{diag}(\mathrm{vec}(C))\mathrm{vec}(ff^T),$$

which is (2.25). □

Combining the covariance identity from the previous lemma with the vectorisation rule in Lemma 2.3, we reduce the matrix-valued covariance dynamics to the linear ODE (2.25) on $q_t^\lambda = vec(\Gamma_t^\lambda)$; this directly gives the existence and an explicit formula for the stationary covariance under the hypothesis that K is negative-definite, and $C = LL^T$ is non-negative entry-wise.

Corollary 2.1. *Assume that $M^\lambda = A_\Delta - B^\lambda$ is negative definite, $y_0 = 0$ and*

$$K^\lambda = I_d \otimes M^\lambda + M^\lambda \otimes I_d + \tau \operatorname{diag}(\operatorname{vec}(C))(D^\lambda \otimes D^\lambda)$$

is negative definite. Assume further that $C = LL^T \geq 0$ component-wise. Then $\lim_{t\to\infty} \Gamma_t^\lambda =: \Gamma_\infty^\lambda$ exists. Further, setting $q^\lambda = \operatorname{vec}(\Gamma_\infty^\lambda)$, we have

$$q^\lambda = (-K^\lambda)^{-1} F^\lambda,$$

Moreover $(-K^\lambda)^{-1} \geq 0$ component-wise.

Proof. Assume for simplicity $\tau = 1$. We drop the dependence on λ for the ease of notation. The first part of the statement consists in observing that the solution of the ODE (2.25) converges if K is negative definite.

Let's now check that, if K is negative definite, then $(-K)^{-1} \geq 0$ component-wise. Write

$$-K = I_d \otimes (-M) + (-M) \otimes I_d - \operatorname{diag}(\operatorname{vec}(C))(D \otimes D).$$

We claim that $-K$ is a Z-matrix, i.e. it has non-positive off-diagonal elements.

First, observe that $-M$ is a Z-matrix. Indeed, the discrete Laplacian A_Δ has non-negative off-diagonal entries and B is diagonal, hence $M = A_\Delta - B$ has non-negative off-diagonals. Therefore $-M$ has non-positive off-diagonals, i.e. $-M$ is a Z-matrix.

Second, both Kronecker products $I_d \otimes (-M)$ and $(-M) \otimes I_d$ have the same sign pattern off-diagonal as $-M$, therefore each of them is a Z-matrix. The same holds for their sum

Third, the term $\operatorname{diag}(\operatorname{vec}(C))(D \otimes D)$ is diagonal and non-negative. Indeed, since D is diagonal, then $D \otimes D$ is diagonal. Hence $\operatorname{diag}(\operatorname{vec}(C))(D \otimes D)$ is diagonal as well. Moreover, $C \geq 0$ entry-wise implies $\operatorname{diag}(\operatorname{vec}(C)) \geq 0$ entry-wise; therefore $\operatorname{diag}(\operatorname{vec}(C))(D \otimes D)$ has non-negative diagonal entries. Consequently, $\operatorname{diag}(\operatorname{vec}(C))(D \otimes D)$ only affects the diagonal of $-K$ and does not change any off-diagonal sign.

In conclusion, we have proved that $-K$ is a Z-matrix. By the hypothesis on K, we have that $-K$ is positive definite. By Theorem 2.1, we deduce that $(-K)^{-1} \geq 0$ component-wise.

□

2.2.4 Monotonicity of the stationary covariance in the radiative forcing parameter

We now study how the stationary covariance of the semi-discrete temperature anomaly depends on the forcing parameter λ. For each λ, let $Y_t^\lambda \in \mathbb{R}^d$ solve the finite-difference SDE (2.23) with $y_0 = 0$, i.e.

$$dY_t^\lambda = M^\lambda Y_t^\lambda \, dt + \sqrt{\tau}\, \mathrm{diag}\big(D^\lambda Y_t^\lambda + f^\lambda\big)\, L\, dW_t, \qquad Y_0^\lambda = 0,$$

where

$$M^\lambda := A_\Delta - B^\lambda, \quad B^\lambda := \mathrm{diag}(b^\lambda), \quad D^\lambda := \mathrm{diag}(d^\lambda), \quad f^\lambda \in \mathbb{R}^d, \quad C := LL^T.$$

Recall that the coefficients are obtained by sampling the equilibrium profile $T^{*,\lambda}$ on the interior grid points z_m:

$$\begin{aligned} b_m^\lambda &= a^\lambda(z_m) = -Q(z_m)\beta'\left(T^{*,\lambda}(z_m)\right) + r_1, \\ d_m^\lambda &= \beta'\left(T^{*,\lambda}(z_m)\right), \\ f_m^\lambda &= \beta\left(T^{*,\lambda}(z_m)\right). \end{aligned} \tag{2.26}$$

Here we used the affine form $\mathcal{R}_e(T) = r_0 + r_1 T$ so that $\mathcal{R}_e'(T) \equiv r_1$. Recall that, under the non-restrictive assumption $y_0 = 0$,

$$\Gamma_t^\lambda = \mathbb{E}\left[Y_t^\lambda (Y_t^\lambda)^T\right], \qquad \Gamma_\infty^\lambda = \lim_{t\to\infty} \Gamma_t^\lambda,$$

whenever the limit exists. By Lemma 2.3 and Corollary 2.1, under the stability assumptions on M^λ and K^λ we have

$$q_\infty^\lambda := \mathrm{vec}(\Gamma_\infty^\lambda) = (-K^\lambda)^{-1} F^\lambda,$$

where

$$F^\lambda = \tau\, \mathrm{diag}(\mathrm{vec}(C))\, \mathrm{vec}(f^\lambda (f^\lambda)^T). \tag{2.27}$$

As in the zero-dimensional case, one expects $\lambda \mapsto T^{*,\lambda}(x)$ to be increasing for each $x \in \mathcal{D}$ (see Section 2.1). Since, for $T \in (T_l, T_u)$, β is increasing, this implies that $\lambda \mapsto f^\lambda$ is increasing component-wise.

To control the λ-dependence of $B^\lambda = \mathrm{diag}(b^\lambda)$ and $D^\lambda = \mathrm{diag}((\beta'(T^{*,\lambda}(x_i))_i))$, we assume, as above, that the equilibrium temperatures remain in a regime where β is increasing, e.g.

$$T^{*,\lambda}(z_m) \in (T_l, T_u), \qquad m = 1, \dots, d, \tag{2.28}$$

so that $\partial_\lambda b^\lambda = 0$ and $\beta'(T^{*,\lambda}) \equiv \frac{\beta_{\max} - \beta_{\min}}{T_u - T_l}$.

Proposition 2.3 (Strict component-wise increase of the stationary covariance)**.** *Let*

$$s := \frac{\beta_{\max} - \beta_{\min}}{T_u - T_l} > 0.$$

Assume that, for every λ under consideration, the equilibrium profile satisfies

$$T^{*,\lambda}(x) \in (T_l, T_u) \qquad \textit{for all } x \in \mathcal{D},$$

so that $\beta'(T^{*,\lambda}(x)) \equiv s$ on $\mathcal{D}$. Assume moreover the coercivity condition

$$r_1 - Q(x)s \geq 0 \qquad \textit{in } \mathcal{D}. \tag{2.29}$$

Let $C = LL^T$ and assume

$$C \geq 0 \textit{ entry-wise}, \qquad C \neq 0.$$

Assume that K^λ is negative definite, where

$$M^\lambda := A_\Delta - B^\lambda, \qquad K^\lambda := I_d \otimes M^\lambda + M^\lambda \otimes I_d + \tau \operatorname{diag}(\operatorname{vec}(C))\,(D^\lambda \otimes D^\lambda).$$

Then $\partial_\lambda \Gamma_\infty^\lambda > 0$ entry-wise.

Proof. Step 1: $\partial_\lambda T^{*,\lambda} > 0$ in the interior. Set $u^\lambda := \partial_\lambda T^{*,\lambda}$. Differentiating the elliptic equilibrium problem (2.17) with respect to λ yields

$$\Delta u^\lambda(x) + Q(x)\beta'(T^{*,\lambda}(x))u^\lambda(x) + 1 - r_1 u^\lambda(x) = 0, \qquad u^\lambda|_{\partial\mathcal{D}} = 0.$$

Since $T^{*,\lambda}(x) \in (T_l, T_u)$ for all x and β is affine on (T_l, T_u), we have $\beta'(T^{*,\lambda}(x)) \equiv s$. Hence

$$-\Delta u^\lambda(x) + (r_1 - Q(x)s)u^\lambda(x) = 1, \qquad u^\lambda|_{\partial\mathcal{D}} = 0.$$

By (2.29) and the maximum principle, see [26, Section 6.4], it follows that

$$u^\lambda(x) > 0 \quad \text{in } \mathcal{D},$$

and in particular $u^\lambda(z_m) > 0$ for all interior grid points z_m.

Step 2: $\partial_\lambda f^\lambda > 0$ component-wise. Recall $f_m^\lambda = \beta(T^{*,\lambda}(z_m))$. Since $\beta'(T^{*,\lambda}(z_m)) \equiv s$,

$$\partial_\lambda f_m^\lambda = \beta'(T^{*,\lambda}(z_m))\partial_\lambda T^{*,\lambda}(z_m) = s u^\lambda(z_m) > 0, \qquad m = 1, \ldots, d.$$

Also $f^\lambda > 0$ component-wise since $\beta \in (0, 1)$.

Step 3: K^λ is λ-independent on (T_l, T_u). Because $\beta'(T^{*,\lambda}(z_m)) \equiv s$, we have $D^\lambda = sI$ and $B^\lambda = \operatorname{diag}(-Q(z_m)s + r_1)$, hence D^λ, M^λ and K^λ do not depend on λ in this regime. We denote them simply by D, M and K.

Step 4: $-K$ is an irreducible nonsingular M-matrix and $(-K)^{-1} > 0$ entry-wise. Since A_Δ is the standard finite-difference Laplacian (five-point stencil) on a connected interior grid, its directed graph is strongly connected, hence A_Δ is irreducible. As B^λ is diagonal, $M^\lambda = A_\Delta - B^\lambda$ has the same off-diagonal pattern as A_Δ, so $-M$ is an irreducible Z-matrix. Consider the Kronecker sum

$$S := I_d \otimes (-M) + (-M) \otimes I_d.$$

Then S is a Z-matrix and is irreducible[1]. Moreover, since D is diagonal, $D \otimes D$ is diagonal, hence $\mathrm{diag}(\mathrm{vec}(C))(D \otimes D)$ is diagonal. Therefore

$$-K = S - \tau\,\mathrm{diag}(\mathrm{vec}(C))(D \otimes D)$$

is still a Z-matrix and remains irreducible (diagonal modifications do not affect irreducibility). By assumption, K is negative definite, hence $-K$ is positive definite and in particular all eigenvalues of $-K$ have strictly positive real part. Since $-K$ is a Z-matrix, this implies that $-K$ is a nonsingular M-matrix. Together with irreducibility, it follows, thanks to [24, Corollary 3.8, Chapter 5], that

$$(-K)^{-1} > 0 \qquad \text{entry-wise.}$$

Step 5: differentiate the stationary covariance formula and conclude strict positivity. By Lemma 2.3 and Corollary 2.1,

$$q^\lambda_\infty := \mathrm{vec}(\Gamma^\lambda_\infty) = (-K)^{-1} F^\lambda, \qquad F^\lambda = \tau\,\mathrm{diag}(\mathrm{vec}(C))\mathrm{vec}(f^\lambda (f^\lambda)^T).$$

Since K is constant in λ, differentiation gives

$$\partial_\lambda q^\lambda_\infty = (-K)^{-1}\,\partial_\lambda F^\lambda,$$

and

$$\partial_\lambda F^\lambda = \tau\,\mathrm{diag}(\mathrm{vec}(C))\,\mathrm{vec}((\partial_\lambda f^\lambda)(f^\lambda)^T + f^\lambda(\partial_\lambda f^\lambda)^T).$$

By Step 2, both f^λ and $\partial_\lambda f^\lambda$ are strictly positive component-wise, hence the matrix

$$G^\lambda := (\partial_\lambda f^\lambda)(f^\lambda)^T + f^\lambda(\partial_\lambda f^\lambda)^T$$

[1]Indeed, write the index set of $\mathbb{R}^{d^2}$ as pairs (i,j) with $i,j \in \{1,\dots,d\}$. By definition of the Kronecker sum, S^λ allows moves that change *only one coordinate at a time*: from (i,j) to (i',j) whenever $(-M)_{ii'} \neq 0$, and from (i,j) to (i,j') whenever $(-M)_{jj'} \neq 0$. Since $-M$ is irreducible, its graph is strongly connected, hence any pair (i,j) can reach any other pair (i',j') by first moving in the i-coordinate and then in the j-coordinate. Therefore S is irreducible.

is strictly positive entry-wise, so $\mathrm{vec}(G^\lambda) > 0$ component-wise. Since $C \geq 0$ entry-wise, $\mathrm{diag}(\mathrm{vec}(C)) \geq 0$ entry-wise, and because $C \neq 0$ we have $\mathrm{diag}(\mathrm{vec}(C))\,\mathrm{vec}(G^\lambda) \neq 0$. Therefore

$$\partial_\lambda F^\lambda \geq 0, \qquad \partial_\lambda F^\lambda \neq 0.$$

Finally, since $(-K)^{-1} > 0$ entry-wise (Step 4), it follows that

$$\partial_\lambda q_\infty^\lambda = (-K)^{-1}\,\partial_\lambda F^\lambda > 0 \quad \text{component-wise},$$

and hence $\partial_\lambda \Gamma_\infty^\lambda > 0$ entry-wise. □

In particular, since the stationary spatial variance is the trace of Γ_∞^λ (see Definition 2.1), the previous result guarantees that it is monotone increasing with respect to λ.

Corollary 2.2 (Monotonicity of the stationary spatial variance)**.** *Under the assumptions of Proposition 2.3, the stationary spatial variance*

$$\mathrm{Var}_{\mathrm{sp},\infty}(\lambda) = \mathrm{Tr}(\Gamma_\infty^\lambda)$$

is monotone increasing in λ.

Remark 2.3 (Stronger forcing, stronger climate spatial co-variability)**.** *We remark that Proposition 2.3 states that*

$$\partial_\lambda(\Gamma_\infty^\lambda)_{ij} > 0 \qquad \textit{for all } i, j,$$

and therefore, for any two distinct grid points $z_i \neq z_j$,

$$\partial_\lambda \mathrm{Cov}\left(Y_\infty^\lambda(z_i), Y_\infty^\lambda(z_j)\right) > 0.$$

In climate terms, increasing radiative forcing increase not only the amplitude of local fluctuations (variance or spatial variance) but also their spatial co-fluctuation*: anomalies at different locations tend to move more "together" in the sense of increasing covariance.*

Note that among the assumptions of Proposition 2.3 there is $C = LL^T \geq 0$ element-wise. This is mandatory. Indeed, in the next example, we show that, if the spatial covariance matrix C of the noise has even one negative entry, then the monotonicity of the spatial variance may fail, even when the noise amplitude is increasing componentwise in λ.

Example 2.1 (Failure of monotonicity with negative correlations)**.** *Consider the two-dimensional SDE with additive noise*

$$dY_t^\lambda = MY_t^\lambda\,dt + \Sigma^\lambda\,dW_t, \qquad Y_0^\lambda = 0,$$

where W_t is a 2-dimensional Brownian motion and

$$\Sigma^\lambda := \mathrm{diag}(f^\lambda)\, L, \quad C := LL^T.$$

We choose

$$M = \begin{pmatrix} -1 & s \\ s & -1 \end{pmatrix}, \qquad 0 < s < 1,$$

so that M is symmetric negative definite (its eigenvalues are $-1 \pm s < 0$). Let

$$C = \begin{pmatrix} 1 & -c \\ -c & 1 \end{pmatrix}, \qquad 0 < c < 1,$$

which is positive definite (its eigenvalues are $1 \pm c > 0$) but has a negative *off-diagonal entry $C_{12} = -c < 0$. Let $L \in \mathbb{R}^{2\times 2}$ such that $LL^T = C$; note that L exists, for instance, thanks to the Cholesky factorisation. Finally, define*

$$f^\lambda = \begin{pmatrix} \lambda \\ 1 \end{pmatrix}, \qquad \lambda \geq 0,$$

which is increasing componentwise in λ.

Let $\Gamma_t^\lambda := \mathbb{E}[Y_t^\lambda (Y_t^\lambda)^T]$. Since the noise is additive, Itô formula gives that Γ_t solves the ODE

$$\frac{d}{dt}\Gamma_t^\lambda = M\Gamma_t^\lambda + \Gamma_t^\lambda M^T + S^\lambda, \quad S^\lambda := \Sigma^\lambda (\Sigma^\lambda)^T.$$

Because $\Sigma^\lambda = \mathrm{diag}(f^\lambda)L$ and $LL^T = C$, we have

$$S^\lambda = \mathrm{diag}(f^\lambda)\, C\, \mathrm{diag}(f^\lambda) = \begin{pmatrix} \lambda^2 & -c\lambda \\ -c\lambda & 1 \end{pmatrix}.$$

Since M is negative definite, Γ_t^λ converges to the unique stationary covariance Γ_∞^λ solving

$$M\Gamma_\infty^\lambda + \Gamma_\infty^\lambda M + S^\lambda = 0.$$

The stationary covariance matrix Γ_∞^λ can also be expressed as

$$\Gamma_\infty^\lambda = \int_0^\infty e^{Mu} S^\lambda e^{Mu} du.$$

Let $\sigma_+ := -1 + s$ and $\sigma_- = -1 - s$ be the eigenvalues, and let v_+, v_- be eigenvectors corresponding to respectively to σ_+ and σ_-. We can take them orthonormal and given by

$$v_+ = \frac{1}{\sqrt{2}} \begin{pmatrix} 1 \\ 1 \end{pmatrix}, \qquad v_- = \frac{1}{\sqrt{2}} \begin{pmatrix} 1 \\ -1. \end{pmatrix}$$

Let

$$V := \begin{pmatrix} | & | \\ v_+ & v_- \\ | & | \end{pmatrix}$$

in such a way that $VV^T = V^TV = I$. *Hence*

$$V^TMV = \begin{pmatrix} -1+s & 0 \\ 0 & -1-s \end{pmatrix} := D_M.$$

Recall that

$$e^{Mu} = Ve^{D_Mu}V^T, \quad e^{D_Mu} = \begin{pmatrix} e^{\sigma_+ u} & 0 \\ 0 & e^{\sigma_- u} \end{pmatrix}.$$

Using the linearity and cyclicity of the trace

$$\begin{aligned} \mathrm{Tr}(\Gamma_\infty^\lambda) &= \mathrm{Tr}(\int_0^\infty e^{Mu}S^\lambda e^{Mu}du) \\ &= \int_0^\infty \mathrm{Tr}(e^{Mu}S^\lambda e^{Mu})du \\ &= \int_0^\infty \mathrm{Tr}(Ve^{D_Mu}V^TS^\lambda Ve^{D_Mu}V^T)du \\ &= \int_0^\infty \mathrm{Tr}(V^TVe^{D_Mu}V^TS^\lambda Ve^{D_Mu})du \\ &= \int_0^\infty \mathrm{Tr}(e^{D_Mu}V^TS^\lambda Ve^{D_Mu})du \\ &= \int_0^\infty \mathrm{Tr}(e^{2D_Mu}V^TS^\lambda V)du. \end{aligned}$$

Setting $\tilde{S}^\lambda := V^TS^\lambda V$, *then*

$$\mathrm{Tr}(\Gamma_\infty^\lambda) = \int_0^\infty \mathrm{Tr}(e^{2D_Mu}\tilde{S}^\lambda)du = \int_0^\infty \left(e^{2u\sigma_+}\tilde{S}_{11}^\lambda + e^{2u\sigma_-}\tilde{S}_{22}^\lambda\right)du = -\frac{\tilde{S}_{11}^\lambda}{2\sigma_+} - \frac{\tilde{S}_{22}^\lambda}{2\sigma_-}.$$

Since

$$\tilde{S}_{11}^\lambda = \frac{\lambda^2 - 2c\lambda + 1}{2}, \quad \tilde{S}_{22}^\lambda = \frac{\lambda^2 + 2c\lambda + 1}{2},$$

we obtain, after some computations

$$\mathrm{Tr}(\Gamma_\infty^\lambda) = \frac{\lambda^2 - 2cs\lambda + 1}{2(1-s^2)}.$$

Computing the derivative with respect to λ, *we observe that*

$$\partial_\lambda \mathrm{Tr}(\Gamma_\infty^\lambda) = \frac{\lambda - cs}{1-s^2}.$$

Since $s \in (0,1)$, *for* $\lambda < cs$ *the spatial variance, i.e. the trace of the stationary covariance matrix, is decreasing.*



Figure 2.1: *Geographical distribution of the Arctic Ocean and its marginal seas. Numbered labels indicate: (1) Norwegian Sea, (2) Barents Sea, (3) Kara Sea, (4) Laptev Sea, (5) East Siberian Sea, (6) Chukchi Sea, (7) Beaufort Sea, (8) Baffin Bay, (9) Greenland Sea, and (10) Arctic Ocean.*

2.3 Analysis of observational sea surface temperature data

In this section we compare our results with data. The real-world data are the product of the net outcome of all the geophysical processes at work within the system and from this perspective, the model presented is highly simplified. We focus on Surface Sea Temperature (SST) during summer (August) in the northern high latitudes, above 60°N, where the ice-albedo feedback is predominant.

In glacial zones small temperature increments can trigger powerful feedbacks that further accelerate the initial warming. In particular, the ice-albedo feedback represents a key mechanism governing Arctic SST, especially during summer months [27]. When the temperature is near a certain threshold, a small temperature increase triggers ice melting, giving way to liquid water; since water has a much lower albedo, this leads to increased heat absorption and then to higher temperatures.
Due to the increase in CO_2, Arctic regions are experiencing the so-called *Arctic Amplification* [28] and a severe retreat of sea ice [29]. Therefore, August SSTs are currently exhibiting higher values than in the past [30] and northern seas are undergoing a condition of abrupt interannual changes [31] , leading to greater fluctuations in

SST [27, 32]. This is the dynamic described by our model in Section 2.1.

Concerning Section 2.2, we addressed the concept of spatial variance. By this term, we intend to examine how the local mechanism described above manifests on a larger scale. This reflects the spatial uniformity of ice-water dynamics across the entire ocean, clarifying whether the process is homogeneous or characterised by a patchwork distribution [33, 34, 35]. In other words, we are assessing the heterogeneity of the phenomenon, looking at the extent to which the system is fragmented into patches, through the spatial variability of SST. In particular, we have shown that temperature variability, under a certain regime, also increases spatially, implying a patchy behaviour and non-homogeneous distribution.

We used observations from NOAA (National Oceanic and Atmospherical Administration), in particular NOAA OI SST V2 High Resolution Dataset (`https://psl.noaa.gov/data/gridded/data.noaa.oisst.v2.highres.html`), provided by the NOAA PSL, Boulder, Colorado, USA (`https://psl.noaa.gov`) [36]. The dataset employed to assess temporal variance analysis contains daily SST values from 1981/09 to 2026/01, with Spatial Coverage of 0.25 degree latitude x 0.25 degree longitude global grid (1440x720). For the spatial variance analysis, we utilised monthly mean SSTs, sharing the same timeframe and geographical extent as the aforementioned dataset.

Initially, to detect signals of temporal SST variability, we first fixed a study area. Than, we extracted data for every August between 1982 and 2025 and we computed the daily spatial mean for each selected month. Subsequently, we calculated statistics (histograms, mean, standard deviation) over overlapping 10-year periods (31×10 data for each period), moving the window forward by one year at a time.

In Figure 2.2 we show the case of the Kara Sea, a marginal sea of the Arctic Ocean. This example is consistent with our results. The top-left panel indicates the location of the study area. The top-right panel shows a comparison between the histograms of the spatial-averaged daily August SST for the first (blue) and the last (red) calculable decade, along with their respective mean and variance. We note that the distribution has evolved significantly over time: the mean is increased and the tails of the distribution have broadened, as confirmed by the increase in the mean value and standard deviation value, respectively. The bottom-left panel shows the decadal spatial mean of August SST over time (centred on the mid-year of each decade) and a significant increasing trend can be observed. The bottom-right panel shows the decadal spatial standard deviation of August SST over time (centred on the mid-year

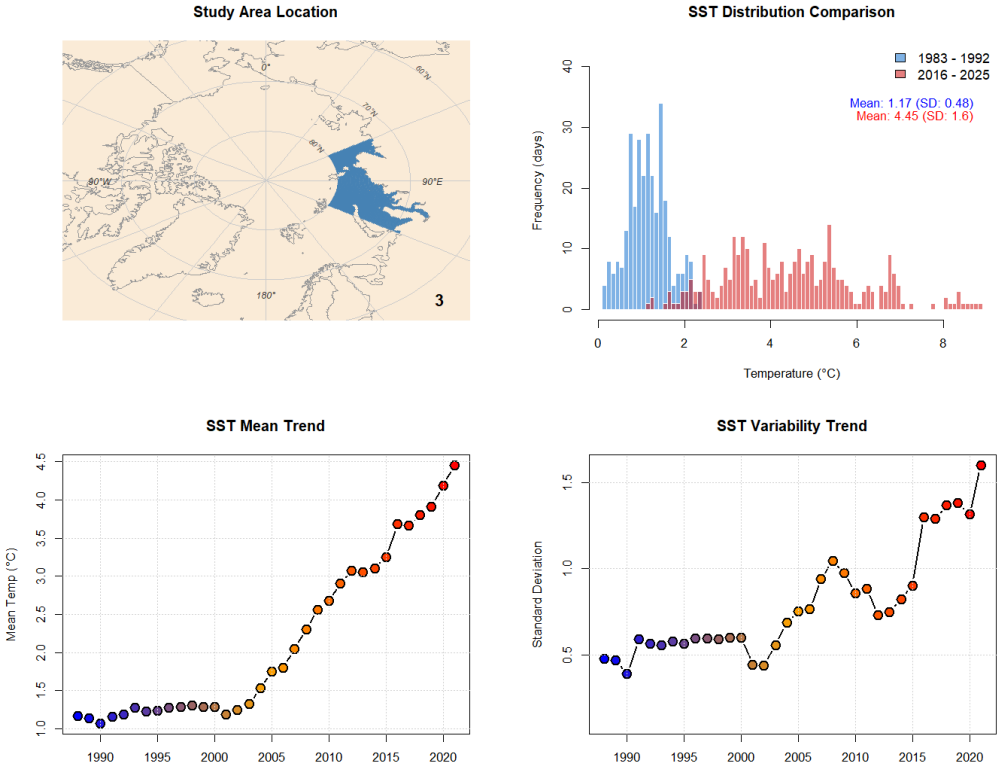

Figure 2.2: *Kara Sea. Top-left: location of the study area. Top-right: comparison between the histograms (number of days) of the spatial-averaged daily August SST for the first decade (1983-1992, blue) and the last calculable decade (2016-2025, red), along with their respective mean and standard deviation values. Bottom-left: decadal spatial mean trend of August SST (centred on the mid-year of each decade, one year moving window). Bottom-right: decadal spatial standard deviation trend of August SST (centred on the mid-year of each decade, one year moving window). The blue-to-red colour scale represents the progression of time across the decades, in accordance with the colour scheme used in the histogram.*

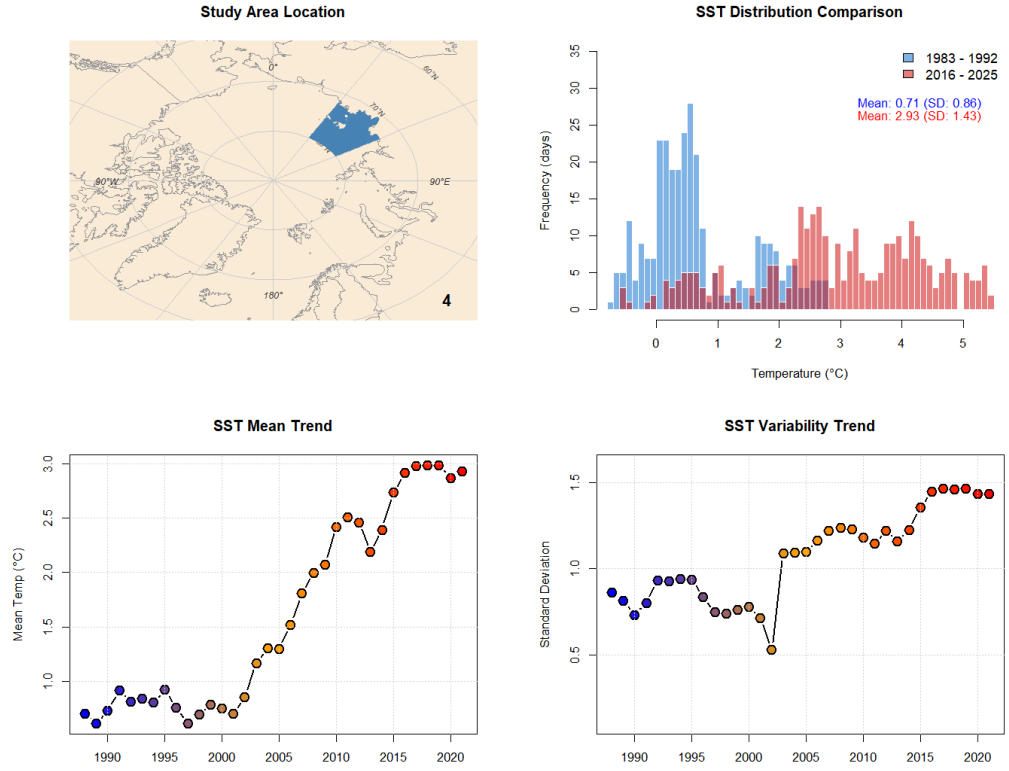

Figure 2.3: *Laptev Sea. Top-left: location of the study area. Top-right: comparison between the histograms (number of days) of the spatial-averaged daily August SST for the first decade (1983-1992, blue) and the last calculable decade (2016-2025, red), along with their respective mean and standard deviation values. Bottom-left: decadal spatial mean trend of August SST (centred on the mid-year of each decade, one year moving window). Bottom-right: decadal spatial standard deviation trend of August SST (centred on the mid-year of each decade, one year moving window). The blue-to-red colour scale represents the progression of time across the decades, in accordance with the colour scheme used in the histogram.*

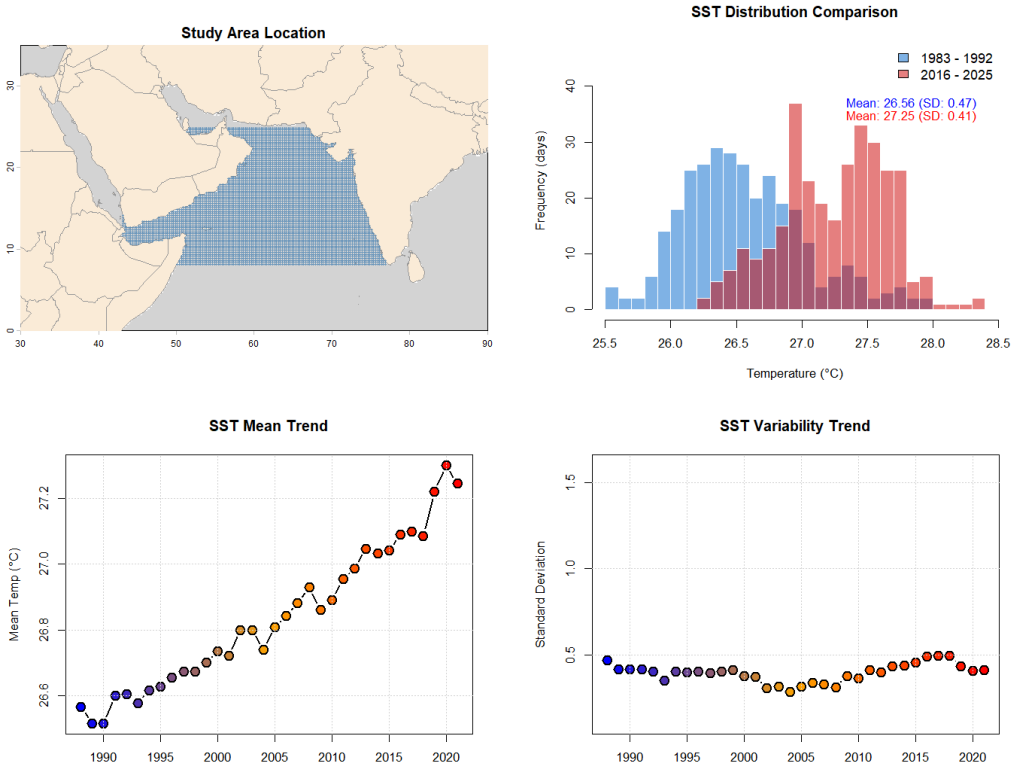

Figure 2.4: *Arabic Sea. Top-left: location of the study area (long-lat). Top-right: comparison between the histograms (number of days) of the spatial-averaged daily August SST for the first decade (1983-1992, blue) and the last calculable decade (2016-2025, red), along with their respective mean and standard deviation values. Bottom-left: decadal spatial mean trend of August SST (centred on the mid-year of each decade, one year moving window). Bottom-right: decadal spatial standard deviation trend of August SST (centred on the mid-year of each decade, one year moving window). The blue-to-red colour scale represents the progression of time across the decades, in accordance with the colour scheme used in the histogram.*

of each decade). After a stationary phase, also observable in the mean trend, a period of growth can be distinctly discerned, i.e. an increased variability. Similar observations can be done for Figure 2.3, which illustrates the Laptev Sea case [37].

Comparing the Arabic Sea (Figure 2.4) to the previous cases, the growth trend of the mean is considerably weaker and the distribution tails do not change in shape. Consequently, the standard deviation shows no growth and remains steady. This could possibly be explained by the fact that the equilibrium temperature of that area far exceeds the reference interval, meaning we are referring to the right-side plateau of the co-albedo curve (equation (2.2)), i.e. in (2.2) $\mathrm{Var}'_\infty \equiv 0$.

Regarding the spatial variability of temperature, as mentioned before, we changed dataset. For each grid point within the study area, we used the August mean SST value to create a density map, where the colour intensity represents the frequency of SST values over time. We then calculated the standard deviation for each year, thus capturing the area's spatial spread, the fluctuations around the average value, i.e. its heterogeneity.

Figures 2.5 and 2.6 illustrate the spatial variability of the previously discussed seas, i.e. the Kara and Laptev Seas, respectively. The top panel shows the density map. In both cases, a clear widening of the spread is visible, indicating greater dispersion. The lower panel displays the interannual standard deviation, together with its growth trend (dashed red line), which is increasing.

In contrast to the aforementioned seas, the Arctic Ocean (panel 10, Figure 2.1) exhibits a different behaviour. As shown in Figure 2.7, the standard deviation remains stationary. This could possibly be explained by the fact that the average temperatures of those seas are still too low; that is, we are referring to the left-side plateau of the co-albedo curve (equation (2.2)), i.e. in (2.2) $\mathrm{Var}'_\infty \equiv 0$. Indeed, persistent ice still characterises this area even during August.

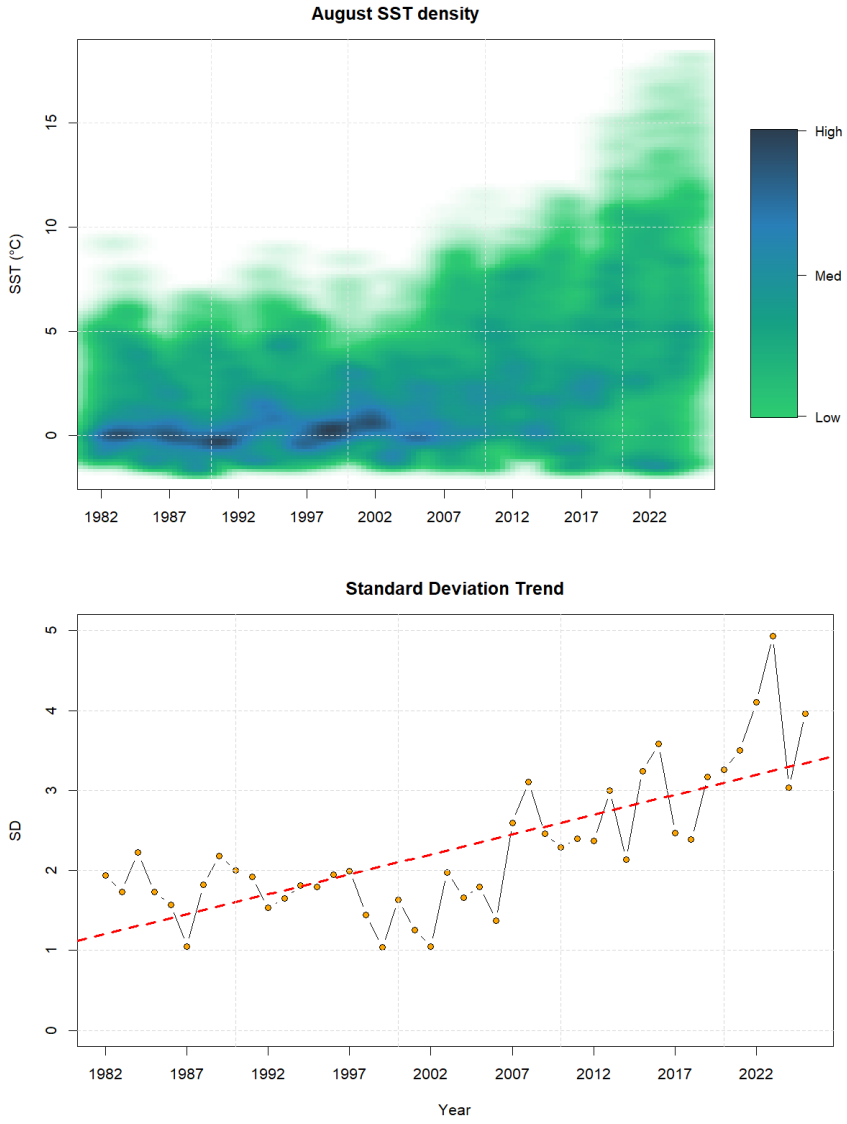

Figure 2.5: *Kara Sea (panel 3, Figure 2.1). Top: density distribution of annual August mean SST values across all individual grid points of the study area. Bottom: interannual standard deviation (dashed line with markers), together with its growth trend (dashed red line).*

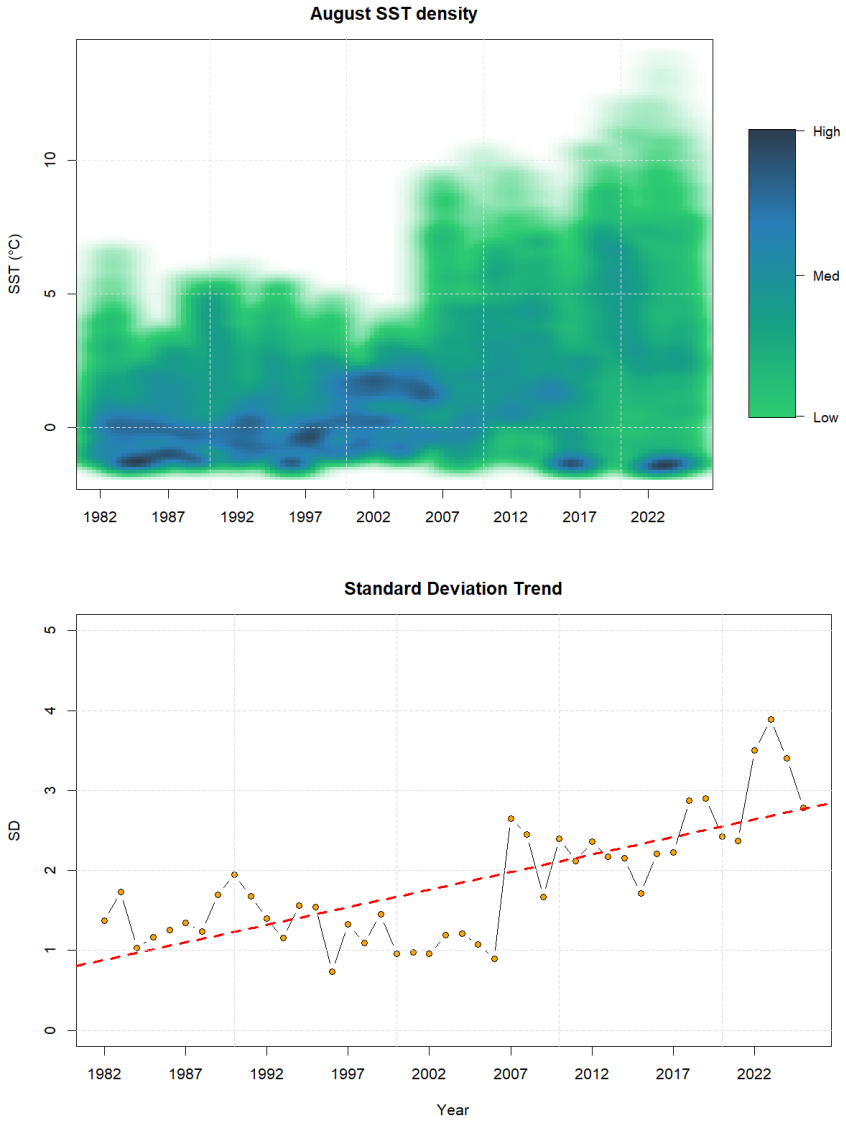

Figure 2.6: *Laptev Sea (panel 4, Figure 2.1). Top: density distribution of annual August mean SST values across all individual grid points of the study area. Bottom: interannual standard deviation (dashed line with markers), together with its growth trend (dashed red line).*

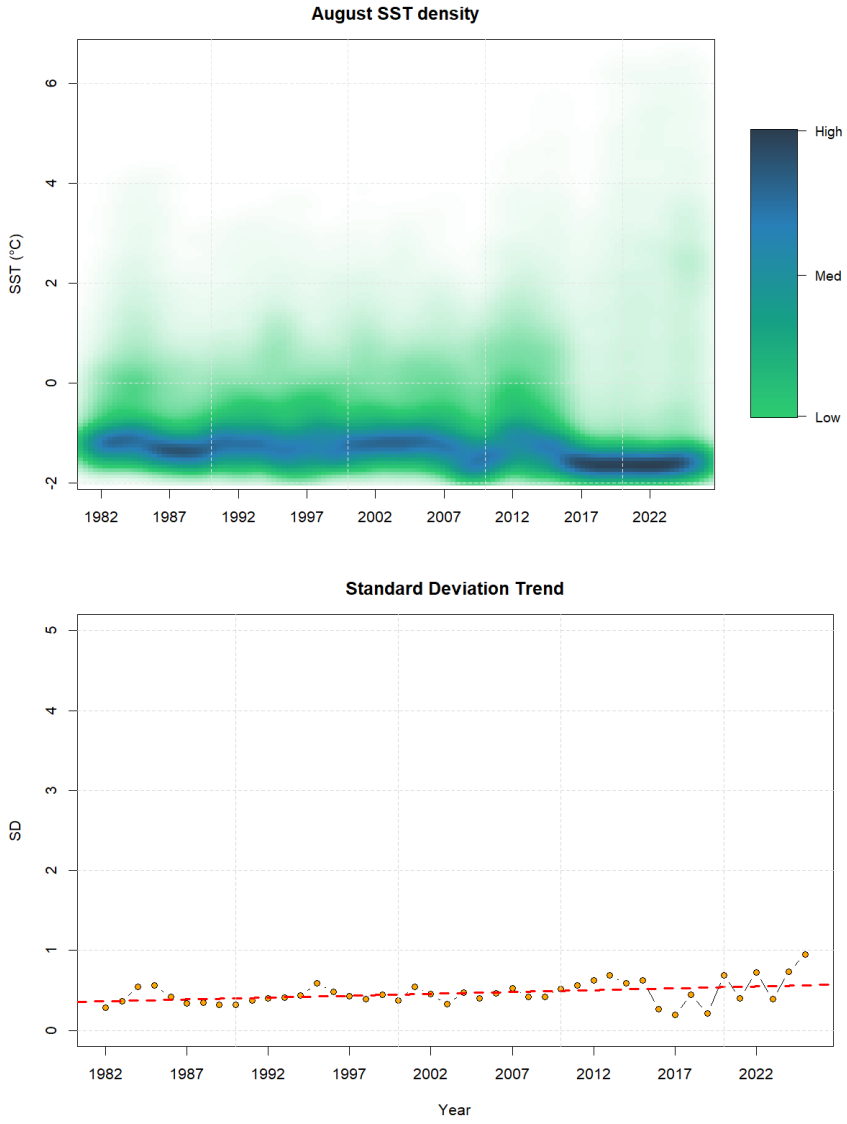

Figure 2.7: *Arctic Ocean (panel 10, Figure 2.1). Top: density distribution of annual August mean SST values across all individual grid points of the study area. Bottom: interannual standard deviation (dashed line with markers), together with its growth trend (dashed red line).*

References

1. North, G. & Kim, K. *Energy balance climate models* doi:10.1002/9783527698844 (John Wiley & Sons, Weinheim, 2017).
2. Budyko, M. The effect of solar radiation variations on the climate of the earth. *Tellus* **21,** 611–619. doi:10.1111/j.2153-3490.1969.tb00466.x (1969).
3. Sellers, W. A global climatic model based on the energy balance of the earth-atmosphere system. *Journal of Applied Meteorology and Climatology* **8,** 392–400. doi:10.1175/1520-0450(1969)008<0392:AGCMBO>2.0.CO;2 (1969).
4. Ghil, M. Climate stability for a sellers-type model. *Journal of Atmospheric Sciences* **33,** 3–20. doi:10.1175/1520-0469(1976)033<0003:CSFAST>2.0.CO;2 (1976).
5. North, G. *et al.* Energy balance climate models. *Reviews of Geophysics* **19,** 91–121. doi:10.1029/RG019i001p00091 (1981).
6. Van de Wal, R. & Oerlemans, J. An energy balance model for the greenland ice sheet. *Global and Planetary Change* **9,** 115–131. doi:10.1016/0921-8181(94)90011-6 (1994).
7. Dortmans, B. *et al.* An energy balance model for paleoclimate transitions. *Climate of the Past* **15,** 493–520. doi:10.5194/cp-15-493-2019 (2019).
8. Goodwin, P. & Williams, R. On the arctic amplification of surface warming in a conceptual climate model. *Physica D: Nonlinear Phenomena* **454,** 133880. doi:10.1016/j.physd.2023.133880 (2023).
9. Rose, B. & Marshall, J. Ocean heat transport, sea ice, and multiple climate states: Insights from energy balance models. *Journal of the Atmospheric Sciences* **66,** 2828–2843. doi:10.1175/2009JAS3039.1 (2009).
10. Eisenman, I. & Wettlaufer, J. S. Nonlinear threshold behavior during the loss of arctic sea ice. *Proceedings of the National Academy of Sciences* **106,** 28–32. doi:10.1073/pnas.0806887106 (2009).
11. Del Sarto, G. *et al.* Variational techniques for a one-dimensional energy balance model. *Nonlinear Processes in Geophysics* **31,** 137–150. doi:10.5194/npg-31-137-2024 (2024).
12. Bastiaansen, R. *et al.* Fragmented tipping in a spatially heterogeneous world. *Environmental Research Letters* **17,** 045006. doi:10.1088/1748-9326/ac59a8 (Mar. 2022).

13. Rombouts, J. & Ghil, M. Oscillations in a simple climate–vegetation model. *Nonlinear Processes in Geophysics* **22,** 275–288. doi:10.5194/npg-22-275-2015 (2015).
14. Eisenman, I. Factors controlling the bifurcation structure of sea ice retreat. *Journal of Geophysical Research: Atmospheres* **117,** D01111. doi:10.1029/2011JD016164 (2012).
15. Díaz, J. I. in *The mathematics of models for climatology and environment* (ed Díaz, J. I.) 217–251 (Springer, Berlin, 1997). doi:10.1007/978-3-642-60603-8_6.
16. Karatzas, I. & Shreve, S. *Brownian motion and stochastic calculus* second. doi:10.1007/978-1-4612-0949-2 (Springer-Verlag, New York, 1991).
17. Ikeda, N. & Watanabe, S. *Stochastic differential equations and diffusion processes* (North-Holland Publishing Co. / Kodansha, Ltd., Amsterdam-New York / Tokyo, 1981).
18. Twardowska, K. Wong-Zakai approximations for stochastic differential equations. *Acta Applicandae Mathematicae* **43,** 317–359. doi:10.1007/BF00047670 (1996).
19. Särkkä, S. & Solin, A. *Applied stochastic differential equations* doi:10.1017/9781108186735 (Cambridge University Press, Cambridge, 2019).
20. Hasselmann, K. Stochastic climate models part I. Theory. *Tellus* **28,** 473–485. doi:10.1111/j.2153-3490.1976.tb00696.x (1976).
21. Da Prato, G. & Zabczyk, J. *Stochastic equations in infinite dimensions* second edition. doi:10.1017/CBO9781107295513 (Cambridge University Press, Cambridge, 2014).
22. Quarteroni, A. *Numerical models for differential problems* third. doi:10.1007/978-3-319-49316-9 (Springer, Cham, 2017).
23. LeVeque, R. J. *Finite difference methods for ordinary and partial differential equations* doi:10.1137/1.9780898717839 (SIAM, Philadelphia, 2007).
24. Plemmons, R. J. M-matrix characterizations. I. Nonsingular M-matrices. *Linear Algebra and its Applications* **18,** 175–188. doi:10.1016/0024-3795(77)90073-8 (1977).
25. Berman, A. & Plemmons, R. J. *Nonnegative matrices in the mathematical sciences* doi:10.1137/1.9781611971262 (SIAM, Philadelphia, 1994).
26. Evans, L. C. *Partial differential equations* second (American Mathematical Society, Providence, RI, 2010).

27. Timmermans, M. & Labe, Z. *Sea Surface Temperature* NOAA Technical Report OAR ARC 23-07. In: Arctic Report Card 2023 (National Oceanic and Atmospheric Administration (NOAA), 2023). doi:10.25923/e8jc-f342.

28. Serreze, M. & Barry, R. Processes and impacts of arctic amplification: A research synthesis. *Global and Planetary Change* **77,** 85–96. doi:10.1016/j.gloplacha.2011.03.004 (2011).

29. Goosse, H. *et al.* Increased variability of the Arctic summer ice extent in a warmer climate. *Geophysical Research Letters* **36,** L23702. doi:10.1029/2009GL040546 (2009).

30. Carvalho, K. & Wang, S. Sea surface temperature variability in the Arctic Ocean and its marginal seas in a changing climate: Patterns and mechanisms. *Global and Planetary Change* **193,** 103265. doi:10.1016/j.gloplacha.2020.103265 (2020).

31. Landrum, L. & Holland, M. M. Extremes become routine in an emerging new Arctic. *Nature Climate Change* **10,** 1108–1115. doi:10.1038/s41558-020-0892-z (2020).

32. Alexander, M. A. *et al.* Projected sea surface temperatures over the 21st century: Changes in the mean, variability and extremes for large marine ecosystem regions of Northern Oceans. *Elementa: Science of the Anthropocene* **6,** 9. doi:10.1525/elementa.191 (2018).

33. Barber, D. *et al.* Perennial pack ice in the southern Beaufort Sea was not as it appeared in the summer of 2009. *Geophysical Research Letters* **36,** L24501. doi:10.1029/2009GL041434 (2009).

34. Strong, C. & Rigor, I. Arctic marginal ice zone trending wider in summer and narrower in winter. *Geophysical Research Letters* **40,** 4864–4868. doi:10.1002/grl.50928 (2013).

35. Timmermans, M.-L. The impact of stored solar heat on Arctic sea ice growth. *Geophysical Research Letters* **42,** 6399–6406. doi:10.1002/2015GL064541 (2015).

36. Huang, B. *et al.* Improvements of the Daily Optimum Interpolation Sea Surface Temperature (DOISST) Version 2.1. *Journal of Climate* **34,** 2923–2939. doi:10.1175/JCLI-D-20-0166.1 (2021).

37. Shabanov, P. *et al.* Decline in Ice Coverage and Ice-Free Period Extension in the Kara and Laptev Seas during 1979–2022. *Remote Sensing* **16,** 1875. doi:10.3390/rs16111875 (2024).

Chapter 3



Temperature-velocity model: boundary noise

This chapter is extensively based on the following publication:
Del Sarto G., Lenzi M., (2026) Global well-posedness for small data in a 3D temperature-velocity model with Dirichlet boundary noise.
https://doi.org/10.1214/26-EJP1522

3 TEMPERATURE-VELOCITY MODEL: BOUNDARY NOISE

This chapter is organised as follows. In Section 3.1 we introduce the notation which will be used throughout the chapter. In Section 3.2 we describe our approach to solving the coupled velocity–temperature problem, the object of this work, and present the main results of our research. In Section 3.3, we present the analysis of the temperature problem, assuming a given velocity field with specified regularity. The strategy is to split the problem into a linear system with non-homogeneous Dirichlet boundary noise, and the remainder system. In Section 3.4, we analyse the velocity system, subject to a prescribed temperature forcing of specified regularity. In particular, we show that the weak Stokes operator admits a bounded $\mathcal{H}^\infty$-calculus and enjoys maximal regularity. We then apply these results to prove a global well-posedness result for small data for our 3D Navier–Stokes equation. Lastly, Section 3.5 is entirely devoted to the proof of the main theorem.

3.1 NOTATIONS AND FUNCTIONAL SETTING

We work on a complete filtered probability space $(\Omega, \mathcal{F}, (\mathcal{F}_t)_t, \mathbb{P})$. A stochastic process Φ, taking values in a measurable space, is adapted if Φ_t is $\mathcal{F}_t$-measurable for any $t \geq 0$. It is progressively measurable if the map $(s, \omega) \mapsto \Phi_s(\omega)$ is measurable on $([0,t] \times \Omega, \mathcal{B}(0,t) \otimes \mathcal{F}_t)$ for every $t \geq 0$, with $\mathcal{B}(0,t)$ being the Borel σ-algebra on $[0,t]$.

Let $\mathcal{D} \subset \mathbb{R}^3$ be a bounded, open domain (i.e. non-empty, connected set) with smooth boundary. We denote by $(W_t)_t$ a $\mathcal{Q}$-Wiener process on $L^2(\partial\mathcal{D})$ defined on $(\Omega, \mathcal{F}, (\mathcal{F}_t)_t, \mathbb{P})$, and represented by

$$W(t,x) = \sum_{k \geq 0} \lambda_k e_k(x) \beta_k(t), \quad t \geq 0,\ x \in \partial\mathcal{D}$$

where $(e_k)_k \subset L^2(\partial\mathcal{D})$ is an orthonormal basis of $L^2(\partial\mathcal{D})$, $(\beta_k(t))_k$ are independent Brownian motions, and $(\lambda_k)_k$ are the non-negative square roots of the eigenvalues of the covariance operator $\mathcal{Q}$. For further details, we refer to [1].

To handle the stochastic forcing on the boundary, we employ the *Dirichlet map* D, following the approach of [2]. It is defined as the linear map

$$D\colon L^2(\partial\mathcal{D}) \to L^2(\mathcal{D}), \quad Dh := u,$$

where u denotes the unique weak solution to the Dirichlet problem

$$\begin{cases} \Delta u = 0, & x \in \mathcal{D}, \\ u|_{\partial\mathcal{D}} = h, & x \in \partial\mathcal{D}. \end{cases}$$

Regarding the functional setting, for $s \in \mathbb{R}$ and $p \in (1,\infty)$, we denote by $W^{s,p}(\mathcal{D})$ the fractional Sobolev space and by $H^{s,p}(\mathcal{D})$ the Bessel potential space. In particular, we set $H^{0,p}(\mathcal{D}) = L^p(\mathcal{D})$, and write $H^s(\mathcal{D}) = H^{s,2}(\mathcal{D})$. Note that $H^{s,p}(\mathcal{D}) = W^{s,p}(\mathcal{D})$ for any $s \in \mathbb{N}$.

We denote by

$$\Delta\colon H^{2,2}(\mathcal{D}) \cap H_0^{1,2}(\mathcal{D}) \subset L^2(\mathcal{D}) \to L^2(\mathcal{D})$$

the Dirichlet Laplacian, and we consider the fractional powers $(-\Delta)^\alpha$, for any $\alpha \in (0,1)$. Their domains are given by

$$D((-\Delta)^\alpha) := {}_0H^{2\alpha}(\mathcal{D}) := \begin{cases} H^{2\alpha}(\mathcal{D}), & 0 < \alpha < \dfrac{1}{4}, \\ H_{00}^{\frac{1}{2}}(\mathcal{D}), & \alpha = \dfrac{1}{4}, \\ H_0^{2\alpha}(\mathcal{D}), & \dfrac{1}{4} < \alpha \leq \dfrac{1}{2}, \\ H^{2\alpha}(\mathcal{D}) \cap H_0^1(\mathcal{D}), & \dfrac{1}{2} < \alpha < 1, \end{cases}$$

where $H_{00}^{\frac{1}{2}}(\mathcal{D})$ consists of all $u \in H^{\frac{1}{2}}(\mathcal{D})$ such that

$$\int_{\mathcal{D}} \rho(x)^{-1} |u(x)|^2 \, dx < \infty,$$

with $\rho(x)$ being any C^∞ function comparable to $dist(x, \partial\mathcal{D})$; see [3, 4] for more details on the domain of the fractional powers of the Dirichlet Laplacian.

We define the space of solenoidal (divergence-free) square-integrable vector fields by

$$L^2_\sigma(\mathcal{D}) = \overline{\{u \in C_c^\infty(\mathcal{D};\mathbb{R}^3) \ : \ \mathrm{div}(u) = 0 \text{ in } \mathcal{D}\}}^{\|\cdot\|_{L^2(\mathcal{D})}}.$$

The space $L^2(\mathcal{D})$ can be decomposed as

$$L^2(\mathcal{D}) = L^2_\sigma(\mathcal{D}) \oplus G_2(\mathcal{D}),$$

where $G_2(\mathcal{D}) := \left\{ u \in L^2(\mathcal{D}) \ : \ u = \nabla \pi, \text{ for some } \pi \in H^{1,2}_{loc}(\mathcal{D}) \right\}$, and there exists a unique projection $P \colon L^2(\mathcal{D}) \to L^2_\sigma(\mathcal{D})$ called the *Helmholtz projection* in $L^2(\mathcal{D})$. We denote by A the Stokes operator with Dirichlet boundary conditions, defined by

$$Au := -P\Delta u, \quad D(A) := H^{2,2}(\mathcal{D}) \cap H^{1,2}_0(\mathcal{D}) \cap L^2_\sigma(\mathcal{D}).$$

In the Hilbert space $X_0 = L^2_\sigma(\mathcal{D})$, the Stokes operator A is a non-negative, self-adjoint operator with compact inverse; see, for instance, [5, Section 2]. In particular, A is sectorial of angle 0 and $-A$ generates a bounded analytic C_0-semigroup on X_0; see, for example, [6, 7]. Moreover, since A is a non-negative self-adjoint operator on a Hilbert space, it admits a bounded $\mathcal{H}^\infty$-functional calculus of angle 0; see [8, Chapters 2 and 7]. In the specific case of the Stokes operator, the domains of the fractional powers A^α in $L^2_\sigma(\mathcal{D})$ have been identified in [9] and are given by

$$D(A^\alpha) = {}_0H^{2\alpha}(\mathcal{D}) \cap L^2_\sigma(\mathcal{D}), \qquad \alpha \in (0,1).$$

For notational convenience, we introduce the following spaces:

$$H^s_\sigma(\mathcal{D}) = H^s(\mathcal{D}) \cap L^2_\sigma(\mathcal{D}), \quad {}_0H^s_\sigma(\mathcal{D}) = {}_0H^s(\mathcal{D}) \cap L^2_\sigma(\mathcal{D}), \quad s \geq 0,$$

and, by duality

$$H^{-s}_\sigma(\mathcal{D}) = \left(H^s(\mathcal{D}) \cap L^2_\sigma(\mathcal{D})\right)', \quad {}_0H^{-s}_\sigma(\mathcal{D}) = \left({}_0H^s(\mathcal{D}) \cap L^2_\sigma(\mathcal{D})\right)', \quad s > 0.$$

We will work with an extension of the classical Stokes operator to a weaker setting, which we denote by A_w. Specifically, for any sufficiently small $\delta_u > 0$, we define the *weak Stokes operator* by

$$\begin{aligned} A_w \colon {}_0H^{\frac{3}{2}-\delta_u}_\sigma(\mathcal{D}) &\to {}_0H^{-\frac{1}{2}-\delta_u}_\sigma(\mathcal{D}) \\ \langle A_w u, v \rangle &:= \langle \nabla u, \nabla v \rangle_{H^{\frac{1}{2}-\delta_u}, H^{-\frac{1}{2}+\delta_u}}, \end{aligned} \tag{3.1}$$

for all pairs $(u,v) \in {}_0H^{\frac{3}{2}-\delta_u}_\sigma(\mathcal{D}) \times {}_0H^{\frac{1}{2}+\delta_u}_\sigma(\mathcal{D})$. Here, $\langle \cdot, \cdot \rangle_{H^{\frac{1}{2}-\delta_u}, H^{-\frac{1}{2}+\delta_u}}$ denotes the duality pairing between $H^{\frac{1}{2}-\delta_u}(\mathcal{D})$ and $H^{-\frac{1}{2}+\delta_u}(\mathcal{D})$.

Lastly, given a final time $T > 0$ and $p \in (1, \infty)$, we set

$$\mathbb{E}^{\delta_u}_{t,p} := W^{1,p}(0,t; {}_0H^{-\frac{1}{2}-\delta_u}_\sigma(\mathcal{D})) \cap L^p(0,t; {}_0H^{\frac{3}{2}-\delta_u}_\sigma(\mathcal{D})),$$

for any $t \in [0,T]$. This space will be the maximal regularity space on which the velocity of our model evolves. Additionally, we define the real interpolation space

$$V^{\delta_u}_p = \left({}_0H^{-\frac{1}{2}-\delta_u}_\sigma(\mathcal{D}), {}_0H^{\frac{3}{2}-\delta_u}_\sigma(\mathcal{D}) \right)_{1-\frac{1}{p},p}.$$

For more information on these function spaces, we refer the reader to [3, 4, 10].

3.2 Preliminaries and main results

For the reader's convenience, we recall here what was already presented in the introduction, namely the system under study, the approach we adopt, and the results obtained.

Let $\mathcal{D} \subset \mathbb{R}^3$ be a bounded, open domain (i.e. non-empty, connected set) with smooth boundary $\partial\mathcal{D}$, and let $T > 0$ be a fixed final time. We study the coupled velocity-temperature system for an incompressible fluid in $\mathcal{D}$, modelled by Navier-Stokes equations with thermal advection-diffusion, and perturbed by Dirichlet boundary noise. Concretely, for each $\varepsilon > 0$ we consider

$$\begin{cases} \partial_t u^\varepsilon + u^\varepsilon \cdot \nabla u^\varepsilon + \nabla p^\varepsilon - \Delta u^\varepsilon = -\theta^\varepsilon e_3, & \text{in } \mathcal{D}\times(0,T), \\ \operatorname{div}(u^\varepsilon) = 0, & \text{in } \mathcal{D}\times(0,T), \\ u^\varepsilon|_{\partial\mathcal{D}} = 0, & \text{in } \partial\mathcal{D}\times(0,T), \\ \partial_t \theta^\varepsilon + u^\varepsilon \cdot \nabla \theta^\varepsilon - \Delta \theta^\varepsilon = 0, & \text{in } \mathcal{D}\times(0,T), \\ \theta^\varepsilon_{|\partial\mathcal{D}} = \sqrt{\varepsilon}\,\dfrac{dW}{dt}, & \text{in } \partial\mathcal{D}\times(0,T), \\ u^\varepsilon|_{t=0} = u_0, \quad \theta^\varepsilon|_{t=0} = \theta_0. \end{cases} \tag{3.2}$$

where $u^\varepsilon \colon \mathcal{D}\times(0,T) \to \mathbb{R}^3$ is the fluid velocity, $\theta^\varepsilon \colon \mathcal{D}\times(0,T) \to \mathbb{R}$ is the temperature field, $p^\varepsilon \colon \mathcal{D}\times(0,T) \to \mathbb{R}$ is the pressure, $e_3 = (0,0,1)^T$, and $(W_t)_{t\geq 0}$ is a $\mathcal{Q}$-Wiener process acting only on the boundary with intensity which scales depending on the parameter ε.

We decouple the model (3.2) into a system for temperature only, given a prescribed fluid velocity, and a system for velocity only, given a prescribed temperature. Namely, we study first the equation for the temperature $\theta^\varepsilon \colon \mathcal{D}\times(0,T) \to \mathbb{R}$, which reads as

$$\begin{cases} \partial_t \theta^\varepsilon + u \cdot \nabla \theta^\varepsilon - \Delta \theta^\varepsilon = 0, & \text{in } \mathcal{D}\times(0,T), \\ \theta^\varepsilon|_{\partial\mathcal{D}} = \sqrt{\varepsilon}\dfrac{dW}{dt}, & \text{in } \partial\mathcal{D}\times(0,T), \\ \theta^\varepsilon|_{t=0} = \theta_0, & \text{in } \mathcal{D}. \end{cases} \tag{3.3}$$

Here, $u \colon \mathcal{D}\times(0,T) \to \mathbb{R}^3$ is a given velocity and θ_0 is the initial condition. Second, we study the 3D Navier-Stokes equations for the velocity $u \colon \mathcal{D}\times(0,T) \to \mathbb{R}^3$ given by

$$\begin{cases} \partial_t u + u \cdot \nabla u + \nabla p - \Delta u = f^\theta, & \text{in } \mathcal{D}\times(0,T), \\ \operatorname{div}(u) = 0, & \text{in } \mathcal{D}\times(0,T), \\ u|_{\partial\mathcal{D}} = 0, & \text{in } \partial\mathcal{D}\times(0,T), \\ u|_{t=0} = u_0, & \text{in } \mathcal{D}. \end{cases} \tag{3.4}$$

Here, $f^\theta \colon \mathcal{D}\times(0,T) \to \mathbb{R}^3$ is a prescribed forcing, $p \colon \mathcal{D}\times(0,T) \to \mathbb{R}$ is the pressure, and u_0 denotes the initial condition.

Then, we split the analysis of (3.3) into two problems, corresponding to the decomposition $\theta_t^\varepsilon = Z_t^\varepsilon + \zeta_t^\varepsilon$. The first term Z_t^ε corresponds to the stochastic linear problem with non-homogeneous Dirichlet boundary conditions given by

$$\begin{cases} \partial_t Z^\varepsilon = \Delta Z^\varepsilon, & \text{in } \mathcal{D}\times(0,T), \\ Z^\varepsilon|_{\partial\mathcal{D}} = \sqrt{\varepsilon}\dfrac{dW}{dt}, & \text{in } \partial\mathcal{D}\times(0,T), \\ Z^\varepsilon|_{t=0} = 0, & \text{in } \mathcal{D}. \end{cases} \tag{3.5}$$

The solution of the previous equation can be interpreted in mild form. Next, we consider the remainder $\zeta_t^\varepsilon := \theta_t^\varepsilon - Z_t^\varepsilon$, which satisfies

$$\begin{cases} \partial_t \zeta^\varepsilon + u\cdot\nabla\zeta^\varepsilon + u\cdot\nabla Z^\varepsilon - \Delta\zeta^\varepsilon = 0, & \text{in } \mathcal{D}\times(0,T), \\ \zeta^\varepsilon|_{\partial\mathcal{D}} = 0, & \text{in } \partial\mathcal{D}\times(0,T), \\ \zeta^\varepsilon|_{t=0} = \theta_0, & \text{in } \mathcal{D}. \end{cases} \tag{3.6}$$

Here, we interpret again the solution $\zeta^\varepsilon\colon \mathcal{D}\times(0,T)\to\mathbb{R}$ in the mild form, namely

$$\zeta_t^\varepsilon = e^{t\Delta}\theta_0 - \int_0^t e^{(t-r)\Delta}\,(u_r\cdot\nabla\zeta_r^\varepsilon)\,dr - \int_0^t e^{(t-r)\Delta}\,(u_r\cdot\nabla Z_r^\varepsilon)\,dr.$$

We continue this section by describing the solution of the linear temperature problem associated to (3.3), i.e. by recalling the following result concerning the mild solution of (3.5), which follows from [2] and the factorisation trick for the stochastic convolution [1, Section 5.3.1].

Proposition 3.1. *For any $\delta_\theta > 0$, fix*

$$\alpha_\theta = \frac{1}{4} + \frac{\delta_\theta}{2}, \quad \beta_\theta = \frac{1}{4} - \frac{\delta_\theta}{4}.$$

Assume that

$$\sum_k \lambda_k^2 \left\| (-\Delta)^{\beta_\theta} D e_k \right\|_2^2 < \infty. \tag{3.7}$$

The following holds.

(i) The process $Z_t^\varepsilon = -\sqrt{\varepsilon}\int_0^t \Delta e^{(t-r)\Delta} D\,dW_r$ is the unique $(\mathcal{F}_t)_t$-adapted mild solution of (3.5), and takes values in $H^{-2\alpha_\theta}(\mathcal{D})$.

(ii) The process

$$\xi_t^\varepsilon := (-\Delta)^{-\alpha_\theta} Z_t^\varepsilon = \sqrt{\varepsilon}\int_0^t (-\Delta)^{1-\alpha_\theta} e^{(t-r)\Delta} D\,dW_r, \tag{3.8}$$

has a continuous version in $L^2(\mathcal{D})$ and Z^ε has a continuous version in $H^{-2\alpha_\theta}(\mathcal{D})$.

(iii) Let $T > 0$. For any $\vartheta > 0$, there exists a positive constant $C = C(\delta_\theta, T)$ such that

$$\mathbb{P}\left(\sup_{0\le t\le T}\|Z_t^\varepsilon\|_{H^{-2\alpha_\theta}(\mathcal{D})} > \vartheta\right) \le \frac{\varepsilon}{\vartheta^2} C \sum_k \lambda_k^2 \left\|(-\Delta)^{\beta_\theta} De_k\right\|_2^2.$$

We remark that point (iii) of the previous result is key since it controls, depending on the noise intensity $\sqrt{\varepsilon}$, the probability of the sup norm of Z_t^ε to be small in an appropriate Bessel potential space.

Now, let $p > 4$ and $s \in (0, \frac{1}{2})$. Choose

$$\gamma := \frac{1}{4} + \varepsilon_\gamma, \qquad 0 < \varepsilon_\gamma < \min\left\{\frac{1-2s}{4},\ \frac{(1-2s)(p-4)}{4p}\right\}, \tag{3.9}$$

and set $a(s,\gamma) := \frac{1}{2} + \gamma + \frac{s}{2}$ and $\lambda_{\max} := p(1 - a(s,\gamma))$. Then

$$a(s,\gamma) = \frac{3}{4} + \frac{s}{2} + \varepsilon_\gamma < 1 \quad \text{(since } \varepsilon_\gamma < \tfrac{1-2s}{4}\text{)},$$

and, using $1 - a(s,\gamma) = \frac{1-2s}{4} - \varepsilon_\gamma$,

$$\lambda_{\max} - \left(\frac{1}{2} - s\right) = p\left(\frac{1-2s}{4} - \varepsilon_\gamma\right) - \frac{1-2s}{2} = \frac{(1-2s)(p-2)}{4} - p\varepsilon_\gamma > 0, \tag{3.10}$$

so $\lambda_{\max} > \frac{1}{2} - s$. Moreover,

$$\lambda_{\max} - (1-2s) = p\left(\frac{1-2s}{4} - \varepsilon_\gamma\right) - (1-2s) = \frac{(1-2s)(p-4)}{4} - p\varepsilon_\gamma > 0, \tag{3.11}$$

by (3.9). Hence the interval $(0, \min\{2s,\ \lambda_{\max} - (1-2s)\})$ is non-empty, and we may choose

$$\lambda := \left(\frac{1}{2} - s\right) + \varepsilon_\lambda, \qquad 0 < \varepsilon_\lambda < \min\left\{2s, \lambda_{\max} - (1-2s)\right\}. \tag{3.12}$$

In particular, $\lambda < \frac{1}{2} + s < 1$ (since $\varepsilon_\lambda < 2s$). Finally, define the thresholds

$$\bar\delta_\theta := \min\left\{\lambda, 2\gamma - \frac{1}{2}\right\}, \qquad \bar\delta_u := \min\left\{\lambda_{\max} - \lambda, 1 - \lambda\right\}. \tag{3.13}$$

The first main result concerns the well-posedness of the system (3.6).

Theorem 3.1. *Let $T > 0$, $s \in (0, \frac{1}{2})$ and $p > 4$, and choose γ, λ as in* (3.9) *and* (3.12). *Let $\bar\delta_\theta(s,p)$ and $\bar\delta_u(s,p)$ be given by* (3.13). *Then for every*

$$0 < \delta_\theta < \bar\delta_\theta(s,p), \qquad 0 < \delta_u < \bar\delta_u(s,p),$$

the following holds. Set

$$\alpha_\theta = \frac{1}{4} + \frac{\delta_\theta}{2}, \qquad \beta_\theta = \frac{1}{4} - \frac{\delta_\theta}{4},$$

and let $Z_t^\varepsilon = -\sqrt{\varepsilon}\int_0^t \Delta e^{(t-r)\Delta} D\, dW_r$ *be the continuous version in* $H^{-2\alpha_\theta}(\mathcal{D})$ *from Proposition 3.1. Then, for every divergence-free velocity field*

$$u \in L^p\big(0,T;{}_0H_\sigma^{\frac{3}{2}-\delta_u}(\mathcal{D})\big) \cap L^\infty\big(0,T;{}_0H_\sigma^{\frac{1}{2}-\delta_u}(\mathcal{D})\big)$$

and every initial datum $\theta_0 \in W^{s,6/5}(\mathcal{D})$*, there exists a unique mild solution* ζ^ε *of* (3.6) *of the form*

$$\zeta_t^\varepsilon = e^{t\Delta}\theta_0 - \int_0^t e^{(t-r)\Delta}\big(u_r\cdot\nabla\zeta_r^\varepsilon\big)\,dr - \int_0^t e^{(t-r)\Delta}\big(u_r\cdot\nabla Z_r^\varepsilon\big)\,dr,$$

with trajectories in

$$\zeta^\varepsilon \in C(0,T;W^{s,6/5}(\mathcal{D})) \qquad \mathbb{P}\text{-a.s.}$$

A straightforward but important consequence of the proof of the previous result is the following estimate.

Corollary 3.1. *Under the assumptions of Theorem 3.1, let* $\zeta \in C(0,T;W^{s,\frac{6}{5}}(\mathcal{D}))$ *and define*

$$\tilde\zeta_t := e^{t\Delta}\theta_0 - \int_0^t e^{(t-r)\Delta}\,(u_r\cdot\nabla\zeta_r)\,dr - \int_0^t e^{(t-r)\Delta}\,(u_r\cdot\nabla Z_r^\varepsilon)\,dr,$$

Then, for any $0<\lambda<1-\delta_u$*, it holds*

$$\begin{aligned}\left\|\tilde\zeta\right\|_{C(0,T;W^{s,\frac{6}{5}}(\mathcal{D}))} &\le \left\|e^{t\Delta}\theta_0\right\|_{C(0,T;W^{s,\frac{6}{5}}(\mathcal{D}))}\\ &\quad + C\,\|u\|_{L^{\frac{p}{\lambda+\delta_u}}(0,T;W^{\frac{1}{2}+\lambda,2}(\mathcal{D}))}\Big(\|\zeta\|_{C(0,T;W^{s,\frac{6}{5}}(\mathcal{D}))} + \|\xi^\varepsilon\|_{C(0,T;L^2(\mathcal{D}))}\Big),\end{aligned} \tag{3.14}$$

where $C = C(p,\lambda,\delta_u,\delta_\theta,s,T) > 0$*.*

So far, in Proposition 3.1, Theorem 3.1, and Corollary 3.1, we have investigated the well-posedness of the temperature equation (3.3). Moreover, we can control the norm of its solution $\theta^\varepsilon = Z^\varepsilon + \zeta^\varepsilon$ with high probability depending on ε, since we are able to estimate the norms of Z^ε (by Proposition 3.1) and ζ^ε (by Corollary 3.1).

We now turn to the analysis of the 3D Navier-Stokes equations (3.4), assuming that f^θ is a prescribed forcing term. In the classical

energy setting one typically assumes $f^\theta \in L^2(0,T;L^2(\mathcal{D}))$ and $u_0 \in H^1(\mathcal{D})$.

In our coupled model the forcing is of buoyancy type, $f^\theta = -\theta^\varepsilon e_3$, and the temperature is decomposed as $\theta^\varepsilon = Z^\varepsilon + \zeta^\varepsilon$. The noise component Z^ε is, in general, only continuous in time with values in $H^{-\frac{1}{2}-\delta_\theta}(\mathcal{D})$, for any $\delta_\theta > 0$ compatible with the covariance summability condition (3.7); the remainder ζ^ε is controlled in $W^{s,6/5}(\mathcal{D})$. We therefore work in the ambient space $H^{-\frac{1}{2}-\delta_u}(\mathcal{D})$ for the Stokes/Navier-Stokes maximal regularity theory, choosing δ_u so that

$$\delta_u \geq \max\{\delta_\theta,\ \tfrac{1}{2} - s\},$$

which ensures that both Z^ε and ζ^ε can be interpreted as forcing terms in $H^{-\frac{1}{2}-\delta_u}(\mathcal{D})$. Accordingly, we formulate the Navier-Stokes well-posedness result for general forcing

$$f^\theta \in L^p(0,T;H^{-\frac{1}{2}-\delta_u}(\mathcal{D})), \quad p > \frac{2}{1-\delta_u},$$

which is the natural class arising from the maximal regularity framework in the low-regularity setting.

The notion of solution considered for the 3D Navier-Stokes problem (3.4) is the one of mild solution in the weak setting determined by the weak Stokes operator A_w. We now formalise this notion.

Definition 3.1. A function u is a solution of the 3D Navier-Stokes equations (3.4) on the time interval $[0,T]$ if

$$u_t = e^{-tA_w}u_0 + \int_0^t e^{-(t-r)A_w} P\left(-u_r \cdot \nabla u_r + f_r^\theta\right) dr, \tag{3.15}$$

for any $0 \leq t \leq T$, and possesses the regularity

$$u \in \mathbb{E}_{T,p}^{\delta_u} = W^{1,p}(0,T;{}_0H_\sigma^{-\frac{1}{2}-\delta_u}(\mathcal{D})) \cap L^p(0,T;{}_0H_\sigma^{\frac{3}{2}-\delta_u}(\mathcal{D})).$$

Here, and throughout the rest of the work, P denotes the Helmholtz projection, defined by interpolation from $H^{-\frac{1}{2}-\delta_u}(\mathcal{D})$ to $H_\sigma^{-\frac{1}{2}-\delta_u}(\mathcal{D})$. The global existence results for the velocity problem read as follows.

Theorem 3.2 (Global well-posedness for small data)**.** *Let $\delta_u \in (0,1)$, $f^\theta \in L^p(0,T;H^{-\frac{1}{2}-\delta_u}(\mathcal{D}))$, with $p > \frac{2}{1-\delta_u}$, and $u_0 \in V_p^{\delta_u}$. There exist $\tilde\eta = \tilde\eta(p,\delta_u,T) > 0$ and $M = M(p,\delta_u,T) > 0$ such that if $\eta \in (0,\tilde\eta)$ and*

$$\max\left(\|u_0\|_{V_p^{\delta_u}}, \left\|f^\theta\right\|_{L^p(0,T;H^{-\frac{1}{2}-\delta_u}(\mathcal{D}))}\right) \leq \frac{\eta}{4M},$$

then there exists a unique solution $u \in \mathbb{E}_{T,p}^{\delta_u}$ with $\|u\|_{\mathbb{E}_{T,p}^{\delta_u}} \leq \eta$ of the 3D Navier-Stokes equation (3.4) *in the sense of Definition 3.1.*

Remark 3.1. *Note that Definition 3.1 is well-posed due to the fact that, as will be demonstrated in Section 3.4.1, the operator A_w admits a bounded $\mathcal{H}^\infty$-calculus on ${}_0H_\sigma^{-\frac{1}{2}-\delta_u}(\mathcal{D})$. Thus, the operator $-A_w$ generates an analytic semigroup on ${}_0H_\sigma^{-\frac{1}{2}-\delta_u}(\mathcal{D})$, ensuring that the variation of constants formula* (3.15) *is meaningful, thanks also to the estimate of the convective term*

$$\|P(u\cdot\nabla u)\|_{L^p(0,T;{}_0H_\sigma^{-\frac{1}{2}-\delta_u}(\mathcal{D}))}\lesssim \|u\|^2_{\mathbb{E}^{\delta_u}_{T,p}},$$

which will be proved in Lemma 3.3.

We now shift our focus to the fully coupled velocity-temperature system (3.2). The corresponding notion of solution is introduced below.

Definition 3.2. The triple $(u^\varepsilon,\theta^\varepsilon,\tau^\varepsilon)$ is a *solution* of (3.2) on $[0,T]$ if $\tau^\varepsilon\colon\Omega\to[0,T]$ is a stopping time and $(u^\varepsilon,\theta^\varepsilon)$ is a stochastic process with trajectories $\mathbb{P}$-a.s. in

$$\mathbb{E}^{\delta_u}_{\tau^\varepsilon,p}\times C\big(0,\tau^\varepsilon;H^{-\frac{1}{2}-\delta_u}(\mathcal{D})\big),$$

where u^ε is adapted to $(\mathcal{F}_t)_t$ as a process in ${}_0H_\sigma^{-\frac{1}{2}-\delta_u}(\mathcal{D})$, and progressively measurable as a process in ${}_0H_\sigma^{\frac{3}{2}-\delta_u}(\mathcal{D})$, while θ^ε is adapted as a process in $H^{-\frac{1}{2}-\delta_u}(\mathcal{D})$, and, for any $0\le t\le\tau^\varepsilon$, it holds

$$\begin{aligned}
u^\varepsilon_t &= e^{-tA_w}u_0+\int_0^t e^{-(t-r)A_w}P\left(-u^\varepsilon_r\cdot\nabla u^\varepsilon_r-\theta^\varepsilon_r e_3\right)dr,\\
\theta^\varepsilon_t &= \zeta^\varepsilon_t+Z^\varepsilon_t,\\
\zeta^\varepsilon_t &= e^{t\Delta}\theta_0-\int_0^t e^{(t-r)\Delta}\left(u^\varepsilon_r\cdot\nabla\zeta^\varepsilon_r\right)dr-\int_0^t e^{(t-r)\Delta}\left(u^\varepsilon_r\cdot\nabla Z^\varepsilon_r\right)dr,\\
Z^\varepsilon_t &= -\sqrt{\varepsilon}\int_0^t\Delta e^{(t-r)\Delta}DdW_r,
\end{aligned}$$

with probability one.

Lastly, we state the main result of our work.

Theorem 3.3. *Let $T>0$, $s\in(0,\frac{1}{2})$ and $p>4$, and choose γ,λ as in* (3.9) *and* (3.12)*. Let $\bar\delta_\theta$ and $\bar\delta_u$ be given by* (3.13)*. Let parameters δ_θ,δ_u satisfy*

$$0<\delta_\theta<\bar\delta_\theta,\qquad 0<\delta_u<\bar\delta_u,$$

subject to the compatibility conditions

$$\delta_u\ge\max\left\{\delta_\theta,\frac{1}{2}-s\right\},\qquad \delta_u<1-\frac{2}{p},\tag{3.16}$$

which define a non-empty set for the given range of s and p. Set

$$\alpha_\theta := \frac{1}{4} + \frac{\delta_\theta}{2}, \qquad \beta_\theta := \frac{1}{4} - \frac{\delta_\theta}{4},$$

and assume

$$\sum_k \lambda_k^2 \|(-\Delta)^{\beta_\theta} De_k\|^2_{L^2(\mathcal{D})} < \infty.$$

Then there exist constants $\eta > 0$ and $\widetilde{M} = \widetilde{M}(\delta_\theta, \delta_u, T) \geq 2$ such that the following holds: if

$$(\theta_0, u_0) \in W^{s,6/5}(\mathcal{D}) \times V_p^{\delta_u}, \qquad \max\{\|\theta_0\|_{W^{s,6/5}(\mathcal{D})},\ \|u_0\|_{V_p^{\delta_u}}\} \leq \frac{\eta}{16\widetilde{M}},$$

then for every $\varepsilon > 0$ there exists a unique solution $(u^\varepsilon, \theta^\varepsilon, \tau^\varepsilon)$ of (3.2) on $[0,T]$ in the sense of Definition 3.2, such that

$$\|u^\varepsilon\|_{\mathbb{E}^{\delta_u}_{\tau^\varepsilon,p}} \leq \eta, \qquad \|\theta^\varepsilon\|_{C\left(0,\tau^\varepsilon;H^{-\frac{1}{2}-\delta_u}(\mathcal{D})\right)} \leq \eta, \qquad \mathbb{P}-a.s.$$

Moreover, there exists a constant $C(\delta_\theta, T) > 0$ such that

$$\mathbb{P}(\tau^\varepsilon = T) \geq 1 - \frac{64\,\widetilde{M}^2\,\varepsilon}{\eta^2}\, C(\delta_\theta, T) \sum_k \lambda_k^2 \|(-\Delta)^{\beta_\theta} De_k\|_2^2.$$

3.3 Temperature problem

In this section we describe how to solve the temperature problem (3.3), which is split in the linear problem (3.5), and the remainder problem (3.6).

3.3.1 Stochastic linear problem with non-homogeneous Dirichlet boundary conditions

We start this section by proving the first part of Proposition 3.1, in particular the well-posedness and the regularity for the mild solution Z_t^ε of the linear problem (3.5) subject to Dirichlet noise boundary conditions. Note that this result is well-known in the literature, see for instance [2, Proposition 3.1].

Proof of Proposition 3.1 (i)-(ii). Since (i)-(ii) do not depend on ε, we assume $\varepsilon = 1$ and omit the dependence on ε of ξ and Z in the following.

(i) First, considering the splitting

$$Z_t = (-\Delta)^{\alpha_\theta} \int_0^t (-\Delta)^{1-\alpha_\theta-\beta_\theta} e^{(t-r)\Delta} (-\Delta)^{\beta_\theta} D dW_r,$$

Z_t is well-defined and takes values in $H^{-2\alpha_\theta}(\mathcal{D})$, assuming (3.7), if

$$\begin{cases} \alpha_\theta + \beta_\theta > \dfrac{1}{2}, \\ \beta_\theta < \dfrac{1}{4}. \end{cases} \tag{3.17}$$

Indeed, the first inequality in (3.17) is a consequence of the square integrability conditions needed to define the Itô integral. The second guarantees that

$$\int_0^t (-\Delta)^{1-\alpha_\theta-\beta_\theta} e^{(t-r)\Delta} (-\Delta)^{\beta_\theta} D dW_r = \sum_k \lambda_k \int_0^t (-\Delta)^{1-\alpha_\theta-\beta_\theta} e^{(t-r)\Delta} (-\Delta)^{\beta_\theta} D e_k \, d\beta_k(r)$$

is well-defined. In particular $De_k \in D((-\Delta)^{\beta_\theta})$, where the explicit characterisation of the domain for fractional powers of the Dirichlet Laplacian was recalled in Section 3.1. Note that (3.17) is satisfied by our choice of $\alpha_\theta, \beta_\theta$.

(ii) We observe that ξ_t is a Gaussian process with values in $L^2(\mathcal{D})$ and with zero mean. If we are able to prove that there exist $M > 0$ and $\eta \in (0, 1]$ such that

$$\mathbb{E}\left[\|\xi_{t_2} - \xi_{t_1}\|_2^2\right] \leq M(t_2 - t_1)^\eta, \quad \forall\, 0 \leq t_1 \leq t_2, \tag{3.18}$$

then the thesis follows from the Kolmogorov test for Gaussian processes, see [1, Proposition 3.16]. Consider

$$\xi_t = \int_0^t (-\Delta)^{1-\alpha_\theta} e^{(t-r)\Delta} D dW_r = \int_0^t (-\Delta)^{1-\alpha_\theta-\beta_\theta} e^{(t-r)\Delta} (-\Delta)^{\beta_\theta} D dW_r,$$

with

$$\alpha_\theta = \frac{1}{4} + \frac{\delta_\theta}{2}, \quad \beta_\theta = \frac{1}{4} - \frac{\delta_\theta}{4}.$$

Then, for any $0 \leq t_1 \leq t_2$, we have

$$\xi_{t_2} - \xi_{t_1} = I_1 + I_2,$$

with

$$I_1 := \sum_k \lambda_k \int_{t_1}^{t_2} \left[(-\Delta)^{1-\alpha_\theta-\beta_\theta} e^{(t_2-r)\Delta} (-\Delta)^{\beta_\theta} D e_k\right] d\beta_k(r)$$

and

$$I_2 := \sum_k \lambda_k \int_0^{t_1} \left[(-\Delta)^{1-\alpha_\theta-\beta_\theta} \left(e^{(t_2-r)\Delta} - e^{(t_1-r)\Delta}\right) (-\Delta)^{\beta_\theta} D e_k\right] d\beta_k(r).$$

For the estimate of the first integral I_1, by the independence of $(\beta_k)_k$, the Itô-isometry, and the estimate for the heat-semigroup, we get

$$\begin{aligned}\mathbb{E}\left[\|I_1\|_2^2\right] &\leq \sum_k \lambda_k^2 \int_{t_1}^{t_2} \left\|(-\Delta)^{1-\alpha_\theta-\beta_\theta} e^{(t_2-r)\Delta}(-\Delta)^{\beta_\theta} De_k\right\|_2^2 dr \\ &\leq C\sum_k \lambda_k^2 \left\|(-\Delta)^{\beta_\theta} De_k\right\|_2^2 \int_{t_1}^{t_2} (t_2-r)^{-2(1-\alpha_\theta-\beta_\theta)} dr.\end{aligned} \tag{3.19}$$

By our choice of α_θ and β_θ, it holds

$$-2(1-\alpha_\theta-\beta_\theta) = -1 + \frac{\delta_\theta}{2}.$$

Since

$$\int_{t_1}^{t_2} (t_2-r)^{-1+\frac{\delta_\theta}{2}}\, dr = \frac{2}{\delta_\theta}(t_2-t_1)^{\delta_\theta/2},$$

we get, up to renaming C,

$$\mathbb{E}\left[\|I_1\|_2^2\right] \leq C(t_2-t_1)^{\frac{\delta_\theta}{2}} \sum_k \lambda_k^2 \left\|(-\Delta)^{\beta_\theta} De_k\right\|_2^2. \tag{3.20}$$

For the estimate of the second integral I_2, fix $0 \leq t_1 \leq t_2$. By the semigroup property,

$$e^{(t_2-r)\Delta} - e^{(t_1-r)\Delta} = e^{(t_1-r)\Delta}(e^{(t_2-t_1)\Delta} - I), \qquad 0 \leq r \leq t_1.$$

Let $\gamma \in (0,1]$ (to be chosen later). Using the commutation of $(-\Delta)^\sigma$ with $e^{t\Delta}$ and inserting $(-\Delta)^\gamma(-\Delta)^{-\gamma}$, we obtain

$$\begin{aligned}\left\|(-\Delta)^{1-\alpha_\theta-\beta_\theta}(e^{(t_2-r)\Delta} - e^{(t_1-r)\Delta})\right\|_{\mathcal{L}(L^2)} &= \|(-\Delta)^{1-\alpha_\theta-\beta_\theta} e^{(t_1-r)\Delta}(e^{(t_2-t_1)\Delta} - I)\|_{\mathcal{L}(L^2)} \\ &= \|(-\Delta)^{1-\alpha_\theta-\beta_\theta+\gamma} e^{(t_1-r)\Delta}(-\Delta)^{-\gamma}(e^{(t_2-t_1)\Delta} - I)\|_{\mathcal{L}(L^2)} \\ &\leq \|(-\Delta)^{1-\alpha_\theta-\beta_\theta+\gamma} e^{(t_1-r)\Delta}\|\, \|(-\Delta)^{-\gamma}(e^{(t_2-t_1)\Delta} - I)\|_{\mathcal{L}(L^2)}.\end{aligned} \tag{3.21}$$

For the first factor we use [11, Theorem 6.13(c)] and we get

$$\|(-\Delta)^{1-\alpha_\theta-\beta_\theta+\gamma} e^{(t_1-r)\Delta}\|_{\mathcal{L}(L^2)} \leq C(t_1-r)^{-(1-\alpha_\theta-\beta_\theta+\gamma)}, \tag{3.22}$$

for a constant C independent of t_1. For the second factor, let $g \in L^2(\mathcal{D})$ and set $x := (-\Delta)^{-\gamma} g \in D((-\Delta)^\gamma)$. Since $(-\Delta)^{-\gamma}$ commutes with the heat semigroup $e^{(t_2-t_1)\Delta}$, we have

$$(-\Delta)^{-\gamma}(e^{(t_2-t_1)\Delta} - I)g = (e^{(t_2-t_1)\Delta} - I)(-\Delta)^{-\gamma} g = (e^{(t_2-t_1)\Delta} - I)x.$$

Applying [11, Theorem 6.13(d)] with exponent γ yields

$$\|(e^{(t_2-t_1)\Delta} - I)x\|_2 \leq C(t_2-t_1)^\gamma \|(-\Delta)^\gamma x\|_2 = C(t_2-t_1)^\gamma \|g\|_2,$$

for a new constant C independent of t_1, t_2. Therefore

$$\|(-\Delta)^{-\gamma}(e^{(t_2-t_1)\Delta} - I)\|_{\mathcal{L}(L^2)} \leq C(t_2 - t_1)^{\gamma}. \tag{3.23}$$

Combining (3.21)-(3.23) we obtain, for all $0 \leq r \leq t_1$,

$$\|(-\Delta)^{1-\alpha_\theta-\beta_\theta}(e^{(t_2-r)\Delta} - e^{(t_1-r)\Delta})\|_{\mathcal{L}(L^2)} \leq C(t_2 - t_1)^{\gamma}(t_1 - r)^{-(1-\alpha_\theta-\beta_\theta+\gamma)}. \tag{3.24}$$

Using independence of $(\beta_k)_k$, Itô isometry, and (3.24), we get

$$\begin{aligned}
\mathbb{E}\|I_2\|_2^2 &= \sum_k \lambda_k^2 \int_0^{t_1} \|(-\Delta)^{1-\alpha_\theta-\beta_\theta}(e^{(t_2-r)\Delta} - e^{(t_1-r)\Delta})(-\Delta)^{\beta_\theta} De_k\|_2^2 \, dr \\
&\leq \sum_k \lambda_k^2 \int_0^{t_1} \|(-\Delta)^{1-\alpha_\theta-\beta_\theta}(e^{(t_2-r)\Delta} - e^{(t_1-r)\Delta})\|_{\mathcal{L}(L^2)}^2 \|(-\Delta)^{\beta_\theta} De_k\|_2^2 \, dr \\
&\leq C(t_2 - t_1)^{2\gamma} \left(\sum_k \lambda_k^2 \|(-\Delta)^{\beta_\theta} De_k\|_2^2 \right) \int_0^{t_1} (t_1 - r)^{-2(1-\alpha_\theta-\beta_\theta+\gamma)} \, dr.
\end{aligned}$$

The time-integral is finite provided $2(1 - \alpha_\theta - \beta_\theta + \gamma) < 1$, i.e.

$$\gamma < \alpha_\theta + \beta_\theta - \frac{1}{2}.$$

Since $\alpha_\theta + \beta_\theta = \frac{1}{2} + \frac{\delta_\theta}{4}$, we may choose any $\gamma \in (0, \frac{\delta_\theta}{4})$, and then

$$\mathbb{E}\|I_2\|_2^2 \leq C\,(t_2 - t_1)^{2\gamma} \sum_k \lambda_k^2 \|(-\Delta)^{\beta_\theta} De_k\|_2^2, \tag{3.25}$$

where $C > 0$ depends on $T, \alpha_\theta, \beta_\theta, \gamma$ but not on t_1, t_2. In conclusion, applying Jensen's inequality and setting $\eta := \min(\delta_\theta/2, 2\gamma) \in (0, 1]$, we obtain (3.18) by combining the estimates for I_1, I_2 in (3.20) and (3.25).

□

We conclude this section by recalling, and then applying, the notion of stochastic convolution to prove point (iii) of Proposition 3.1.

Given U, H, Hilbert spaces, let $U_0 := \mathcal{Q}^{1/2}(U)$ and set $L_2^0 = L_2(U_0, H)$ the space of Hilbert-Schmidt operators from U_0 to H, with norm

$$\|R\|_{L_2^0} = \left\| R \circ \mathcal{Q}^{1/2} \right\|_{L_2(U,H)},$$

where $L_2 = L_2(U, H)$ is the space of Hilbert-Schmidt operators from U to H with norm

$$\|R\|_{L_2}^2 = \sum_k \|Re_k\|_H^2,$$

where again $(e_k)_k \subset U$ denotes an orthonormal basis of U. Consider $(W_t)_t$ to be a U-valued $\mathcal{Q}$-Wiener process and $\mathcal{A}\colon D(\mathcal{A}) \subset H \to H$ a linear operator which generates a C_0-semigroup $(e^{t\mathcal{A}})_{t\geq 0}$ in H. Then, we consider the following space of stochastic processes

$$\mathcal{N}_W^2(0,T) := \left\{\Phi\colon [0,T]\times\Omega \to L_2^0 \;\middle|\; \Phi \text{ is predictable and } \|\Phi\|_T < \infty\right\},$$

where

$$\|\Phi\|_T := \left(\mathbb{E}\left[\int_0^T \|\Phi(t)\|_{L_2^0}^2\, dt\right]\right)^{\frac{1}{2}}.$$

Lastly, for $\Phi \in \mathcal{N}_W^2(0,T)$ we recall that the stochastic convolution $W_{\mathcal{A}}^{\Phi}$ is defined as

$$W_{\mathcal{A}}^{\Phi}(t) = \int_0^t e^{(t-r)\mathcal{A}}\Phi(r)\, dW_r, \quad t\in[0,T],$$

and we refer to [1] for more information. We can now move to the proof of the last part of Proposition 3.1.

Proof of Proposition 3.1 (iii). By Markov's inequality, for any $\vartheta > 0$, we have

$$\mathbb{P}\left(\sup_{0\leq t\leq T}\|Z_t^\varepsilon\|_{H^{-2\alpha_\theta}(\mathcal{D})} > \vartheta\right) \leq \frac{1}{\vartheta^2}\mathbb{E}\left[\sup_{0\leq t\leq T}\|Z_t^\varepsilon\|_{H^{-2\alpha_\theta}(\mathcal{D})}^2\right]. \tag{3.26}$$

To obtain the thesis, we thus need to bound the expectation on the right-hand side. We start to observe that, since $Z_t^\varepsilon = (-\Delta)^{\alpha_\theta}\xi_t^\varepsilon$, then

$$\|Z_t^\varepsilon\|_{H^{-2\alpha_\theta}(\mathcal{D})} = \|(-\Delta)^{\alpha_\theta}\xi_t^\varepsilon\|_{H^{-2\alpha_\theta}(\mathcal{D})} \cong \|\xi_t^\varepsilon\|_2\,.$$

Second, recall that

$$\xi_t^\varepsilon = \sqrt{\varepsilon}\int_0^t (-\Delta)^{1-\alpha_\theta-\beta_\theta}e^{(t-r)\Delta}(-\Delta)^{\beta_\theta}D\, dW_r.$$

Set $\Phi := (-\Delta)^{\beta_\theta}D$, and observe that $\Phi \in L_2^0$ since

$$\|\Phi\|_{L_2^0}^2 = \sum_k \lambda_k^2\|(-\Delta)^{\beta_\theta}De_k\|_2^2 < \infty,$$

where $(e_k)_k$ is an orthonormal basis of U made of eigenvectors for the covariance operator $\mathcal{Q}$. Thus, it is well-defined the $L^2(\mathcal{D})$-stochastic convolution $W_\Delta^\Phi(t) := \int_0^t e^{(t-r)\Delta}\Phi\, dW_r$, for $t\in[0,T]$, and $\xi_t^\varepsilon = \sqrt{\varepsilon}(-\Delta)^{\frac{1}{2}-\frac{\delta_\theta}{4}}W_\Delta^\Phi(t)$. Choose now $\rho \in (\frac{1}{2}-\frac{\delta_\theta}{4}, \frac{1}{2})$, and set

$$Y_\rho(t) := \int_0^t (t-r)^{-\rho}e^{(t-r)\Delta}\Phi dW_r, \quad t\in[0,T].$$

By the factorisation method, see [1, Section 5.3.1], since $\int_0^T t^{-2\rho}\|e^{t\Delta}\Phi\|_{L_2^0}^2 dt < \infty$, it holds

$$W_\Delta^\Phi(t) = \frac{\sin(\pi\rho)}{\pi}\int_0^t (t-r)^{\rho-1}e^{(t-r)\Delta}Y_\rho(r)\,dr.$$

Thus, using the estimate for the fractional powers as in (3.22), we have

$$\begin{aligned}\|\xi_t^\varepsilon\|_2 &\le C\sqrt{\varepsilon}\int_0^t (t-r)^{\rho-1}\|(-\Delta)^{\frac{1}{2}-\frac{\delta_\theta}{4}}e^{(t-r)\Delta}\|_{\mathcal{L}(L^2)}\|Y_\rho(r)\|_2 dr\\ &\le C\sqrt{\varepsilon}\int_0^t (t-r)^{\rho-\frac{3}{2}+\frac{\delta_\theta}{4}}\|Y_\rho(r)\|_2 dr.\end{aligned}$$

Fix now $q>2$ such that $\frac{1}{q} < \rho - (\frac{1}{2}-\frac{\delta_\theta}{4})$, and let q' be the conjugate exponent of q, i.e. $q' = \frac{q}{q-1}$. Then $g(\sigma) := \sigma^{\rho-1-(\frac{1}{2}-\frac{\delta_\theta}{4})} \in L^{q'}(0,T)$, and by Hölder inequality

$$\sup_{0\le t\le T}\|\xi_t^\varepsilon\|_2 \le C\sqrt{\varepsilon}\|g\|_{L^{q'}(0,T)}\|Y_\rho\|_{L^q(0,T;L^2(\mathcal{D}))}.$$

Considering the q-th moment, we have

$$\mathbb{E}\left[\sup_{0\le t\le T}\|\xi_t^\varepsilon\|_2^q\right] \le C\varepsilon^{q/2}\mathbb{E}\left[\int_0^T \|Y_\rho(r)\|_2^q\,dr\right]. \tag{3.27}$$

Since Y_ρ is a centered Gaussian random variable in $L^2(\mathcal{D})$, there exists $c_q>0$ such that $\mathbb{E}[\|Y_\rho(r)\|_2^q] \le c_q\left(\mathbb{E}[\|Y_\rho(r)\|_2^2]\right)^{q/2}$. By Itô isometry and the contraction of $e^{t\Delta}$ on L^2, we have

$$\begin{aligned}\mathbb{E}\left[\|Y_\rho(r)\|_2^2\right] &= \int_0^r (r-\sigma)^{-2\rho}\|e^{(r-\sigma)\Delta}\Phi\|_{L_2^0}^2\,d\sigma\\ &\le \|\Phi\|_{L_2^0}^2\int_0^r (r-\sigma)^{-2\rho}\,d\sigma\\ &= \|\Phi\|_{L_2^0}^2\frac{r^{1-2\rho}}{1-2\rho}.\end{aligned}$$

Therefore

$$\mathbb{E}\left[\int_0^T \|Y_\rho(r)\|_2^q\,dr\right] \le c_q\|\Phi\|_{L_2^0}^q\int_0^T r^{\frac{(1-2\rho)q}{2}}dr \le c_{q,\rho,T}\|\Phi\|_{L_2^0}^q. \tag{3.28}$$

Thus, substituting (3.28) inside (3.27), we obtain

$$\mathbb{E}\left[\sup_{0\le t\le T}\|\xi_t^\varepsilon\|_2^q\right] \le C(\delta_\theta,T,q)\varepsilon^{q/2}\|\Phi\|_{L_2^0}^q.$$

Lastly, since $q > 2$, by Jensen inequality we deduce

$$\begin{aligned}\mathbb{E}\left[\sup_{0\le t\le T}\|\xi_t^\varepsilon\|_2^2\right] &\le \left(\mathbb{E}\left[\sup_{0\le t\le T}\|\xi_t^\varepsilon\|_2^q\right]\right)^{2/q}\\ &\le \varepsilon C(\delta_\theta,T)\|\Phi\|_{L_2^0}^2\\ &= \varepsilon C(\delta_\theta,T)\sum_k \lambda_k^2\|(-\Delta)^{\beta_\theta}De_k\|_2^2.\end{aligned}$$

The thesis then follows by substituting the previous bound into (3.26). □

3.3.2 The remainder temperature equation

Let $\delta_u > 0$ be a small regularity exponent for the velocity. Given a prescribed divergence-free velocity field

$$u \in L^p(0,T;H_\sigma^{\frac{3}{2}-\delta_u}(\mathcal{D}))\cap L^\infty(0,T;H_\sigma^{\frac{1}{2}-\delta_u}(\mathcal{D})),\quad p\in(1,\infty)$$

in this section we consider the remainder $\zeta_t^\varepsilon := \theta_t^\varepsilon - Z_t^\varepsilon$ between the solution θ_t^ε of the system (3.3), and the solution Z_t^ε of the linear problem (3.5) considered in the previous section.

We start by proving an auxiliary interpolation result for the velocity field u, which will be used throughout this section.

Corollary 3.2. *Let $\delta_u \in (0,1)$ and $p\in(1,\infty)$. If*

$$u \in L^p(0,T;H^{\frac{3}{2}-\delta_u}(\mathcal{D}))\cap L^\infty(0,T;H^{\frac{1}{2}-\delta_u}(\mathcal{D})),$$

then for all $0<\lambda\le 1-\delta_u$, we have

$$u \in L^{\frac{p}{\lambda+\delta_u}}\left(0,T;H^{\frac{1}{2}+\lambda}(\mathcal{D})\right).$$

Proof. Note that if $\lambda = 1-\delta_u$, then the statement is trivial. Thus, fix $0<\lambda<1-\delta_u$, and define $\delta' := 1-\lambda$. Then $\delta_u < \delta' < 1+\delta_u$. Since $\frac{3}{2}-\delta' \in (\frac{1}{2}-\delta_u, \frac{3}{2}-\delta_u)$, there exists $\vartheta\in(0,1)$ such that

$$\frac{3}{2}-\delta' = (1-\vartheta)\left(\frac{1}{2}-\delta_u\right)+\vartheta\left(\frac{3}{2}-\delta_u\right),$$

which yields

$$\vartheta = 1-\delta'+\delta_u.$$

Using the interpolation inequality

$$\|u_t\|_{H^{\frac{3}{2}-\delta'}(\mathcal{D})} \le C\,\|u_t\|_{H^{\frac{1}{2}-\delta_u}(\mathcal{D})}^{\delta'-\delta_u}\,\|u_t\|_{H^{\frac{3}{2}-\delta_u}(\mathcal{D})}^{1-\delta'+\delta_u},$$

for a constant $C > 0$. Therefore, for any $q \geq 1$, we have

$$\int_0^T \|u_t\|^q_{H^{\frac{3}{2}-\delta'}(\mathcal{D})}\, dt \leq C \int_0^T \|u_t\|^{(\delta'-\delta_u)q}_{H^{\frac{1}{2}-\delta_u}(\mathcal{D})} \|u_t\|^{(1-\delta'+\delta_u)q}_{H^{\frac{3}{2}-\delta_u}(\mathcal{D})}\, dt$$
$$\leq C \|u\|^{(\delta'-\delta_u)q}_{L^\infty\left(0,T;H^{\frac{1}{2}-\delta_u}(\mathcal{D})\right)} \|u\|^{(1-\delta'+\delta_u)q}_{L^{(1-\delta'+\delta_u)q}\left(0,T;H^{\frac{3}{2}-\delta_u}(\mathcal{D})\right)}.$$

This is finite if $(1-\delta'+\delta_u)q = p$, which gives

$$q = \frac{p}{1-\delta'+\delta_u} = \frac{p}{\lambda+\delta_u}.$$

Further, observe that $\frac{3}{2} - \delta' = \lambda + \frac{1}{2}$ by definition of λ. Thus, we have proved

$$\int_0^T \|u_t\|^{\frac{p}{\lambda+\delta_u}}_{H^{\lambda+\frac{1}{2}}(\mathcal{D})} < \infty,$$

which gives the thesis. □

To make sense of the mild solution, we next establish a space-time integrability result for the product $u_t \cdot Z^\varepsilon_t$. Recall that, for any $\delta_\theta > 0$, $\alpha_\theta = \frac{1}{4} + \frac{\delta_\theta}{2}$ and $\beta_\theta = \frac{1}{4} - \frac{\delta_\theta}{4}$, we have introduced the stochastic processes

$$Z^\varepsilon_t = (-\Delta)^{\alpha_\theta}\xi^\varepsilon_t, \quad \xi^\varepsilon_t = \int_0^t (-\Delta)^{1-\alpha_\theta} e^{(t-r)\Delta} D dW_r.$$

Further, if

$$\sum_k \lambda_k^2 \left\|(-\Delta)^{\beta_\theta} D e_k\right\|_2^2 < \infty,$$

then by Proposition 3.1 we know that the trajectories of ξ^ε are in $C(0,T;L^2(\mathcal{D}))$.

Lemma 3.1. *Let $0 < \lambda < 1$ and $\gamma > \frac{1}{4}$. Set*

$$\bar{\delta}_\theta(\lambda,\gamma) := \min\{\lambda, 2\gamma - \frac{1}{2}\}.$$

For any $0 < \delta_\theta < \bar{\delta}_\theta$, any velocity field

$$u \in L^p(0,T;H^{\frac{3}{2}-\delta_u}(\mathcal{D})) \cap L^\infty(0,T;H^{\frac{1}{2}-\delta_u}(\mathcal{D})), \qquad p > 1,\ \delta_u \in (0, 1-\lambda],$$

we have

$$t \mapsto (-\Delta)^{-\gamma-\frac{1}{2}}\mathrm{div}\,(u_t(-\Delta)^{\alpha_\theta}\xi^\varepsilon_t) \in L^{\frac{p}{\lambda+\delta_u}}\left(0,T;L^{\frac{6}{5}}(\mathcal{D})\right), \qquad \alpha_\theta = \frac{1}{4} + \frac{\delta_\theta}{2}.$$

Moreover,

$$\left\|(-\Delta)^{-\gamma-\frac{1}{2}}\mathrm{div}(u_t(-\Delta)^{\alpha_\theta}\xi^\varepsilon_t)\right\|_{L^{\frac{p}{\lambda+\delta_u}}(0,T;L^{\frac{6}{5}}(\mathcal{D}))} \leq C \|\xi^\varepsilon\|_{C(0,T;L^2(\mathcal{D}))} \|u\|_{L^{\frac{p}{\lambda+\delta_u}}(0,T;W^{\frac{1}{2}+\lambda,2}(\mathcal{D}))}, \tag{3.29}$$

where $C = C(\lambda,\gamma,\delta_\theta) > 0$.

Proof. To simplify the notation, we set $\varepsilon = 1$ and drop the dependence on ε of ξ^ε. We start by recalling that, by [12, Theorem A.1] (which we can apply after extending functions on $\mathcal{D}$ to $\mathbb{R}^3$ via a bounded extension operator), the pointwise multiplication

$$\begin{aligned} W^{s_1,p_1}(\mathcal{D}) \times W^{s_2,p_2}(\mathcal{D}) &\hookrightarrow W^{s,p}(\mathcal{D}) \\ (f,g) &\mapsto fg \end{aligned}$$

is bilinear and continuous if

(i) $s_1 \geq s$ and $s_2 \geq s$;

(ii) $s_1 \geq s + 3\left(\frac{1}{p_1} - \frac{1}{p}\right)$ and $s_2 \geq s + 3\left(\frac{1}{p_2} - \frac{1}{p}\right)$;

(iii) $s_1 + s_2 > s + 3\left(\frac{1}{p_1} + \frac{1}{p_2} - \frac{1}{p}\right)$;

(iv) if $s_i = s \notin \mathbb{N}$ for some $i \in \{1,2\}$, then one must additionally assume $p_i \leq p$.

Step 1. As a first step of the proof, we show that

$$\left\langle (-\Delta)^{-\gamma-\frac{1}{2}} \mathrm{div}\left(u_t(-\Delta)^{\alpha_\theta}\xi_t\right), \phi \right\rangle \leq K_t \|\phi\|_{L^6(\mathcal{D})},$$

where the integrability in time of $t \mapsto K_t$ will be investigated in Step 2. Here, 6 is the conjugate exponent of $\frac{6}{5}$, $\phi \in L^6(\mathcal{D})$ is a test function, and $\alpha_\theta = \frac{1}{4} + \frac{\delta_\theta}{2}$. Further, we denote by $\langle \cdot, \cdot \rangle$ the duality pairing. Since Δ is self-adjoint, by Hölder inequality and integration by parts, we obtain

$$\begin{aligned} \left\langle (-\Delta)^{-\gamma-\frac{1}{2}} \mathrm{div}\left(u_t(-\Delta)^{\alpha_\theta}\xi_t\right), \phi \right\rangle &= \left\langle \mathrm{div}(u_t(-\Delta)^{\alpha_\theta}\xi_t), (-\Delta)^{-\gamma-\frac{1}{2}}\phi \right\rangle \\ &= -\langle u_t(-\Delta)^{\alpha_\theta}\xi_t, \nabla(-\Delta)^{-\gamma-\frac{1}{2}}\phi \rangle \\ &= -\left\langle (-\Delta)^{\alpha_\theta}\xi_t, u_t \cdot \nabla(-\Delta)^{-\gamma-\frac{1}{2}}\phi \right\rangle \\ &= -\left\langle \xi_t, (-\Delta)^{\alpha_\theta}\left(u_t \cdot \nabla(-\Delta)^{-\gamma-\frac{1}{2}}\phi\right) \right\rangle \\ &\leq \|\xi_t\|_{L^2(\mathcal{D})} \left\| (-\Delta)^{\alpha_\theta}\left(u_t \cdot \nabla(-\Delta)^{-\gamma-\frac{1}{2}}\phi\right) \right\|_{L^2(\mathcal{D})} \\ &= \|\xi_t\|_{L^2(\mathcal{D})} \left\| u_t \cdot \nabla(-\Delta)^{-\gamma-\frac{1}{2}}\phi \right\|_{W^{2\alpha_\theta,2}(\mathcal{D})}. \end{aligned}$$

Next, we show that $u_t \cdot \nabla(-\Delta)^{-\gamma-\frac{1}{2}}\phi \in W^{2\alpha_\theta,2}(\mathcal{D})$. Since $2\alpha_\theta = \frac{1}{2} + \delta_\theta$, this is equivalent to

$$u_t \cdot \nabla(-\Delta)^{-\gamma-\frac{1}{2}}\phi \in W^{\frac{1}{2}+\delta_\theta,2}(\mathcal{D}). \tag{3.30}$$

By the norm equivalence between $W^{\frac{1}{2}+\lambda,2}(\mathcal{D})$ and $H^{\frac{1}{2}+\lambda}(\mathcal{D})$, and by Corollary 3.2, we have $u_t \in W^{\frac{1}{2}+\lambda,2}(\mathcal{D})$ a.e., and since $\phi \in L^6(\mathcal{D})$,

we deduce $\nabla(-\Delta)^{-\gamma-\frac{1}{2}}\phi \in W^{2\gamma,6}(\mathcal{D})$. Thus (3.30) follows from the pointwise multiplication embedding

$$\begin{aligned} W^{\frac{1}{2}+\lambda,2}(\mathcal{D}) \times W^{2\gamma,6}(\mathcal{D}) &\hookrightarrow W^{\frac{1}{2}+\delta_\theta,2}(\mathcal{D}) \\ (u_t, \nabla(-\Delta)^{-\gamma-\frac{1}{2}}\phi) &\mapsto u_t \cdot \nabla(-\Delta)^{-\gamma-\frac{1}{2}}\phi, \end{aligned}$$

provided that the following conditions hold

(i) $\frac{1}{2}+\lambda \geq \frac{1}{2}+\delta_\theta$ and $2\gamma \geq \frac{1}{2}+\delta_\theta$;

(ii) $\frac{1}{2}+\lambda \geq \frac{1}{2}+\delta_\theta+3\left(\frac{1}{2}-\frac{1}{2}\right)$ and $2\gamma \geq \frac{1}{2}+\delta_\theta+3\left(\frac{1}{6}-\frac{1}{2}\right)$;

(iii) $\frac{1}{2}+\lambda+2\gamma > \frac{1}{2}+\delta_\theta+3\left(\frac{1}{2}+\frac{1}{6}-\frac{1}{2}\right)$.

The previous conditions are equivalent to

(a) $\delta_\theta \leq \lambda$ and $\delta_\theta \leq 2\gamma-\frac{1}{2}$;

(b) $\delta_\theta \leq \frac{1}{2}+2\gamma$;

(c) $\delta_\theta < \lambda+2\gamma-\frac{1}{2}$.

Since in general $s=\frac{1}{2}+\delta_\theta \notin \mathbb{N}$ and here $p_2=6>p=2$, condition (iv) in [12, Theorem A.1] forbids the borderline case $s_2=s$. Hence we impose

$$s_2 > s \quad\Longleftrightarrow\quad 2\gamma > \frac{1}{2}+\delta_\theta \quad\Longleftrightarrow\quad \delta_\theta < 2\gamma-\frac{1}{2}.$$

In contrast, the endpoint $\delta_\theta=\lambda$ is admissible since then $s_1=s$ but $p_1=p=2$.

Therefore, we can choose

$$\bar{\delta}_\theta(\lambda,\gamma) := \min\left\{\lambda, 2\gamma-\frac{1}{2}\right\} > 0, \tag{3.31}$$

and note that $\bar{\delta}_\theta$ is positive since $\gamma>\frac{1}{4}$ and $\lambda \in (0,1)$.

Step 2. Fix now $0<\delta_\theta \leq \bar{\delta}_\theta(\lambda,\gamma)$. The computations of the previous step yield

$$\begin{aligned} \left\|(-\Delta)^{-\gamma-\frac{1}{2}}\mathrm{div}\left(u_t(-\Delta)^{\alpha_\theta}\xi_t\right)\right\|_{L^{\frac{6}{5}}(\mathcal{D})} &= \sup_{\|\phi\|_{L^6(\mathcal{D})}\leq 1}\left\langle(-\Delta)^{-\gamma-\frac{1}{2}}\mathrm{div}\left(u_t(-\Delta)^{\alpha_\theta}\xi_t\right),\phi\right\rangle \\ &\leq C\|\xi_t\|_{L^2(\mathcal{D})}\sup_{\|\phi\|_6\leq 1}\left\|u_t\cdot\nabla(-\Delta)^{-\gamma-\frac{1}{2}}\phi\right\|_{W^{2\alpha_\theta,2}(\mathcal{D})} \\ &\leq C\|\xi_t\|_{L^2(\mathcal{D})}\|u_t\|_{W^{\frac{1}{2}+\lambda,2}(\mathcal{D})}\sup_{\|\phi\|_6\leq 1}\left\|\nabla(-\Delta)^{-\gamma-\frac{1}{2}}\phi\right\|_{W^{2\gamma,6}(\mathcal{D})} \\ &\leq C\|\xi_t\|_{L^2(\mathcal{D})}\|u_t\|_{W^{\frac{1}{2}+\lambda,2}(\mathcal{D})}\sup_{\|\phi\|_6\leq 1}\|\phi\|_{L^6(\mathcal{D})} \\ &\leq C\|\xi_t\|_{L^2(\mathcal{D})}\|u_t\|_{W^{\frac{1}{2}+\lambda,2}(\mathcal{D})}, \end{aligned}$$

where $C = C(\lambda, \gamma, \delta_\theta)$ is a constant from the multiplication results. Thus, up to positive constants, we obtain from Hölder's inequality that

$$\begin{aligned}\int_0^T \left\|(-\Delta)^{-\gamma-\frac{1}{2}}\operatorname{div}\left(u_t(-\Delta)^{\alpha_\theta}\xi_t\right)\right\|_{L^{\frac{6}{5}}(\mathcal{D})}^{\frac{p}{\lambda+\delta_u}} dt &\leq \int_0^T \left(\|\xi_t\|_{L^2(\mathcal{D})}\,\|u_t\|_{W^{\frac{1}{2}+\lambda,2}(\mathcal{D})}\right)^{\frac{p}{\lambda+\delta_u}} dt \\ &= \int_0^T \|\xi_t\|_{L^2(\mathcal{D})}^{\frac{p}{\lambda+\delta_u}}\,\|u_t\|_{W^{\frac{1}{2}+\lambda,2}(\mathcal{D})}^{\frac{p}{\lambda+\delta_u}} dt \\ &\leq \sup_{0\leq t\leq T}\|\xi_t\|_{L^2(\mathcal{D})}^{\frac{p}{\lambda+\delta_u}} \int_0^T \|u_t\|_{W^{\frac{1}{2}+\lambda,2}(\mathcal{D})}^{\frac{p}{\lambda+\delta_u}} dt.\end{aligned}$$

Note that all the terms on the right-hand side are finite thanks to Proposition 3.1, Corollary 3.2, and the norm equivalence between $W^{\frac{1}{2}+\lambda,2}(\mathcal{D})$ and $H^{\frac{1}{2}+\lambda}(\mathcal{D})$; the last corollary can be applied since by hypothesis $\delta_u \leq 1-\lambda$. □

Recall that the mild solution of the remainder's problem (3.6) has the form

$$\zeta_t^\varepsilon = e^{t\Delta}\theta_0 - \int_0^t e^{(t-r)\Delta}\left(u_r^\varepsilon\cdot\nabla\zeta_r^\varepsilon\right)dr - \int_0^t e^{(t-r)\Delta}\left(u_r^\varepsilon\cdot\nabla Z_r^\varepsilon\right)dr.$$

By the previous auxiliary results, we can deduce the regularity of the third term on the right-hand side of the previous identity.

Corollary 3.3. *Let $s\in(0,\frac{1}{2})$, $p>1$ and $\gamma>\frac{1}{4}$ be given. Assume that*

$$a(s,\gamma) := \frac{1}{2}+\gamma+\frac{s}{2} < 1. \tag{3.32}$$

Let $\lambda\in(0,1)$ such that

$$\lambda < p(1-a(s,\gamma)). \tag{3.33}$$

Fix $0<\delta_\theta<\bar{\delta}_\theta = \min\{\lambda, 2\gamma-\frac{1}{2}\}$, and consider $\alpha_\theta := \frac{1}{4}+\frac{\delta_\theta}{2}$. Define

$$\bar{\delta}_u(p,s,\gamma,\lambda) := \min\{p(1-a(s,\gamma))-\lambda, 1-\lambda\} > 0.$$

Then, for every $\delta_u\in(0,\bar{\delta}_u)$, and every velocity field

$$u\in L^p(0,T;H_\sigma^{\frac{3}{2}-\delta_u}(\mathcal{D}))\cap L^\infty(0,T;H_\sigma^{\frac{1}{2}-\delta_u}(\mathcal{D})),$$

the function

$$\chi_t := \int_0^t e^{(t-r)\Delta}\big(u_r\cdot\nabla Z_r^\varepsilon\big)\,dr$$

belongs to $C(0,T;W^{s,\frac{6}{5}}(\mathcal{D}))$ and satisfies

$$\|\chi^\varepsilon\|_{C(0,T;W^{s,\frac{6}{5}})} \leq C\,\|\xi^\varepsilon\|_{C(0,T;L^2)}\,\|u\|_{L^{\frac{p}{\lambda+\delta_u}}(0,T;W^{\frac{1}{2}+\lambda,2})}, \tag{3.34}$$

where $C = C(s, p, \gamma, \lambda, \delta_\theta, T) > 0$. *Lastly, given* $s \in (0, \frac{1}{2}), p > 1$ *as before, there always exists* $\gamma = \gamma(s) > \frac{1}{4}$ *and* $\lambda = \lambda(s, p) \in (0, 1)$ *such that* (3.32) *and* (3.33) *hold.*

Proof. To simplify the notation, we set $\varepsilon = 1$ and drop the dependence of ε of ξ^ε.

Step 1. Fix $\delta_\theta > 0$ such that $0 < \delta_\theta < \bar{\delta}_\theta = \min\{\lambda, 2\gamma - \frac{1}{2}\}$. Define the function

$$f_\lambda(\delta_u) = (\gamma + \frac{s}{2} + \frac{1}{2}) \frac{1}{1 - \frac{\lambda}{p} - \frac{\delta_u}{p}} = \frac{a(s,\gamma)}{1 - \frac{\lambda + \delta_u}{p}}, \quad \lambda \geq 0.$$

If $\delta_u < \bar{\delta}_u$, then $\lambda + \delta_u < p(1 - a(s, \gamma))$, which implies

$$f_\lambda(\delta_u) = \left(\gamma + \tfrac{s}{2} + \tfrac{1}{2}\right) \frac{1}{1 - \frac{\lambda}{p} - \frac{\delta_u}{p}} < 1. \tag{3.35}$$

Step 2. Thanks to the commuting properties of the fractional Laplacian with the heat semigroup and the divergence free condition of u, it holds

$$\chi_t = (-\Delta)^{-\frac{s}{2}} \rho_t,$$
$$\rho_t = \int_0^t (-\Delta)^{\gamma + \frac{s}{2} + \frac{1}{2}} e^{(t-r)\Delta} (-\Delta)^{-\gamma - \frac{1}{2}} \operatorname{div}\left(u_r (-\Delta)^{\alpha_\theta} \xi_r\right) dr.$$

By the estimate

$$\left\| (-\Delta)^{\varsigma} e^{(t-r)\Delta} y \right\|_{L^{\frac{6}{5}}(\mathcal{D})} \leq \frac{c}{(t-r)^{\varsigma}} \|y\|_{L^{\frac{6}{5}}(\mathcal{D})},$$

where $\varsigma := \gamma + \frac{s}{2} + \frac{1}{2}$ and $c = c(\varsigma)$ is a positive constant, we get

$$\begin{aligned} \|\rho_t\|_{L^{\frac{6}{5}}(\mathcal{D})} &\leq \int_0^t \frac{c}{(t-r)^{\gamma + \frac{s}{2} + \frac{1}{2}}} \left\| (-\Delta)^{-\gamma - \frac{1}{2}} \operatorname{div}\left(u_r (-\Delta)^{\alpha_\theta} \xi_r\right) \right\|_{L^{\frac{6}{5}}(\mathcal{D})} dr \\ &\leq \left(\int_0^t \left(\frac{c}{(t-r)^{\gamma + \frac{s}{2} + \frac{1}{2}}} \right)^{\frac{p}{p - \lambda - \delta_u}} dr \right)^{\frac{p - \lambda - \delta_u}{p}} \left(\int_0^t \left\| (-\Delta)^{-\gamma - \frac{1}{2}} \operatorname{div}\left(u_r (-\Delta)^{\alpha_\theta} \xi_r\right) \right\|_{L^{\frac{6}{5}}(\mathcal{D})}^{\frac{p}{\lambda + \delta_u}} dr \right)^{\frac{\lambda + \delta_u}{p}}. \end{aligned} \tag{3.36}$$

The second term is finite thanks to Lemma 3.1 (that we can apply since $\lambda \leq 1 - \delta_u$ and $\delta_\theta \in (0, \bar{\delta}_\theta]$), while the first term is finite thanks to (3.35). Taking the supremum over $t \in [0, T]$ in (3.36), using Lemma 3.1 to bound the second term on the right-hand side of (3.36), and the boundedness of $(-\Delta)^{-s/2} \colon L^{6/5} \to W^{s, 6/5}$, we obtain (3.34).

Step 3. We now prove that $t \mapsto \rho_t$ is continuous as a map $(0, T) \to L^{\frac{6}{5}}(\mathcal{D})$. For notational convenience, write

$$\rho_t = \int_0^t (-\Delta)^{\gamma + \frac{s}{2} + \frac{1}{2}} e^{(t-\tau)\Delta} g_\tau \, d\tau, \qquad g_\tau := (-\Delta)^{-\gamma - \frac{1}{2}} \operatorname{div}\left(u_\tau (-\Delta)^{\alpha_\theta} \xi_\tau\right),$$

so that $g \in L^{\frac{p}{\lambda+\delta_u}}(0,T;L^{\frac{6}{5}}(\mathcal{D}))$ by Lemma 3.1. Fix $r \in (0,T]$ and let $t \in [r,T]$. Then

$$\begin{aligned}\rho_t - \rho_r &= \int_0^t (-\Delta)^{\gamma+\frac{s}{2}+\frac{1}{2}} e^{(t-\tau)\Delta} g_\tau \, d\tau - \int_0^r (-\Delta)^{\gamma+\frac{s}{2}+\frac{1}{2}} e^{(r-\tau)\Delta} g_\tau \, d\tau \\ &= \int_r^t (-\Delta)^{\gamma+\frac{s}{2}+\frac{1}{2}} e^{(t-\tau)\Delta} g_\tau \, d\tau + \int_0^r \Big[(-\Delta)^{\gamma+\frac{s}{2}+\frac{1}{2}} e^{(t-\tau)\Delta} - (-\Delta)^{\gamma+\frac{s}{2}+\frac{1}{2}} e^{(r-\tau)\Delta}\Big] g_\tau \, d\tau \\ &=: I_1(t,r) + I_2(t,r).\end{aligned}$$

Using the estimate for the fractional powers as in (3.22) and Hölder's inequality with $q := \frac{p}{\lambda+\delta_u} > 1$, $q' = \frac{q}{q-1}$, we obtain

$$\|I_1(t,r)\|_{L^{\frac{6}{5}}} \le C\Big(\int_r^t (t-\tau)^{-\left(\gamma+\frac{s}{2}+\frac{1}{2}\right)q'} \, d\tau\Big)^{1/q'} \Big(\int_r^t \|g_\tau\|^q_{L^{\frac{6}{5}}} \, d\tau\Big)^{1/q},$$

for $C = C(\gamma, s, p, \lambda, \delta_u) > 0$. The first factor I_1 is bounded uniformly in $t \in [r,T]$ thanks to condition (3.35), while the second factor tends to 0 as $t \downarrow r$ by the absolute continuity of the integral, since $g \in L^q(0,T;L^{\frac{6}{5}}(\mathcal{D}))$. Hence $\|I_1(t,r)\|_{L^{\frac{6}{5}}} \to 0$ as $t \downarrow r$.

For the second term I_2, for every fixed $\tau \in (0,r)$ the map

$$\theta \mapsto (-\Delta)^{\gamma+\frac{s}{2}+\frac{1}{2}} e^{\theta\Delta} g_\tau, \qquad \theta > 0,$$

is continuous in $L^{\frac{6}{5}}(\mathcal{D})$ by strong continuity of the heat semigroup; therefore the integrand in $I_2(t,r)$ converges to 0 in $L^{\frac{6}{5}}$ as $t \downarrow r$ for a.e. $\tau \in (0,r)$. Moreover, using again the estimate for the fractional power (3.22), for t close to r we have

$$\|(-\Delta)^{\gamma+\frac{s}{2}+\frac{1}{2}} e^{(t-\tau)\Delta} g_\tau - (-\Delta)^{\gamma+\frac{s}{2}+\frac{1}{2}} e^{(r-\tau)\Delta} g_\tau\|_{L^{\frac{6}{5}}} \le C(r-\tau)^{-\gamma-\frac{s}{2}-\frac{1}{2}} \|g_\tau\|_{L^{\frac{6}{5}}},$$

and the right-hand side is integrable on $(0,r)$ by the same computation as in (3.36). Hence, by the dominated convergence theorem, $\|I_2(t,r)\|_{L^{\frac{6}{5}}} \to 0$ as $t \downarrow r$. We deduce that $\|\rho_t - \rho_r\|_{L^{\frac{6}{5}}(\mathcal{D})} \to 0$ for every $r \in (0,T]$, that is $\rho \in C(0,T;L^{\frac{6}{5}}(\mathcal{D}))$. Consequently, $\chi_t = (-\Delta)^{-\frac{s}{2}} \rho_t$ belongs to $C(0,T;W^{s,\frac{6}{5}}(\mathcal{D}))$.

Step 4. Existence of γ, λ, given s, p. Assume that, as before, $s \in (0, \frac{1}{2})$ and $p > 1$ are given. We now check that we can always find $\gamma = \gamma(s) > \frac{1}{4}$ and $\lambda = \lambda(s,p)$ such that (3.32) and (3.33) are satisfied, and thus this corollary is non-trivial. Indeed, with the notation of Step 1, from $a(\frac{1}{4}) = \frac{3}{4} + \frac{s}{2} < 1$, it follows that there exists $\gamma = \gamma(s) > \frac{1}{4}$ sufficiently close to $\frac{1}{4}$ such that $a(s,\gamma) < 1$, that is (3.32). Hence, also $p(1-a) > 0$ holds, and we may choose $\lambda = \lambda(s,p) \in (0,1)$ so small that $\lambda < p(1-a)$, that is (3.33). □

Remark 3.2. *From the proof of Corollary 3.3, it follows that if* $s \in (0, \frac{1}{2}), p > 1, \gamma > \frac{1}{4}$ *and* $\lambda \in (0,1)$ *satisfy* (3.32) *and* (3.33)*, then*

$$\left(\gamma + \tfrac{s}{2} + \tfrac{1}{2}\right) \frac{1}{1 - \frac{\lambda}{p} - \frac{\delta_u}{p}} < 1$$

for any $\delta_u < \bar{\delta}_u = \min\{p(1 - a(s,\gamma)) - \lambda, 1 - \lambda\}$.

Lastly, we show the proof of Theorem 3.1.

Proof of Theorem 3.1. For simplicity we set $\varepsilon = 1$ and drop the superscript, writing ζ and Z instead of ζ^ε and Z^ε. Let $s \in (0, \frac{1}{2})$ and $p > 4$ be given.

Step 1. Setup of parameters and auxiliary embeddings. We work with the parameters $\gamma, \lambda, \bar{\delta}_\theta, \bar{\delta}_u$ fixed in the statement of the theorem. In particular,

$$a(s,\gamma) := \frac{1}{2} + \gamma + \frac{s}{2} < 1, \qquad \lambda_{\max} := p(1 - a(s,\gamma)),$$

and, by (3.10), we have $\lambda_{\max} > \frac{1}{2} - s$. Moreover, $\lambda_{\max} - (1 - 2s) > 0$ by the choice of ε_γ in (3.9) as shown in (3.11). We have set

$$\lambda := (\frac{1}{2} - s) + \varepsilon_\lambda, \qquad 0 < \varepsilon_\lambda < \min\{2s, \lambda_{\max} - (1 - 2s)\}.$$

Note that

$$\lambda < (\tfrac{1}{2} - s) + 2s = \tfrac{1}{2} + s < 1, \qquad \lambda < (\tfrac{1}{2} - s) + \lambda_{\max} - (1 - 2s) = \lambda_{\max} - (\tfrac{1}{2} - s) < \lambda_{\max}.$$

Hence $\lambda \in (\frac{1}{2} - s, \min\{1, \lambda_{\max}\})$. The thresholds are

$$\bar{\delta}_\theta = \min\left\{\lambda, 2\gamma - \frac{1}{2}\right\}, \qquad \bar{\delta}_u = \min\left\{\lambda_{\max} - \lambda, 1 - \lambda\right\}.$$

Finally, fix $0 < \delta_\theta < \bar{\delta}_\theta$ and $0 < \delta_u < \bar{\delta}_u$.

Choice of q, q'. Set

$$q := \frac{6}{5 - 2s}, \qquad \frac{1}{q} + \frac{1}{q'} = 1.$$

Then the Sobolev embedding

$$W^{s,\frac{6}{5}}(\mathcal{D}) \hookrightarrow L^q(\mathcal{D}) \tag{3.37}$$

holds, and a direct computation gives

$$1 - \frac{3}{q'} = \frac{1}{2} - s. \tag{3.38}$$

Product embedding. Since $\gamma > \frac{1}{4}$, the Sobolev embedding yields

$$W^{2\gamma,6}(\mathcal{D}) \hookrightarrow L^{\infty}(\mathcal{D}). \tag{3.39}$$

Moreover, again by the Sobolev embedding,

$$W^{\frac{1}{2}+\lambda,2}(\mathcal{D}) \hookrightarrow L^{r_\lambda}(\mathcal{D}), \qquad r_\lambda := \frac{3}{1-\lambda}. \tag{3.40}$$

Recalling that $q' = \frac{6}{1+2s}$, it can be checked that $r_\lambda \geq q'$ is equivalent to $\lambda \geq \frac{1}{2} - s$. Hence, by (3.40) and the embedding $L^{r_\lambda}(\mathcal{D}) \hookrightarrow L^{q'}(\mathcal{D})$ on bounded $\mathcal{D}$,

$$W^{\frac{1}{2}+\lambda,2}(\mathcal{D}) \hookrightarrow L^{q'}(\mathcal{D}). \tag{3.41}$$

Combining (3.39), (3.41) with Hölder's inequality yields the continuous multiplication map

$$W^{\frac{1}{2}+\lambda,2}(\mathcal{D}) \times W^{2\gamma,6}(\mathcal{D}) \hookrightarrow L^{q'}(\mathcal{D}). \tag{3.42}$$

In particular, for every $\phi \in L^6(\mathcal{D})$,

$$\left\| u_t \cdot \nabla (-\Delta)^{-\gamma-\frac{1}{2}} \phi \right\|_{L^{q'}(\mathcal{D})} \leq C \left\| u_t \right\|_{W^{\frac{1}{2}+\lambda,2}(\mathcal{D})} \left\| \phi \right\|_{L^6(\mathcal{D})}. \tag{3.43}$$

Time integrability condition. Since $\delta_u < \bar{\delta}_u \leq 1 - \lambda$, we have $\lambda \leq 1 - \delta_u$ and therefore Corollary 3.2 implies

$$u \in L^{\frac{p}{\lambda+\delta_u}}\left(0, T; W^{\frac{1}{2}+\lambda,2}(\mathcal{D})\right). \tag{3.44}$$

Moreover, $\delta_u < \bar{\delta}_u \leq \lambda_{\max} - \lambda$ gives $\lambda + \delta_u < \lambda_{\max} = p(1 - a(s,\gamma))$, and hence, by Remark 3.2,

$$\left(\gamma + \frac{s}{2} + \frac{1}{2}\right) \frac{1}{1 - \frac{\lambda}{p} - \frac{\delta_u}{p}} < 1. \tag{3.45}$$

Step 2. Fixed point argument. Observe that, using the notation introduced in Corollary 3.3, we can write ζ_t in the form

$$\zeta_t = e^{t\Delta}\theta_0 - (-\Delta)^{-\frac{s}{2}} \int_0^t (-\Delta)^{\gamma+\frac{s}{2}+\frac{1}{2}} e^{(t-r)\Delta} (-\Delta)^{-\gamma-\frac{1}{2}} \operatorname{div}\left(u_r \zeta_r\right) dr - \chi_t,$$

Let $X := C\left(0, T_1; W^{s,\frac{6}{5}}(\mathcal{D})\right)$, where $T_1 \leq T$ will be chosen later, and for $\zeta \in X$ consider $\Psi(\zeta) := \tilde{\zeta}$, where $\tilde{\zeta}$ is defined as follows

$$\tilde{\zeta}_t := e^{t\Delta}\theta_0 - (-\Delta)^{-\frac{s}{2}} \int_0^t (-\Delta)^{\gamma+\frac{s}{2}+\frac{1}{2}} e^{(t-r)\Delta} (-\Delta)^{-\gamma-\frac{1}{2}} \operatorname{div}\left(u_r \zeta_r\right) dr - \chi_t. \tag{3.46}$$

We are going to apply a fixed point argument to obtain the thesis. First, since $\chi_t \in X$ thanks to Corollary 3.3, to show that $\Psi(\zeta) \in X$ it is sufficient to prove that the linear application

$$\Lambda(\zeta)_t := \int_0^t (-\Delta)^{\gamma+\frac{s}{2}+\frac{1}{2}} e^{(t-r)\Delta} (-\Delta)^{-\gamma-\frac{1}{2}} \operatorname{div}(u_r \zeta_r)\, dr$$

maps X to $C(0,T_1; L^{\frac{6}{5}}(\mathcal{D}))$. Second, we will show that $\Psi\colon X \to X$ is a contraction. We divide the remaining part of the proof into three steps.

Step 3. We want to show that, for any fixed $0 < \delta_u < \bar{\delta}_u(s,p)$ and any u as in the statement of the theorem, it holds

$$(-\Delta)^{-\gamma-\frac{1}{2}} \operatorname{div}(u_t \zeta_t) \in L^{\frac{p}{\lambda+\delta_u}}\big(0,T_1; L^{\frac{6}{5}}(\mathcal{D})\big). \tag{3.47}$$

Let $\phi \in L^6(\mathcal{D})$. As in the proof of Lemma 3.1, using integration by parts and the self-adjointness of Δ, we obtain

$$\begin{aligned}
\Big\langle (-\Delta)^{-\gamma-\frac{1}{2}} \operatorname{div}(u_t\zeta_t), \phi \Big\rangle &= \Big\langle \operatorname{div}(u_t\zeta_t), (-\Delta)^{-\gamma-\frac{1}{2}}\phi \Big\rangle \\
&= -\Big\langle u_t\zeta_t, \nabla(-\Delta)^{-\gamma-\frac{1}{2}}\phi \Big\rangle \\
&= -\Big\langle \zeta_t, u_t \cdot \nabla(-\Delta)^{-\gamma-\frac{1}{2}}\phi \Big\rangle .
\end{aligned}$$

Let q, q' be the conjugate exponents introduced in Step 1, namely $q = \frac{6}{5-2s}$ and $1/q + 1/q' = 1$. By Hölder's inequality,

$$\Big|\Big\langle \zeta_t, u_t \cdot \nabla(-\Delta)^{-\gamma-\frac{1}{2}}\phi \Big\rangle\Big| \le \|\zeta_t\|_{L^q(\mathcal{D})}\, \|u_t \cdot \nabla(-\Delta)^{-\gamma-\frac{1}{2}}\phi\|_{L^{q'}(\mathcal{D})}.$$

Using the product estimate (3.43) from Step 1, we infer

$$\|u_t \cdot \nabla(-\Delta)^{-\gamma-\frac{1}{2}}\phi\|_{L^{q'}(\mathcal{D})} \le C\, \|u_t\|_{W^{\frac{1}{2}+\lambda,2}(\mathcal{D})}\, \|\phi\|_{L^6(\mathcal{D})},$$

and therefore

$$\Big|\Big\langle (-\Delta)^{-\gamma-\frac{1}{2}} \operatorname{div}(u_t\zeta_t), \phi \Big\rangle\Big| \le C\, \|\zeta_t\|_{L^q(\mathcal{D})}\, \|u_t\|_{W^{\frac{1}{2}+\lambda,2}(\mathcal{D})}\, \|\phi\|_{L^6(\mathcal{D})}.$$

Taking the supremum over $\|\phi\|_{L^6} \le 1$ yields

$$\|(-\Delta)^{-\gamma-\frac{1}{2}} \operatorname{div}(u_t\zeta_t)\|_{L^{\frac{6}{5}}(\mathcal{D})} \le C\, \|\zeta_t\|_{L^q(\mathcal{D})}\, \|u_t\|_{W^{\frac{1}{2}+\lambda,2}(\mathcal{D})}. \tag{3.48}$$

Since $\zeta \in X = C(0,T_1; W^{s,\frac{6}{5}}(\mathcal{D}))$, the Sobolev embedding (3.37) implies $\sup_{t\in[0,T_1]} \|\zeta_t\|_{L^q} < \infty$. Hence, raising (3.48) to the power $\frac{p}{\lambda+\delta_u}$ and integrating, we obtain

$$\int_0^{T_1} \|(-\Delta)^{-\gamma-\frac{1}{2}} \operatorname{div}(u_t\zeta_t)\|_{L^{\frac{6}{5}}}^{\frac{p}{\lambda+\delta_u}}\, dt \le C\Big(\sup_{t\in[0,T_1]} \|\zeta_t\|_{L^q}\Big)^{\frac{p}{\lambda+\delta_u}} \int_0^{T_1} \|u_t\|_{W^{\frac{1}{2}+\lambda,2}}^{\frac{p}{\lambda+\delta_u}}\, dt. \tag{3.49}$$

The last integral is finite by (3.44), i.e. $u \in L^{\frac{p}{\lambda+\delta_u}}(0,T_1;W^{\frac{1}{2}+\lambda,2}(\mathcal{D}))$. This proves (3.47)

Step 4. Repeating the same arguments in Corollary 3.3, we obtain $\Lambda(\zeta)_t \in C\left(0,T;L^{\frac{6}{5}}(\mathcal{D})\right)$, and thus $\Psi(\zeta)=\tilde{\zeta}\in X$.

Step 5. We conclude the proof by showing that Ψ is a contraction in $X = C(0,T_1;W^{s,\frac{6}{5}}(\mathcal{D}))$ for $T_1>0$ sufficiently small. Let $\zeta_1,\zeta_2\in X$ and set $\zeta := \zeta_1-\zeta_2$. From

$$\Psi(\zeta_i) = e^{t\Delta}\theta_0 - (-\Delta)^{-\frac{s}{2}}\Lambda(\zeta_i)_t - \chi_t,$$

we deduce that, for every $t\in[0,T_1]$,

$$\Psi(\zeta_1)(t)-\Psi(\zeta_2)(t) = -(-\Delta)^{-\frac{s}{2}}\int_0^t (-\Delta)^{\gamma+\frac{s}{2}+\frac{1}{2}}e^{(t-r)\Delta}(-\Delta)^{-\gamma-\frac{1}{2}}\mathrm{div}\big(u_r\zeta_r\big)\,dr.$$

Set

$$\sigma := \gamma+\frac{s}{2}+\frac{1}{2}, \qquad h(r) := (-\Delta)^{-\gamma-\frac{1}{2}}\mathrm{div}(u_r\zeta_r),$$

and recall that $q := \frac{p}{\lambda+\delta_u}$ and $q' = \frac{q}{q-1}$. Using the smoothing estimate for the heat semigroup, we obtain for every $t\in[0,T_1]$

$$\begin{aligned}\|\Psi(\zeta_1)(t)-\Psi(\zeta_2)(t)\|_{W^{s,\frac{6}{5}}(\mathcal{D})} &\le C\int_0^t \|(-\Delta)^{\sigma}e^{(t-r)\Delta}h(r)\|_{L^{\frac{6}{5}}(\mathcal{D})}\,dr\\ &\le C\int_0^t (t-r)^{-\sigma}\|h(r)\|_{L^{\frac{6}{5}}(\mathcal{D})}\,dr.\end{aligned}$$

Applying Hölder's inequality in time with exponents q,q', we get

$$\begin{aligned}\|\Psi(\zeta_1)(t)-\Psi(\zeta_2)(t)\|_{W^{s,\frac{6}{5}}} &\le C\left(\int_0^t (t-r)^{-\sigma q'}\,dr\right)^{\frac{1}{q'}}\left(\int_0^t \|h(r)\|^q_{L^{\frac{6}{5}}}\,dr\right)^{\frac{1}{q}}\\ &\le C\left(\int_0^{T_1}\tau^{-\sigma q'}\,d\tau\right)^{\frac{1}{q'}}\|h\|_{L^q(0,T_1;L^{\frac{6}{5}}(\mathcal{D}))}.\end{aligned}$$

The integral in τ is finite thanks to condition (3.45), i.e. $\sigma q'<1$. Hence,

$$\|\Psi(\zeta_1)-\Psi(\zeta_2)\|_X \le C(\int_0^{T_1}\tau^{-\sigma q'}\,d\tau)^{\frac{1}{q'}}\|h\|_{L^q(0,T_1;L^{\frac{6}{5}}(\mathcal{D}))}. \tag{3.50}$$

Finally, repeating the argument of Step3 in (3.48)-(3.49) we obtain

$$\|h\|_{L^q(0,T_1;L^{\frac{6}{5}}(\mathcal{D}))} \le C\|u\|_{L^{\frac{p}{\lambda+\delta_u}}\left(0,T_1;W^{\frac{1}{2}+\lambda,2}(\mathcal{D})\right)}\|\zeta\|_X.$$

Substituting into (3.50) yields

$$\|\Psi(\zeta_1)-\Psi(\zeta_2)\|_X \le K(T_1)\|u\|_{L^{\frac{p}{\lambda+\delta_u}}(0,T_1;W^{\frac{1}{2}+\lambda,2}(\mathcal{D}))}\|\zeta_1-\zeta_2\|_X, \tag{3.51}$$

where

$$K(T_1) := C\left(\int_0^{T_1} \tau^{-\sigma q'}\, d\tau\right)^{\frac{1}{q'}}.$$

Since $u \in L^{\frac{p}{\lambda+\delta_u}}(0,T;W^{\frac{1}{2}+\lambda,2}(\mathcal{D}))$, we have $\|u\|_{L^{\frac{p}{\lambda+\delta_u}}(0,T_1;W^{\frac{1}{2}+\lambda,2})} \to 0$ as $T_1 \downarrow 0$, and moreover $K(T_1) < \infty$ for every $T_1 > 0$ by $\sigma q' < 1$. Therefore, choosing $T_1 > 0$ sufficiently small makes the right-hand side of (3.51) strictly less than $\|\zeta_1 - \zeta_2\|_X$, so Ψ is a contraction on X. This yields a unique fixed point $\zeta \in C(0,T_1;W^{s,\frac{6}{5}}(\mathcal{D}))$. If $T_1 < T$, we may iterate the fixed point argument finitely many times to cover $[0,T]$. □

Remark 3.3. *Note that Corollary 3.1 follows by applying to the definition of $\tilde{\zeta}_t$ in* (3.46) *the same arguments that were used to prove* (3.34) *and* (3.49)*.*

3.4 Velocity problem

Let $\delta_u > 0$ be a small regularity exponent for the velocity. In this section, we consider the velocity problem (3.4), assuming that the temperature is a given forcing term $f^\theta \in L^p(0,T;H^{-\frac{1}{2}-\delta_u}(\mathcal{D}))$. By exploiting the weak-Stokes operator $A_w \colon {}_0H_\sigma^{\frac{3}{2}-\delta_u}(\mathcal{D}) \to {}_0H_\sigma^{-\frac{1}{2}-\delta_u}(\mathcal{D})$ introduced in (3.1) as

$$\langle A_w u, v\rangle = \langle \nabla u, \nabla v\rangle_{H^{\frac{1}{2}-\delta_u}, H^{-\frac{1}{2}+\delta_u}}, \quad (u,v) \in {}_0H_\sigma^{\frac{3}{2}-\delta_u}(\mathcal{D}) \times {}_0H_\sigma^{\frac{1}{2}+\delta_u}(\mathcal{D}),$$

then the velocity problem can be reformulated as a Cauchy problem in ${}_0H_\sigma^{-\frac{1}{2}-\delta_u}(\mathcal{D})$ as follows

$$\begin{cases} \partial_t u + A_w u = P(-u\cdot\nabla u + f^\theta), & t \in (0,T), \\ u|_{t=0} = u_0, \end{cases} \tag{3.52}$$

where P denotes the Helmholtz projection, and $u_0 \in V_p^{\delta_u}$ denotes the initial condition, with

$$V_p^{\delta_u} = \left({}_0H_\sigma^{-\frac{1}{2}-\delta_u}(\mathcal{D}), {}_0H_\sigma^{\frac{3}{2}-\delta_u}(\mathcal{D})\right)_{1-\frac{1}{p},p}.$$

Note that here, and in the remainder of the section, we drop the dependence of u on ε.

In Section 3.4.1, we investigate the properties of the weak Stokes operator A_w, in particular the $\mathcal{H}^\infty$-calculus and maximal regularity. Then, in Section 3.4.2 we apply these results to prove a global for small-data result for (3.52), according to the mild notion of solution stated in Definition 3.1.

3.4.1 Stokes operator in weak setting, $\mathcal{H}^\infty$-calculus and maximal regularity

We start this section by recalling how the weak Stokes operator A_w inherits the property of a bounded $\mathcal{H}^\infty$-calculus with $\mathcal{H}^\infty$-angle $\phi^\infty_{A_w} = 0$ from the (strong) Stokes operator A. This is obtained by following the approach in [13, Section 5].

From this, it follows the maximal regularity property for the (weak) Stokes operator and the mixed derivative theorem, which are summarised in Proposition 3.3 and Lemma 3.2, respectively. Then, we conclude the section showing how it is possible to estimate the non-linear convective term $u \cdot \nabla u$ in $L^p(0,T;{}_0H_\sigma^{-\frac{1}{2}-\delta_u}(\mathcal{D}))$ using the maximal regularity space $\mathbb{E}^{\delta_u}_{T,p}$, for any $p > \frac{2}{1-\delta_u}$. This is key to prove the global existence result for small data in Section 3.4.2.

Proposition 3.2. *The weak Stokes operator*

$$A_w \colon {}_0H_\sigma^{\frac{3}{2}-\delta_u}(\mathcal{D}) \to {}_0H_\sigma^{-\frac{1}{2}-\delta_u}(\mathcal{D})$$

admits a bounded $\mathcal{H}^\infty$-calculus on ${}_0H_\sigma^{-\frac{1}{2}-\delta_u}(\mathcal{D})$ with angle $\phi^\infty_{A_w} = 0$.

Proof. Let $A_0 = A$ and $X_0 = L^2_\sigma(\mathcal{D})$. By [14, Theorem V.1.5.1 and Theorem 1.5.4], it follows that the pair (X_0, A_0) generates an interpolation-extrapolation scale (X_α, A_α) with respect to the complex interpolation functor. Note that for $\alpha \in (0,1)$, A_α is the X_α-realization of A_0 (the restriction of A_0 to X_α) and

$$X_\alpha = D(A_0^\alpha).$$

Let $X_0^\sharp := (X_0)'$ and $A_0^\sharp := (A_0)'$ with $D(A_0^\sharp) =: X_1^\sharp$. Then $(X_0^\sharp, A_0^\sharp)$ generates an interpolation-extrapolation scale $(X_\alpha^\sharp, A_\alpha^\sharp)$, the dual scale, and by [14, Theorem V.1.5.12], it holds that

$$(X_\alpha)' = X^\sharp_{-\alpha} \quad \text{and} \quad (A_\alpha)' = A^\sharp_{-\alpha}$$

for $\alpha \in \mathbb{R}$. Further, the domain of the fractional power of the Stokes operator can be characterised as

$$X_\alpha = D((-\Delta)^\alpha) \cap L^2_\sigma(\mathcal{D}), \quad \alpha \in (0,1),$$

see [9]. In the particular case of

$$\alpha = 1 - \theta = \frac{3}{4} - \frac{\delta_u}{2},$$

then from the characterisation of the fractional powers of the Dirichlet Laplacian, we get

$$X_{1-\theta} = \left\{ u \in H^{\frac{3}{2}-\delta_u}(\mathcal{D}) \ : \ u|_{\partial\mathcal{D}} = 0 \right\} \cap L^2_\sigma(\mathcal{D}),$$

where $u|_{\partial\mathcal{D}}$ is understood in trace-sense. Hence, the operator $A_{-\theta}$ from the scale (X_α, A_α), $\alpha \in \mathbb{R}$, is given by

$$A_{-\theta}\colon X_{1-\theta} \to X_{-\theta},$$

where by reflexivity $X_{-\theta} = \left(X_\theta^\sharp\right)'$. Since $A_0^\sharp \in \mathcal{H}^\infty(X_0^\sharp)$, we have

$$X_\theta^\sharp = D((A_0^\sharp)^\theta) = [X_0^\sharp, X_1^\sharp]_\theta = \left\{u \in H^{\frac{1}{2}+\delta_u}(\mathcal{D}) \ : \ u|_{\partial\mathcal{D}} = 0\right\} \cap L^2_\sigma(\mathcal{D}).$$

Moreover, we have $A_{-\theta} = (A_\theta^\sharp)'$. Since $A_0^\sharp$ admits a bounded $\mathcal{H}^\infty$-calculus on $X_0^\sharp$ with angle 0, by duality the operator $A_{-\theta}\colon X_{1-\theta} \to X_{-\theta}$ has a bounded $\mathcal{H}^\infty$-calculus with $\mathcal{H}^\infty$-angle $\phi^\infty_{A_{-\theta}} = 0$.

It remains to identify $A_{-\theta}$ with the weak Stokes operator A_w. Since $A_{-\theta}$ is the closure of A_0 in $X_{-\theta}$, it coincides with A_0 on the dense subspace X_1. For any $u \in X_1$ and $v \in X_1^\sharp$, we have via integration by parts

$$\langle A_{-\theta}u, v\rangle = (A_0 u, v)_{L^2(\mathcal{D})} = \int_{\mathcal{D}} \nabla u \cdot \nabla v \, dx.$$

Since $X_1^\sharp$ is dense in $X_\theta^\sharp$, this identity extends to all $v \in X_\theta^\sharp$ by interpreting the integral as duality pairing. Note that for $u \in X_{1-\theta}$ and $v \in X_\theta^\sharp$, the gradients satisfy $\nabla u \in H^{\frac{1}{2}-\delta_u}(\mathcal{D})$ and $\nabla v \in H^{-\frac{1}{2}+\delta_u}(\mathcal{D})$. Thus, the identity extends continuously with respect to u to the duality pairing

$$\langle A_{-\theta}u, v\rangle = \langle \nabla u, \nabla v\rangle_{H^{\frac{1}{2}-\delta_u}, H^{-\frac{1}{2}+\delta_u}}.$$

Since X_1 is dense in $X_{1-\theta}$, this identity holds for all $u \in X_{1-\theta} = {}_0H^{\frac{3}{2}-\delta_u}_\sigma(\mathcal{D})$ and $v \in X_\theta^\sharp = {}_0H^{\frac{1}{2}+\delta_u}_\sigma(\mathcal{D})$. Therefore, the abstract operator $A_{-\theta}$ coincides with the weak Stokes operator A_w defined in (3.1), and A_w inherits the bounded $\mathcal{H}^\infty$-calculus. □

The first result that we recall is the maximal regularity of the weak Stokes operator, which is a consequence of the $\mathcal{H}^\infty$-calculus recalled above, see [15, Section II.4].

Proposition 3.3 (Maximal regularity for the weak-Stokes operator)**.** *Let $T > 0$ be a given time, $J = (0,T)$, $\delta_u \in (0,1)$. Consider the problem*

$$\begin{cases} \partial_t z + A_w z = g, & t \in (0,T), \\ z|_{t=0} = z_0. \end{cases} \tag{3.53}$$

(i) If $g \in L^p(J; {}_0H^{-\frac{1}{2}-\delta_u}_\sigma(\mathcal{D}))$ and $z_0 \in V_p^{\delta_u}$, then there exists a unique solution

$$z \in \mathbb{E}^{\delta_u}_{T,p} = W^{1,p}(J; {}_0H^{-\frac{1}{2}-\delta_u}_\sigma(\mathcal{D})) \cap L^p(J; {}_0H^{\frac{3}{2}-\delta_u}_\sigma(\mathcal{D}))$$

of (3.53)*.*

(ii) There exists $C = C(p, \delta_u, T) > 0$ *such that*

$$\|z\|_{\mathbb{E}^{\delta_u}_{T,p}} \leq C \left(\|g\|_{L^p(J;H^{-\frac{1}{2}-\delta_u}(\mathcal{D}))} + \|z_0\|_{V_p^{\delta_u}} \right). \tag{3.54}$$

Second, we recall the mixed derivative theorem, see e.g. [15, Corollary 4.5.10].

Lemma 3.2 (Mixed derivative)**.** *Let* $T > 0$ *be a given time and* $J = (0, T)$*. Then*

$$\mathbb{E}^{\delta_u}_{T,p} = W^{1,p}(J; {}_0H_\sigma^{-\frac{1}{2}-\delta_u}(\mathcal{D})) \cap L^p(J; {}_0H_\sigma^{\frac{3}{2}-\delta_u}(\mathcal{D})) \hookrightarrow H^{r,p}(J; D(A_w^{1-r})), \tag{3.55}$$

for any $r \in [0, 1]$.

We conclude with an auxiliary result, which is based on Lemma 3.2, for the estimate of the non-linear convective term of the NSEs (3.52).

Lemma 3.3. *Let* $T > 0$ *be a given time,* $\delta_u \in (0, 1)$ *and set* $J = (0, T)$*. If* $p > \frac{2}{1-\delta_u}$*, then there exists* $C = C(p, \delta_u, T) > 0$ *such that*

$$\|P(u \cdot \nabla v)\|_{L^p(J;{}_0H_\sigma^{-\frac{1}{2}-\delta_u}(\mathcal{D}))} \leq C \|u\|_{\mathbb{E}^{\delta_u}_{T,p}} \|v\|_{\mathbb{E}^{\delta_u}_{T,p}}$$

for any $u, v \in \mathbb{E}^{\delta_u}_{T,p}$*, where* $P : H^{-\frac{1}{2}-\delta_u}(\mathcal{D}) \to {}_0H_\sigma^{-\frac{1}{2}-\delta_u}(\mathcal{D})$ *is the extension of the Helmholtz projection.*

Proof. Assume that $s_1, s_2 \in \mathbb{R}$ are such that the following pointwise multiplication is bilinear and continuous

$$\begin{aligned} W^{s_1,2}(\mathcal{D}) \times W^{s_2,2}(\mathcal{D}) &\hookrightarrow W^{-\frac{1}{2}-\delta_u,2}(\mathcal{D}) \\ (f, g) &\mapsto fg. \end{aligned} \tag{3.56}$$

Combining the previous multiplication embedding with the boundedness of P on $H^{-\frac{1}{2}-\delta_u}(\mathcal{D})$ and the norm equivalence $H^s(\mathcal{D}) \cong W^{s,2}(\mathcal{D})$, there exists $C = C(s_1, s_2, \delta_u) > 0$ such that

$$\|P(u \cdot \nabla v)\|_{{}_0H_\sigma^{-\frac{1}{2}-\delta_u}(\mathcal{D})} \leq C \|u\|_{W^{s_1,2}(\mathcal{D})} \|\nabla v\|_{W^{s_2,2}(\mathcal{D})} \leq C \|u\|_{W^{s_1,2}(\mathcal{D})} \|v\|_{W^{1+s_2,2}(\mathcal{D})}.$$

Considering the L^p norm in time and applying Hölder's inequality, we obtain

$$\begin{aligned} \|P(u \cdot \nabla v)\|_{L^p(J;{}_0H_\sigma^{-\frac{1}{2}-\delta_u}(\mathcal{D}))} &\leq C \|u \cdot \nabla v\|_{L^p(J;H^{-\frac{1}{2}-\delta_u}(\mathcal{D}))} \\ &\leq C \|u\|_{L^\infty(J;W^{s_1,2}(\mathcal{D}))} \|v\|_{L^p(J;W^{1+s_2,2}(\mathcal{D}))}. \end{aligned}$$

Assuming that

$$\mathbb{E}^{\delta_u}_{T,p} \hookrightarrow L^\infty(J; H^{s_1}(\mathcal{D})) \tag{3.57}$$

and

$$\mathbb{E}^{\delta_u}_{T,p} \hookrightarrow L^p(J; H^{1+s_2}(\mathcal{D})), \tag{3.58}$$

we conclude, from the norm equivalence $H^s(\mathcal{D}) \cong W^{s,2}(\mathcal{D})$, that

$$\|P(u\cdot\nabla v)\|_{L^p(J;{}_0H^{-\frac{1}{2}-\delta_u}_\sigma(\mathcal{D}))} \leq C\,\|u\|_{\mathbb{E}^{\delta_u}_{T,p}}\,\|v\|_{\mathbb{E}^{\delta_u}_{T,p}}.$$

It remains to check that (3.56), (3.57) and (3.58) hold. First, using Lemma 3.2, it holds

$$\mathbb{E}^{\delta_u}_{T,p} \hookrightarrow H^{r,p}(J; D(A_w^{1-r})),$$

for any $r \in [0,1]$. Second, using the notation of the proof of Proposition 3.2, recall that the pair (X_0, A_0), where A_0 denotes the Stokes operator $A_0 = A$, and $X_0 = L^2_\sigma(\mathcal{D})$, generates the interpolation-extrapolation scale (X_α, A_α). Further, the weak Stokes operator is $A_w = A_{-\theta} : X_{1-\theta} \to X_{-\theta}$ and $D(A_w^{1-r}) = X_{-\theta+(1-r)} = {}_0H^{2(1-\theta-r)}_\sigma(\mathcal{D})$. Since $1-\theta = \frac{3}{4} - \frac{\delta_u}{2}$ (see the proof of Proposition 3.2), we have $D(A_w^{1-r}) = {}_0H^{\frac{3}{2}-\delta_u-2r}_\sigma(\mathcal{D})$, and in conclusion

$$\mathbb{E}^{\delta_u}_{T,p} \hookrightarrow H^{r,p}(J; D(A_w^{1-r})) \hookrightarrow H^{r,p}\big(J; H^{\frac{3}{2}-\delta_u-2r}(\mathcal{D})\big).$$

Further, it can be checked that (3.57) holds if

$$\begin{cases} r > \dfrac{1}{p}, \\ \dfrac{3}{2} - \delta_u - 2r \geq s_1, \end{cases} \tag{3.59}$$

is satisfied for some $r \in [0,1]$. On the other hand, (3.58) holds if $s_2 \leq \frac{1}{2} - \delta_u$. Lastly, choosing

$$s_1 := \frac{3}{2} - \delta_u - 2r, \quad s_2 := \frac{1}{2} - \delta_u,$$

the pointwise multiplication embedding (3.56) holds, thanks to [12, Theorem 8.2] if $\delta_u \in (0, \frac{1}{2})$ and [12, Theorem 8.1] if $\delta_u \in [\frac{1}{2}, 1)$, if $r < \frac{1-\delta_u}{2}$. Thus, we can find $r \in (0,1)$ such that (3.56) and (3.59) hold if

$$\frac{1}{p} < \frac{1-\delta_u}{2},$$

which is true thanks to our hypothesis $p > \frac{2}{1-\delta_u}$. This completes the proof. □

3.4.2 Global for small data for the 3D Navier-Stokes problem

The auxiliary results presented in the previous section will be employed to demonstrate Theorem 3.2, i.e. the global existence result for small data for the 3D Navier-Stokes problem (3.52), within the weak setting for the Stokes operator A_w. In particular, if we assume that the initial condition u_0 and the forcing term f^θ are sufficiently small, we show that the solution, in the sense of Definition 3.1, exists on the whole time interval $[0,T]$.

Proof of Theorem 3.2. Let v_* denote the reference solution for (3.52), i.e., the solution to the linear problem

$$\begin{cases} \partial_t v_* + A_w v_* = P f^\theta, & t \in (0,T), \\ v_*|_{t=0} = u_0, \end{cases} \tag{3.60}$$

and define the ball

$$\mathbb{B}\left(v_*, \frac{\eta}{2}\right) = \left\{ v' \in \mathbb{E}^{\delta_u}_{T,p} \ : \ \left\| v' - v_* \right\|_{\mathbb{E}^{\delta_u}_{T,p}} \leq \frac{\eta}{2} \right\} \subset \mathbb{E}^{\delta_u}_{T,p}.$$

Consider the map

$$\begin{aligned} \Gamma \colon \mathbb{B}\left(v_*, \frac{\eta}{2}\right) \subset \mathbb{E}^{\delta_u}_{T,p} &\to \mathbb{E}^{\delta_u}_{T,p} \\ \Gamma(v') &= v, \end{aligned}$$

where v is the unique solution of

$$\begin{cases} \partial_t v + A_w v = P(-v' \cdot \nabla v' + f^\theta), & t \in (0,T), \\ v|_{t=0} = u_0. \end{cases}$$

We will show that, there exists $\tilde{\eta} = \tilde{\eta}(p, \delta_u, T) > 0$ such that for any $\eta \in (0, \tilde{\eta})$, the following two conditions hold

(i) $\|\Gamma(v') - v_*\|_{\mathbb{E}^{\delta_u}_{T,p}} \leq \frac{\eta}{2}$ for all $v' \in \mathbb{B}(v_*, \frac{\eta}{2})$,

(ii) $\|\Gamma(v_1') - \Gamma(v_2')\|_{\mathbb{E}^{\delta_u}_{T,p}} \leq d \cdot \|v_1' - v_2'\|_{\mathbb{E}^{\delta_u}_{T,p}}$, where $d \in [0,1)$, for all $v_1', v_2' \in \mathbb{B}(v_*, \frac{\eta}{2})$.

(i). Let $v = \Gamma(v')$ and define $w := v - v_*$, which satisfies

$$\begin{cases} \partial_t w + A_w w = P(-v' \cdot \nabla v'), & t \in (0,T), \\ w|_{t=0} = 0. \end{cases} \tag{3.61}$$

By the maximal regularity of the weak Stokes operator (see Proposition 3.3), Lemma 3.3 and Jensen's inequality, we obtain

$$\begin{aligned}\|w\|_{\mathbb{E}_{T,p}^{\delta_u}} &\leq C \left\|P(v'\cdot\nabla v')\right\|_{L^p(J;{}_0H_\sigma^{-\frac{1}{2}-\delta_u}(\mathcal{D}))}\\ &\leq C\left\|v'\right\|_{\mathbb{E}_{T,p}^{\delta_u}}^2\\ &\leq 2C\left(\left\|v'-v_*\right\|_{\mathbb{E}_{T,p}^{\delta_u}}^2+\|v_*\|_{\mathbb{E}_{T,p}^{\delta_u}}^2\right),\end{aligned}$$

for a positive constant $C=C(p,\delta_u,T)$ and $J=(0,T)$. Further, again by the maximal regularity of the weak Stokes operator, there exists a constant $M=M(p,\delta_u,T)$ such that

$$\|v_*\|_{\mathbb{E}_{T,p}^{\delta_u}} \leq M\left(\left\|f^\theta\right\|_{L^p(J;H^{-\frac{1}{2}-\delta_u}(\mathcal{D}))}+\|u_0\|_{V_p^{\delta_u}}\right)\leq\frac{\eta}{2}. \tag{3.62}$$

Thus, we have

$$\|v-v_*\|_{\mathbb{E}_{T,p}^{\delta_u}}=\|w\|_{\mathbb{E}_{T,p}^{\delta_u}}\leq 2C\left(\left\|v'-v_*\right\|_{\mathbb{E}_{T,p}^{\delta_u}}^2+\|v_*\|_{\mathbb{E}_{T,p}^{\delta_u}}^2\right)\leq 2C\left(\frac{\eta^2}{4}+\frac{\eta^2}{4}\right)=C\eta^2. \tag{3.63}$$

By choosing η such that

$$\eta^2\leq\frac{\eta}{2C},$$

we conclude that Γ maps $\mathbb{B}\left(v_*,\frac{\eta}{2}\right)$ into itself.

(ii). Let $v_i=\Gamma(v_i')$ for $i=1,2$, and define $\tilde{w}:=v_1-v_2$, $\tilde{w}'=v_1'-v_2'$. Then, $\tilde{w}$ satisfies

$$\begin{cases}\partial_t\tilde{w}+A_w\tilde{w}=P(-v_1'\cdot\nabla v_1'+v_2'\cdot\nabla v_2'), & t\in(0,T),\\ \qquad\tilde{w}|_{t=0}=0.\end{cases} \tag{3.64}$$

By the maximal regularity of the Stokes operator, Lemma 3.3, the definition of v_i' and (3.62), we have

$$\begin{aligned}\left\|\Gamma(v_1')-\Gamma(v_2')\right\|_{\mathbb{E}_{T,p}^{\delta_u}} &\leq C\left\|-\tilde{w}'\cdot\nabla v_1'-v_2'\cdot\nabla\tilde{w}'\right\|_{L^p(J;H^{-\frac{1}{2}-\delta_u}(\mathcal{D}))}\\ &\leq C\left\|\tilde{w}'\right\|_{\mathbb{E}_{T,p}^{\delta_u}}\left(\left\|v_1'\right\|_{\mathbb{E}_{T,p}^{\delta_u}}+\left\|v_2'\right\|_{\mathbb{E}_{T,p}^{\delta_u}}\right)\\ &\leq C\left\|\tilde{w}'\right\|_{\mathbb{E}_{T,p}^{\delta_u}}(\eta+\eta)\\ &= 2C\left\|v_1'-v_2'\right\|_{\mathbb{E}_{T,p}^{\delta_u}}\eta,\end{aligned}$$

where $C=C(p,\delta_u,T)$ is a positive constant changing from line to line. Up to choosing η sufficiently small, (ii) is verified.

In conclusion, by the Banach fixed point theorem, there exists a unique fixed point $v = \Gamma(v) \in \mathbb{B}(v_*, \frac{\eta}{2})$. Furthermore, by the triangle inequality, (3.62), and (3.63), we also obtain

$$\|v\|_{\mathbb{E}^{\delta_u}_{T,p}} \leq \|v - v_*\|_{\mathbb{E}^{\delta_u}_{T,p}} + \|v_*\|_{\mathbb{E}^{\delta_u}_{T,p}} \leq \frac{\eta}{2} + \frac{\eta}{2} = \eta.$$

This concludes the proof. □

3.5 Well-posedness for the 3D-coupled temperature-velocity model with boundary noise

We are now in position to prove the main result of our work.

Proof of Theorem 3.3. Fix $T > 0$, $s \in (0, \frac{1}{2})$ and $p > 4$. Choose, as in (3.9),

$$\gamma := \frac{1}{4} + \varepsilon_\gamma, \qquad 0 < \varepsilon_\gamma < \min\left\{\frac{1-2s}{4}, \frac{(1-2s)(p-4)}{4p}\right\},$$

and set

$$a(s,\gamma) := \frac{1}{2} + \gamma + \frac{s}{2}, \qquad \lambda_{\max} := p(1 - a(s,\gamma)), \qquad \lambda_{\min} := \frac{1}{2} - s.$$

Then $\lambda_{\max} > \lambda_{\min}$, thanks to the same computation as in (3.10). Hence the interval $(\lambda_{\min}, \lambda_{\max})$ is non-empty. Thus, we may choose $\lambda \in (\lambda_{\min}, \lambda_{\max})$. In particular, as in (3.12), we pick

$$\lambda := \frac{1}{2} - s + \varepsilon_\lambda \qquad 0 < \varepsilon_\lambda < \min\{2s, \lambda_{\max} - (1-2s)\}.$$

Lastly, as in (3.13), define the thresholds

$$\bar{\delta}_\theta := \min\left\{\lambda, 2\gamma - \frac{1}{2}\right\}, \qquad \bar{\delta}_u := \min\left\{1 - \lambda, \lambda_{\max} - \lambda\right\}.$$

With this choice we have

$$1 - \lambda > \frac{1}{2} - s, \qquad \lambda_{\max} - \lambda > \frac{1}{2} - s, \qquad \text{hence} \qquad \bar{\delta}_u > \frac{1}{2} - s.$$

In preparation for the application of Sobolev embeddings used below and Theorem 3.2, we now fix $\delta_u \in (0, \bar{\delta}_u)$ and $0 < \delta_\theta < \bar{\delta}_\theta$ satisfying the compatibility conditions (3.16), namely

$$\delta_u \geq \max\left\{\delta_\theta, \frac{1}{2} - s\right\}, \qquad \delta_u < 1 - \frac{2}{p}.$$

These constraints are consistent: indeed $p > 4$ implies $1 - \frac{2}{p} > \frac{1}{2}$ and, by the choice of λ, we have $\bar{\delta}_u > \frac{1}{2} - s$, hence one can pick

δ_u in the non-empty interval $\left[\frac{1}{2}-s, \min\{\bar{\delta}_u, 1-\frac{2}{p}\}\right)$ and then choose any $\delta_\theta \in (0, \min\{\bar{\delta}_\theta, \delta_u\})$. Finally, note that $\delta_u < 1-\frac{2}{p}$ is equivalent to $p > \frac{2}{1-\delta_u}$, which is the integrability requirement needed to apply maximal regularity in Theorem 3.2.

Define

$$\alpha_\theta = \frac{1}{4} + \frac{\delta_\theta}{2}, \qquad \beta_\theta = \frac{1}{4} - \frac{\delta_\theta}{4}.$$

Let $\tilde{\eta} = \tilde{\eta}(p, \delta_u, T) > 0$ and $M = M(p, \delta_u, T) > 0$ be the constants given by Theorem 3.2. Since $\delta_u \geq \max\{\delta_\theta, \frac{1}{2}-s\}$ thanks to the compatibility conditions (3.16), the embeddings

$$H^{-2\alpha_\theta}(\mathcal{D}) \hookrightarrow H^{-\frac{1}{2}-\delta_u}(\mathcal{D}), \quad W^{s,\frac{6}{5}}(\mathcal{D}) \hookrightarrow H^{s-1}(\mathcal{D}) \hookrightarrow H^{-\frac{1}{2}-\delta_u}(\mathcal{D}),$$

hold. Thus, there exists a constant $C_{emb} = C_{emb}(\delta_\theta, \delta_u, s)$ such that for all $g_1 \in H^{-2\alpha_\theta}(\mathcal{D})$ and $g_2 \in W^{s,\frac{6}{5}}(\mathcal{D})$, we have

$$\|g_1\|_{H^{-\frac{1}{2}-\delta_u}(\mathcal{D})} \leq C_{emb}\|g_1\|_{H^{-2\alpha_\theta}(\mathcal{D})}, \quad \|g_2\|_{H^{-\frac{1}{2}-\delta_u}(\mathcal{D})} \leq C_{emb}\|g_2\|_{W^{s,\frac{6}{5}}(\mathcal{D})}.$$

We define $\widetilde{M} := \max\{2, M, MT^{1/p}C_{emb}\}$. For any $\eta \in (0, \tilde{\eta})$, define the stopping time $\tau^\varepsilon \colon \Omega \to [0,T]$ as

$$\tau^\varepsilon := \inf\left\{t \in [0,T] \ : \ \|Z_t^\varepsilon\|_{H^{-2\alpha_\theta}(\mathcal{D})} > \frac{\eta}{8\widetilde{M}}\right\},$$

with the understanding that $\tau^\varepsilon = T$ if the previous set is empty. Note that

$$\{\omega \ : \ \tau^\varepsilon = T\} = \left\{\omega \ : \ \sup_{0\leq t\leq T}\|Z_t^\varepsilon\|_{H^{-2\alpha_\theta}(\mathcal{D})} \leq \frac{\eta}{8\widetilde{M}}\right\}.$$

From Proposition 3.1, we deduce that

$$\mathbb{P}\left(\tau^\varepsilon = T\right) \geq 1 - \frac{64\widetilde{M}^2\varepsilon}{\eta^2}\, C(\delta_\theta, T) \sum_k \lambda_k^2 \left\|(-\Delta)^{\beta_\theta} De_k\right\|_2^2,$$

where $C = C(\delta_\theta, T)$ is a positive constant. Consider

$$\mathbb{B}_1 := \left\{z \in C(0,\tau^\varepsilon; W^{s,\frac{6}{5}}(\mathcal{D})) \ : \ \|z\|_{C(0,\tau^\varepsilon;W^{s,\frac{6}{5}}(\mathcal{D}))} \leq \frac{\eta}{8\widetilde{M}}\right\},$$

and the map

$$\begin{aligned} \Gamma \colon \mathbb{B}_1 &\to C(0,\tau^\varepsilon; W^{s,\frac{6}{5}}(\mathcal{D})) \\ \zeta' &\mapsto \zeta^\varepsilon \end{aligned}$$

where

$$\zeta_t^\varepsilon := e^{t\Delta}\theta_0 - \int_0^t e^{(t-r)\Delta}\left(u_r^\varepsilon \cdot \nabla \zeta_r'\right)\, dr - \int_0^t e^{(t-r)\Delta}\left(u_r^\varepsilon \cdot \nabla Z_r^\varepsilon\right)\, dr, \quad 0 \le t \le \tau^\varepsilon.$$

Here $u^\varepsilon \in \mathbb{E}^{\delta_u}_{\tau^\varepsilon,p}$ is the unique solution of

$$\begin{cases} \partial_t u^\varepsilon + A_w u^\varepsilon = P(-u^\varepsilon \cdot \nabla u^\varepsilon - \theta_t^{\varepsilon,\prime} e_3), & t \in (0, \tau^\varepsilon), \\ u^\varepsilon|_{t=0} = u_0, \end{cases}$$

where

$$\theta_t^{\varepsilon,\prime} := Z^\varepsilon_{t\wedge\tau^\varepsilon} + \zeta_t'.$$

Note that u^ε is well defined thanks to Theorem 3.2, once we check the corresponding smallness condition on the forcing $-\theta^{\varepsilon,\prime}e_3$. First, by the definition of τ^ε we have

$$\sup_{0\le t\le T} \left\| Z^\varepsilon_{t\wedge\tau^\varepsilon}\right\|_{H^{-2\alpha_\theta}(\mathcal{D})} = \sup_{0\le t\le T} \left\| Z^\varepsilon_{t\wedge\tau^\varepsilon}\right\|_{H^{-\frac{1}{2}-\delta_\theta}(\mathcal{D})} \le \frac{\eta}{8\widetilde{M}}.$$

Further, by definition of $\mathbb{B}_1$, we also have

$$\sup_{0\le t\le \tau^\varepsilon} \|\zeta_t'\|_{W^{s,\frac{6}{5}}(\mathcal{D})} \le \frac{\eta}{8\widetilde{M}}.$$

Using the embedding constant C_{emb} defined above, we estimate the forcing in $L^p(0,\tau^\varepsilon; H^{-\frac{1}{2}-\delta_u}(\mathcal{D}))$

$$\begin{aligned} \|\theta^{\varepsilon,\prime}\|_{L^p(0,\tau^\varepsilon;H^{-\frac{1}{2}-\delta_u}(\mathcal{D}))} &\le T^{1/p} \sup_{0\le t\le\tau^\varepsilon} \left(\|Z_t^\varepsilon\|_{H^{-\frac{1}{2}-\delta_u}(\mathcal{D})} + \|\zeta_t'\|_{H^{-\frac{1}{2}-\delta_u}(\mathcal{D})}\right) \\ &\le T^{1/p} C_{emb} \left(\sup_{0\le t\le\tau^\varepsilon} \|Z_t^\varepsilon\|_{H^{-2\alpha_\theta}(\mathcal{D})} + \sup_{0\le t\le\tau^\varepsilon} \|\zeta_t'\|_{W^{s,\frac{6}{5}}(\mathcal{D})}\right) \\ &\le T^{1/p} C_{emb} \left(\frac{\eta}{8\widetilde{M}} + \frac{\eta}{8\widetilde{M}}\right) \\ &= T^{1/p} C_{emb} \frac{\eta}{4\widetilde{M}}. \end{aligned}$$

Since we defined $\widetilde{M} \ge M T^{1/p} C_{emb}$, we deduce

$$\|\theta^{\varepsilon,\prime}\|_{L^p(0,\tau^\varepsilon;H^{-\frac{1}{2}-\delta_u}(\mathcal{D}))} \le \frac{\eta}{4M}.$$

This is exactly the smallness assumption required in Theorem 3.2, so u^ε is well defined.

To apply the Banach fixed point theorem, we first check that Γ maps $\mathbb{B}_1$ into itself. We can use (3.14) by Corollary 3.1 since its hypothesis, namely $\delta_\theta < \bar\delta_\theta$ and $\delta_u < \bar\delta_u$ are satisfied; further, we

have the embedding $\mathbb{E}^{\delta_u}_{\tau^\varepsilon,p} \hookrightarrow L^{\frac{p}{\lambda+\delta_u}}(0,\tau^\varepsilon; W^{\frac{1}{2}+\lambda,2}(\mathcal{D}))$, which holds for our fixed λ thanks to the assumption $\delta_u < 1-\lambda$. Thus,

$$\begin{aligned}\|\zeta^\varepsilon\|_{C(0,\tau^\varepsilon;W^{s,\frac{6}{5}}(\mathcal{D}))} &\leq \sup_{0\leq t\leq\tau^\varepsilon} \left\|e^{t\Delta}\right\|_{W^{s,\frac{6}{5}}(\mathcal{D})} \|\theta_0\|_{W^{s,\frac{6}{5}}(\mathcal{D})} \\ &\quad + C\,\|u^\varepsilon\|_{\mathbb{E}^{\delta_u}_{\tau^\varepsilon,p}} \left(\left\|\zeta'\right\|_{C(0,\tau^\varepsilon;W^{s,\frac{6}{5}}(\mathcal{D}))} + \|\xi^\varepsilon\|_{C(0,\tau^\varepsilon;L^2(\mathcal{D}))}\right) \\ &\leq \frac{\eta}{16\widetilde{M}} + C\eta\left(\frac{\eta}{8\widetilde{M}} + \frac{\eta}{8\widetilde{M}}\right) \\ &= \frac{\eta}{16\widetilde{M}} + \frac{C\eta^2}{4\widetilde{M}}.\end{aligned}$$

Thus, if η is small enough, $\Gamma(\mathbb{B}_1) \subset \mathbb{B}_1$.

Now we verify the contraction property. Consider $\zeta_i^\varepsilon = \Gamma(\zeta_i')$, $i = 1,2$. By the definition of Γ, for every $t \in [0,\tau^\varepsilon]$ we have

$$\begin{aligned}\zeta_1^\varepsilon(t) - \zeta_2^\varepsilon(t) = &-\int_0^t e^{(t-r)\Delta}\Big(u^\varepsilon_{1,r}\cdot\nabla\zeta'_{1,r} - u^\varepsilon_{2,r}\cdot\nabla\zeta'_{2,r}\Big)\,dr \\ &-\int_0^t e^{(t-r)\Delta}\Big(u^\varepsilon_{1,r} - u^\varepsilon_{2,r}\Big)\cdot\nabla Z^\varepsilon_r\,dr.\end{aligned}$$

We split the first integral by adding and subtracting the same quantity and then, using Corollary 3.3 and the bilinear estimate proved in (3.49), we obtain

$$\begin{aligned}\|\zeta_1^\varepsilon - \zeta_2^\varepsilon\|_{C(0,\tau^\varepsilon;W^{s,\frac{6}{5}})} \leq C\Big(&\|u_1^\varepsilon\|_{\mathbb{E}^{\delta_u}_{\tau^\varepsilon,p}} \|\zeta_1' - \zeta_2'\|_{C(0,\tau^\varepsilon;W^{s,\frac{6}{5}})} \\ &+ \|u_1^\varepsilon - u_2^\varepsilon\|_{\mathbb{E}^{\delta_u}_{\tau^\varepsilon,p}} \|\zeta_2'\|_{C(0,\tau^\varepsilon;W^{s,\frac{6}{5}})} \\ &+ \|u_1^\varepsilon - u_2^\varepsilon\|_{\mathbb{E}^{\delta_u}_{\tau^\varepsilon,p}} \|Z^\varepsilon\|_{C(0,\tau^\varepsilon;H^{-2\alpha_\theta})}\Big).\end{aligned}$$

Let $w^\varepsilon := u_1^\varepsilon - u_2^\varepsilon$. It satisfies

$$\begin{cases}\partial_t w^\varepsilon + A_w w^\varepsilon = P(-u_1^\varepsilon\cdot\nabla u_1^\varepsilon + u_2^\varepsilon\cdot\nabla u_2^\varepsilon - \big(\zeta'_{t,1} - \zeta'_{t,2}\big)\,e_3), \qquad t\in(0,\tau^\varepsilon), \\ \qquad w^\varepsilon|_{t=0} = 0.\end{cases}$$

By the maximal regularity of the weak Stokes operator (Proposition 3.3) and Lemma 3.3, there exists $C = C(p,\delta_u,T)$ such that

$$\begin{aligned}\|w^\varepsilon\|_{\mathbb{E}^{\delta_u}_{\tau^\varepsilon,p}} &\leq C\left(\|w^\varepsilon\cdot\nabla u_1^\varepsilon\|_{L^p(0,\tau^\varepsilon;H^{-\frac{1}{2}-\delta_u}(\mathcal{D}))} + \|u_2^\varepsilon\cdot\nabla w^\varepsilon\|_{L^p(0,\tau^\varepsilon;H^{-\frac{1}{2}-\delta_u}(\mathcal{D}))}\right. \\ &\qquad \left. + \left\|\zeta_1' - \zeta_2'\right\|_{L^p(0,\tau^\varepsilon;H^{-\frac{1}{2}-\delta_u}(\mathcal{D}))}\right) \\ &\leq C\left(\|w^\varepsilon\|_{\mathbb{E}^{\delta_u}_{\tau^\varepsilon,p}} \|u_1^\varepsilon\|_{\mathbb{E}^{\delta_u}_{\tau^\varepsilon,p}} + \|u_2^\varepsilon\|_{\mathbb{E}^{\delta_u}_{\tau^\varepsilon,p}} \|w^\varepsilon\|_{\mathbb{E}^{\delta_u}_{\tau^\varepsilon,p}} + \left\|\zeta_1' - \zeta_2'\right\|_{L^p(0,\tau^\varepsilon;H^{-\frac{1}{2}-\delta_u}(\mathcal{D}))}\right) \\ &\leq C\left(2\eta\,\|w^\varepsilon\|_{\mathbb{E}^{\delta_u}_{\tau^\varepsilon,p}} + \left\|\zeta_1' - \zeta_2'\right\|_{L^p(0,\tau^\varepsilon;H^{-\frac{1}{2}-\delta_u}(\mathcal{D}))}\right).\end{aligned}$$

Up to choosing η sufficiently small, using the embedding $W^{s,\frac{6}{5}}(\mathcal{D}) \hookrightarrow H^{s-1}(\mathcal{D}) \hookrightarrow H^{-\frac{1}{2}-\delta_u}(\mathcal{D})$, which holds for $\delta_u \geq \frac{1}{2} - s$, we obtain

$$\|w^\varepsilon\|_{\mathbb{E}^{\delta_u}_{\tau^\varepsilon,p}} \leq C \left\|\zeta_1' - \zeta_2'\right\|_{L^p(0,\tau^\varepsilon;H^{-\frac{1}{2}-\delta_u}(\mathcal{D}))} \leq C \left\|\zeta_1' - \zeta_2'\right\|_{C(0,\tau^\varepsilon;W^{s,\frac{6}{5}}(\mathcal{D}))}.$$

Up to renaming C, we get

$$\begin{aligned}\|\zeta_1^\varepsilon - \zeta_2^\varepsilon\|_{C(0,\tau^\varepsilon;W^{s,\frac{6}{5}}(\mathcal{D}))} &\leq C\left(\eta \|\zeta_1' - \zeta_2'\|_{C(0,\tau^\varepsilon;W^{s,\frac{6}{5}}(\mathcal{D}))} + \|\zeta_1' - \zeta_2'\|_{C(0,\tau^\varepsilon;W^{s,\frac{6}{5}}(\mathcal{D}))} \frac{\eta}{8\widetilde{M}}\right) \\ &= d \|\zeta_1' - \zeta_2'\|_{C(0,\tau^\varepsilon;W^{s,\frac{6}{5}}(\mathcal{D}))}\end{aligned}$$

where $d := C\eta(1 + \frac{1}{8\widetilde{M}})$. Thus, $d < 1$ if η is small enough.

Lastly, regarding the adaptedness of the solution process, fix a time $t_0 \in [0,T]$. For any $\omega \in \Omega$, the contraction principle applied in the proof above, starting with a deterministic initial condition, generates an adapted sequence $(\tilde{u}_n^{\varepsilon,t_0}(\omega), \tilde{\theta}_n^{\varepsilon,t_0}(\omega))_n$ which converges to a limiting sequence $(\tilde{u}^{\varepsilon,t_0}(\omega), \tilde{\theta}^{\varepsilon,t_0}(\omega))$. This latter stochastic process is adapted, being the limit of adapted processes. By uniqueness, the restriction to $[0,t_0]$ of the solution $(u^\varepsilon(\omega), \tilde{\theta}^\varepsilon(\omega))$ needs to coincide with the adapted solution $(\tilde{u}^{\varepsilon,t_0}, \tilde{\theta}^{\varepsilon,t_0})$. This proves adaptedness. The progressive measurability of the solution can be obtained by a similar reasoning. The proof is thus complete. □

References

1. Da Prato, G. & Zabczyk, J. *Stochastic equations in infinite dimensions* second. MR3236753. doi:10.1017/CBO9781107295513 (Cambridge University Press, Cambridge, 2014).
2. Da Prato, G. & Zabczyk, J. Evolution equations with white-noise boundary conditions. *Stochastics and Stochastics Reports* **42.** MR1291187, 167–182. doi:10.1080/17442509308833817 (1993).
3. Lions, J.-L. & Magenes, E. *Non-homogeneous boundary value problems and applications. Vol. I* MR350177. doi:10.1007/978-3-642-65161-8 (Springer-Verlag, New York-Heidelberg, 1972).
4. Triebel, H. *Theory of function spaces* MR3024598. doi:10.1007/978-3-0346-0416-1 (Birkhäuser/Springer Basel AG, Basel, 2010).
5. Temam, R. *Navier-Stokes equations and nonlinear functional analysis* second. doi:10.1137/1.9781611970050 (SIAM, Philadelphia, PA, 1995).

6. Engel, K.-J. & Nagel, R. *One-parameter semigroups for linear evolution equations* doi:10.1007/b97696 (Springer, New York, 2000).
7. Hytönen, T. *et al. Analysis in Banach spaces. Vol. II. Probabilistic methods and operator theory* doi:10.1007/978-3-319-69808-3 (Springer, Cham, 2017).
8. Haase, M. *The functional calculus for sectorial operators* doi:10.1007/3-7643-7698-8 (Birkhäuser Verlag, Basel, 2006).
9. Giga, Y. Domains of fractional powers of the Stokes operator in L_r spaces. *Archive for Rational Mechanics and Analysis* **89.** MR786549, 251–265. doi:10.1007/BF00276874 (1985).
10. Lunardi, A. *Interpolation theory* third. MR3753604. doi:10.1007/978-88-7642-638-4 (Edizioni della Normale, Pisa, 2018).
11. Pazy, A. *Semigroups of linear operators and applications to partial differential equations* doi:10.1007/978-1-4612-5561-1 (Springer-Verlag, New York, 1983).
12. Behzadan, A. & Holst, M. Multiplication in Sobolev spaces, revisited. *Arkiv för Matematik* **59.** MR4339668, 275–306. doi:10.4310/ARKIV.2021.v59.n2.a2 (2021).
13. Prüss, J. & Wilke, M. On critical spaces for the Navier-Stokes equations. *Journal of Mathematical Fluid Mechanics* **20.** MR3808592, 733–755. doi:10.1007/s00021-017-0342-5 (2018).
14. Amann, H. *Linear and quasilinear parabolic problems. Vol. I* MR1345385. doi:10.1007/978-3-0348-9221-6 (Birkhäuser Boston, Inc., Boston, MA, 1995).
15. Prüss, J. & Simonett, G. *Moving interfaces and quasilinear parabolic evolution equations* MR3524106. doi:10.1007/978-3-319-27698-4 (Birkhäuser/Springer, Cham, 2016).

Chapter 4



Climate, Sustainability, and Volcanoes

4 CLIMATE, SUSTAINABILITY, AND VOLCANOES

This chapter is organised as follows. In Section 4.1 we give an overview of the state of the art concerning volcanic eruptions and their past and present effects from the point of view of climate change and CO_2 emissions. We describe the *warming effect* and the *cooling effect*, providing for the latter a toy model to simulate it. In Section 4.2 we exploit this investigation of volcanoes to address the sustainability of human life in the specific case of the Campi Flegrei caldera, explaining what bradyseism is and what damage it may cause to the population; we then attempt to build a simple model of the subsurface capable of explaining the intense seismic activity.

4.1 The effects of volcanic eruptions

The aim of this section is to characterize the role of present-day volcanic emissions within the framework of climate change, i.e. to determine whether large-scale eruptions can release enough greenhouse gases to contribute to global temperature increases. The analysis that follows traces the impact of volcanic activity through time, with the aim of defining its modern counterpart.

Large volcanic eruptions inject great amounts of particles and gases into the stratosphere. The bulk of the emitted volatiles consists of H_2O, CO_2 and N_2, together with sulfur species released mainly as SO_2 and, in some cases, H_2S [1, 2]. From the radiative point of view, the potentially climate-perturbing species are the greenhouse gases H_2O, CO_2 and the SO_2: the former may, in principle, reinforce the greenhouse effect, whereas the latter is converted into sulfate aerosols on a timescale of weeks, thereby altering the planetary albedo [1, 3, 4]. In the most energetic events, hot convective plumes can penetrate the tropopause and deliver these gases directly into the stratosphere, and deliver these gases directly into the stratosphere, where they acquire longer residence times than in the troposphere [2].

The analysis reveals two distinct and competing mechanisms operating on different time scales. The first, driven by the accomulation of volcanic CO_2 emissions and acting on millennial-to-

geological timescales, induces a *warming effect*. Conversely, the second mechanism is caused by the injection of sulfur dioxide (SO_2) into the stratosphere, operating on a short-term (1-3 yr) timescale and resulting in a temporary *cooling effect*.

4.1.1 Warming effect

Taking a chronological perspective, the earliest manifestation of the warming effect of volcanic activity is associated with the transitions out of the Snowball Earth states. During a global glaciation, silicate-weathering consumption of CO_2 collapses, so that volcanic CO_2 accumulates in the atmosphere until a sufficiently strong greenhouse forcing drives deglaciation [5]. The comparison between the two Neoproterozoic events is instructive, as their contrasting durations point to two distinct routes out of the frozen state. The longer Sturtian glaciation, lasting of the order of tens of millions of years, is consistent with deglaciation driven by the slow, sustained accumulation of volcanic CO_2 [5]. By contrast, the much shorter Marinoan glaciation ($\sim$4 Myr) is widely held to be too brief for gradual CO_2 build-up alone to have reached the deglaciation threshold, requiring instead an additional radiative perturbation [5, 6].

Moving closer to the present, further manifestations of volcanically induced warming emerge during more recent periods. During the last deglaciation, specifically between 12 and 7 ka, volcanic eruptions played a pivotal role in climate dynamics. In this case, the widely discussed hypothesis, proposed by [7], suggests that volcanic activity acted as an accelerating factor for ice melt. In more detail, as ice caps and glaciers retreat, the load imposed on the crust and mantle is removed; this unloading induces mantle decompression, which in turn enhances magma production and ascent, and hence eruptive activity. The increased subaerial volcanism releases additional CO_2, thereby warming the climate and driving further ice melt. This constitutes a positive feedback loop where ice unloading promotes volcanism, which subsequently accelerates deglaciation through greenhouse gas emissions.
However, this mechanism remains debated, and its two limbs have been questioned separately. The deglaciation–eruption-rate link is re-examined in [8], where the empirical support is found to be equivocal, too weak to confirm such a causal relationship conclusively. By contrast, in [9] a volcanism–ice-melt coupling is accepted but its cause is reassigned: abrupt melting events are shown to coincide with volcanogenic aerosol emissions, and the enhanced runoff is attributed primarily to a reduction in surface albedo from ash deposition rather than to large-scale CO_2 warming.



Figure 4.1: *On the scale of carbon dioxide emissions, human sources far outweigh volcanoes. NOAA Climate.gov cartoon by Emily Greenhalgh.*

In the present-day context, by contrast, the warming contribution of volcanic CO_2 is minor, and this can be appreciated from two complementary standpoints. First, the CO_2 released by individual eruptions is negligible relative to the large atmospheric reservoir, so that even a major event does not appreciably enhance the greenhouse effect [1, 3]. Second, the integrated global volcanic CO_2 flux is more than two orders of magnitude smaller than the anthropogenic one: so much so that the entire volcanic excess released over the several millennia of the last deglaciation is comparable to only about a century of present-day anthropogenic output [7], as illustrated in Fig. 4.2. In other words, a source that required thousands of years to leave a discernible imprint on the glacial–interglacial CO_2 record is, on a human timescale, far outweighed by fossil-fuel emissions.
This result answers directly to the question posed at the beginning of this section, namely, whether a large present-day eruption could release enough CO_2 to intensify the greenhouse effect and thereby contribute to global warming. The evidences founded indicate that it could not: the geological episodes in which volcanic CO_2 acted as an effective warming agent all relied on sustained emission integrated over millennial-to-geological timescales and, for the Snowball terminations, under a background CO_2 level orders of magnitude higher than today's. The present-day counterpart of those paleoclimatic warming events is therefore effectively absent.

4.1.2 Cooling effect

Large, explosive volcanic eruptions can have a significant, albeit temporary, cooling effect on the global mean temperature. As well

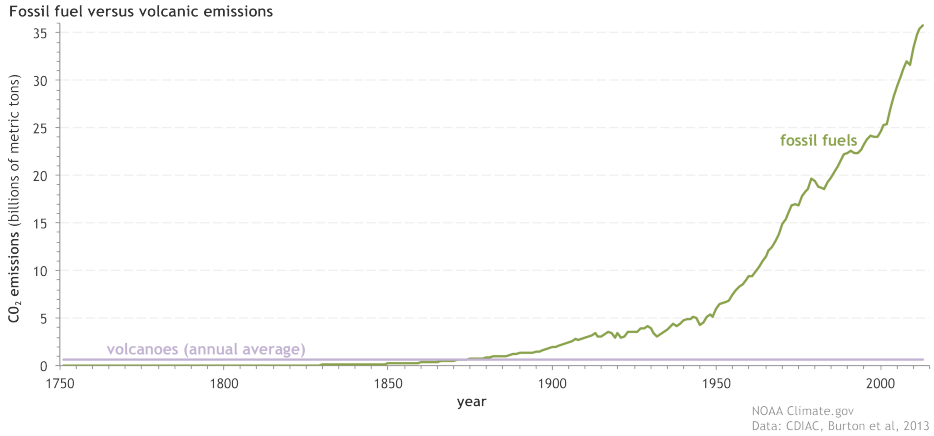

Figure 4.2: *Comparison between human emissions of carbon dioxide from fossil fuels and cement production (green line) and volcanoes emissions of carbon dioxide (purple line), since the start of the Industrial Revolution. NOAA Climate.gov graph, based on data from the Carbon Dioxide Information Analysis Center (CDIAC) at the DOE's Oak Ridge National Laboratory and Burton et al., 2013.*

described in [1], this phenomenon occurs when eruptions are powerful enough to inject large quantities of sulfur dioxide (SO_2) gas into the stratosphere. In the stratosphere, SO_2 reacts with water vapor to form sulfuric acid (H_2SO_4) aerosols. These tiny droplets are highly reflective and can persist for up to a few years, creating a hazy layer that scatters a portion of the incoming solar radiation back into space. In [3] the resulting radiative forcing is quantified through Earth-system model simulations, showing that this reduction in absorbed solar energy leads to a net cooling of the Earth's surface and lower atmosphere, as observed after the 1991 Pinatubo eruption [1]. This phenomenon is corroborated by instrumental evidence: in [10] the 1963 eruption of Mount Agung is used as an early observational test of the modelled surface cooling induced by a stratospheric aerosol perturbation.

The cooling mechanism is well-documented in the historical record. For instance, Figure 4.3 displays a tree-ring-based reconstruction of the Northern Hemisphere's summer temperature anomaly for the period 1590-1710. The chart highlights several major volcanic eruptions from that era. It is visually apparent that a noticeable drop in the temperature anomaly often occurs in the years immediately following these major eruptions, such as the significant cooling event after the 1600 eruption of Huaynaputina in Peru. The pronounced cooling and its societal repercussions during the mid-17th-century eruption cluster have likewise been reconstructed in

[11].

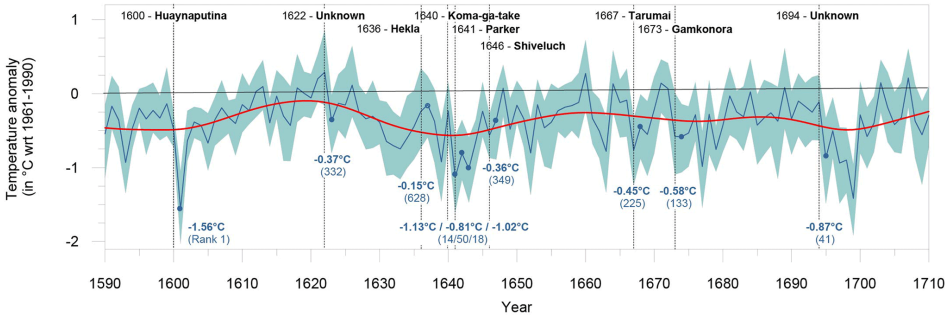

Figure 4.3: *Tree ring based summer temperature anomaly for the Northern hemisphere of the period* $1590 - 1710$ *with respect to the period* $1961 - 1990$*. The volcanic eruptions of* $1600, 1622, 1636, 1640, 1641, 1646, 1667, 1673,$ *and* 1694 *are highlighted by vertical dotted lines. Source: [11]*

Beyond these instrumental and historical instances, the cooling potential of volcanic sulfur has been invoked to explain climate perturbations of far greater magnitude in the deep geological past. In particular, [2] propose that the onset of the first Snowball Earth, the same glaciation whose CO_2-driven termination was discussed in the previous section, was triggered by a massive injection of volcanic sulfate aerosols, whose albedo increase was sufficient to tip the planet into runaway global glaciation.
Such an outcome, however, is exceedingly unlikely under present-day conditions: [4] show that, in an idealized energy-balance model admitting three climate equilibria (a warm, largely ice-free state, an intermediate cold state, and a fully glaciated Snowball), forcing a transition into the Snowball state, even starting from the cold equilibrium, would require a radiative perturbation comparable to that of the Toba super-eruption, the largest known volcanic event of the past $\sim$2 Myr, sustained continuously for several decades, far beyond the transient, few-year signal of any single historical eruption.

From the standpoint of climate change, the question of interest is whether there exists a mechanism based on volcanic activity — and specifically on its cooling effect — capable of operating on a multidecadal scale, so as to partially offset the ongoing rise in temperatures and thus act as a counterweight, without either forcing a state transition or being as unpredictable and short-lived as a single super-eruption. The literature suggests what such a mitigator would require: not an isolated event but a cluster of closely spaced, decadally paced eruptions, sustaining the stratospheric aerosol load, and hence the radiative forcing, well beyond the one-to-two-year lifetime of a single eruption's aerosol [3, 1];

and, beyond this direct forcing, ocean conditions favourable enough for the induced cooling to persist on multidecadal to centennial timescales [3]. Neither condition is guaranteed: the required clustering is rare, the mid-17th-century eruption cluster being one historical instance [11], and the longer-term persistence of the cooling is itself uncertain [3].

A toy model with numerical simulations

The goal of this section is to model the temporary cooling behavior using a simplified climate model. To treat this phenomenon, we consider a one-dimensional energy balance model (1D-EBM) for the surface temperature anomaly $T = T(t, x)$, which is coupled with an advection-diffusion-reaction equation describing the atmospheric concentration of sulfuric acid aerosols $c = c(t, x)$. The coupled system is given by:

$$\begin{cases} \partial_t c + u \cdot \nabla c - \kappa \Delta c = f - \lambda c + \dfrac{dW^1}{dt}, & \text{in } (0,\infty) \times (-1,1), \\ \partial_t T - \nu \Delta T = \beta(T,c) Q(x) - |T|^3 T + \dfrac{dW^2}{dt} & \text{in } (0,\infty) \times (-1,1), \\ \partial_n T = \partial_n c = 0, & \text{in } \partial(-1,1), \\ c(0) = c_0, \quad T(0) = T_0, & \text{in } (-1,1). \end{cases} \tag{4.1}$$

where x represents the spatial coordinate (e.g., latitude), t is time, and $(W_t^1)_t$, $(W_t^2)_t$ are independent cylindrical Wiener processes.

In the first equation, the evolution of the aerosol concentration c is governed by three main processes:

- advective transport ($u \cdot \nabla c$), where aerosols are carried by the atmospheric flow u;
- diffusion ($\kappa \Delta c$), representing the spatial spreading of the aerosol cloud, with $\kappa > 0$ being the diffusion coefficient;
- source and sink terms ($f - \lambda c$), where $f = f(t, x)$ is a source term modeling the injection of aerosols from a volcanic eruption, and $-\lambda c$ represents the gradual removal of aerosols from the stratosphere with a characteristic decay rate $\lambda > 0$.

The second equation in (4.1) is the classical 1D-EBM.

The crucial coupling between the two equations lies in the coalbedo $\beta(T, c)$, which represents the fraction of solar radiation absorbed by the Earth. We assume β is a decreasing function of the

aerosol concentration c. This encapsulates the core physical mechanism: an increase in aerosols (c) reduces the co-albedo (β), causing more solar radiation to be reflected and thus cooling the system.

The atmospheric flow u is modeled as a stochastic process to capture the unpredictable nature of atmospheric circulation:

$$u(t,x) = \theta \sum_{k=1}^{K} \sigma_k(x) Z_t^k,$$

where $\theta > 0$ is a parameter representing intensity, $\sigma_k(x) = sin(k\pi x)$, and $(Z_t^k)_k$ are independent Ornstein-Uhlenebeck processes which are obtained as the solution of the SDEs

$$dZ_t^k = -\frac{1}{\tau} dZ_t^k dt + \frac{1}{\sqrt{\tau}} dW_t^k,$$

where $\tau = \frac{7}{365}$ is the parameter relating to the time correlation (in years).

We simulate the system of equations (4.1) to illustrate the cooling mechanism described [1]. The volcanic eruption is modeled by a source term $f(t,x)$ that is localized in both space (at a specific latitude) and time. As shown in Figure 4.4, the forcing acts as a pulse, injecting aerosols into the atmosphere over a short duration.

Due to the stochastic nature of the wind field u, each simulation run, or "realization," produces a unique spatio-temporal evolution. We present two such realizations to demonstrate the model's typical behavior.

Figure 4.5 and Figure 4.6 show the results. The top panels in each figure (4.5a and 4.6a) display the spatio-temporal evolution of the temperature $T(t,x)$ and the aerosol concentration $c(t,x)$. Following the eruption, a sulphuric acid forms and it is diffused and transported across the domain by the Laplacian and the stochastic wind field.

The impact on the global climate is best seen in the global mean temperature (GMT), which is the spatial average of $T(t,x)$. The bottom panels (4.5b and 4.6b) show the evolution of the GMT for each realization. In both cases, a sharp drop in GMT occurs shortly after the eruption begins. The temperature lower for a period, and then start to increase, due to the presence of the damping term $-\lambda c$ in the equation for c in our model (4.1).

[1] We thank Dr. Gianmarco Del Sarto for providing the code used in the simulations.

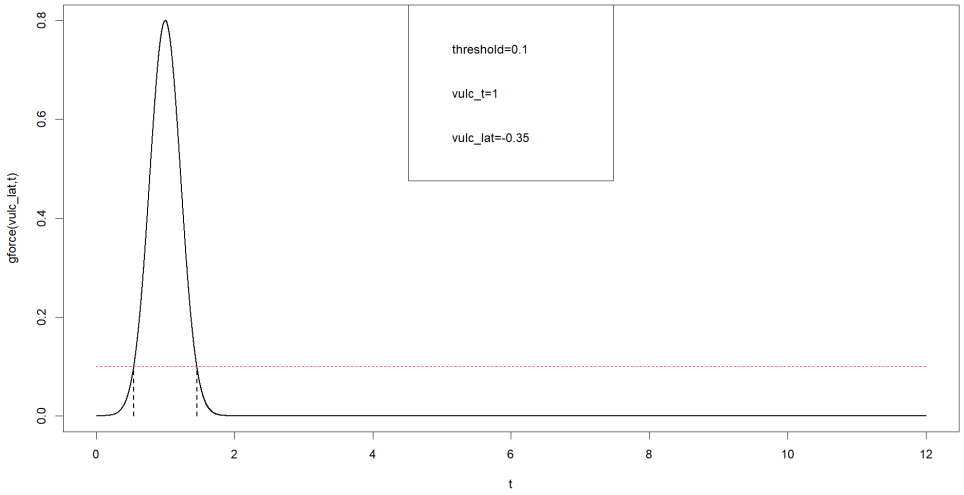

Figure 4.4: *Evolution of $f(t,x)$ with respect to t in $x = x_* = -0.35$ source latitude. Red dashed line is a 0.1 threshold and vertical dashed lines are initial and final times corresponding to the values of f greater than the threshold.*

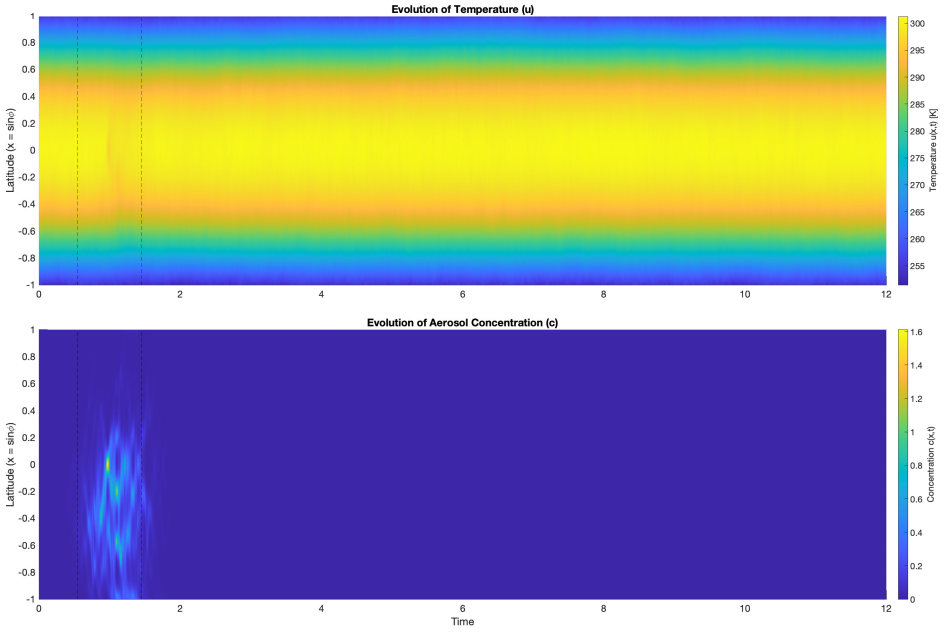

(a) *Simulation of the model* (4.1). *The horizontal axis represents time (in years), while the vertical axis represents space* $x = \sin(\phi)$, *with* ϕ *denoting the latitude. (Top) temperature* $T = T(t, x)$, *and (Bottom) aerosol concentration* $c = c(t, x)$. *The volcano explodes in the point* $x = -0.35$.

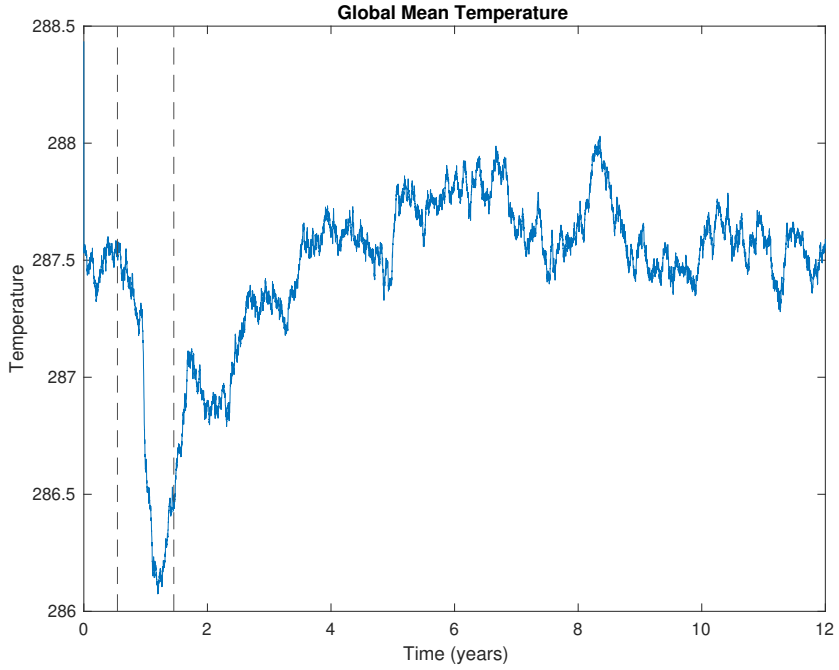

(b) *The evolution of the global mean temperature (GMT) for the realization shown above.*

Figure 4.5: *Simulation number 1.*

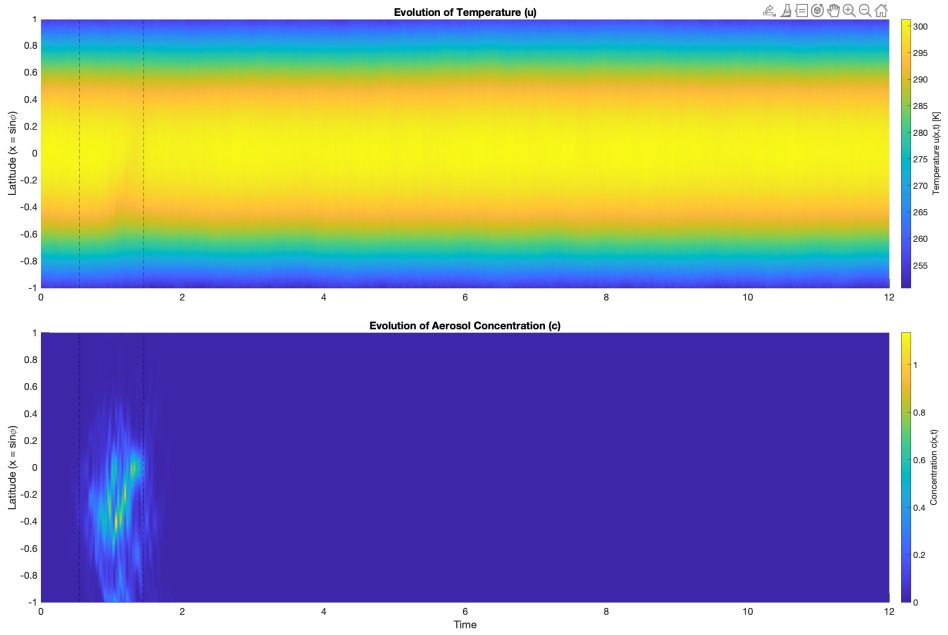

(a) *A second simulation of the model* (4.1)*. The horizontal axis represents time (in years), while the vertical axis represents space* $x = \sin(\phi)$*, with* ϕ *denoting the latitude. (Top) temperature* $T = T(t, x)$*, and (Bottom) aerosol concentration* $c = c(t, x)$*. The volcano explodes in the point* $x = -0.35$*.*

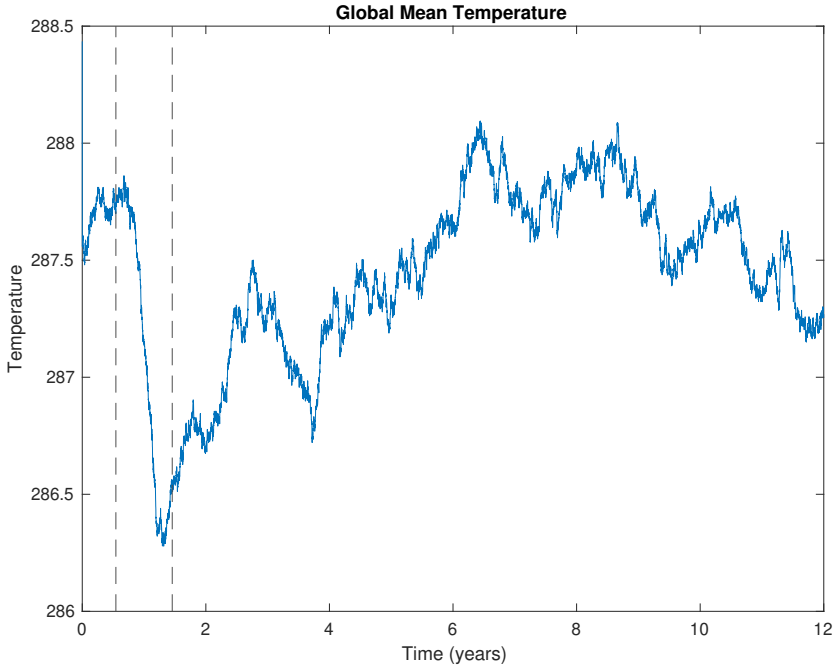

(b) *The evolution of the global mean temperature (GMT) for the second simulation.*

Figure 4.6: *Simulation number 2.*



Figure 4.7: *Location of the Campi Flegrei caldera (source: INGV-OV).*

4.2 The case of Campi Flegrei Caldera

The Campi Flegrei (CF) caldera represents a unique example of an active volcanic system. A caldera is a large volcanic depression, typically circular or elliptical in shape, that forms through the collapse of the ground when an underlying magma chamber empties rapidly, usually during a large-volume explosive eruption. The case of CF is a ∼12–15 km-wide nested caldera and it is the consequence of two major eruptions implying collapses: the Campanian Ignimbrite (∼39–40 ka) and the Neapolitan Yellow Tuff (∼15 ka) [12, 13]. The last eruption, called Monte Nuovo, occurred in A.D. 1538, after a prolonged period of inactivity [14].

The most characteristic feature of this area is bradyseismic activity, which consists of a succession of short-term to long-term periods of marked inflation and deflation of the ground (the *breathing* of the caldera [15]). In the past, the Campi Flegrei caldera experienced several bradyseismic crises, most notably in 1950-1952 (with

a maximum uplift of 0.73m), 1969-1972 (1.77m) and 1982-1984 (1.79m) [16]. After the last crisis, the caldera underwent about 20 years of subsidence until 2005, when the ground began to inflate again, starting a new unrest phase which is still ongoing today [17, 12, 13]. The ground deformation at Campi Flegrei displays an approximately radially symmetric geometry: the vertical uplift decreases with distance from a central maximum near Pozzuoli, following a bell-shaped profile, while the horizontal displacements point radially outward. [18, 19, 12].

The bradyseism is accompanied by intense seismic activity, especially during uplift phases, with hypocentres that over the years have reached a maximum depth of about 3–4 km [17]. The large majority of these earthquakes are of very low magnitude, yet the strongest event recorded so far attained a duration magnitude of Md 4.4 with a 2.6 km of depth, on May 2024 [20]. During the previous crisis (1982-1984), the intense seismicity caused severe building damage and led to the evacuation of a large part of Pozzuoli, on the order of tens of thousands of residents, after a 4.0 Md event [21, 20].

Furthermore, the uplift phases are accompanied by an intensification of gas release from the ground, reflected in the progressively increasing fumarolic degassing [22, 23, 20].

Because of these peculiar features, with which the local population has to cope on a daily basis, the Campi Flegrei caldera has undergone decades of geodetic, geochemical, volcanological, and seismic monitoring. The most immediate hazard is the occurrence of strong, shallow earthquakes [24, 12], whereas a renewed volcanic eruption remains a possibility on a much longer time scale and it is currently debated [24, 21, 25]. However, the area is now covered and continuously monitored by the INGV–Osservatorio Vesuviano through integrated seismic, geodetic (GNSS/GPS) and geochemical networks, comprising several tens of permanent seismic and GNSS stations progressively upgraded over the last decades; further details are available at the INGV–Osservatorio Vesuviano website (see `https://www.ov.ingv.it/index.php/home-campi-flegrei`). In particular, weekly surveillance bulletins are available, and the catalogue of seismic events can be consulted through the public seismological database GOSSIP of the INGV–Osservatorio Vesuviano (see `https://terremoti.ov.ingv.it/gossip/flegrei/`).

Building on this extensive observational effort, a wide body of theoretical and modelling studies has addressed the aforementioned different aspects of the caldera's behaviour.
Research on ground deformation at Campi Flegrei spans a broad methodological range: from the geodetic reconstruction and map-

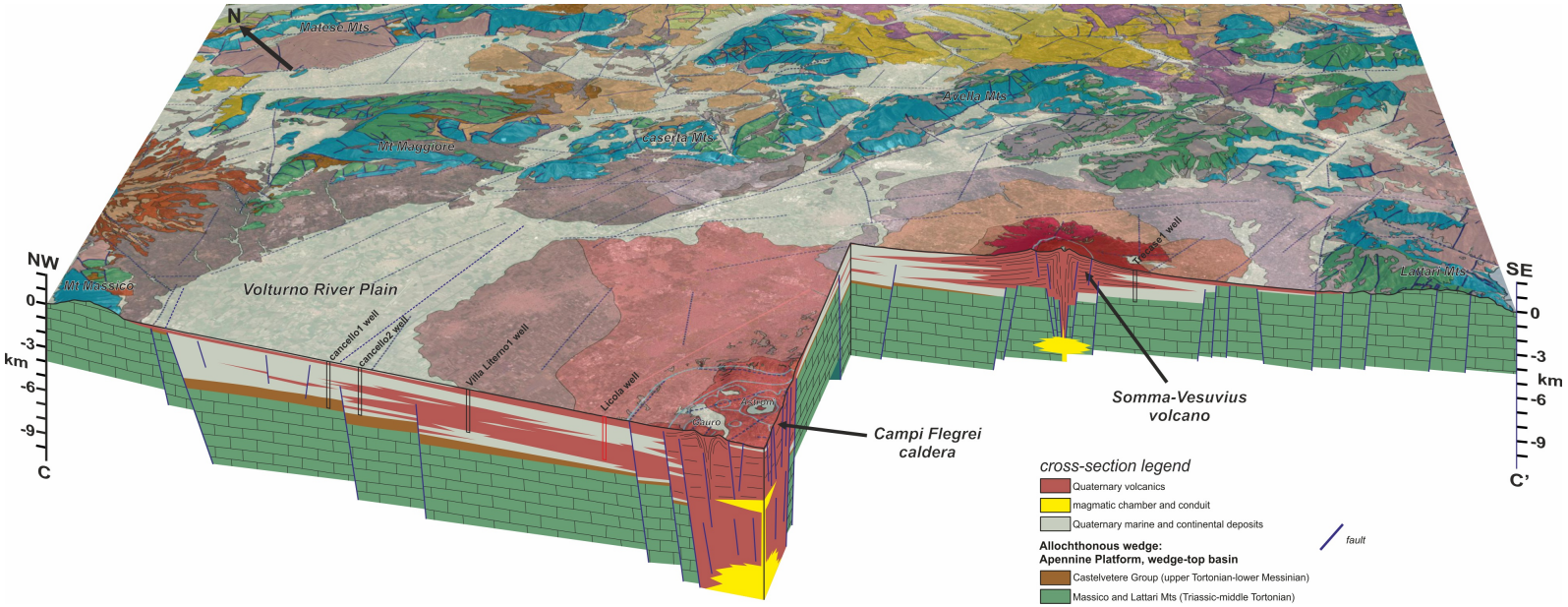

Figure 4.8: *Geological map of Campania, from University of Naples Federico II, Department of Earth, Environmental and Resources Sciences. Available at:* `https://www.distar.unina.it/en/carta-geologica-campania-in-google-earth`

ping of the deformation field [18], through the statistical characterization of the accelerating, seismicity-coupled uplift signal [19, 12], to the physical modelling of its source — mainly hydrothermal/-poroelastic mechanisms [15, 26] — and to failure-based forecasting of the crust's approach to rupture [21].
In terms of seismicity, the research spans from the precise relocation and mapping of earthquakes onto active fault zones [24, 23], through the statistical and rheological characterization of the seismic field via energy-release analyses and via b-value (the scaling coefficient of the so-called *Gutenberg–Richter law*, which expresses the relationship between earthquake magnitude and the total number of events of at least that magnitude in a given region and time period)[13, 17], to the recognition of specific seismic signatures diagnostic of critical unrest, such as burst-like swarms [20], and, more broadly, to the joint analysis of accelerating seismicity and ground uplift as a coupled deformation–seismicity process [12].
Studies targeting the fumarolic gases focus on tracking their chemical composition over time to infer the conditions of the underlying magmatic–hydrothermal system and its role in driving unrest [27], and more broadly use gas signals as evidence of deep magma degassing [28] or as one feature in integrated statistical analyses of the caldera's dynamics [29], while geophysical imaging characterizes the structure and fluid pathways feeding the fumarolic vents [22].
Finally, studies aiming to model the subsurface of Campi Flegrei range from numerical simulations of the geothermal and hydrothermal system [30, 31] and geophysical/tomographic imaging of its structure and plumbing [22, 25] to poroelastic modelling of the shallow deformation source [15] and integrated conceptual models of the layered magmatic–hydrothermal reservoirs driving unrest [27].

The precise mechanisms and triggering causes remain the subject of ongoing debate and research. A transversal objective underlying all these studies is to characterize the distinctive dynamics of CF through rigorous and reliable methods, thereby enabling, to some degree and with sufficient lead time, the forecasting of extreme events, such as a violent, shallow earthquake, that could disrupt the habitability of the area, cause substantial damage, or even pose a threat to the inhabitants' lives.

The present situation, as noted above, is that of a persistent crisis of ground uplift: as of February 2026, uplift has reached approximately 160 cm, and more than 20,000 seismic events have been recorded since 2005 [32]. This ongoing unrest poses a critical challenge for local sustainability and risk management, as the area is currently inhabited by over 350,000 people. Consequently, under-

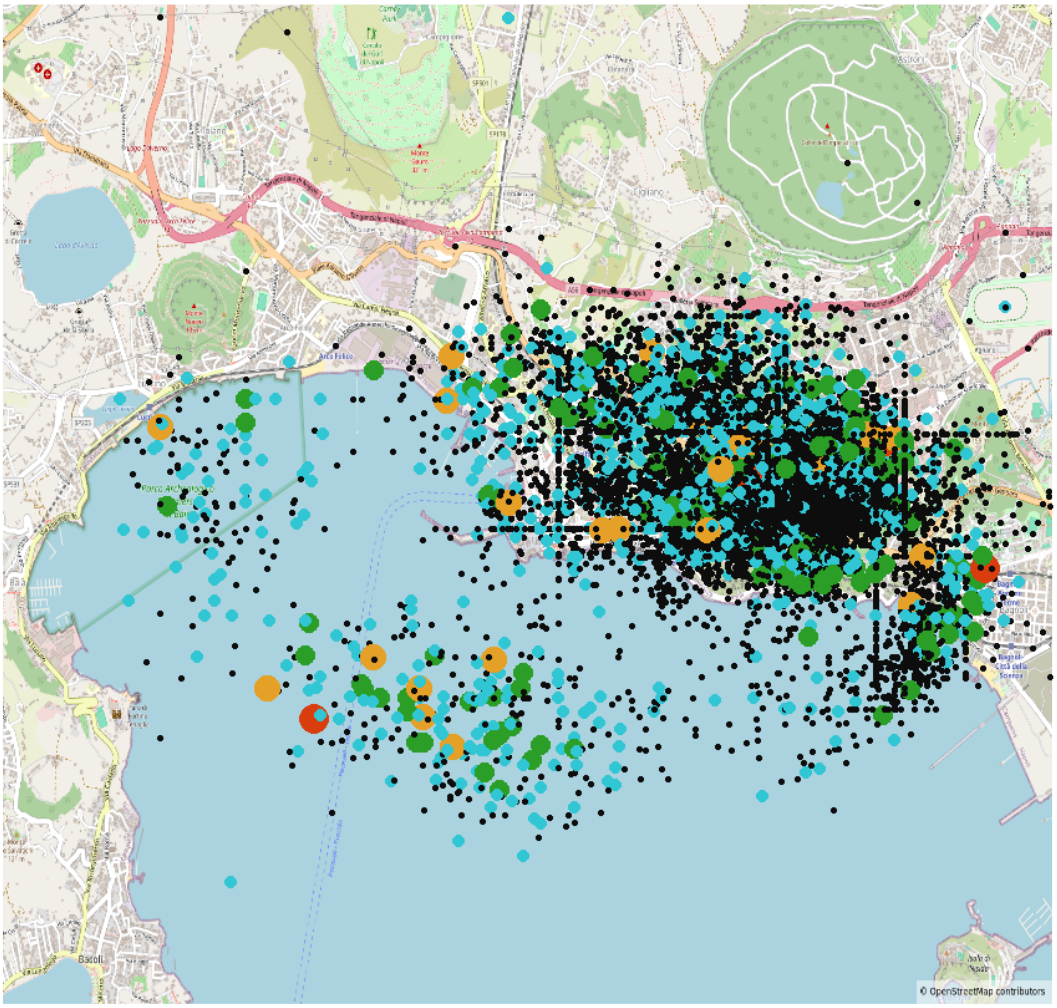

Figure 4.9: *Localization of earthquakes from 2005 to 2025. Red circles are earthquakes with magnitude higher than 4. Base map: © OpenStreetMap contributors (ODbL). Data overlay by the author.*

standing the mechanisms governing this behaviour is of paramount importance, not only to mitigate risks in a timely manner but also to contribute to the broader discourse on the long-term sustainability of daily life in the region, a reflection already initiated during previous crises.

To address these challenges, the aim of this study is to model the caldera's subsurface. The investigation relies on two decades of data from the continuous GNSS (Global Navigation Satellite System) monitoring network, in particular the daily observations of ground uplift at the RITE (Rione Terra) station[2], located in Pozzuoli at the point of maximum ground deformation of the caldera and therefore taken as the reference station for the uplift, together with the sequence of daily records of seismic events (from GOSSIP). Although certain statistical and functional relationships between uplift and seismicity have already been proposed and applied [12], combining these records with a plausible model of the subsurface may represent a promising strategy for supporting the long-term sustainability of daily life in the area and for risk mitigation.

To achieve this, the subsurface structure must first be characterized. Given the inherent complexity of reproducing every geological peculiarity from a geophysical standpoint, a simplified yet realistic model is initially adopted, that is, an idealized representation of the underground hydrothermal system and its interaction with deep-seated magma (for examples see [27, Figure 5] or [28, Figure 6]). This model incorporates heterogeneous layers and low-permeability barriers — characterized by depth-dependent geophysical properties — that communicate with each other and with the surface. A dynamic process of magmatic fluid (gas) ascent from depth is imposed, inducing sequential pressurisation of the overlying layers. This pressurisation deforms the barriers, triggering a chain reaction that manifests as surface deformation, depending on the depth of the involved layers and their mutual interactions. This approach aims to explain the driving mechanisms of the uplift, enabling day-by-day simulations to be validated against empirical data.

In a second model, the layered representation adopted above is replaced by a more realistic structure composed of interconnected cavities. Rather than a rigid vertical sequence of layers, these cavities are distributed in three dimensions and communicate both vertically and laterally. Their geometry is delineated primarily from the spatial distribution of earthquake, which outline the active subsur-

[2]We thank INGV–Sezione di Pisa for the collaboration during the research period and for providing the data.

face structures. As before, a dynamic ascent of magmatic fluid (gas) from depth is imposed, sequentially pressurising the cavities and propagating through their connections until the resulting deformation manifests at the surface. The ultimate goal remains the same: to simulate the observed uplift.
In a subsequent stage, seismicity will be integrated into the models as a direct consequence of the simulated ground deformation.

Quantifying the occurrence probability of a suite of plausible scenarios, especially those posing the highest risk to the local population, is fundamental. For instance, estimating the probability of a high-magnitude seismic event occurring within a specific short-term horizon is a primary focus. Provided that the uplift can be robustly forecast, the statistical and functional relationships between seismicity and deformation could then be used to forecast seismicity across all magnitudes via the Gutenberg–Richter law. A possible direction for future research is the refinement of these models, in order to fully assess their fitting capabilities and predictive power.

The analysis is performed using R [33], a widely adopted open-source environment for statistical computing and data analysis.

4.2.1 First model: layers

The pourpose of this model is to hypothesise the possible dynamic governing the unrest phase of uplift at CF, starting from a plausible description of the underground hydrothermal system and its behaviour with respect to the magma present at great depth. In this way, we would like to be able to simulate the uplift and make its forecast.

Filling phase

It is known that under Campi Flegrei area there is a magmatic chamber at a depth of about 7.5 km [13]. In this model, we suppose that there is a solid barrier that separates this magmatic chamber from the ground above it. We also suppose that the ground between this barrier and the soil, i.e. the subsurface of CFs, consists of a series of heterogeneous layers and barriers that can be identified on the basis of their different geochemical and physical composition. We refer to them as

- $\underline{M}$: the barrier in contact with the magmatic source;
- $\overline{M}$: soil, the barrier which identifies the surface of CF;
- $\underline{M} < M_1 < M_2 < \cdots < M_n < \overline{M}$: intermediate layers, where "$<$" stands for their depth.

The layers are separeted by their own barriers too. Each layer-barrier has its own combination of characteristics, such as the type of material present, porosity, elasticity. In particular, all these features define the different geochemical and physical nature of each layer-barrier in terms of their ability to let magmatic fluids enter or exit. These characteristics are summarised, for each layer M_i, by the *maximum volume* V_i, i.e. the maximum volume they can hold without deforming:

$$V_i = \text{maximum capacity of layer } i,\ V_i \in \mathbb{R}_+.$$

We assume that the magmatic chamber fills the overlying ground from below with a mixture of water and gas, that is we assume that there is a bottom-up push of magmatic fluids originating from the magmatic chamber that can potentially pass through the various layers. To do so, we introduce the quantity

$$v_i(t) = \text{volume of fluid injected at time } t \text{ in layer } i.$$

At time $t = 0$, we suppose $v_i(0) = 0 \quad \forall i$.

The dynamics described here begin with a push of fluid from $\underline{M}$ towards layer M_1, passing through the existing gaps. Then, this fluid begins to invade the porosity of the layer and $v_1(t)$ increases. We assume a linear growth with respect to time for each layer:

$$v_i'(t) = r_i \quad \forall i \in \{1, \dots, n\}$$

where r_i depends on the structure of M_i, i.e. on its own features. Looking at the first step, as long as $v_1(t) < V_1$, M_1 is saturating its volumes, filling its spaces with fluids coming from below it, pressurising itself. In the model, this mechanism does not affect either the other layers or the soil, meaning that nothing is visible from these points of view. In particular, in this phase of the dynamics, we assume that there is no deformation of the existing barriers. We call this phase the *filling phase*.

Deformation phase

At a certain time t_1, it happens that v_1 is equal to V_1, which means that the layer has filled every free space, all its volumes, is under pressure and it is no longer able to host fluids. Then, it begins the second phase of the dynamics: the continuous push of fluids from below together with the inability to accept them, induce pressure on the M_1 barrier, which separates M_1 from M_2, causing it to bulge, for example by insisting on a potentially more fragile area of the barrier itself, invading the adjacent layer M_2. This excess of

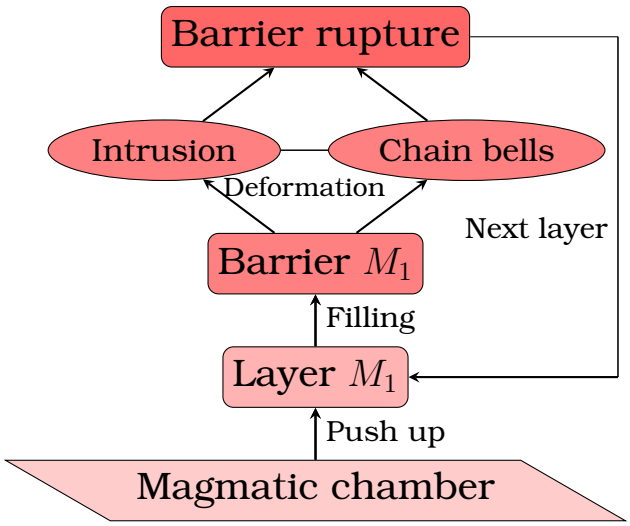

Figure 4.10: *Model dynamics.*

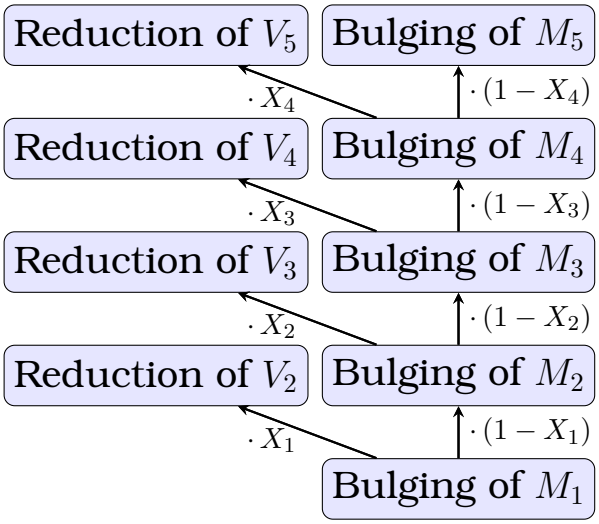

Figure 4.11: *Chain bells effect.*

material, compared to the capacity to absorb fluids without deforming, entering the layer has two different effects caused by swelling, one on M_2 maximum volume and one on the entire system. We refer to them as *intrusion effect* and *chain bells effect*, respectively.
The intrusion effect consists in a partial occupation of the free volume of the adjacent layer, i.e. we suppose that the invasion of the M_1 deformed barrier into the next layer causes movements in the rock material present that reduce the free spaces, that is, the layer adjusts itself to the invasion and therefore its maximum volume is reduced.
The chain bells effect is, in a certain sense, complementary. We assume that it occurs because the bulging (bell-shaped) is very localised and M_2, the invaded layer, does not have the capacity to instantly absorb all the pressure by filling its spaces. Then, it happens that the M_1 barrier deformation triggers a chain reaction through all the other layers, swelling up (bell-shaped) all the other barriers in a dampened manner, until it reaches the surface. So, the visible consequence of this effect is the soil uplift, at level $\overline{M}$.
In this model, the chain bells effect will exist whenever a layer is in the second phase. Due to the intrusion effect described above, we assume that the extent of visible deformation on the surface, caused by chain bulges of the barriers, is not equal to the extent of the bulging of the barrier that first triggered the reaction, i.e. that relating to the state under pressure. In fact, going upwards, this quantity is dampened due to the intrusion effect that occurs in each layer. To summarise: the bulging of barrier M_1 partly causes the maximum volume of M_2 to decrease and partly causes a damped deformation of M_2 barrier; the latter in turn causes an intrusion effect on the maximum volume of M_3 and a damped deformation on M_3 barrier, and so on until it reaches the surface. The chain of deformations is the chain bells effect. We call this phase the *deformation phase*.

Looking at the first step, this phase begins at t_1 and ends at a certain moment t_1^*, that is the moment of the *barrier rupture*. Whit this term, we highlight the phenomenon whereby the barrier under pressure, stressed by the bulging, breaks due to the excessive number of fractures that have formed. In fact, as there is still pressure from below, the barrier can no longer withstand the pressure and volume of fluids introduced, deforming itself, then it fractures, allowing the fluids to pass through to the next layer. From time t_1^* onwards, we assume that M_1 remains under pressure and the dynamics described above, with the two different phases, are repeated in M_2, starting again with the filling phase, now from a maximum volume that has been reduced by the intrusion effect and with all

the barriers of the system deformed. This cycle will repeat until it reaches the surface.
At any time t after the beginning of the second phase of the dynamics, for each layer M_i, the volume of fluid introduced from below, when the layer involved is already full, is

$$\text{exc}_i(t) := v_i(t) - V_i$$

If we denote the fraction related to the intrusion effect by $X_i \in [0, 1]$, the maximum volume of the layer $i + 1$ will we updated as follows

$$V_{i+1} \to V_{i+1} - X_i \cdot \text{exc}_i(t_i^*). \tag{4.2}$$

Meanwhile, the volume $(1 - X_i) \cdot \text{exc}_i(t_i^*)$ will be the bell-shaped volume that plastically invades M_{i+1} and therefore will be responsible for the reduction of the maximum volume of the other layers. It will also be reponsible for the deformation of the barriers of the other layers (chain bells effect), thus causing the uplift. We will describe the precise manner in which this occurs in the following section.

Soil uplift

Let us consider a 2D-section of the subsfarce, in particular let's consider the x-z coordinates, where both x and z belong to a bounded interval. The aim is to consider a portion of the subsurface, looking at the layers. In this setting, for simplicity, we refer to all the quantities described above as planar quantities, that is, volumes will be areas. We assume that the beginning of the deformation phase is localised at a specific point on the first barrier, for example in a more fragile area that can therefore break more easily. In 2D view, we propose a bell-shaped bulge, i.e. the bulge has the shape of the probability density function of a Gaussian, at every time t.
Let p be the mean and σ^2 the variance of the chosen Gaussian distribution. We assume that every time there is a bulge, it will have p as its point of maximum height in terms of deformation, which means that p will be the point of greatest stress at any moment during the dynamics. So, the bulging of each barrier will be bell-shaped, centred at p, and p will be the point at which we will measure the visible uplift of the soil.
Note that, considering a generic layer M_i, its barrier will deform when:

1. a layer M_j with $j < (i - 1)$ is in deformation phase, thanks to the chain reaction, in a dampened manner due to the various intrusion effects affecting the layers below it;

2. the layer M_{i-1} is in deformation phase, thanks to the bulging of the M_{i-1} barrier, in a manner which involves the quantity $(1 - X_{i-1}) \cdot \text{exc}_{i-1}(t^*_{i-1})$;

3. it is in deformation phase.

To model the shape of the barrier swelling, at any time t and at any point x, when the layer M_i is in second phase, we propose the following function

$$h_i(t, x) := \text{exc}_i(t) \cdot (1 - X_i) \cdot \frac{1}{\sqrt{2\pi\sigma^2}} \exp\left\{\left(-\frac{(x-p)^2}{2\sigma^2}\right)\right\}.$$

The maximum height of the bell $c_i(t)$ at time t of the M_i barrier will be

$$c_i(t) := h_i(t, p) = \frac{\text{exc}_i(t) \cdot (1 - X_i)}{\sqrt{2\pi\sigma^2}} \tag{4.3}$$

while

$$\int h_i(t, x)dx = \text{exc}_i(t) \cdot (1 - X_i) = (v_i(t) - V_i) \cdot (1 - X_i) \tag{4.4}$$

will be its area.
In accordance with the above, we leave the final portion of volume introduced $(v_i(t^*_i) - V_i) \cdot X_i$ for the intrusion effect, i.e. to update the maximum volume of M_{i+1} as in (4.2). Meanwhile, the M_{i+1} barrier will bulge at any time t and, according to the dynamics, its area will be equal to

$$(\text{exc}_i(t) \cdot (1 - X_i)) \cdot (1 - X_{i+1}).$$

Infact, the quantity $\text{exc}_i(t) \cdot (1 - X_i)$, the area of the main bell, will be splitted into two parts:

1. $\text{exc}_i(t) \cdot (1 - X_i) \cdot X_{i+1}$, the reduction of the V_{i+2} volume (intrusion effect);

2. $\text{exc}_i(t) \cdot (1 - X_i) \cdot (1 - X_{i+1})$, the area of the bell-shaped bulge in M_{i+1} barrier (chain bells effect).

The above steps will be repeated until the soil is reached.
The visible uplift will be determined by the maximun height of the last bell, so, according to (4.3), it will be increased by an amount equal to

$$\Delta_i(t) = \frac{\text{exc}_i(t)}{\sqrt{2\pi\sigma^2}} \prod_{j=i}^{n} (1 - X_j). \tag{4.5}$$

A schematic representation of the described mechanism is shown in Fig 4.10, Fig 4.11 and Fig 4.12.

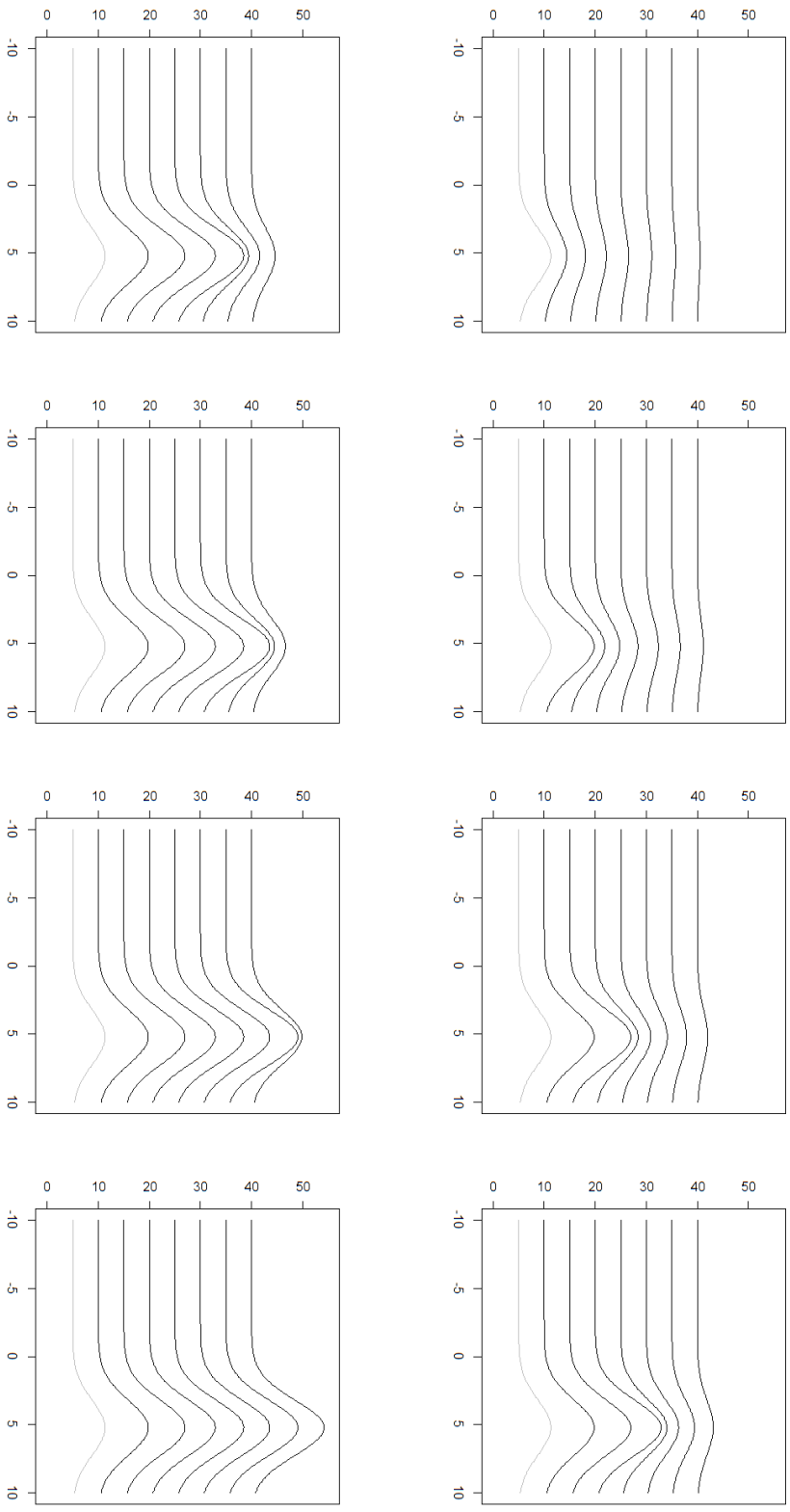

Figure 4.12: *Chain bells effect (from top-left to bottom-right)*

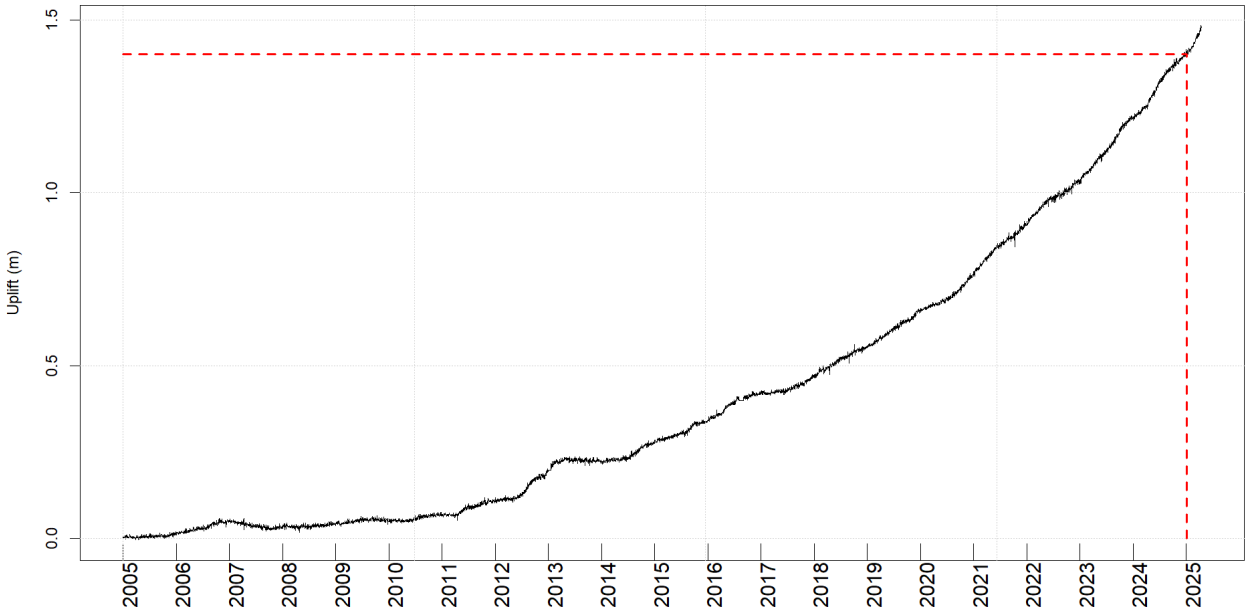

Figure 4.13: *Real uplift of the RITE station from 2005 to 2025. The red dashed lines highlight the value at January 2025.*

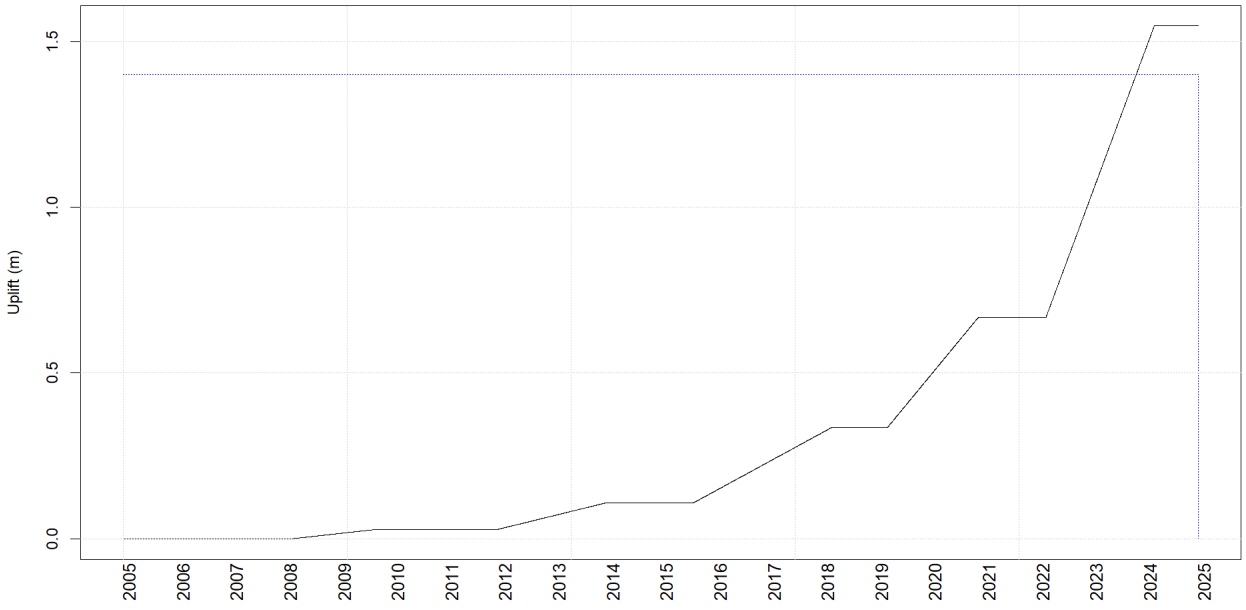

Figure 4.14: *Simulated soil uplift. Blue dashed lines highlight the real uplift value at January 2025.*

Simulations

Figure 4.13 shows the ground uplift, expressed in metres, recorded at the RITE station over the period 2005–2025. The time series is characterised by an initially slow uplift whose rate increases steadily from approximately 2015 onwards. Superimposed on this long-term trend, and most evident during the earlier part of the record, is a marked alternation between near-stationary intervals and episodes of remarkable uplift of varying extent. For example, two growth phases occur between 2005–2007 and 2011–2013, whereas the corresponding pause intervals (approximately 2007–2011 and mid-2013 to mid-2014) represent phases of relative quiescence.
This episodic, step-like behaviour is the primary motivation for the development of the layered model adopted in this study (filling phases correspond to flat periods, while deformation phases correspond to increasing uplift), and also it subsequently guides the calibration of the model during the simulation stage. In particular, the observed alternation of loading and pause intervals constrains the tuning of the free parameters, namely the number of layers, the initial volumes, the filling rate, the various damping terms, the rupture times, and the height of the deformation bell.
From 2015 onwards, the alternation between flat and rising phases becomes considerably more subdued, with the near-stationary intervals progressively shortening as the overall uplift rate increases. This is precisely the behaviour that the volume-reduction mechanism is intended to reproduce: since the maximum volume has already been partially reduced by the dynamics occurring in the previous layers, when the layer involved reaches its filling turn, less time is required to complete the filling phase, so that the curve exhibits a shorter flat interval.

Figure 4.14 shows the simulated uplift as a function of time, based on the calibration described above and on the rules outlined in the previous sections. The flat intervals correspond to the phases during which the filling of a given layer is taking place, so that no increase is observed at the ground surface, whereas the intervals with a positive slope correspond to the phases during which the deformation phase occurs, producing a measurable increase in surface uplift. Consistent with the observations discussed above, the flat intervals are initially very long and become progressively much shorter thereafter.

Although this first model immediately proves to be a suitable starting point to reproduce the real data, it soon becomes apparent that it is far too simplistic in several key aspects. First, the simulated curve is perfectly smooth, whereas the real signal is inherently

affected by noise. Second, the model lacks physical realism, since there is no direct interaction between adjacent layers, nor between any layer and the surface. Third, its adherence to the observed signal is poor: the filling phase produces an exaggerated flatness, whereas the real uplift record exhibits vigorous, cyclically recurring growth episodes followed by near-stationary intervals that are, however, never as flat as those generated by the model.
These limitations define the primary directions for improvement, namely introducing a sort of coupling between the layers, removing the excessive flatness, and adding a realistic noise component. It is worth stressing that the role of noise is not merely visual but substantial: if a noise component is introduced with a characteristic scale h, representing, for instance, its intensity, the step-like features of the signal remain distinguishable only when their duration exceeds h, whereas shorter steps become blended with the noise and are effectively no longer visible. A final objective is to improve the overall physical realism of the model and to train it over a fixed time interval, specifically up to 2015.

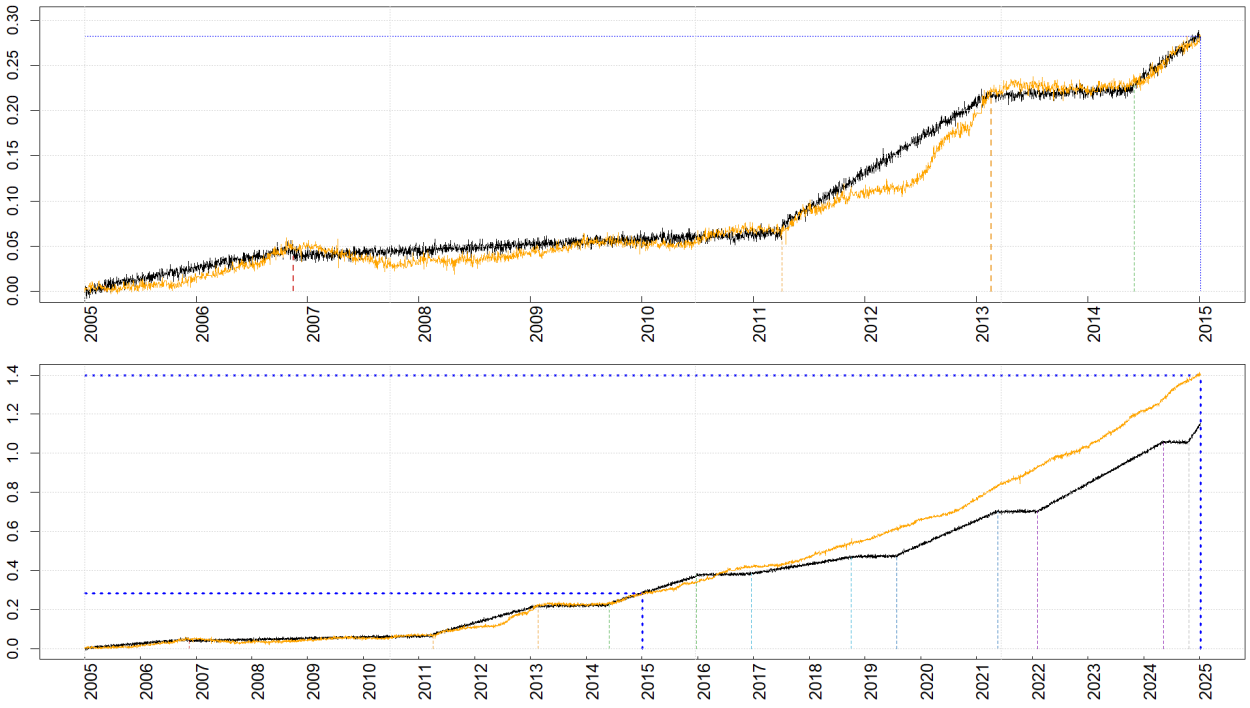

Figure 4.15: *Refined model: simulated soil uplift (m) together with the real data from 2005 to 2015 (top) and from 2005 to 2025 (bottom). Blue dashed lines highlight the real uplift value at January 2015 and January 2025, while the other coloured dashed lines highlight the alternation between the two phases.*

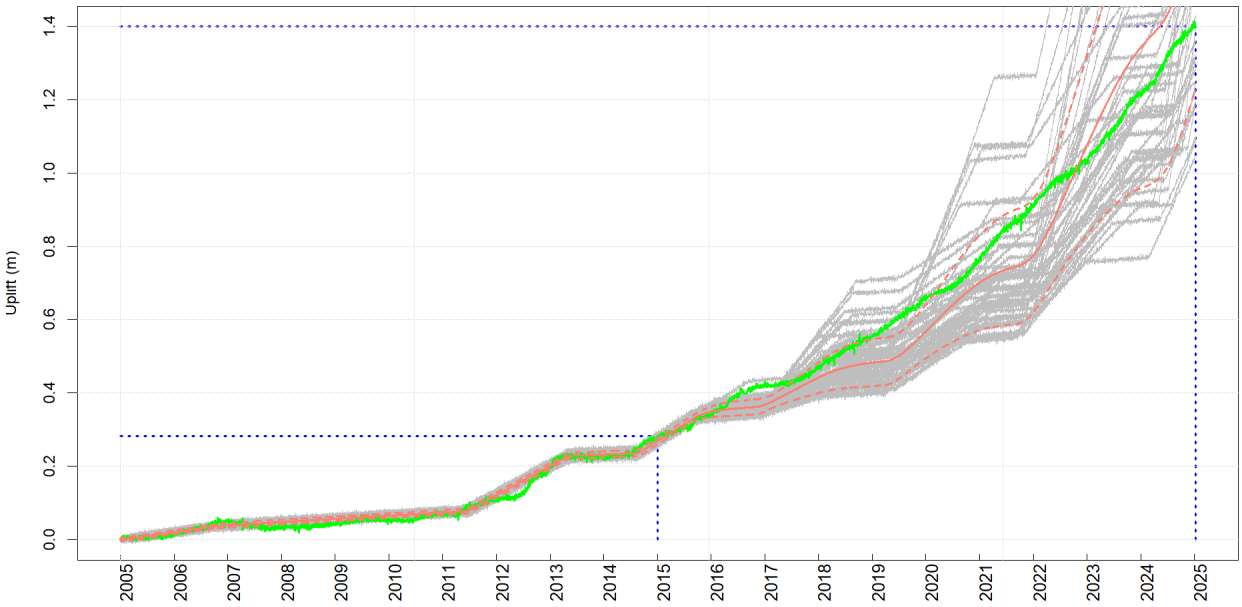

Figure 4.16: *Refined model: simulated soil uplift, with random inizialization of variables. The model is trained on data from 2005 to 2015 (blue dashed lines highlight the real values at January 2015 and January 2025). Grey lines represent different trajectories. The green line is the real uplift, while the pink one is the mean trajectory together with its standard deviation.*

Figures 4.15 and 4.16 show the results for the refined model. Unlike the theoretical formulation, a direct interaction between the ground surface and every other layer is imposed. Specifically, the main effect of the filling phase is to pressurise the layer involved, but there is also a side effect that acts as a sort of dispersion: a small fraction of the injected gas reaches the surface directly through the imposed connection, causing it to bulge. As a result, a very small uplift is observed even during the filling phase of each layer, and the flat intervals are therefore no longer perfectly flat. This connection is also fed during the deformation phase, that is, the injected fluid is now partitioned into three components. The number of layers is set to 9, based on the literature ([27, figure 5]); the filling rate is constant in time and identical for every layer, thereby modelling a steady push from below, as is the percentage of volume reduction; the initial volumes, the rupture times, the fraction of volume transferred directly to the surface and the height of the bell are set by inspecting the first two or three layers, since these are the ones involved in the dynamics prior to 2015 — that is, the data from 2005 to 2015 are used as a sort of training set. The corresponding quantities for the remaining layers are set as a ran-

dom combination of the choices made for the first layers. The noise is obtained by identifying the characteristic frequency of the noise affecting the real uplift record. No connection between individual layers is imposed.
With all these improvements, the model is now more realistic, as can be seen in Figure 4.15: the calibration adopted allows the simulation to adhere closely to the real data before 2015 and to begin exhibiting a certain forecasting ability afterwards, although after a few years the simulated and the observed dynamics diverge. This divergence is particularly evident in Figure 4.16, which shows an ensemble of possible trajectories (in grey), together with the mean trajectory (pink, solid line) and the confidence band defined by the standard deviation (pink, dashed lines): the observed uplift (green line) is not well reproduced by the mean behaviour and barely remains within the confidence band. Even the final uplift value, in January 2025, is likely off by almost a quarter of a metre, which corresponds to a rather unreliable forecast.

Despite the improvements introduced and in light of the considerations drawn from the simulations, this model still proves too rigid to capture the complexity of the natural system. In particular, the layered structure appears excessively schematic and needs to be made more realistic. This is precisely the purpose of the second model presented in the following section.

4.2.2 Second model: cavities

In this second model, we hypothesise that the subsurface geometry is more complicated than a rigid sequence of layers. In fact, we propose that the dynamics also have a horizontal component, meaning that there are subsurface zones that are connected to each other not only vertically. Furthermore, we abandon the concept of layers in favour of a structural system made up of compartments or cavities, with more complex and realistic interconnections.
We thus maintain the dynamics of filling and pressurisation (ascending gas originating from the magmatic chamber), but now we assume that the gas developed from the deep zones proceeds to occupy various zones, various cavities, more or less simultaneously, perhaps venting slightly up to the surface, but not enough to deactivate the pressure increase in various zones. These cavities are spatially located in three dimensions and are connected to each other. These connections allow the passage of gas, thereby creating a consequentiality. The pressurisation of these zones then causes the uplift, as in the previous model.

The first objective is therefore to identify the subsoil zones that

become pressurised, namely to determine the precise subsurface geometry. To this end, we use seismicity. Indeed, we believe that the rock walls affected by the deformation of a cavity, due to gas filling and consequent pressurisation, are subject to stress that tends to be released through fractures, which manifest as earthquakes. That is, a pressurised zone will accumulate stress, which induces ruptures, which induce earthquakes.
The available seismic data indicate the coordinates of the earthquakes that have occurred and the available geodetic data suggest that the uplift takes a bell-shaped form, of which we know the centre is very close to the RITE station. Therefore, a posteriori and in good approximation, the earthquake coordinates can indicate the location of the zones. In particular, if the earthquakes are clustered in 3D, those clusters could correspond to the filling zones. In this way, as mentioned, we abandon the layers, introduce smaller basins that are not necessarily overlapping but are spatially located in 3D, we enhance the horizontal component, and we restructure the connections between zones.
Regarding the structure of the connections, our guess is that certain pressure activities generate stress and earthquakes relative to one zone, and then induce the same mechanism in a zone connected to it. If the zones correspond to the earthquake clusters, we look at the times, in addition to the coordinates, of the earthquakes to try to understand if the events in certain clusters have a statistical tendency to follow those in another cluster. This signifies the presence of a connection.

Simulations

First of all, we consider the period from 2005 to 2020, which we assume to be long enough to identify the cavities. For this period, we consider the seismic activity, namely the earthquakes of every magnitude, and we apply a simple clustering method, i.e. PAM (Partitioning Around Medoids), imposing a priori a total of 18 clusters: the data are first clustered horizontally into 9 clusters, and subsequently vertically into 9 further clusters (see figure 4.17 for the correspondence between cluster labels and colours). Figure 4.18 shows the seismic activity over the prescribed period, viewed from above, i.e. in the longitude–latitude plane, superimposed on a stylised outline of the Campi Flegrei coastline (black line). Each point represents an earthquake, and its colour corresponds to the assigned cluster. The orange and red circles delimit the area affected by ground uplift. Figure 4.19, in turn, provides a three-dimensional view of the cluster centres (medoids), including depth, together with

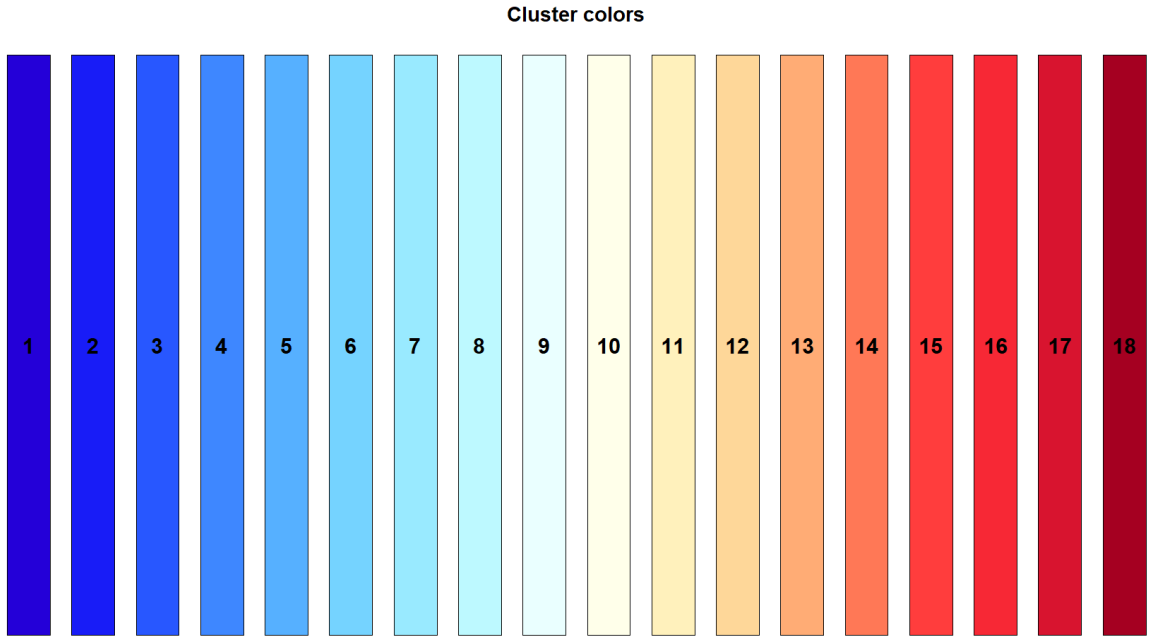

Figure 4.17: *Cluster colours-numbers.*

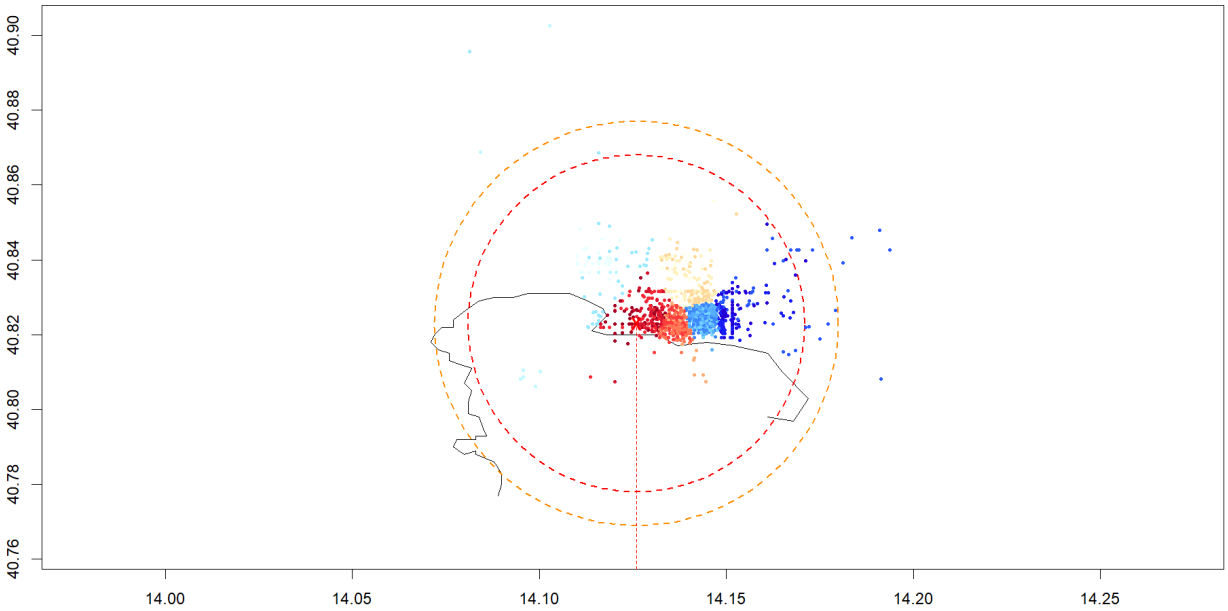

Figure 4.18: *Localization of cluster (long-lat) from 2005 to 2020. The red X is the RITE station. The circles delimit the area affected by uplift (5km and 6km).*

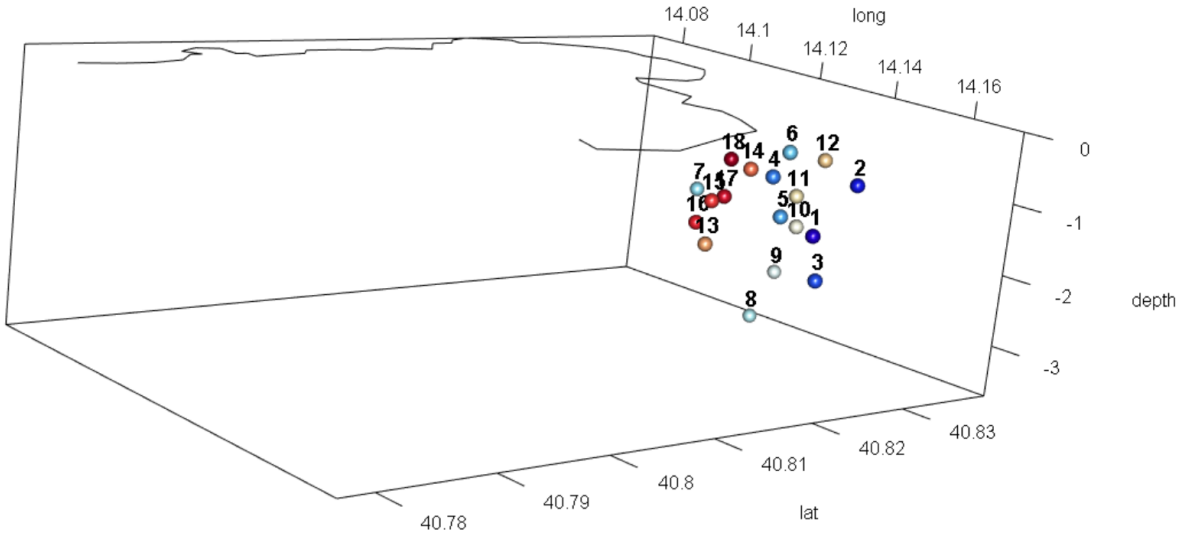

Figure 4.19: *Localization of medoids of the clusters 3D.*

the same coastline at the surface level.
The clearest insight is provided by Figure 4.20. Each panel (from top-left to bottom-right, one per year) shows the three-dimensional seismic activity that has occurred since the date reported in the caption; the figure therefore highlights the seismic evolution. The colours are the same as before, but each point now has a radius proportional to the magnitude of the earthquake it represents, thereby emphasising the higher-magnitude events.
At a glance, a clear temporal sequence emerges: the first to activate are the clusters in the blue range of the colour scale, then the orange ones, and finally the red ones, which are the last to become active. It is worth recalling that the clustering does not rely on any temporal information, but only on the spatial one; this method for identifying the connections between the cavities therefore seems to work.
If an ascending gas develops from the deep zones, at about 8 km depth, it will occupy several regions, so that pressure increases simultaneously in several zones. From this figure we therefore interpret the first zones directly reached by the initial injection as being four, namely the dark blue, blue, light blue and white clusters. These begin their process of filling, pressurisation and rupture, each with its own timescale, but approximately in parallel. Then, after several years, they fill other zones not directly involved at the outset, namely the orange, light red and dark red ones. With

regard to the connections, we therefore propose a connection between the magma and the four clusters, then connections between these and the surface in order to allow outgassing, and the development of connections between them and the orange–red zones, which activate slowly.

The last figure to be discussed is figure 4.21, which reports, for each cluster (first column), the number of earthquakes recorded in each year of the investigated period. The table provides further support for the interpretation given above. The clusters corresponding to the red tones, including their lighter shades, begin to activate in 2013 and then become definitively and increasingly active from 2015 onwards, whereas the blue clusters and their shades are already active in 2006 and remain so until the end of the investigated period. We therefore regard the table as additional evidence of a potentially statistically relevant temporal sequence. The persistence of seismicity in the "older" clusters, from the point of view of their activation time, is interpreted as an indication that these zones remain pressurised, so that the surrounding rock continues to fracture and readjust, with each such movement manifesting itself as an earthquake.

The present investigation goes no further, owing to logistical and time constraints. A natural continuation, however, would be to apply once again the filling, pressurisation and deformation dynamics of the previous model, embedding it within this new framework, with the usual objective of forecasting the uplift. The advantage would be that the earthquakes would now already be integrated into the dynamics, unlike in the previous model, where it still remains to be decided how and why they should be incorporated into the mechanism imposed by the model itself.

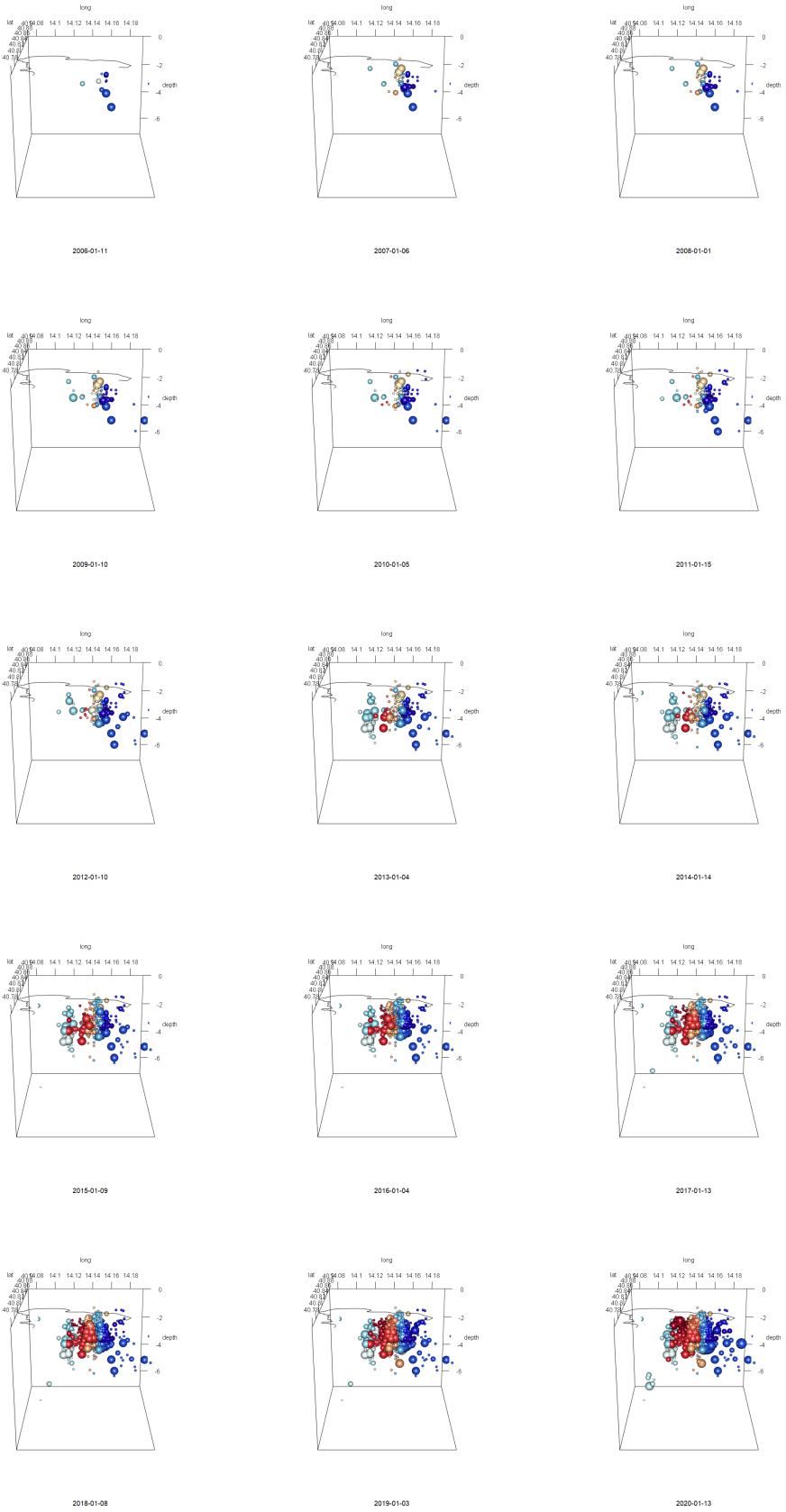

Figure 4.20: *Evolution of earthquakes.*

	2006	2007	2008	2009	2010	2011	2012	2013	2014	2015	2016	2017	2018	2019	2020
1	2	9	0	4	3	6	1	0	2	7	4	9	10	11	23
2	2	3	0	2	4	3	0	5	0	1	7	0	0	13	29
3	4	2	0	3	0	9	5	8	1	4	2	3	10	7	6
4	1	1	0	0	0	0	0	0	1	5	7	17	15	38	90
5	0	3	1	0	0	2	2	6	3	2	15	16	6	19	53
6	0	1	0	0	0	0	1	1	0	21	19	20	13	32	45
7	1	2	0	2	1	0	1	6	1	1	2	8	1	3	10
8	0	0	0	0	0	1	0	6	0	1	0	1	0	0	4
9	0	0	0	0	0	0	0	38	0	0	0	1	0	0	1
10	1	2	0	4	2	1	4	1	2	4	3	5	3	16	16
11	0	5	0	0	0	0	0	2	2	0	5	7	12	26	27
12	0	2	0	1	1	2	2	2	2	2	5	4	9	17	44
13	0	2	0	0	1	0	0	12	1	6	4	11	1	7	7
14	0	1	0	0	1	0	0	3	0	6	4	6	7	21	55
15	0	0	0	0	0	1	0	3	0	11	9	12	13	25	42
16	0	0	0	0	2	1	2	7	0	8	8	9	5	13	15
17	0	0	0	0	0	0	0	1	0	3	5	8	4	11	28
18	0	0	0	0	0	0	0	0	1	2	5	9	5	13	24

Figure 4.21: *Number of earthquakes for each cluster, for each year. Useful to determine the activation times.*

References

1. Robock, A. Volcanic eruptions and climate. *Reviews of Geophysics* **38,** 191–219. doi:10.1029/1998RG000054 (2000).
2. Macdonald, F. & Wordsworth, R. Initiation of Snowball Earth with volcanic sulfur aerosol emissions. *Geophysical Research Letters* **44,** 1938–1946. doi:10.1002/2016GL072335 (2017).
3. Timmreck, C. Modeling the climatic effects of large explosive volcanic eruptions. *Wiley Interdisciplinary Reviews: Climate Change* **3,** 545–564. doi:10.1002/wcc.192 (2012).
4. Gupta, M. *et al.* Triggering global climate transitions through volcanic eruptions. *Journal of Climate* **32,** 3727–3742. doi:10.1175/JCLI-D-18-0883.1 (2019).
5. Tasistro-Hart, A. *et al.* Four-million-year Marinoan snowball shows multiple routes to deglaciation. *Proceedings of the National Academy of Sciences* **122,** e2418281122. doi:10.1073/pnas.2418281122 (2025).
6. Chaverot, G. *et al.* Resilience of Snowball Earth to stochastic events. *Geophysical Research Letters* **51,** e2024GL109512. doi:10.1029/2024GL109512 (2024).
7. Huybers, P. & Langmuir, C. Feedback between deglaciation, volcanism, and atmospheric CO_2. *Earth and Planetary Science Letters* **286,** 479–491. doi:10.1016/j.epsl.2009.07.014 (2009).
8. Conway, C. *et al.* An assessment of potential causal links between deglaciation and eruption rates at arc volcanoes. *Frontiers in Earth Science* **11,** 1082342. doi:10.3389/feart.2023.1082342 (2023).
9. Muschitiello, F. *et al.* Enhanced ice sheet melting driven by volcanic eruptions during the last deglaciation. *Nature Communications* **8,** 1020. doi:10.1038/s41467-017-01273-1 (2017).
10. Hansen, J. *et al.* Mount Agung eruption provides test of a global climatic perturbation. *Science* **199,** 1065–1068. doi:10.1126/science.199.4333.1065 (1978).
11. Stoffel, M. *et al.* Climatic, weather and socio-economic conditions corresponding with the mid-17th century eruption cluster. *Climate of the Past Discussions* **2021,** 1–48. doi:10.5194/cp-18-1083-2022 (2021).

12. Bevilacqua, A. *et al.* Accelerating upper crustal deformation and seismicity of Campi Flegrei caldera (Italy), during the 2000–2023 unrest. *Communications Earth & Environment* **5,** 742. doi:10.1038/s43247-024-01865-y (2024).

13. Tramelli, A. *et al.* b value enlightens different rheological behaviour in Campi Flegrei caldera. *Communications Earth & Environment* **5,** 275. doi:10.1038/s43247-024-01447-y (2024).

14. Bevilacqua, A. *et al.* Temporal models for the episodic volcanism of Campi Flegrei caldera (Italy) with uncertainty quantification. *Journal of Geophysical Research: Solid Earth* **121,** 7821–7845. doi:10.1002/2016JB013171 (2016).

15. Todesco, M. Caldera's Breathing: Poroelastic Ground Deformation at Campi Flegrei (Italy). *Frontiers in Earth Science* **9,** 702665. doi:10.3389/feart.2021.702665 (2021).

16. Del Gaudio, C. *et al.* Unrest episodes at Campi Flegrei: A reconstruction of vertical ground movements during 1905–2009. *Journal of Volcanology and Geothermal Research* **195,** 48–56. doi:10.1016/j.jvolgeores.2010.05.014 (2010).

17. Danesi, S. *et al.* Evolution in unrest processes at Campi Flegrei caldera as inferred from local seismicity. *Earth and Planetary Science Letters* **626,** 118530. doi:10.1016/j.epsl.2023.118530 (2024).

18. Bevilacqua, A. *et al.* Radial interpolation of GPS and leveling data of ground deformation in a resurgent caldera: application to Campi Flegrei (Italy). *Journal of Geodesy* **94,** 24. doi:10.1007/s00190-020-01355-x (2020).

19. Bevilacqua, A. *et al.* Data analysis of the unsteadily accelerating GPS and seismic records at Campi Flegrei caldera from 2000 to 2020. *Scientific Reports* **12,** 19175. doi:10.1038/s41598-022-23628-5 (2022).

20. Giudicepietro, F. *et al.* Burst-like swarms in the Campi Flegrei caldera accelerating unrest from 2021 to 2024. *Nature Communications* **16,** 1548. doi:10.1038/s41467-025-56723-y (2025).

21. Kilburn, C. R. J. *et al.* Potential for rupture before eruption at Campi Flegrei caldera, Southern Italy. *Communications Earth & Environment* **4,** 190. doi:10.1038/s43247-023-00842-1 (2023).

22. Troiano, A. *et al.* The Pisciarelli main fumarole mechanisms reconstructed by electrical resistivity and induced polarization imaging. *Scientific Reports* **11,** 18639. doi:10.1038/s41598-021-97413-1 (2021).

23. Tramelli, A. *et al.* The seismicity of Campi Flegrei in the contest of an evolving long term unrest. *Scientific Reports* **12,** 2900. doi:10.1038/s41598-022-06928-8 (2022).

24. Scotto di Uccio, F. *et al.* Delineation and Fine-Scale Structure of Fault Zones Activated During the 2014–2024 Unrest at the Campi Flegrei Caldera (Southern Italy) From High-Precision Earthquake Locations. *Geophysical Research Letters* **51,** e2023GL107680. doi:10.1029/2023GL107680 (2024).

25. Giacomuzzi, G. *et al.* Tracking transient changes in the plumbing system at Campi Flegrei Caldera. *Earth and Planetary Science Letters* **637,** 118744. doi:10.1016/j.epsl.2024.118744 (2024).

26. Nespoli, M. *et al.* The effects of hot and pressurized fluid flow across a brittle layer on the recent seismicity and deformation in the Campi Flegrei caldera (Italy). *Journal of Volcanology and Geothermal Research* **443,** 107930. doi:10.1016/j.jvolgeores.2023.107930 (2023).

27. Marini, L. *et al.* Time changes during the last 40 years in the Solfatara magmatic–hydrothermal system (Campi Flegrei, Italy): new conceptual model and future scenarios. *Solid Earth* **16,** 551–578. doi:10.5194/se-16-551-2025 (2025).

28. Buono, G. *et al.* New Insights Into the Recent Magma Dynamics Under Campi Flegrei Caldera (Italy) From Petrological and Geochemical Evidence. *Journal of Geophysical Research: Solid Earth* **127,** e2021JB023773. doi:10.1029/2021JB023773 (2022).

29. Petrillo, Z. *et al.* Principal component analysis on twenty years (2000–2020) of geochemical and geophysical observations at Campi Flegrei active caldera. *Scientific Reports* **13,** 18445. doi:10.1038/s41598-023-45108-0 (2023).

30. Petrillo, Z. *et al.* Defining a 3D physical model for the hydrothermal circulation at Campi Flegrei caldera (Italy). *Journal of Volcanology and Geothermal Research* **264,** 172–182. doi:10.1016/j.jvolgeores.2013.08.008 (2013).

31. Afanasyev, A. *et al.* Investigation of hydrothermal activity at Campi Flegrei caldera using 3D numerical simulations: Extension to high temperature processes. *Journal of Volcanology and Geothermal Research* **299,** 68–77. doi:10.1016/j.jvolgeores.2015.04.004 (2015).

32. INGV-OV. *Campi Flegrei - Bollettino di Sorveglianza mensile – Febbraio 2026* Bollettino di Sorveglianza. https://www.ov.ingv.it/index.php/monitoraggio-e-infrastrutture/bollettini-tutti/bollett-mensili-cf/anno-2026-2/1945-bollettino-mensile-campi-flegrei-2026-02/file (Feb. 2026).

33. R Core Team. *R: A Language and Environment for Statistical Computing* https://www.R-project.org/. R Foundation for Statistical Computing (Vienna, Austria, 2024).

Chapter 5



Conclusions

5 CONCLUSIONS

This thesis has approached climate change and environmental sustainability from a mathematical standpoint, through a set of idealised models built around two recurring threads: the role of CO_2-driven mechanisms and the interplay between climate variables acting on different timescales.

In Chapter 2, starting from a fast-slow OU/EBM system, a reduced model à la Hasselmann was derived, driven by a multiplicative stochastic noise whose amplitude depends on temperature itself through the co-albedo. Its stationary variance was computed explicitly and shown to be an increasing function of λ, which stands for the CO_2 radiative forcing. As a consequence, once the equilibrium point enters the ice-sensitive regime of the co-albedo, the stationary variance grows as CO_2 increases, thus offering a mechanism for the enhanced temperature variability observed in the Arctic seas. The same result was then recovered in a spatial setting: by introducing a model that also accounts for horizontal heat transport, it is shown that increasing radiative forcing increases the stationary spatial variance (the trace of the stationary covariance matrix), which is used as a proxy for fluctuation intensity.

In Chapter 3, the fast-slow paradigm was reinterpreted in a spatial form: a three-dimensional Navier-Stokes system, coupled through a buoyancy term to an advection-diffusion equation for the temperature subject to boundary noise. For this velocity-temperature system, a global well-posedness result for small data was established.

In Chapter 4, the discussion moved towards environmental sustainability through the lens of volcanic activity. After an overview of the past and present role of volcanic emissions in terms of greenhouse gases, the case of the Campi Flegrei was addressed, and simplified models of subsurface layers and cavities were proposed, with the aim of reproducing the observed ground uplift through numerical simulations.

Finally, it is worth acknowledging that, despite being grounded in physical laws, the models presented here remain, to a large extent, phenomenological and conceptual. Several assumptions were

made for the sake of tractability, and each chapter leaves room for refinement. In Chapter 2, the stability of the equilibrium point is currently imposed as a modelling assumption; a natural development would be to incorporate a seasonal cycle, so that this stability follows from the dynamics rather than being postulated. In Chapter 3, an interesting direction would be to clarify in which precise sense the system studied can be regarded as the outcome of a Hasselmann-type reduction, thereby connecting the analytical result to the physical picture that motivates it. In Chapter 4, models are still at an early stage: they drastically simplify the enormous complexity of the subsurface and do not yet incorporate seismicity, whose inclusion represents the most immediate next step. These limitations, far from diminishing the value of the models, delineate the space in which future work can meaningfully proceed.